



Virginia Commonwealth University
VCU Scholars Compass

Theses and Dissertations

Graduate School

2018

Aerosolized Surfactants: Formulation Development and Evaluation of Aerosol Drug Delivery to the Lungs of Infants

Susan Boc

Virginia Commonwealth University

Follow this and additional works at: <https://scholarscompass.vcu.edu/etd>

 Part of the [Pharmaceuticals and Drug Design Commons](#)

© Susan Boc

Downloaded from

<https://scholarscompass.vcu.edu/etd/5577>

This Dissertation is brought to you for free and open access by the Graduate School at VCU Scholars Compass. It has been accepted for inclusion in Theses and Dissertations by an authorized administrator of VCU Scholars Compass. For more information, please contact libcompass@vcu.edu.

© Susan Boc 2018
All Rights Reserved

**AEROSOLIZED SURFACTANTS: FORMULATION DEVELOPMENT
AND EVALUATION OF AEROSOL DRUG DELIVERY TO THE LUNGS
OF INFANTS**

A dissertation submitted in partial fulfillment of the requirements for the degree of
Doctor of Philosophy at Virginia Commonwealth University.

by

Susan Boc,
B.Sc., University of California, Los Angeles, 2005

Director: Michael Hindle, Ph.D.,
Professor, Department of Pharmaceutics

Virginia Commonwealth University
Richmond, Virginia
August, 2018

ACKNOWLEDGEMENT

I feel incredibly grateful to have reached this point where I am able to give thanks to all those who have helped me along this journey. This has truly been a great experience.

I would like to express my sincere gratitude to my advisor, Professor Michael Hindle, for his support and patience in guiding me through these last four years. He has been a great mentor and the research that I am so proud to be a part of would not have been possible if it were not for him. I would like to thank my Graduate Advisory Committee members: Dr. Sandro da Rocha, Dr. Matthew Halquist, Dr. Rebecca Heise, and Dr. P. Worth Longest for their support, their time, and their expert advice. I would also like to thank Dr. Masahiro Sakagami and Dr. Peter Byron for their curiosity and insightful comments. Many thanks to Dr. Phillip Gerk for opening up his lab to me and allowing me to use equipment essential to my research.

Also, I would like to acknowledge the members of the Aerosol Research Group, past and present, that have helped me along the way and whom I have built lifelong friendships with Dr. Mandana Azimi, Dr. Tien Truong, Dr. Xiangyin Wei, Dr. Sneha Dhapare, Anuja Raut, Serena Bonasera and Varsha Nair. A special thanks to the members of the VCU Department of Mechanical and Nuclear Engineering: Dr. Dale Farkas, Benjamin Spence and Karl Bass for their willingness to help and their general good nature.

A warm thanks to my former colleagues at Novartis, Nani Kadrichu, John Le, Ralph Niven, and Jeffry Weers; your words of encouragement not only started me on this path but have stayed with me through the years.

Thanks to my family and friends who have supported and encouraged me through this process even though it kept us three thousand miles apart. A special thanks to my mom and my sisters who have been strong role models throughout my life and who have wholeheartedly supported me through this process as they have in every other aspect of my life. And to my fiancé, these last two years have been a whirlwind of excitement and I am eternally grateful to have had you by my side. Thanks for all your love and support, I am truly blessed.

TABLE OF CONTENTS

LIST OF FIGURES	ii
LIST OF TABLES.....	viii
GLOSSARY OF ABBREVIATIONS	xiii
ABSTRACT	xvii
CHAPTER 1	
BACKGROUND AND INTRODUCTION.....	1
1.1 Anatomy and physiology of the respiratory tract	1
1.1.1 Respiratory tract epithelium and airway surface fluid	2
1.2 Pulmonary surfactant	4
1.2.1 Surface tension and surfactant function	4
1.2.2 Adsorption and self-assembly.....	6
1.2.3 Surfactant proteins	7
1.3 Surfactant therapy	8
1.3.1 Animal-derived exogenous surfactants	9
1.4 Neonatal respiratory distress syndrome (RDS)	10
1.4.1 Treatment.....	11
1.4.2 Issues with surfactant therapy for RDS.....	11
1.5 Bronchiolitis	12
1.5.1 Treatment.....	13
1.6 Non-invasive ventilation in infants	14
1.6.1 Constant airway pressure ventilation	14
1.6.1.1 Continuous positive airway pressure (CPAP)	14
1.6.1.2 High-flow nasal cannula (HFNC) therapy	15

1.6.2	Variable airway pressure ventilation.....	15
1.6.3	NIV in infants with respiratory distress	16
1.7	Pulmonary drug delivery	16
1.7.1	Excipient enhanced growth	17
1.7.2	Aerosol delivery devices	18
1.7.3	Aerosol therapy in infants	19
1.8	Aerosolized surfactants	20
1.8.1	Dry powder surfactants	20
1.8.1.1	Dry powder production	21
1.8.1.2	Spray drying of surfactants.....	24
1.8.2	Nebulized surfactants	25
1.9	Surfactant-EEG formulation characterization	26
1.9.1	Phospholipid detection	26
1.9.2	Surface activity	28
1.9.3	Surfactant protein analysis	29
1.9.3.1	Protein purification by precipitation	30
1.9.3.2	Protein purification by analytical separation.....	32
1.9.3.3	Protein detection	32
1.9.4	Dispersion stability	33
1.10	Objectives	35
 CHAPTER 2		
	HYPOTHESIS AND SPECIFIC AIMS.....	36
 CHAPTER 3		
	ASSESSMENT OF THE EFFECT OF SPRAY DRYING PROCESS PARAMETERS AND FORMULATION FACTORS ON POWDER CHARACTERISTICS AND AEROSOL PERFORMANCE OF DPPC-EEG POWDERS	39
3.1	Introduction	39
3.2	Materials and methods	41
3.2.1	Materials	41

3.2.2	Development of methods to produce DPPC-EEG feed dispersions for spray drying	41
3.2.2.1	Spray dried powder formation.....	42
3.2.2.2	Aerodynamic particle size characterization in ambient conditions	42
3.2.2.3	Liquid chromatography-mass spectrometry for DPPC	43
3.2.2.4	Thermogravimetric analysis	44
3.2.3	Development of methods for surface tension sample preparation and measurement	45
3.2.4	Full factorial design of experiment (DOE) to assess selected formulation factors and spray drying parameters.....	47
3.2.4.1	Particle size determination	48
3.2.5	Statistical analysis	49
3.3	Results and discussion.....	50
3.3.1	Development of methods to produce DPPC-EEG feed dispersions for spray drying	50
3.3.1.1	Preliminary studies on the effect of formulation excipients on powder yield.....	50
3.3.1.2	Preliminary studies on the effect of mannitol-to-sodium chloride ratio on aerosol performance	52
3.3.1.3	Preliminary studies on the effect of feed dispersion preparation method on DPPC content	53
3.3.2	Development of methods for surface tension measurements of DPPC-EEG powders	55
3.3.2.1	Effect of sample preparation and measurement temperature on DPPC surface activity measurements	55
3.3.2.2	Effect of DPPC concentration on DPPC surface activity measurements.....	60
3.3.2.3	Surface tension measurements with preliminary spray dried DPPC-EEG powders.....	62
3.3.2.4	Effect of powder age on DPPC surface activity measurements	63
3.3.3	Full factorial design of experiment (DOE) to assess select formulation factors and spray drying parameters	64
3.3.3.1	Effect of formulation factors and spray drying parameters on powder yield and DPPC content of DPPC-EEG formulations	65
3.3.3.2	Effect of formulation factors and spray drying parameters on the primary particle size distribution of DPPC-EEG formulations.....	68
3.3.3.3	Effect on aerosol performance.....	70

3.3.3.4	Effect of formulation factors and spray drying parameters on the surface tension of DPPC-EEG formulations	74
3.3.4	Preliminary assessment of EEG formulations with commercial surfactants.....	77
3.3.4.1	Feed dispersion preparation and powder formation of commercial surfactant-EEG formulations.....	77
3.3.4.2	Evaluation of the primary particle size of commercial surfactant-EEG formulations	82
3.3.4.3	Aerosol performance of commercial surfactant-EEG formulations	85
3.3.4.4	Surface tension of commercial surfactant-EEG formulations.....	86
3.4	Conclusions	90

CHAPTER 4

	DETERMINATION OF THE EFFECT OF DISPERSION ENHANCERS AND SPRAY VEHICLE ALCOHOL CONCENTRATION ON THE DISPERSIBILITY OF EEG POWDERS PREPARED WITH COMMERCIAL REPLACEMENT SURFACTANTS	92
4.1	Introduction	92
4.2	Materials and methods	93
4.2.1	Materials	93
4.2.2	Feed dispersion preparation.....	94
4.2.2.1	Stability of feed dispersions	95
4.2.3	Spray dried powder formation.....	95
4.2.4	Particle size characterization	97
4.2.5	DPPC content analysis	98
4.2.6	Aerosol performance of leucine powder formulation	98
4.2.6.1	Modified low-volume dry powder inhaler	98
4.2.6.2	Malvern Spraytec [®] aerosol characterization	99
4.2.6.3	Emitted mass determination	100
4.2.7	Spray dried powder analysis.....	101
4.2.7.1	Scanning electron microscopy.....	101
4.2.7.2	Solid state powder characteristics.....	102
4.2.8	Statistical analysis	102

4.3	Results and discussion.....	103
4.3.1	Effect of bypass flow on feed dispersion DPPC content	103
4.3.2	Effect of sonication time on feed dispersion and spray dried powder characteristics	104
4.3.3	Effect of spray atomizer size on particle size distribution	105
4.3.4	Selection of dispersion enhancer	109
4.3.4.1	Effect of dispersion enhancer on feed dispersion characteristics	109
4.3.4.2	Effect of dispersion enhancer on primary particle size distribution	110
4.3.5	Evaluation of leucine formulation	116
4.3.5.1	Effect of ethanol concentration in feed dispersion on the primary particle size distribution.....	116
4.3.5.2	Effect of ethanol concentration in feed dispersion on DPI emitted mass	117
4.3.5.3	Effect of ethanol concentration in feed dispersion on aerosol characteristics.....	118
4.3.5.4	Effect of ethanol concentration in feed dispersion on solid state powder characteristics	126
4.4	Conclusions	130

CHAPTER 5

	ASSESSMENT OF THE EFFECTS OF DESIGN MODIFICATIONS TO A LOW AIR VOLUME ACTUATED DRY POWDER INHALER ON AEROSOL PERFORMANCE CHARACTERISTICS	132
5.1	Introduction	132
5.2	Materials and methods	134
5.2.1	Spray dried powder formulations.....	134
5.2.2	Low dispersion air volume actuation dry powder inhalers	135
5.2.3	Aerosol performance of modified containment unit DPIs	139
5.2.4	Aerosol performance with micronized powder	140
5.2.5	Statistical analysis	142
5.3	Results and discussion.....	142
5.3.1	Effect of powder chamber volume, design configuration, and number of air inlet holes	142
5.3.2	Effect of outlet delivery tube internal diameter on aerosol performance.....	146

5.3.3	Effect of outlet delivery tube length and fill mass on powder performance	148
5.3.4	Aerosol plume characteristics.....	156
5.3.5	Aerosol performance with micronized powder	164
5.4	Conclusions	165

CHAPTER 6

	EVALUATION OF THE <i>IN VITRO</i> AEROSOL DELIVERY EFFICIENCY OF SURFACTANT-EEG FORMULATIONS USING NOVEL LOW-VOLUME MIXER-HEATERS	167
6.1	Introduction	167
6.2	Materials and methods	169
6.2.1	VCU mixer-heater systems.....	169
6.2.1.1	Low-volume mixer-heater design.....	169
6.2.1.2	Very low-volume mixer-heater design.....	170
6.2.2	Realistic infant nose-throat model	171
6.2.3	<i>In vitro</i> nasal delivery experimental set up.....	172
6.2.3.1	VCU low-volume mixer-heater with streamlined infant nasal cannula.....	173
6.2.3.2	Face mask standard of care system.....	174
6.2.3.3	High flow nasal cannula standard of care system.....	175
6.2.4	Breathing conditions	176
6.2.4.1	Optimization of breath synchronized aerosol drug delivery	177
6.2.5	Droplet sizing experiments with the Andersen Cascade Impactor	178
6.2.6	High performance liquid chromatography assay.....	179
6.2.7	Statistical analysis	180
6.3	Results and discussion.....	180
6.3.1	Droplet aerosol sizing experiments with the ACI.....	180
6.3.1.1	Effect of modified controller on nebulizer initial aerosol droplet size	180
6.3.1.2	Effect of mixer-heater on nebulizer aerosol droplet size	181
6.3.2	<i>In vitro</i> aerosol deposition with a realistic infant nose-throat model.....	185
6.3.2.1	Effect of aerosol delivery system on <i>in vitro</i> drug deposition.....	185
6.3.2.2	Effect of a realistic breath cycle on <i>in vitro</i> aerosol deposition	188

6.3.3	Optimization of aerosol delivery synchronization with realistic breathing cycle .	190
6.3.3.1	Effect of nebulizer aerosol output rate on <i>in vitro</i> aerosol deposition	190
6.3.3.2	Effect of nebulizer synchronization on <i>in vitro</i> aerosol deposition	192
6.3.3.3	Effect of nebulization duration on <i>in vitro</i> aerosol deposition	195
6.3.4	Optimized <i>in vitro</i> deposition with a realistic infant nose-throat airway model ...	196
6.3.5	<i>In vitro</i> aerosol deposition with a realistic infant nose-throat airway model from the VCU very low-volume mixer-heater	200
6.3.5.1	Surfactant-EEG dispersion for nebulization.....	201
6.3.5.2	Effect of nebulizer formulation composition on aerosol concentration.....	202
6.3.5.3	VCU very low-volume mixer-heater with the modified controller	203
6.3.5.3.1	Effect of the VCU very low-volume mixer-heater on the aerosol droplet size.....	203
6.3.5.3.2	Effect of the VCU very low-volume mixer-heater on <i>in vitro</i> regional aerosol deposition	207
6.3.5.4	VCU very low-volume mixer-heater with the commercial controller.....	210
6.3.5.4.1	Effect of the commercial controller on the aerosol droplet size from the VCU very low-volume mixer-heater	211
6.3.5.4.2	Effect of the commercial controller on the <i>in vitro</i> regional aerosol deposition from the VCU very low-volume mixer-heater.....	214
6.3.5.4.3	Assessment of DPPC recovered dose using steady state inhalation flow with the very low-volume mixer-heater and the commercial controller	218
6.3.5.4.4	Assessment of DPPC recovered dose using room temperature ventilation gas with using the very low-volume-mixer-heater and the commercial controller with steady state inhalation flow	220
6.4	Conclusions	221

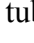
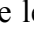
CHAPTER 7

	ASSESSMENT OF THE EFFECT OF SPRAY DRYING PROCESSES ON SURFACTANT PROTEIN CONCENTRATION	224
7.1	Introduction	224
7.2	Materials and methods	226
7.2.1	Protein purification by precipitation	226
7.2.1.1	Hexane/isopropanol	228
7.2.1.2	Methanol/chloroform	228

7.2.1.3	Acetone.....	228
7.2.1.4	Trichloroacetic acid in acetone.....	229
7.2.2	Analysis by direct infusion into mass spectrometer	229
7.2.3	Protein purification by analytical chromatographic separation.....	230
7.2.4	Non-specific assay of proteins.....	231
7.2.5	Enzymatic assay of proteins	232
7.3	Results and discussion.....	233
7.3.1	Protein precipitation.....	233
7.3.2	Analytical separation of Survanta [®] components	241
7.3.3	Non-specific assay of surfactant proteins.....	252
7.3.4	Enzyme linked assay of surfactant proteins	254
7.4	Conclusion.....	256
CHAPTER 8		
	SUMMARY AND CONCLUSIONS.....	258
	LIST OF REFERENCES	267
	VITA.....	282

LIST OF FIGURES

Figure 1.1 Schematic of the conducting and respiratory regions of the human respiratory tract, adapted from [3].	2
Figure 1.2 Cell types of the respiratory epithelium, adapted from [4].	3
Figure 1.3 Chemical structure of dipalmitoylphosphatidylcholine (DPPC, 16:0/16:0 PC).	5
Figure 1.4 Schematic representation of solid-gel to liquid-crystalline phase transition of a DPPC bilayer, adapted from [17].	6
Figure 1.5 Schematic of free energy with particle separation according to DVLO theory [120].	34
Figure 1.6 Zeta potential of Survanta (1 mg/mL phospholipids) as a function of pH [121].	35
Figure 3.1 Dynamic tensiogram for the commercial Survanta formulation (0.75 mg/mL phospholipids) at 37 °C [104].	46
Figure 3.2 Effect of sample temperature on surface activity of 1.2 mg/mL dispersion of unprocessed DPPC in 154 mM NaCl vehicle performed using method 1. The surface activity of 154 mM NaCl solution is also shown for comparison. Markers represent individual values. RT=room temperature.	59
Figure 3.3 Effect of sample preparation method effect on surface activity measurement of DPPC (1.0-1.2 mg/mL) dispersed in NaCl aqueous vehicle at 50 °C. Method 1: heat and bath sonication at elevated temperature; method 2: heat, stirring and bath sonication at elevated temperature; method 3: probe sonication at elevated temperature. The surface activity of water is also shown for comparison. Markers represent individual values.	60
Figure 3.4 Correlation of final surface tension values with DPPC concentration for samples measured at 50 °C using method 3. Markers represent individual values.	61
Figure 3.5 Surface tension activity comparison of unprocessed DPPC and spray dried formulation P9 with a nominal DPPC concentration of 0.86 mg/mL measured at 50 °C using method 3. The surface activity of water is also shown for comparison. Markers represent individual values.	63

- Figure 3.6** Combined experimental conditions ordered by increasing primary particle size (primary y-axis) with corresponding MMAD values on the secondary y-axis. Markers represent the mean, error bars represent the SD, n=3. 73
- Figure 3.7** Correlation of MMAD with Dv50 values for DPPC-EEG powders. Markers represent mean values, n=3..... 74
- Figure 3.8** Particle size distribution comparisons for commercial surfactant-EEG powders with DPPC-EEG formulation 3 determined on the Sympatec HELOS with RODOS dispersion pressure of 3.0 bar. Markers represent the mean value, error bars represent the SD, n=3. 84
- Figure 3.9.** Surface tension activity comparison of commercial replacement surfactant formulations with EEG powder formulations of Curosurf[®] (top) and Survanta[®] (bottom) with nominal DPPC content of 1.5 mg/mL measured at 50 °C using method 3. Markers represent individual values. 88
- Figure 3.10** Surface tension activity comparison of unprocessed DPPC with commercial surfactant EEG powder formulations of Curosurf (circles) and Survanta (diamonds) with nominal DPPC content of 1.5 mg/mL measured at 50 °C using method 3. The surface activity of water is also shown for comparison. Markers represent individual values. 89
- Figure 4.1** Axial cross-section view of the assembled modified containment unit DPI with 55 mm delivery tube length. Inlet body () and outlet body () portions differentiated by fill pattern. 99
- Figure 4.2** Representative time history plot for the aerosol plume of Survanta-EEG powder generated with the modified containment unit DPI using 3 mL volume of dispersion air as captured by the Malvern Spraytec[®] 100
- Figure 4.3** DPPC content in replicate runs of recycled dispersions of Survanta-EEG formulations with trileucine in 5% v/v ethanol in water spray vehicle. Markers represent the mean value, error bars represent the SD, n=3. 104
- Figure 4.4** Primary particle size characteristics of spray dried Survanta-EEG powders determined on the Sympatec HELOS with RODOS dispersion pressures of 1.0 and 4.5 bar. Bars represent the mean value, error bars represent the SD, n≥3. 111
- Figure 4.5** Cumulative mass emitted (% nominal, circles) and mass emitted (% remaining, triangles) for leucine-Survanta-EEG powders with the modified containment unit DPI with 10 mg powder fill mass using 3 mL pulses of dispersion air. Markers represent the mean value, error bars represent the SD, n=3; EtOH=ethanol..... 118
- Figure 4.6** Mass emitted (% nominal, squares) and Dv50 (diamonds) values for leucine-Survanta-EEG powders with the modified containment unit DPI with 10 mg powder fill mass using 3 mL pulses of dispersion air. Markers represent the mean value, error bars represent the SD, n=3; EtOH=ethanol. 119

- Figure 4.7** Obscuration-time profiles for the (a) first actuation, (b) second actuation, and (c) third actuation replicate aerosol plumes from the modified containment unit DPI filled with 10 mg of leucine-Survanta-EEG powders dispersed with 3 mL volume of dispersion air, EtOH=ethanol. 124
- Figure 4.8** Log-linear plots showing comparisons of mean volume fraction/ μm distributions for each actuation of Survanta-EEG formulations prepared with 5% and 20% v/v ethanol in water concentrations; EtOH=ethanol. 125
- Figure 4.9** SEM images of leucine-Survanta-EEG spray dried powder formulations prepared in (a) 5% v/v ethanol in water, and (b) 20% v/v ethanol in water feed dispersions. 127
- Figure 4.10** Characteristic plots showing (a) thermogravimetric analyzer profiles with isothermal hold at 100 °C and (b) dynamic scanning calorimetry thermograms heated from 25 to 100 °C at a rate of 5 °C/min for spray dried leucine-Survanta-EEG formulations. 129
- Figure 5.1** Cumulative (primary y-axis) and density (secondary y-axis) particle size distribution of the spray dried surfactant-EEG powder batches determined using the Sympatec RODOS dispersion pressure of 4.5 bar. Markers represent the mean value, error bars represent the SD, n=10. 135
- Figure 5.2** Axial cross-section of assembled single side device showing the inlet and outlet capillaries inside the capsule. 136
- Figure 5.3** Axial cross-section of assembled containment unit DPIs: (a) SS with 0.68 mL powder chamber, (b) SS with 0.21 mL powder chamber, (c) ST with 90 mm delivery tube. Open powder chamber view of studied inlets (d) and delivery tube internal diameters (e); SS: single side, ST: straight through. 139
- Figure 5.4** Cumulative (primary y-axis) and density (secondary y-axis) particle size distribution of the micronized albuterol sulfate powder determined using the Sympatec RODOS dispersion pressure of 4.5 bar. Markers represent the mean value, error bars represent the SD, n=4. 141
- Figure 5.5** Cumulative mass emitted (% nominal) for each actuation by delivery tube length and fill mass. Markers represent the mean value, error bars represent the SD, n=3. 156
- Figure 5.6** Replicate obscuration-time profiles for different fill masses of surfactant-EEG powder studied with the (a) 90 mm (b) 55 mm, and (c) 45 mm delivery tube lengths of the optimized containment unit DPI on the first 3 mL actuation of dispersion air, n=3. 160
- Figure 5.7** Correlation of delivery tube length of the optimized containment unit DPI with a) D_{v50} , b) particle fraction $<1 \mu\text{m}$, and c) particle fraction $<5 \mu\text{m}$ of surfactant-EEG powders on the first 3 mL actuation of air with 5 mg powder fill mass. Markers represent individual values. 163
- Figure 6.1** Computer aided design rendered image of the VCU low-volume mixer-heater. 170

- Figure 6.2** VCU very low-volume mixer-heater and modified Aerogen® Solo..... 171
- Figure 6.3** Infant nose-throat model, based on the computed tomography scan of a 20-week-old male infant weighing 7.7 kg, with streamlined infant nasal cannula..... 172
- Figure 6.4** Experimental setup for the VCU low-volume mixer-heater system with streamlined nasal cannula..... 174
- Figure 6.5** Face mask standard of care system experimental setup..... 175
- Figure 6.6** High flow nasal cannula standard of care system experimental setup..... 176
- Figure 6.7** Two cycles of a realistic breathing profile based on an 8 kg infant. The ventilation gas flow rate is 100 mL/s (6 L/min) delivered continuously. Ideally, drug aerosol is delivered to the patient in the ventilation gas flow only during inhalation and the delivery time should be synchronized such that delivery occurs when the inhalation flow rate is greater than the ventilation gas flow as shown by the nebulization duration. To achieve this delivery through the low-volume mixer heater, nebulization must be triggered during the exhalation cycle, as shown by the trigger time. In this example, the nebulization trigger time was 0.8 s before the next breath and the nebulization duration was 0.3 s..... 177
- Figure 6.8** Droplet size distributions of mass fraction/ μm (top) and cumulative percent mass undersize (bottom) of 0.5% w/v albuterol sulfate in water from the Aeroneb® Pro nebulizer determined by cascade impaction with the ACI in an environmental chamber set to 99% RH. Aerosol size was determined at the nebulizer exit using the (i) commercial controller and (ii) modified controller, together with (iii) the aerosol size at the exit of the streamlined cannula following aerosol generation into the VCU low-volume mixer-heater. Markers represent the mean value, error bars represent the SD, $n \geq 3$ 183
- Figure 6.9** Aerosol drug deposition comparison for the face mask standard of care system and the VCU low-volume mixer-heater system using steady state inhalation conditions. Delivery device: face mask system = nebulizer outlet; mixer-heater system = nebulizer outlet, mixer-heater, tubing. Bars represent the mean value, error bars represent SD, $n=3$. *Significant difference; Student's t-test, $p < 0.05$ 186
- Figure 6.10** Estimated *in vitro* lung dose at different nebulization trigger times relative to the start of inhalation (top) and relative to the realistic breathing profile (bottom) with nebulization duration of 0.3 s. Markers represent the mean value, error bars represent the SD, $n=3$. 194
- Figure 6.11** Comparison of *in vitro* aerosol deposition when varying the nebulization duration using the VCU low-volume mixer-heater. Bars represent the mean value, error bars represent the SD, $n \geq 3$. *Significant difference; Student's t-test, $p < 0.05$ 199
- Figure 6.12** Aerosol particle concentration of albuterol sulfate and surfactant-EEG nebulizer formulation aerosols generated as a function of dilution gas flow rate measured using the condensation particle counter from aerosols generated by the modified Aerogen® Solo operated by the modified controller. Markers represent the mean value, error bars represent the SD, $n=4$ 203

- Figure 6.13** Aerosol droplet size distributions of the modified Aeroneb[®] Solo nebulizer output (exit nebulizer) and following delivery from the very low-volume mixer-heater (exit tubing) of 0.5% w/v surfactant-EEG formulation generated by the Aerogen[®] Solo with the modified controller. Markers represent the mean value, error bars represent the SD, $n \geq 3$.
..... 205
- Figure 6.14** Comparison of *in vitro* aerosol DPPC deposition when varying the nebulization duration using the VCU very low-volume mixer-heater with surfactant-EEG and the modified controller initiating nebulization at the start of a realistic inhalation breathing cycle. Bars represent the mean value, error bars represent the SD, $n=3$. *Significant difference; Student's t-test, $p < 0.05$.
..... 210
- Figure 6.15** Aerosol droplet size distributions of the Aeroneb[®] Solo nebulizer output (exit of nebulizer) and following delivery from the very low-volume mixer-heater (exit of tubing) of 0.5% w/v surfactant-EEG formulation generated by the Aerogen[®] Solo with the commercial controller. Markers represent the mean value, error bars represent the SD, $n=5$.
..... 213
- Figure 6.16** Comparison of *in vitro* aerosol DPPC deposition when varying the nebulization duration using the VCU very low-volume mixer-heater with surfactant-EEG and the commercial controller initiating nebulization at the start of a realistic inhalation breathing cycle. Bars represent the mean value, error bars represent the SD, $n=3$. *Significant difference; Student's t-test, $p < 0.05$.
..... 215
- Figure 6.17** Comparison of DPPC aerosol deposition from the VCU very low-volume mixer heater captured using a realistic breathing cycle and a steady state inhalation flow of 30 L/ min. Steady state inhalation deposition experiments were performed using heated and room temperature ventilation gas flowing through the VCU very low-volume mixer heater with the commercial controller with 0.1 s nebulization duration. Bars represent the mean value, error bars represent the SD, $n=3$. *Significant difference; Student's t-test, $p < 0.05$. RT=room temperature
..... 220
- Figure 7.1** Solubility of SP-B (top) and SP-C (bottom) in different organic solvent/water mixtures; TFE = trifluoroethanol (circles), MeOH = methanol (triangles), ACN = acetonitrile (squares) [6].
..... 227
- Figure 7.2** Mass spectrum comparison of protein precipitation method on Survanta[®] with (a) hexane/isopropanol, (b) methanol/chloroform, (c) acetone, and (d) TCA in acetone. ... 235
- Figure 7.3** Transform spectrum comparison of protein precipitation methods on Survanta[®] with (a) hexane/isopropanol, (b) methanol/chloroform, (c) acetone, and (d) TCA in acetone with output mass range set from 3500 to 18500 Da. 238
- Figure 7.4** MaxEnt spectrum comparison of protein precipitation methods on Survanta[®] with (a) hexane/isopropanol, (b) methanol/chloroform, (c) acetone, and (d) TCA in acetone for output mass range set from 3500 to 18500 Da. 239

- Figure 7.5** MaxEnt spectrum for acetone precipitate sample on Survanta[®] with output mass range of 4000 to 5000 Da with a resolution of 0.5 Da/channel..... 240
- Figure 7.6** Repeat acetone protein precipitation sample (a) electrospray spectrum (b) Transform spectrum and (c) MaxEnt spectrum of Survanta[®]..... 240
- Figure 7.7** Comparison of total ion count chromatograms obtained for commercial Survanta[®] formulation (top) and Survanta-EEG spray dried powder (bottom) separation in mobile phase of 80/20% v/v methanol/water with 0.1% formic acid with 5 μ L injection volume, 0.2 mL/min flow rate and a 22 min run time. 242
- Figure 7.8** Mass spectra of Survanta[®] components separated using with 80:20% v/v methanol/water with 0.1% formic acid with injection volume of 5 μ L, 0.2 mL/min flow rate and 22 min run time. MS settings: capillary=3.5 kV, cone=35 V, source temperature=120 $^{\circ}$ C, desolvation temperature=300 $^{\circ}$ C. 243
- Figure 7.9** Comparison of mobile phase solvents (a) 80:20% v/v MeOH/H₂O with 0.1% formic acid, (b) 80:20% v/v ACN/H₂O with 0.1% formic acid, and (c) 60:40% v/v ACN/H₂O with 0.1% formic acid on separation of Survanta[®] components with 5 μ L injection volume and 0.2 mL/min flow rate. MeOH=methanol, H₂O=water, ACN=acetonitrile..... 245
- Figure 7.10** Comparison of commercial Survanta[®] formulation (top) with Survanta-EEG spray dried powder (bottom) separation in mobile phase of 60:40% v/v acetonitrile/water with 0.1% formic acid with 5 μ L injection volume, 0.2 mL/min flow rate and a 15 min run time. 246
- Figure 7.11** Mass spectra of Survanta[®] components separated using with 60:40% v/v ACN/water with 0.1% formic acid with injection volume of 5 μ L, 0.2 mL/min flow rate and 15 min run time. MS settings: capillary=3.5 kV, cone=35 V, source temperature=120 $^{\circ}$ C, desolvation temperature=300 $^{\circ}$ C..... 248
- Figure 7.12** Mass spectra of Survanta-EEG components separated using with 60:40% v/v ACN/water with 0.1% formic acid with injection volume of 5 μ L, 0.2 mL/min flow rate and 15 min run time. MS settings: capillary=3.5 kV, cone=35 V, source temperature=120 $^{\circ}$ C, desolvation temperature=300 $^{\circ}$ C..... 249
- Figure 7.13** Comparison of mass spectra of peak at tR 1.21 min for the commercial Survanta[®] formulation (top) with Survanta-EEG spray dried powder (bottom). MS settings: capillary=3.5 kV, cone=35 V, source temperature=120 $^{\circ}$ C, desolvation temperature=300 $^{\circ}$ C..... 250

LIST OF TABLES

Table 1.1 Commercially available in the US animal-derived surfactant phospholipid and protein concentration comparison, from [35].	10
Table 1.2 Nozzle, droplet and particle size comparison of the traditional Mini Spray Dryer B-290 with the Nano Spray Dryer B-90 and B-90 HP, from [94, 96].	22
Table 3.1 Factors and levels for full factorial DOE assessment of DPPC-EEG formulation optimization.	47
Table 3.2 Weight and volume amounts used for the formulation factors studied.	48
Table 3.3 Effect of formulation excipients on spray dried powder yield and DPPC content of DPPC-EEG powders.	51
Table 3.4 Aerosol performance with the Aerolizer [®] of DPPC-EEG spray dried formulations using mannitol, sodium chloride and leucine as excipients.	52
Table 3.5 DPPC content of feed dispersions (nominal concentration = 20% w/w) prepared by probe sonication and resultant spray dried powder (nominal concentration = 40% w/w). Values are mean (SD), n=3.	54
Table 3.6 Comparison of surface activity of unprocessed DPPC following different preparation methods.	58
Table 3.7 Comparison of surfactant activity for unprocessed DPPC and spray dried formulation P9 at a nominal DPPC concentration of 0.86 mg/mL dispersed in 1 mM NaCl measured at 50 °C using method 3. Values are mean (SD), n=3.	62
Table 3.8 Surfactant activity characteristics of preliminary formulation P9 when stored at 2-8 °C for 14 days. Values are mean (SD), n=3.	64
Table 3.9 Effect of formulation factors and spray drying parameters on the powder characteristics of spray dried DPPC-EEG powders.	67
Table 3.10 Primary particle size measurements and aerosol properties of spray dried DPPC-EEG powders for each experiment varying formulation factors and spray drying parameters. Values are mean (SD), n=3.	69

Table 3.11 Summary of primary particle size of spray dried DPPC-EEG powders by study factor. Values are mean (SD), n=8.....	70
Table 3.12 Summary of aerosol properties of spray dried DPPC-EEG powders by study factor. Values are mean (SD), n=8.....	71
Table 3.13 Effect of formulation factors and spray drying parameters on the surface tension for spray dried DPPC-EEG powder with DPPC concentration of 0.86 mg/mL dispersed in 1 mM NaCl at 50 °C. Values are mean (SD), n=3.....	76
Table 3.14 Characteristics of EEG formulations prepared with commercial surfactant. Values are mean (SD), n=3.....	80
Table 3.15 Commercial surfactant-EEG formulation contents.	81
Table 3.16 Comparison of primary particle size characteristics of DPPC-EEG formulation with commercial surfactant-EEG formulations. Values are mean (SD), n=3.....	83
Table 3.17 Comparison of aerosol performance of DPPC-EEG formulation with spray dried commercial surfactant-EEG powders. Values are mean (SD), n=3.....	86
Table 3.18 Comparison of surfactant activity for EEG formulations prepared with commercial surfactant with nominal DPPC content of 1.5 mg/mL measured at 50 °C using method 3. Values are mean (SD), n=3.....	87
Table 4.1 Spray drying parameters to produce Survanta-EEG powders.....	96
Table 4.2 Effect of sonication time on feed dispersion characteristics (Malvern Zetasizer) and primary particle size characteristics (Sympatec HELOS with RODOS dispersion pressure of 4.5 bar). Values are mean (SD), n≥3.....	107
Table 4.3 Effect of spray atomizer size on particle size characteristics: primary particle size determined on the Sympatec HELOS with RODOS dispersion pressure of 4.5 bar, aerosol performance determined on Malvern Spraytec® with the modified containment unit DPI using 5 mg powder fill mass and 3 mL volume dispersion air. Values are mean (SD), n≥3.	108
Table 4.4 Effect of dispersion enhancer on the zeta potential (ζ), particle size (z-Ave), and polydispersity index (PDI) of the spray drying dispersion. Values are mean (SD), n≥3.	110
Table 4.5 Effect of dispersion enhancer on the primary particle size characteristics, span and particle fractions of the spray dried powders determined using the Sympatec HELOS with RODOS dispersion pressure of 4.5 bar. Values are mean (SD), n=3.	114
Table 4.6 Effect of dispersion enhancer on the primary particle size characteristics, span and particle fractions of the spray dried powders determined using the Sympatec HELOS with RODOS dispersion pressure of 1.0 bar. Values are mean (SD), n=3.	115

Table 4.7 Aerosol characteristics of leucine-Survanta-EEG spray dried powders using the modified containment unit DPI with 10 mg powder fill mass and 3 mL pulses of dispersion air. Values are mean (SD), n=3.....	121
Table 5.1 Device design parameters explored for the modified containment unit DPI with 3 mL volume of dispersion air.	140
Table 5.2 Effect of powder chamber volume, design configuration, number of air inlet holes, and delivery tube internal diameter on aerosol performance of surfactant-EEG spray dried powders (fill mass: 3 mg, values are mean (SD), n \geq 3).	145
Table 5.3 Correlation statistics of outlet delivery tube internal diameter with aerosol performance characteristics.....	148
Table 5.4 Effect of delivery tube length and fill mass on aerosol performance of surfactant-EEG spray dried powders. Values are mean (SD), n=3.....	154
Table 5.5 Correlation statistics of powder fill mass with powder dispersion characteristics for the three delivery tube lengths during the first actuation.....	155
Table 5.6 Aerosol plume characteristics of the first actuation of surfactant-EEG spray dried powders delivered with the optimized containment unit DPI. Values are mean (SD), n=3.	157
Table 5.7 Effect of delivery tube length on aerosol performance of surfactant-EEG spray dried powders (fill mass: 5 mg, values are mean (SD), n=3).....	162
Table 5.8 Aerosol performance of micronized albuterol sulfate powder with the optimized containment unit DPI (fill mass: 10 mg, values are mean (SD), n \geq 3).....	164
Table 6.1 Droplet size characteristics of 0.5% w/v albuterol sulfate in water from the Aeroneb [®] Pro nebulizer determined by cascade impaction with the ACI. Aerosol size was determined at the nebulizer exit using the (i) commercial controller and (ii) modified controller, together with (iii) the aerosol size at the streamlined cannula exit following aerosol generation into the VCU low-volume mixer-heater. Values are mean (SD), n \geq 3.....	184
Table 6.2 Total and regional aerosol drug deposition comparison for the standard of care systems with the VCU mixer-heater delivery system using steady state inhalation conditions. Values are mean (SD), n=3.....	187
Table 6.3 Deposition comparison of standard of care systems with the VCU low-volume mixer-heater delivery system with realistic breathing conditions and constant nebulization. Values are mean (SD), n=4.....	189
Table 6.4 Comparison of nebulizer output rate of the modified controller on estimated % lung dose and total delivered lung dose. Values are mean (SD), n \geq 3.	192

Table 6.5 Comparison of <i>in vitro</i> aerosol deposition for nebulization trigger times relative to the start of inhalation with a nebulization duration of 0.3 s and realistic breathing conditions. Values are mean (SD), n=3.....	195
Table 6.6 Comparison of <i>in vitro</i> aerosol deposition when varying the nebulization duration for nebulization trigger time of 0.4 s prior to the next inhalation with realistic breathing conditions. Values are mean (SD), n≥3.....	196
Table 6.7 Comparison of <i>in vitro</i> aerosol deposition when varying the nebulization duration with breath-actuated nebulization with 0.4 s nebulization trigger time prior to the start of inhalation and realistic breathing conditions. Values are mean (SD) percent of nominal dose, n≥3.....	199
Table 6.8 Surfactant-EEG nebulizer formulation dispersion stability and DPPC content over time. Values are mean (SD), n≥3.....	202
Table 6.9 Aerosol droplet size characteristics of the modified Aeroneb® Solo nebulizer output and following delivery from the very low-volume mixer-heater (delivery tubing exit) of 0.5% w/v surfactant-EEG formulation determined by cascade impaction with the ACI. Aerosols were generated using the modified and commercial Aerogen® controllers. Values are mean (SD), n≥3.	206
Table 6.10 Comparison of <i>in vitro</i> aerosol DPPC deposition when varying the nebulization duration using the VCU very low-volume mixer-heater with surfactant-EEG. The modified controller and commercial controller was used to initiate nebulization at the start of a realistic inhalation breathing cycle. Values are mean (SD) percent of nominal dose, n=3.	209
Table 6.11 Comparison of estimated delivered doses and respiratory losses for the nebulization durations of 0.3 s and 0.1 s with the modified and commercial controllers using the VCU very low-volume mixer-heater. Values are mean (SD), n=3.....	217
Table 6.12 Comparison of DPPC aerosol deposition and recovery from the very low-volume mixer heater captured using a realistic breathing cycle and a steady state inhalation flow of 30 L/min. Steady state inhalation deposition experiments were performed using heated and room temperature ventilation gas flowing through the very low-volume mixer heater with the commercial controller with 0.1 s nebulization duration. Values are mean (SD), n=3....	219
Table 7.1 Starting electrospray mass spectrometer settings for analysis of surfactant samples.	230
Table 7.2 Comparison of bovine SP-B and SP-C characteristics [169-173].....	231
Table 7.3 Prepared protein samples and theoretical protein content for fluorescamine assay...	232
Table 7.4 Identified peaks from mass spectra of Survanta® separated using with 60/40% v/v acetonitrile/water with 0.1% formic acid with injection volume of 5 µL, 0.2 mL/min flow rate and 15 min run time. MS settings: capillary=3.5 kV, cone=35 V, source temperature=120 °C, desolvation temperature=300 °C. Exact mass values from [182].	250

- Table 7.5** Predicted mass charges of SP-B dimer (17395.5 Da), SP-B monomer (8699.8 Da) and SP-C monomer (4041.7 Da), including sodium adducts and single methylation, within the range of the triple quadrupole MS (200-2000 m/z). H=hydrogen, Na=sodium, Me=methyl. 252
- Table 7.6** Fluorescence results for primary amino groups for three batches of spray dried Survanta-EEG formulations and feed dispersions, presented as percentages of the initial values obtained for the unprocessed Survanta[®] formulation. Values are mean (SD), n=3. 254
- Table 7.7** Absorbance results of the spray dried Survanta-EEG formulation and feed dispersions relative to the commercial Survanta[®] formulation using ELISA kits for bovine SP-B and SP-C. 256

GLOSSARY OF ABBREVIATIONS

Å	angstrom
°C	degree Celsius
μL	microliter
γ	surface tension
μg	microgram
μm	micrometer
μmol	micromole
× g	times gravity
ζ	zeta potential
ACI	Andersen Cascade Impactor
ACN	acetonitrile
ANOVA	analysis of variance
APCI	atmospheric pressure chemical ionization
API	active pharmaceutical ingredient
BEH	bridged ethyl hybrid
BiPAP	bilevel positive airway pressure
C	solute concentration
CHCl ₃	chloroform
CI	chemical ionization
cm	centimeter
CO ₂	carbon dioxide
conc	concentration
cP	centipoise = 0.01 gram per centimeter-second
CPAP	continuous positive airway pressure
d _{droplet}	droplet diameter
d _{particle}	particle diameter
DOE	design of experiment
DPI	dry powder inhaler

DPPC	dipalmitoylphosphatidylcholine
DSC	differential scanning calorimetry
Dv10	volume diameter at the 10 th percentile
Dv50	volume median diameter
Dv90	volume diameter at the 90 th percentile
EEG	excipient enhanced growth
EI	electron ionization
ELISA	enzyme-linked immunosorbent assay
ESI	electrospray ionization
EtOH	ethanol
Expt	experiment
g	gram
GRAVY	grand average of hydrophathy
GSD	geometric standard deviation
h	hour
H ₂ O	water
HFNC	high flow nasal cannula
HFV	high-frequency ventilation
HILIC	hydrophobic interaction liquid chromatography
HPMC	hydroxypropyl methylcellulose
HRP	horseradish peroxidase
ID	internal diameter
kDa	kilodalton
kg	kilogram
kHz	kilohertz
kV	kilovolts
L	liter
LC-MS	liquid chromatography-mass spectrometry
LV-DPI	low volume-dry powder inhaler
M	molar; moles per liter
MALDI	matrix-assisted laser desorption ionization
mbar	millibar
MeOH	methanol
mg	milligram
min	minute
mL	milliliter

mm	millimeter
mM	millimolar
MMAD	mass median aerodynamic diameter
mN/m	millinewton per meter
ms	millisecond
MS	mass spectrometer
mV	millivolt
m/z	mass-to-charge ratio
n	number of experimental replicates
NaCl	sodium chloride
NGI	Next Generation Impactor
NIPPV	non-invasive positive pressure ventilation
NIV	non-invasive ventilation
nm	nanometer
p	p -value
P_0	hydrostatic pressure
PdI	polydispersity index; describes the distribution width
PEEP	positive end expiratory pressure
pI	isoelectric point
PL	phospholipids
P_{\max}	maximum pressure
pMDI	pressurized metered dose inhaler
PMPC	palmitoyl-oleoyl phosphatidylcholine, PC 16:0/14:0
POPC	1-palmitoyl-2-oleylphosphatidylcholine, PC 16:0/18:1
POPG	1-palmitoyl-2-oleoyl- <i>sn</i> -glycero-3-phosphoglycerol, PG 16:0/18:1
PS	pulmonary surfactant
PSD	particle size distribution
Q.S.	Quantum sufficit; add enough solvent to bring the total volume to...
r	Pearson correlation coefficient
R^2	coefficient of determination
r_c	capillary radius
RDS	Respiratory Distress Syndrome
RESS	rapid expansion of supercritical solutions
RF	radio frequency
RH	relative humidity
RSV	Respiratory Syncytial Virus

RT	room temperature
RTV	room temperature vulcanizing
s	second
SCF	supercritical fluid
SD	standard deviation
SEM	scanning electron microscopy
<i>sn</i>	single acyl chain
soln	solution
SP-A	surfactant protein A
SP-B	surfactant protein B
SP-C	surfactant protein C
SP-D	surfactant protein D
SS	single side
ST	straight through
TCA	trichloroacetic acid
TFE	trifluoroethanol
T _g	transition temperature
TGA	thermogravimetric analysis
TIC	total ion count
TOF	time-of-flight
T _r	retention time
Tukey's HSD	Tukey's honest significant difference test
USP	United States Pharmacopeia
V	volts
VCU	Virginia Commonwealth University
V _{rms}	root mean square voltage
v/v	volume fraction
w/v	gram of solute per 100 mL of solution
w/w	mass fraction
z-Ave	z-average; hydrodynamic diameter

ABSTRACT

AEROSOLIZED SURFACTANTS: FORMULATION DEVELOPMENT AND EVALUATION OF AEROSOL DRUG DELIVERY TO THE LUNGS OF INFANTS

By Susan Boc, B.Sc.

A dissertation submitted in partial fulfillment of the requirements for the degree of Doctor of Philosophy at Virginia Commonwealth University.

Virginia Commonwealth University, 2018

Major director: Michael Hindle, Ph.D., Professor, Department of Pharmaceutics

The overall aim of this research project was to develop surfactant dry powder formulations and devices for efficient delivery of aerosol formulations to infants using the excipient enhanced growth (EEG) approach. Use of novel formulations and inline delivery devices would allow for more efficient treatment of infants suffering from neonatal respiratory distress syndrome and bronchiolitis.

A dry powder aerosol formulation has been developed using the commercial product, Survanta[®] (beractant) and EEG technology to produce micrometer-sized hygroscopic particles. Spray drying and formulation parameters were initially determined with dipalmitoylphosphatidylcholine (DPPC, the dominant phospholipid in pulmonary surfactant), which produced primary particles 1 μm in size with a mass median aerodynamic diameter of 1-2 μm .

Investigation of dry powder dispersion enhancers and alcohol concentration on the effect of powder aerosol characteristics were performed with the Survanta-EEG formulation. The optimal formulation consisted of Survanta[®], mannitol and sodium chloride as hygroscopic excipients, and leucine as the dry powder dispersion enhancer, prepared in 20% v/v ethanol/water. The powders produced primary particles of 1 μm with >50% of the particles less than 1 μm . The presence of surfactant proteins and surface activity were demonstrated with the Survanta-EEG formulation following processing.

A novel containment unit dry powder inhaler (DPI) was designed for delivery of the surfactant-EEG formulation using a low volume of dispersion air. Studies explored optimization of air entrainment pathway, inlet hole pattern, delivery tube internal diameter and length. With 3-10 mg fill masses of spray dried surfactant powder, the DPI enabled delivery of >2 mg using one 3-mL actuation of dispersion air. Overall, it was possible to deliver >85% of the loaded fill mass using three actuations.

Nebulized aerosol formulations are characterized with low delivered doses. Using a novel mixer-heater delivery system, the highest estimated percent lung dose achieved during realistic *in vitro* testing of a Survanta-EEG formulation aerosolized with a commercial mesh nebulizer was when nebulization was synchronized with inhalation of the breathing profile. Design changes to the mixer-heater system eliminated the need for synchronization, achieving an estimated percent lung dose of 31% of the nominal, an improvement compared with existing systems that achieve approximately <2% lung dose.

CHAPTER 1 BACKGROUND AND INTRODUCTION

1.1 Anatomy and physiology of the respiratory tract

Anatomically, the respiratory tract can be classified into two broad divisions, the upper and lower airways. The upper airways consist of the extrathoracic regions from the nasal cavity and mouth to the larynx, one function of which is to warm and humidify the inhaled ambient air. The lower airways include the trachea, bronchi, bronchioles and the alveoli, which can be functionally divided into the conducting (trachea, bronchi, bronchioles) and respiratory (alveoli) regions (Figure 1.1) [1-3]. The main function of the respiratory system is gas exchange – to take in oxygen and remove waste carbon dioxide – which is done by (i) exchanging gases between the external environment and the alveolar space through breathing, and (ii) exchanging gases between the alveolar space and the blood by diffusion [4]. The conducting airways are a conduit for the transport of gases to and from the external environment to the respiratory regions where gas exchange occurs. From the trachea, the airways repeatedly bifurcate creating a series of airway generations that terminate in the alveolar sacs, each of which contain a collection of alveoli. The diameters of the airways decrease with increasing generations as the surface area of the airways increase [4].

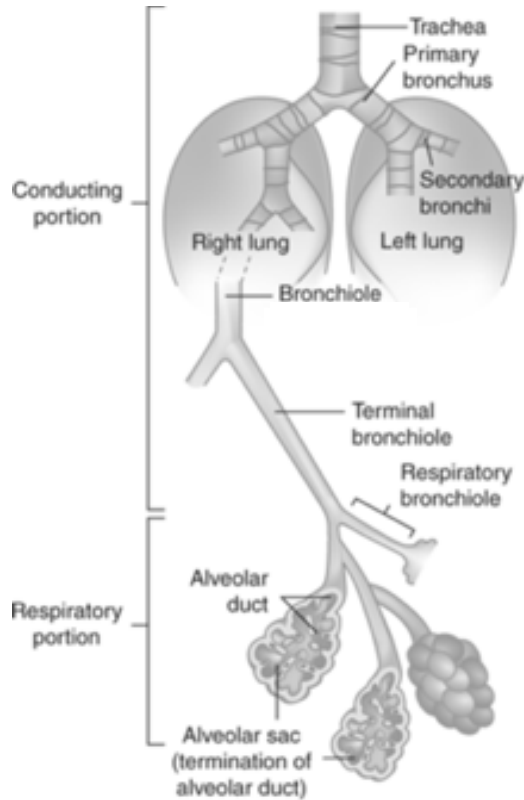


Figure 1.1 Schematic of the conducting and respiratory regions of the human respiratory tract, adapted from [3].

1.1.1 Respiratory tract epithelium and airway surface fluid

The different regions of the respiratory tract are lined with two main cell types, secretory and ciliated epithelial cells, which change in concert with its physiological function (Figure 1.2). In the conducting airways, the secretory cells are goblet cells; they, along with submucosal glands, produce and secrete mucus. Airway mucus, which consists mainly of water and mucins (high molecular weight glycoproteins), has multiple important functions which include protection of the epithelium from dehydration, promoting saturation of inhaled air, and trapping inhaled foreign particles [4, 5]. The mucus layer is separated from the epithelium by an aqueous sol layer, also referred to as periciliary fluid. The low viscosity sol layer surrounds the cilia of the columnar

epithelium allowing it to beat and propel the mucus layer with trapped particles to the pharynx where it is swallowed or expectorated. This movement of mucus from the lower respiratory tract to the pharynx is driven by air flow and mucociliary clearance [6]. The two layers are separated by a thin layer of surfactant, which promotes spreading of the mucus and allows for efficient transfer of energy from the beating cilia, therefore influencing the effectiveness of mucociliary clearance [7].

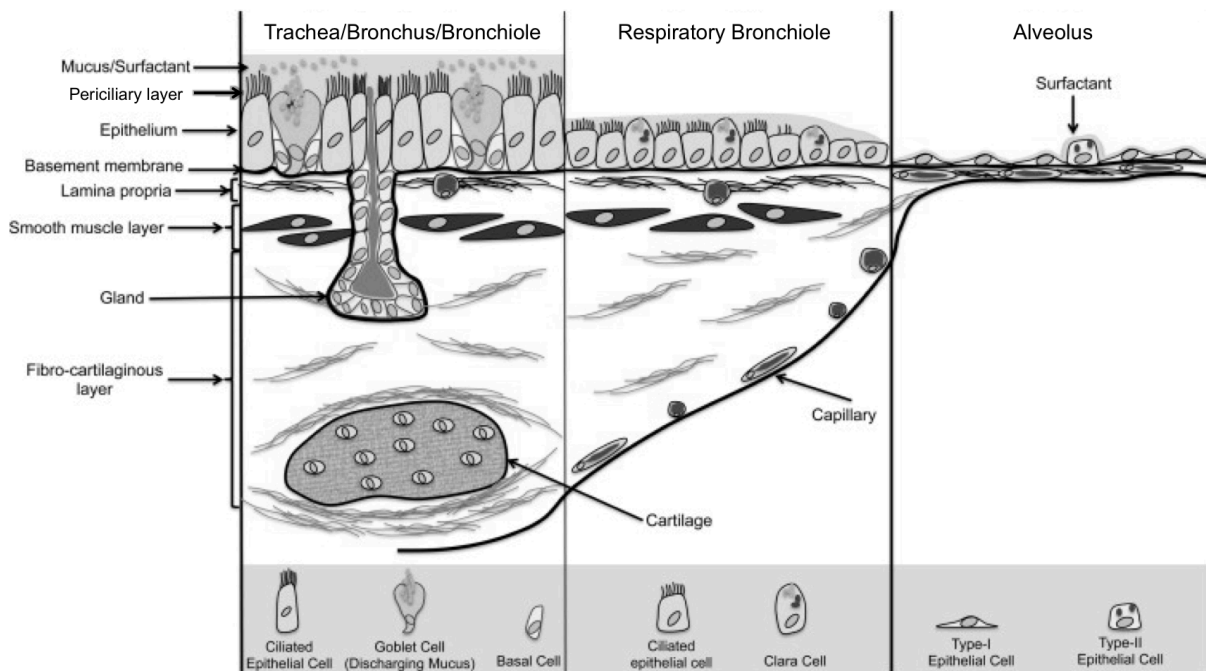


Figure 1.2 Cell types of the respiratory epithelium, adapted from [4].

The goblet cells and mucous glands are not present in the respiratory tract beyond the terminal bronchioles, therefore no mucus is produced in the peripheral airways [4]. The secretory cells in the transition region from the conducting airways to the respiratory region are club cells (Clara cells in Figure 1.2). The ciliated epithelial cells observed in this region are cuboidal in shape with shortened cilia compared to the columnar epithelial cells of the conducting airways.

The alveolar epithelium consists of type I and type II pneumocytes (Figure 1.2). Simple squamous type I cells cover over 90% of the alveoli and are responsible for gas-exchange with blood in the pulmonary capillaries [8, 9]. The type II cells are cuboidal cells that secrete collagen and elastin, creating a fluid extracellular matrix (aqueous alveolar hypophase) that supports the structure of the alveoli and allows for dissolution of gases for passive diffusion with capillaries [8]. The type II cells are also responsible for the production and secretion of pulmonary surfactant, a complex mixture of lipids and proteins, vital for proper lung function [2]. The presence of pulmonary surfactant extends into the bronchioles where it prevents cohesion of the bronchiolar walls and decreases the surface tension of the airway mucus lining [5, 7].

1.2 Pulmonary surfactant

Pulmonary surfactant consists roughly of 90% lipids and 10% proteins, with a disaturated phospholipid, dipalmitoylphosphatidylcholine (DPPC) as the dominant lipid present (30-70% of the total lipid concentration) [10-12]. Its primary role is to facilitate breathing by forming a surface-active layer at the respiratory interface.

1.2.1 Surface tension and surfactant function

The presence of the alveolar hypophase at the airway surface of the alveoli results in high surface tension due to an imbalance of forces – the cohesive forces between the fluid molecules are stronger than the interactive forces between the air and fluid molecules – causing an inward force into the bulk of the fluid [13]. Surface tension is related to the work needed to counter this inward force and expand the surface of the fluid. The work of breathing is mainly having to inflate the alveoli against the high surface tension at the air-liquid interface across the large surface area of the lungs, 3-5 m² at birth which increases to 70-150 m² in adults [14]. The required energy is

reduced by the presence of pulmonary surfactant. Pulmonary surfactant (PS) creates a surface-active layer that lowers and varies the surface tension as a function of alveolar size during breathing [13]. By doing so, PS reduces the work of breathing while stabilizing alveoli from collapse or over distention.

For proper pulmonary function, the surfactant present in the lungs must be rigid enough to resist collapse during exhalation, yet fluid enough to allow for rapid adsorption during inhalation to spread and cover the alveolar surface [10]. DPPC, the dominant lipid in PS, is the primary component responsible for resisting high surface pressures during exhalation due to its high transition temperature that maintains the chemical rigidity of the saturated acyl chains (Figure 1.3), which allow for tight packing at normal physiological temperature [15].

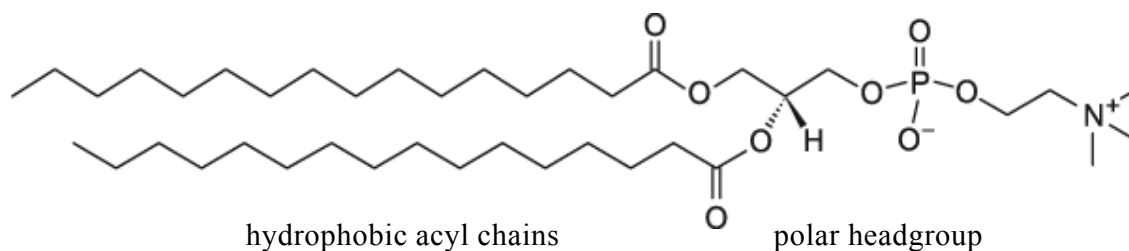


Figure 1.3 Chemical structure of dipalmitoylphosphatidylcholine (DPPC, 16:0/16:0 PC).

Phospholipids have the unique thermal characteristic of a phase transition at temperatures lower than their final melting point. Known as the glass-transition temperature (T_g ; or solid-gel to liquid-crystalline temperature), T_g is the temperature at which the lipid bilayer loses its ordered packing while increasing fluidity (Figure 1.4). The T_g of phospholipids is dependent on: (i) the polar headgroup, (ii) the acyl chain length, (iii) the degree of hydrocarbon chain saturation, and (iv) the nature and ionic strength of the suspension medium [16]. Generally, T_g is lowered by

decreased chain length, unsaturation of the acyl chains and presence of branched chains and bulky headgroups.

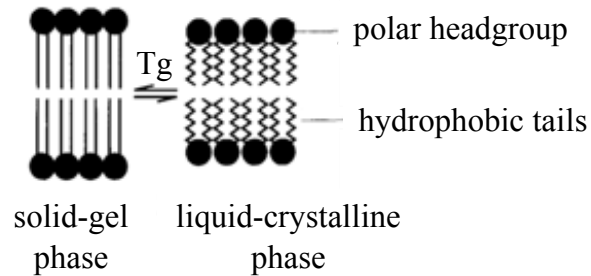


Figure 1.4 Schematic representation of solid-gel to liquid-crystalline phase transition of a DPPC bilayer, adapted from [17].

The relatively long, saturated acyl chains of DPPC results in a high transition temperature relative to other phospholipids, 41 °C [15, 17]. At normal physiological temperature of 37 °C, DPPC exists in the solid-gel phase making it chemically rigid enough to withstand the pressure of compression from exhalation, but results in its slow adsorption and re-spreading when compression is relieved [18, 19]. The presence of unsaturated phospholipids, neutral lipids, and protein components in pulmonary surfactant help to fluidize the interfacial layer during compression and expansion cycles of the alveoli during breathing.

1.2.2 Adsorption and self-assembly

The amphiphilic nature of surfactants – polar headgroup and hydrophobic tails (acyl chains) – allow them to adsorb at interfaces and self-assemble in solution. At the alveolar air-liquid interface, the polar head group of the phospholipid molecules are submerged in the liquid phase

with the hydrophobic chains protruding out into the air phase. Within the airway surface fluid, the phospholipids self-assemble into mixed-lipid bilayers.

The classic model to explain the stability of lung surfactant is the “squeeze-out” model in which it is hypothesized that the less stable fluid components (non-DPPC) are gradually removed from the interfacial monolayer into the subphase during film compression, resulting in a DPPC monolayer at the interface [11, 12]. When compression is relieved, the fluid components return to the interface from the subphase. Dynamic compression-expansion cycling studies indicate that phospholipid uptake into the interface occurs too quickly to be explained by de novo adsorption of phospholipid vesicles from the subphase [20]. It has been proposed that at least part of the PS film is thicker than a single monolayer; in places, the surface monolayer plus one or more lipid bilayers are closely and functionally associated with the interfacial monolayer, which forms the surface-associated “surfactant reservoir” [11, 20].

The non-DPPC components of endogenous surfactant include phosphatidylglycerol (POPG), phosphatidylethanolamine, phosphatidylinositol, some neutral lipids (mainly cholesterol), and four surfactant specific proteins: SP-A, SP-B, SP-C, and SP-D [21, 22].

1.2.3 Surfactant proteins

Surfactant proteins A and D (SP-A and SP-D) are large hydrophilic glycoproteins (26-38 and 43 kDa, respectively [15]) that are involved in pulmonary host defense with the primary role of binding to inhaled particles and pathogens to enhance phagocytic clearance [23]. SP-A is essential for the formation of tubular myelin (loosely packed surfactant in the alveolar hypophase) and regulates phospholipid insertion into the monolayer [24]. SP-A does not have a large effect on surfactant adsorption alone, but is capable of further enhancing adsorption in the presence of SP-

B and calcium [15, 25]. The smaller hydrophobic surfactant proteins, SP-B and SP-C, are necessary for regulating the surface tension in the lungs by independently promoting rapid adsorption of phospholipids from the subphase to the interface [10, 15]. SP-B, an 8.7 kDa protein with 79-amino acid residues, exists as a disulfide linked homodimer with a molecular weight of 17.4 kDa [26]. SP-B plays a role in formation of tubular myelin and influences the molecular ordering of the phospholipid layer as well as SP-C processing [24]. Absence of SP-B results in lethal respiratory distress, whereas SP-C deficiency is associated with chronic interstitial lung disease [10]. SP-C is the most hydrophobic and smallest of the surfactant proteins with 34-amino acid residues at 4.0 kDa [26].

1.3 Surfactant therapy

The basic concept of surfactant therapy involves the delivery of exogenous surfactant to replace or supplement endogenous surfactant that is deficient or has become dysfunctional [13]. The treatment is intended only as an immediate course of action as the lungs are presumed to eventually establish or recover the ability to produce their own surfactant and maintain normal pulmonary function. Surfactant therapy has been shown to be highly effective in the treatment of immaturity-related respiratory distress in preterm infants [27]. Surfactant therapy in infants results in mucus that is more hydrated and better transported by mucociliary clearance compared to mucus in untreated infants, suggesting that surfactant therapy may also be useful in other lung diseases with airway mucus obstruction, such as severe bronchiolitis [6, 28, 29]. The success of the therapy mainly depends on the surfactant composition and efficient and uniform delivery to the targeted regions of the lungs.

1.3.1 Animal-derived exogenous surfactants

Natural surfactant preparations commercially available in the United States include beractant (minced bovine lung extract) [30], calfactant (bovine lung lavage extract) [31], and poractant alfa (minced porcine lung extract) [32]. Trembath et al. [33] found no significant differences in outcomes of air leak syndromes, death and bronchopulmonary dysplasia among the three formulations. Similarly, a Cochrane review concluded that there were no differences in clinical outcome for the two bovine-derived preparations, but concluded that it is unclear if a difference exists from the porcine-derived preparation as there have been a lack of dose-equivalent comparison groups with appropriate sample size [33, 34].

The surfactant formulations are obtained by animal lung lavage or by mincing animal lung tissue, which is then purified by lipid extraction removing hydrophilic components, including the surfactant proteins A and D. The purified extract retains surfactant proteins B and C, neutral lipids, and phospholipids [34, 35]. Table 1.1 compares the phospholipid and protein concentrations in the three formulations. After purification, beractant (Survanta[®], Abbott Laboratories, Columbus, OH) supplements its formulation with the addition of DPPC, palmitic acid, and tripalmitin [30]. Calfactant (Infasurf[®], Forest Pharmaceutical, St Louis, MO) has higher concentrations of SP-B presumably due to the differing processes involved in preparing extracts from lung lavage compared to minced lung processes [35]. Following extraction, poractant (Curosurf[®], Chiesi Farmaceutici, Prima, Italy) undergoes additional purification to remove neutral lipids [35].

Table 1.1 Commercially available in the US animal-derived surfactant phospholipid and protein concentration comparison, from [35].

Formulation	Extract origin	Phospholipid concentration, mg/mL	Phospholipid dose, mg/kg	SP-B, $\mu\text{g}/\mu\text{mol}$	SP-C, $\mu\text{g}/\mu\text{mol}$
Beractant (Survanta [®])	minced bovine lung	25	100	0-1.3	1-20
Calfactant (Infasurf [®])	bovine lung lavage	35	105	5.4	8.1
Poractant (Curosurf [®])	minced porcine lung	76	200, then 100	2-3.7	5-11.6

1.4 Neonatal respiratory distress syndrome (RDS)

About 15 million babies are born prematurely each year – more than one in ten of all births per year worldwide [36]. Respiratory distress syndrome (RDS) results from the insufficient production of surfactant in the lungs of preterm infants, most prevalent in infants born <32 weeks gestational age [13]. The pulmonary surfactant system is one of the last systems to develop before birth as it matures between 29-32 weeks of gestation [9]. Type II pneumocytes, the specialized cells that produce pulmonary surfactant, differentiate and begin to produce surfactant between 24-34 weeks of gestation [7, 9, 37]. Although small quantities of surfactant can be detected at 24 weeks of gestation, it is not found in physiologically relevant amounts until after 30 weeks [7, 9]. Premature birth, consequently, can result in surfactant deficiency due to the immature development of the lungs. The deficiency can lead to reduced pulmonary compliance, increased surface tension and risk of alveoli collapse at end-expiration resulting in a reduction of surface area for gas exchange and consequently respiratory distress [38].

1.4.1 Treatment

Exogenous surfactant replacement therapy for immaturity-related respiratory distress has been shown to be effective in reducing mortality and morbidity of infants since it was introduced in the 1980s leading to its use being approved in the early 1990s [39, 40]. Current respiratory care practice guidelines describe two treatment strategies for immaturity-related respiratory distress: (i) prophylactic, in which high risk infants receive surfactant at the time of birth or shortly after; and (ii) rescue, in which surfactant is administered to mechanically ventilated infants with confirmed respiratory distress [41]. There are drawbacks to both strategies. The prophylactic therapy strategy increases the number of treated infants, exposing more infants to the potential risks of intubation, mechanical ventilation and surfactant administration; while the rescue strategy has the potential to delay surfactant administration allowing lung inflammation and fluid influx to impair gas exchange [41].

Amid findings from recent random controlled trials, the Committee on Fetus and Newborn of the American Academy of Pediatrics has made recommendations for alternative methods over the current guidelines [42]. The Committee recommends to provide nasal continuous positive airway pressure to infants immediately after birth with subsequent selective surfactant administration by intubation to those with persistent severe respiratory distress; and if respiratory support with a ventilator is likely needed, then early administration of surfactant followed by rapid extubation is suggested rather than prolonged ventilation.

1.4.2 Issues with surfactant therapy for RDS

While the treatment is straightforward and effective, delivery of a liquid bolus is associated with non-uniform distribution of surfactant within the airways and requires a high dosage regimen.

Current treatments instruct for surfactant administration to be delivered in partial doses with the infant oriented in different positions, which is done in an effort to achieve a uniform dose by relying on gravity to coat the airspaces of the lungs [30]. The optimal dose and volume of exogenous surfactant is uncertain, however recommended doses are based on the size of the surfactant pool in healthy term infants, estimated to be 100 mg/kg, even though only 3 mg/kg of surfactant phospholipids are needed to coat the inside airspaces with a monolayer [25]. Additionally, the invasive endotracheal intubation procedure is often unsuccessful, nearly 40%, and typically requires >30 seconds to perform [43]. Dosing concerns include plugging the endotracheal tube and single lung deposition. In addition, liquid bolus delivery results in the increased risk of hypoxemia, bradycardia, hypertension, increased intracranial pressure, and increased pulmonary vascular resistance [44].

1.5 Bronchiolitis

Increased mucus production is observed in bronchiolitis, which results in acute inflammation and obstruction of the bronchioles [45]. Signs and symptoms usually start with rhinitis and cough, possibly progressing to tachypnea, wheezing, rales, use of accessory muscles and/or nasal flaring. It is an infection of small airways in the lungs and one of the most common causes of respiratory failure in infants and children less than two years of age. It is a major cause of hospitalization in infants as moderate and severe infections lead to intensive care and mechanical ventilation. Approximately 2-3% of all children in the United States (57,000-172,000) less than 12 months of age are hospitalized with bronchiolitis annually; approximately 8% of which are admitted into intensive care for severe illness [46].

The most common cause of bronchiolitis is respiratory syncytial virus (RSV), but can also be caused by rhinovirus, or the influenza virus [46]. RSV first infects the epithelial cells in the

upper respiratory tract and are thought to spread to the lower respiratory tract by direct cell-to-cell spreading and by aspiration of nasopharyngeal secretions [47]. The pathogen triggers lymphocyte infiltration to the airway walls and tissues resulting in edema and narrowing of air passages [48]. The bronchioles are further narrowed by accumulated cellular debris and increased mucus production leading to respiratory distress, wheezing and tachypnea [45, 48].

1.5.1 Treatment

A guideline released by the American Academy of Pediatrics provides an evidence-based approach to the diagnosis, management and prevention of bronchiolitis [49]. The guideline states that albuterol, epinephrine, and corticosteroids should not be administered; and nebulized hypertonic saline should not be administered unless the infant is hospitalized. Treatment is focused on supportive care, which involves intravenous hydration – intravenous or nasogastric fluids may be used for children who cannot maintain hydration orally – and discretionary use of supplemental oxygen [49, 50]. Overall, there is no treatment that shortens the course of bronchiolitis or hastens the resolution of symptoms [46]. An antiviral treatment for RSV is currently approved, however, its use is recommended only for patients with severe, potentially life-threatening infections since the antiviral (ribavirin) has shown variable efficacy results in clinical trials and exposes health care workers to potential toxic effects [51].

A method of treatment being explored to support breathing in afflicted infants is the use of blended, heated, humidified air and oxygen, through a high-flow nasal cannula interface. The delivery of heated, humidified gas reduces complications of decreased airway function resulting from increased mucous viscosity and reduced cilia beat frequency; it also has a role in the maintenance of body temperature in infants [52]. A Cochrane review concluded that there is insufficient evidence to determine the effectiveness of high-flow nasal cannula therapy for treating

infants with bronchiolitis, but that there is some indication that HFNC therapy is feasible and well tolerated [53].

1.6 Non-invasive ventilation in infants

Non-invasive ventilation (NIV) refers to respiratory support that delivers a constant or variable pressure without tracheal intubation, used both as a method of weaning following a period of mechanical ventilation and as a primary mode of respiratory support [54]. Forms of NIV that deliver a constant airway pressure include continuous positive airway pressure (CPAP) and high-flow nasal cannula (HFNC) therapy, while variable pressure NIV modes include nasal intermittent positive airway pressure (NIPPV), ventilation bilevel positive airway pressure (BiPAP), and high-frequency ventilation (HFV) [55].

1.6.1 Constant airway pressure ventilation

1.6.1.1 Continuous positive airway pressure (CPAP)

CPAP delivers a continuous distending pressure, greater than atmospheric pressure, to the proximal airway, which splints the upper airway, assists in expansion of the lungs and prevents alveolar collapse [56]. CPAP systems are able to maintain a positive end expiratory pressure (PEEP), usually set between 5 and 10 cm H₂O [57], but tidal ventilation is completely dependent on the respiratory muscles of the infant [58]. CPAP systems include: (i) a gas source to provide continuous delivery of warm humidified air and/or oxygen; (ii) a pressure generator to create a positive pressure in the circuit; and (iii) an interface that connects the system tubing to the patient.

Pressure generator devices for CPAP systems can be constant or variable flow devices. The pressure in constant flow devices are generated by adjusting the exhalation orifice (ventilator PEEP) or by altering the length of the expiratory limb of the respiratory circuit that is submerged

under a known depth of water (bubble CPAP). Variable flow devices have an integrated nasal interface and generate CPAP pressure by varying the flow in response to the infant's respiratory efforts [55, 56]. Common CPAP interfaces include binasal prongs (short, wide tubes that extend ~1 cm into the nostrils, also called nasal cannulas) and nasal masks; less common interfaces include single nasopharyngeal prongs and face masks.

1.6.1.2 High-flow nasal cannula (HFNC) therapy

High-flow nasal cannulas are small, thin, tapered binasal tubes that sit just inside each nostril without occluding them [59]. HFNC therapy delivers heated and humidified air or air/oxygen blends at gas flows typically in the range of 1 to 8 L/min for infants [60]. In contrast to CPAP units, HFNC therapy circuits do not routinely measure the positive distending pressure. Important features of HFNC have been identified, such as (i) washout of nasopharyngeal dead-space [61]; (ii) more comfortable for infants due to the smaller nasal prongs compared to those for CPAP [62] and (iii) a preferred treatment to administer by nurses due to ease of use [60].

1.6.2 Variable airway pressure ventilation

The different types of variable ventilation include nasal intermittent positive airway pressure ventilation (NIPPV), bilevel positive airway pressure (BiPAP), and high-frequency ventilation (HFV). NIPPV provides nasal CPAP with intermittent pressure increases applied at the nose [63]. BiPAP cycles between two levels of CPAP, a higher pressure during inhalation and lower pressure during exhalation, which can be triggered by the infant's breathing efforts in a synchronized mode or preset in a non-synchronized mode [55]. HFV uses pressure oscillations to cause small displacements of ventilation gases, considerably smaller than tidal volumes, which

allows for higher PEEP values with lower inspiratory pressures to minimize barotrauma, in an effort to reduce ventilator-associated morbidity [64].

1.6.3 NIV in infants with respiratory distress

The use of nasal CPAP in preterm infants has been shown as an effective and safe alternative to mechanical ventilation [65], requiring fewer days of ventilation [66, 67] and decreased incidence of air leaks with reduction in the need for subsequent mechanical ventilation [68]. A Cochrane review concluded that HFNC therapy has shown similar rates of efficacy compared to other forms of non-invasive respiratory support (CPAP, NIPPV) in preterm infants for preventing treatment failure, chronic lung disease and death, with its main use as post-extubation support [69]. Although CPAP and HFNC therapy systems offer a non-invasive means of treatment over mechanical ventilation, they are not without adverse effects; the nasal prongs used in CPAP are associated with trauma to the nasal septum and deformity on healing of the nares [70], and concern with the lack of knowledge of the actual level of PEEP with HFNC therapy, which may lead to significant lung overexpansion [71].

1.7 Pulmonary drug delivery

Aerosolized drugs for the treatment of pulmonary diseases, such as RDS and bronchiolitis, is an attractive route of administration since it could provide (i) targeted delivery to the peripheral lungs, resulting in lower dose requirements and consequently lower incidence of systemic side effects, and (ii) flexibility in delivery as administration can utilize non-invasive ventilation techniques [1]. Although attractive, there are challenges with delivering drugs to the lungs, especially if the target site is the alveoli. The complex branching and narrowing diameter of the airways (trachea diameter of 1.8 cm to alveolar ducts of 450 μm [72]) requires inhaled particles to

travel a tortuous path in order to reach the alveoli (Figure 1.1). Consequently, drug delivery by inhalation requires aerosolization of the drug formulation to an appropriate small size for deposition to the targeted peripheral regions of the lungs [73].

Deposition of aerosols in the airways occurs by one of three mechanisms: (i) inertial impaction (larger particles, $>5\ \mu\text{m}$, that cannot follow the change in direction which occurs in the upper respiratory tract), (ii) gravitational sedimentation (intermediate particles, $1\text{-}5\ \mu\text{m}$, which tend to settle in the central and peripheral regions), or (iii) Brownian diffusion (very small particles, $<1\ \mu\text{m}$, that deposit as a result of random collisions that occur primarily in the alveolar region), thus particles too large tend to impact in the mouth-throat region and particles too small tend to be exhaled [74]. The desired size of inhaled particles can be controlled by drug formulation and device design optimization.

1.7.1 Excipient enhanced growth

An approach to deal with the challenges of efficient aerosol generation and delivery to the peripheral regions of the lungs is the dynamic particle size strategy of excipient enhanced growth (EEG) developed by Hindle and Longest [75]. The EEG method is an approach in which the particle or droplet size of an aerosol is increased after inhalation due to the addition of hygroscopic excipients (i.e. mannitol and/or sodium chloride). The combination submicrometer (or sufficiently small sized) particles, containing drug, a hygroscopic excipient, and a dispersion enhancing agent (for powder formulations), are inhaled and aerosol growth occurs due to the inherent humidity of the lungs. Since submicrometer-sized aerosols do not have enough inertia to deposit efficiently in the lungs, the use of a hygroscopic excipient allows the initial small sized aerosols to grow when exposed to the natural relative humidity in the lungs, which results in sufficient size increase to

enable deposition. The EEG method has been shown to demonstrate high dispersion efficiency and low mouth-throat deposition when developed both as a spray-dried powder (with mannitol as the hygroscopic excipient and leucine as a dispersion enhancer) [76] and as a liquid formulation (with mannitol or sodium chloride as the hygroscopic excipient) [77].

1.7.2 Aerosol delivery devices

Aerosol delivery devices are based on one of three main platforms: pressurized metered-dose inhalers (pMDIs), dry powder inhalers (DPIs) and nebulizers. The most common inhalers are the pMDIs, which contain liquid propellant-drug formulations and are designed to deliver a precise amount of aerosol when actuated. The drawback with pMDIs are that they require coordination between device actuation and patient inhalation for maximum delivery. The use of spacers and valved holding chambers have been introduced to mitigate this issue, but lung deposition is still often poor even when technique is good [72].

There are two types of DPIs, passive and active. Passive DPIs rely on the patient inhalation to aerosolize the powder, which eliminates the need for coordination as in the pMDIs, but the force needed to disperse and deliver the powder may not always be achieved. Active or power-assisted DPIs, on the other hand, have an alternative energy source to deaggregate the powders for inhalation. DPIs do not contain propellants and lung deposition is often higher and less variable than pMDIs [72].

The third platform, nebulizers, convert liquid formulations and suspensions into aerosols for inhalation. Nebulizers do not require a precise inhalation technique as normal tidal breathing is often adequate. There are three types of nebulizers: jet, ultrasonic, and vibrating mesh. There are advantages and disadvantages to each type. With jet nebulizers, they are less expensive

compared to the ultrasonic and vibrating mesh nebulizers, but require a compressed gas source and are inefficient with higher residual volumes (0.8-1.2 mL) and result in an increase in solute concentration due to evaporative effects [78]. Ultrasonic nebulizers are capable of nebulizing large volumes of liquid in a shorter delivery time than jet nebulizers, but usually have similar residual volumes to jet nebulizers and generate heat, which possibly cause complex molecules to breakdown. In addition, ultrasonic nebulizers are not suitable for suspensions. The vibrating mesh nebulizers generate aerosol by using electricity to vibrate a mesh plate to produce droplet sizes partially determined by the diameter of the apertures. The mesh nebulizers have lower residual volumes (0.1-0.3 mL) and shorter delivery times than the jet nebulizer and are able to deliver highly uniform and respirable droplets, but are more expensive and cleaning can be difficult [78].

1.7.3 Aerosol therapy in infants

There are additional challenges with delivering aerosolized drugs to infants. The smaller airways in infants result in higher aerosol deposition in the upper and central airways as compared to adults, consequently delivering a lower dose to the peripheral regions of the lungs [28, 78, 79]. Also, the breathing pattern of infants are rapid and shallow (30-60 breaths per minute; tidal volume of 10-60 mL [81]) compared to that of larger children and adults (12-15 breaths per minute; tidal volume of 500 mL), resulting in short residence-time for aerosols to deposit in the airways, which further contributes to the predominantly central rather than peripheral drug deposition in the lungs. Another challenge with delivering aerosols to infants arises from their characteristic nasal breathing [82]. Aerosols delivered through the nasal route must navigate the narrow passages of the nasal cavity, which has high filtration efficiency resulting in reduced drug available for pulmonary deposition [1, 72]. For efficient delivery of inhaled drugs via the nasal route, a particle or droplet size of $< 2 \mu\text{m}$ is desired to efficiently bypass the upper respiratory tract [1, 73].

1.8 Aerosolized surfactants

With increasing emphasis towards non-invasive methods of treatment, the delivery of aerosolized surfactant during NIV has been studied as a promising surfactant therapy method. Studies of dry powder surfactant aerosols with animal models have shown improved outcomes with doses as low as 2-3 mg phospholipids/kg [83] and with more uniform distribution within the lung [84] compared to instilled methods. However, delivery of nebulized liquid surfactant has been met with mixed results in clinical studies [85-87]. Berggren et al. [85] found that delivery of surfactant aerosol generated with a jet nebulizer and delivered during nasal CPAP over 3 hours resulted in no beneficial effects compared to the control group that did not receive surfactant, which, as the authors stated, probably reflects low lung deposition attributed to administration techniques.

1.8.1 Dry powder surfactants

Dry powder aerosols are an attractive means of improving the dose delivery of surfactant to the lungs; with no dilution effects of having to be suspended in liquid, so a high concentration aerosol can be delivered. Dry powder formulations have higher stability and are less susceptible to environmental factors. Studies have explored the delivery of dry powder surfactants prepared by micronization [88], spray drying [89] and drying inline from a nebulizer [90] into animal models using novel delivery devices. The novel devices described in the studies required an external gas line for aerosol delivery [88] or included bulky components [89, 90], which would be difficult to incorporate into a NIV circuit.

1.8.1.1 Dry powder production

For dry powders to be effectively delivered to the lungs, the particles must be in the respirable range, $<5\ \mu\text{m}$ in diameter. Common particle formation techniques include milling, spray drying, spray freeze drying, and supercritical fluid crystallization. Milling, or micronization to produce powders in the respirable range, involves crystallization, which results in polydispersed particles $>10\ \mu\text{m}$ in size [91], followed by one of several milling techniques (fluid-energy mills, such as the jet mill; high-peripheral-speed mills, such as the pin-mill; and the ball mill, [92]). Micronization of crystalline particles results in powders with high surface charge that are more surface-active leading to cohesive powders that are prone to aggregation and therefore have poor dispersibility [93].

Preparation of dry powders using the bottom-up method of spray drying is a popular approach as it is a simple, fast, and scalable method that produces particles of uniform size and shape with diameters in the respirable range [91]. The spray drying process consists of three fundamental steps in which a feed solution or suspension is (i) atomized to produce liquid droplets that are (ii) dried by exposure to heated drying gas resulting in dried particles, which is then (iii) separated from the drying gas and collected [94]. A nozzle atomizes the feed stock into droplets creating particles with increased surface area. In the drying chamber, the solvent (a mixture of water and organic solvents) is evaporated from the droplets by hot drying gas producing particles with low moisture content. Droplet drying can be controlled by the inlet temperature, the drying gas flow rate, the feed stock flow rate, and the solvents used in the feed stock. The dried particles are then separated from the drying gas by either a cyclone and collected in a collection vessel, as in the Büchi Mini Spray Dryer B-290, or using an electrostatic particle collector, as with the Büchi Nano Spray Dryer B-90 and B-90 HP.

The particle size of the powder is largely influenced by the solids concentration of the feed stock and also by the size of the droplets produced from atomization as shown in Equation 1.1 [95]. The geometric diameter of the dry particle is governed by mass balance:

$$d_{particle} = \sqrt[3]{\frac{C}{\rho}} d_{droplet} \quad \text{Equation 1.1}$$

When a total solute concentration in the feedstock of C is atomized into droplets of diameter $d_{droplet}$, the geometric diameter of the spray dried particle $d_{particle}$ is produced with density ρ . Traditional spray dryers employ atomizers with a nozzle tip. The desire to produce smaller particles has led to advancements in spray drying technology in which atomization occurs via a vibrating mesh system (Büchi Nano Spray Dryer B-90 and B-90 HP). A comparison of the spray nozzle/meshes of the traditional Büchi Mini Spray Dryer B-290 with the newer Nano Spray Dryers is shown in Table 1.2.

Table 1.2 Nozzle, droplet and particle size comparison of the traditional Mini Spray Dryer B-290 with the Nano Spray Dryer B-90 and B-90 HP, from [94, 96].

	Mini B-290	Nano B-90	Nano B-90 HP
Atomizer size	0.7, 1.4, 2.0 mm (nozzle diameter)	4.0, 5.5, 7.0 μm (spray mesh hole size)	small, medium, large
Water droplet size range	5-30 μm (0.7 mm tip)	3-8 μm (4.0 μm spray mesh), 4-12 μm (5.5 μm spray mesh), 5-15 μm (7.0 μm spray mesh)	3-15 μm
Dried particle size range	2-25 μm	0.3-5 μm	0.2-5 μm

With the traditional spray dryer, the larger mean droplet size range was due to the larger spray nozzle diameters, resulting in spray dried particles of a broader size range. The newer vibrating mesh spray dryers make it possible to produce particles in the submicrometer range with a narrower size distribution compared to that of the traditional spray dryer, which has been shown to have low collection efficiency for fine particles less than 2 μm [97].

Spray freeze drying is a two-step process: (i) atomization of the feedstock into a freezing medium, commonly liquid nitrogen, that produces frozen droplets of the sprayed feedstock, then (ii) lyophilization to remove the ice via sublimation, leaving behind a powder [91]. Spray freeze drying is performed at sub-ambient temperatures, therefore has the advantage of preserving the integrity of thermolabile therapeutics but is less utilized compared to spray drying due to its higher complexity and more tedious scale-up and higher costs [93].

A supercritical fluid (SCF) is a compressed gas or liquid above its critical pressure and temperature that exists as a single phase with liquid-like density and gas-like transport properties. SCFs exhibit pressure-tunable solubility enabling them to be used for recrystallization processes [92]. The most common SCF used is supercritical CO_2 due to its low critical temperature (31.1 $^\circ\text{C}$) and pressure (73.9 bar). Supercritical CO_2 is used as a solvent in rapid expansion of supercritical solutions (RESS) in which drug containing SCF is passed through a nozzle allowing for precipitation of the drug through rapid expansion of CO_2 in the vessel [91]. This method is limited by the poor solubility of most active pharmaceutical ingredients (APIs) in supercritical CO_2 . The use of supercritical CO_2 as an anti-solvent has been developed to overcome this limitation by dissolving drug in a solvent miscible with CO_2 , but the use of SCFs in particle manufacturing still has the challenge of predictive control of particle size [91, 93].

1.8.1.2 Spray drying of surfactants

The relatively high phospholipid T_g of DPPC is regarded as being at a low temperature in terms of dry powder formulation via spray drying. Therefore, phospholipids are difficult to formulate as dry powders due to their T_g values and amorphous nature, which lead to powders that are cohesive and difficult to deaggregate and aerosolize [98]. The transition temperature determines the chemical and physical stability of the amorphous solid and becomes a critical factor when it is approached or exceeded by the product during processing (e.g. drying temperature for spray drying and storage temperature) [99]. For spray drying, a T_g value lower than the outlet air temperature of the dryer causes the components to remain in a more cohesive form, even though they are dried to a low moisture content; while a storage temperature close to the T_g of the formulation increases the possibility of the amorphous powder to transition to the more stable crystalline state. The addition of materials with higher transition temperatures would raise the T_g of the system and allow for more flexibility during processing and storage [99].

The inclusion of sodium chloride in the formulation of a spray dried surfactant-EEG powder would serve two functions: (i) to act as a hygroscopic excipient, and (ii) to raise the T_g of the formulation allowing for particle formation. Sodium chloride exists as a crystalline solid, so its presence in the feed dispersion for spray drying would raise the T_g of the system. The other component materials need to be accounted for to determine the T_g of the system, which would include mannitol (T_g of 6 °C), leucine (dispersion enhancer with T_g of 122 °C) or trileucine (alternative dispersion enhancer with T_g of 110 °C) plus the other components of the commercial formulation (the other major lipid component in Survanta[®] aside from DPPC is POPG, with a transition temperature of -2 °C [100]).

The low aqueous solubility of components in the commercial surfactant formulation results in the production of a dispersion for spray drying in an aqueous media. The homogeneity of the feed dispersion is important to ensure uniformly sprayed particles. A method to prepare homogenous dispersions involves the use of sonication. Sonication can be introduced to the liquid suspension either by immersing an ultrasonic probe in the suspension (direct sonication) or by introducing a vessel with the suspension into a bath sonicator (indirect sonication). Direct sonication yields higher energy output into the suspension requiring less sonication time, but has the side effect of introducing impurities into the suspension as titanium metal erodes from the probe tip [101].

1.8.2 Nebulized surfactants

With nebulized surfactant, studies in animal models have shown that approximately 4 to 11% of the administered dose was recovered from the lungs [84, 102]. In infants, deposition of <1% of nominal dose [103, 104] has been observed. The main challenge with nebulized surfactants is efficient delivery to the targeted regions of the lungs, which suggests the need for development of improved drug formulations and delivery techniques for more effective treatment.

For bronchiolitis, where surfactant therapy does not need to be administered in the quick manner that RDS necessitates, the use of nebulizers to deliver surfactant aerosols containing mannitol would provide supplemental treatment. Mannitol has been shown to have little effect on the surface activity of a dilute Survanta suspension (0.75 mg/mL phospholipids) at different concentrations of mannitol (0.1, 0.5 and 1.0 mg/mL) when measured at 37 °C [105]. The combination of surfactant and mannitol would help facilitate mucociliary clearance since surfactant decreases the adhesion of mucus to the airway epithelium [7], and mannitol, with

hygroscopic properties at > 75% relative humidity [106], has been shown to increase mucociliary clearance [107].

1.9 Surfactant-EEG formulation characterization

Preparation of surfactant-EEG formulations for aerosolization utilizes methods of sonication and nebulization, which may raise concerns of possible adverse effects on the components and surfactant function of the commercial suspensions; specifically, the role of surfactant in reducing the surface tension at the air-liquid interface.

1.9.1 Phospholipid detection

DPPC has two 16-carbon chains with a phosphate group and a quaternary amine (Figure 1.3). The nitrogen is positively charged and the oxygen of the phosphate is negatively charged resulting in a zwitterionic headgroup with a molecular weight of 734.04 Da (exact mass of DPPC is 733.56 Da) when the oxygen of the phosphate group is not protonated. A challenge with DPPC analysis arises when performing quantitative detection of the phospholipid following separation by high performance liquid chromatography (HPLC). DPPC lacks UV chromophores and fluorophores, which eliminates the option of employing commonly utilized UV absorption- and fluorescence-based detectors without first performing derivatization reactions. A common method of detection employed is the use of mass spectrometry.

Mass spectrometry (MS) is a method that separates ions based on their mass-to-charge ratios (m/z). Typical instruments include an ion source, a mass analyzer, and a detector. The ion source induces either a loss or gain of a charge from a neutral species, which are then electrostatically directed into a mass analyzer where they are separated by their m/z and then measured and detected. The result is a mass spectrum.

Common ion source methods include electron ionization (EI), chemical ionization (CI), matrix-assisted laser desorption ionization (MALDI) and electrospray ionization (ESI). Of all the source types, EI results in the highest fragmentation (hardest ionization) and is most widely used with gas chromatography (GC) MS. CI is a softer ionization technique that uses a reagent gas (such as methane or ammonia) for ionization. CI is performed in both closed sources (under vacuum) and in atmospheric pressure (APCI). APCI is typically coupled to HPLC systems and does not generate multiply charged ions. It is commonly used to analyze smaller, thermally stable compounds as it operates at higher temperatures.

The most common ionization methods used for biochemical analyses are MALDI and ESI. Both techniques can operate in positive and negative modes. MALDI results in higher analyte fragmentation when compared to ESI and is not attached to a separation instrument as described with the previous methods. MALDI samples are first dissolved in a volatile solvent and mixed with a matrix prior to application onto a sample plate, which is then inserted into the MS under high vacuum. MALDI primarily produces singly charged species. ESI is the softest of the ionization methods. It can be coupled to a separation instrument, but direct infusion with a syringe pump is possible for simple matrix samples. The analyte containing eluent is introduced into the source via a capillary, at low flow rates (1 $\mu\text{L}/\text{min}$ to 1 mL/min), that is surrounded by drying gas (usually nitrogen), which helps to aerosolize the solvent. A high voltage is applied to the tip of the capillary, producing an aerosol of highly charged droplets. Sample ionization occurs at atmospheric pressure.

There are two types of mass analyzers: scanning and pulsed. Scanning mass analyzers, such as the single and triple quadrupoles, detect ions successively along a time scale, while pulsed mass analyzers (e.g. time-of-flight, orbitrap) detect ions simultaneously. For triple quadrupole MS,

ions are sampled through a series of orifices into the first quadrupole where filtering occurs based on the m/z . Mass separated by ions pass into the hexapole collision cell that either undergo collision induced decomposition (CID) or pass unhindered to the second quadrupole. The fragmented ions are mass analyzed by the second quadrupole and the transmitted ions detected by a conversion dynode, phosphor and photomultiplier detector system. Triple quadrupole is low resolution given that they cannot fully distinguish a change in the m/z of less than 0.5 in a mass spectrum. Time-of-flight (TOF) analyzers, used to detect ionization from MALDI sources, measure arrival times of ions to the detector assuming that the same kinetic energy is applied to all the ions which are allowed to travel the same fixed distance.

1.9.2 Surface activity

Static surface tension is the surface tension value in thermodynamic equilibrium independent of time, whereas the dynamic surface tension (or interfacial tension) is the surface tension at a particular surface (or interface) age. For fluids containing surface-active materials, this value can differ from the equilibrium surface tension value. A newly formed interface of a surfactant solution has a surface tension close to that of the solvent, however, over time, the surface tension will decay to the equilibrium value and this period of time ranges from milliseconds to days depending on the surfactant type and concentration [108].

Methods commonly used to determine surface activity include the Langmuir-Wilhelmy balance, the pulsating bubble surfactometer, captive bubble surfactometer and constrained sessile drop. There are advantages and disadvantages to each method. The Langmuir-Wilhelmy balance is used to study surface rheology properties of surfactant monolayers and phospholipid phase behaviors. The method can be combined with microscopic and spectroscopic techniques [109], but its environment is difficult to control and is not capable of studying adsorbed films. The pulsating

bubble surfactometer provides a quick comparison of surface activity and is able to simulate breathing, but the surface tension at low values tend to be inaccurate. The method of the captive bubble surfactometer allows for simulation of the alveolar environment and is capable of studying both adsorbed and spread films, although it has a limitation on the maximum surfactant concentration used when studying adsorption. The instruments used in captive bubble measurements are often difficult to operate and clean. The constrained sessile drop method uses a precisely-controlled environment and requires low sample volumes (in μL range). The method is also capable of studying both adsorbed and spread films and does not have a limitation on the surfactant concentration.

1.9.3 Surfactant protein analysis

Of the four surfactant proteins known to be present in endogenous surfactant (SP-A, SP-B, SP-C, SP-D), only the hydrophobic proteins, SP-B and SP-C, are present in the commercial formulations processed for human use. The vital role that proteins play in the proper function of pulmonary surfactant deems it necessary to determine that their presence and activity following the processes endured during formulation preparation (i.e. sonication, spray drying) are maintained. During processing, the proteins are subject to various stresses (e.g. sheer, thermal, dehydration) that can lead to high inter-particle interactions and physicochemical degradation that can affect the primary, secondary and tertiary structures of the proteins, possibly resulting in partial or complete loss of biological activity. Physical degradation results from denaturation and non-covalent aggregation, while chemical degradation results from covalent aggregation, oxidation, deamidation, and/or glycation [110].

The challenge with analysis of surfactant proteins is the difficulty in separation of its low content from the other components in the formulation, especially due to the hydrophobic nature of both the proteins and lipids. Protein separation and purification can be performed by exploiting differences in solubility, size, charge, and binding affinity; the most common methods of which are precipitation and analytical separation.

1.9.3.1 Protein purification by precipitation

Protein precipitation can be induced by causing changes in the solvent properties to manipulate the electrostatic forces between proteins. Some common reagents used for precipitation of proteins are ammonium sulfate, hexane/isopropanol, methanol/chloroform, acetone, and trichloroacetic acid.

Ammonium sulfate uses the mechanism of salting-out based on preferential solvation; water molecules are titrated away from hydration layer around the protein to the hydration layer around the ions that make up the salt. This causes increased hydrophobic interaction between protein and water due to increased surface tension, and in response, the protein decreases its surface area to minimize contact with the solvent [111]. Salts high in the Hofmeister series are most efficient at protein precipitation since they form large, stable hydration layers. The use of ammonium sulfate is preferred for salting-out due to its high solubility and that both NH_4^+ and SO_4^{2-} are at the high ends of their respective Hofmeister series [112]. Disadvantages with salting-out are that contaminants often precipitate with the protein, requiring further purification steps and there exists a high concentration of salt at the end of precipitation, which may lead to analytical issues if the salt is not removed [112].

Hexane is nonpolar, and when combined with a polar solvent such as isopropanol, the mixture is able to interact with and extract phospholipids and triglycerides that have both nonpolar and polar regions. The use of a hexane/isopropanol mixture has been shown successful in the determination of hydrophobic proteins and allowed for simultaneous extraction and determination of lipids using very small volumes of samples (5-50 μL) [113]. However, use of hexane/isopropanol to extract lipids is not selective as the method was shown to have < 80% protein recoveries [113] and has been shown to also extract a high proportion of proteins when the hexane-to-isopropanol ratio was increased [114].

Methanol/chloroform extraction involves partitioning of components into the binary mixture. Methanol disrupts the hydrogen bonding or electrostatic forces between cell-membrane lipids (i.e. phospholipids, glycoproteins and cholesterol) and proteins. When chloroform is added (nonpolar), the two-phase system forms and enables extraction of neutral lipids (i.e. triglycerides) [115].

Acetone causes precipitation of proteins by lowering the dielectric constant of the aqueous solution containing protein (dielectric constant of acetone at 20 °C is 21.3, while that of water is 80.0 [116]). Organic solvents with small dielectric constants discourage the dispersion of protein molecules in the media, reducing their solubility. Therefore, adding a water-soluble solvent such as acetone to an aqueous solution of protein induces precipitation by lowering the effective dielectric constant of the media.

Trichloroacetic acid (TCA) induces protein precipitation by disrupting hydration layers and decreasing the pH, partially denaturing proteins, exposing more of the hydrophobic surface to the solvent [117, 118]. TCA is a relatively weak acid and therefore does not hydrolyze the peptide

bonds of proteins. Drawbacks of TCA precipitation include protein denaturing, which limits the use of this method if protein activity is to be retained.

1.9.3.2 Protein purification by analytical separation

Analytical purification methods can utilize protein properties for separation: (i) ion-exchange chromatography by isoelectric point, (ii) reverse-phase chromatography by polarity/hydrophobicity, and (iii) size-exclusion chromatography by size or molecular weight.

Successful protein separation from a majority of the phospholipids (> 96%) has been reported [119]. The method separates proteins by gel-exclusion with a Sephadex LH-60 column using chloroform/methanol and requires a large amount of starting material (which is identical to the commercial Curosurf formulation), 300-500 mg, in which pooled fractions from several preparations are needed for a second separation on a longer Sephadex LH-60 column to obtain the separated proteins.

1.9.3.3 Protein detection

Pellets collected from protein precipitation must be solubilized in appropriate buffers before they can be analyzed further. Detergents (surfactants or a mixture of surfactants) are frequently used to enhance solubilization and stabilize proteins as well as deaggregate membrane-bound protein complexes [120, 121]. However, detergents interfere with mass spectrometry as they are preferentially ionized and are typically present in high concentrations, which can obscure the detection or suppress ionization of the protein. Loo et al. [121] observed poor-to-no protein signal at 1.0% surfactant concentration with better results obtained at lower surfactant concentrations in ESI-MS.

The detection and quantitation of the hydrophobic surfactant proteins in bronchoalveolar lavage fluid (without preprocessing of samples) has been performed using enzyme-linked immunosorbent assay (ELISA) [122]. The assay uses a sandwich enzyme technique in which an antibody specific for the individual proteins was precoated onto a microplate. Protein in the standards and samples are bound by the antibody and any unbound substances are removed. A biotin-conjugated antibody specific for the protein was added, then washed and followed by addition of an avidin conjugated Horseradish Peroxidase (HRP). Once this was washed, a substrate was added and color developed in proportion to the amount of the protein bound in the initial step. Color development was stopped after and the intensities were measured. Disadvantages with ELISA include: (i) the cumbersome washing procedures, (ii) the lengthy incubation times and (iii) the high cost of each kit.

1.9.4 Dispersion stability

Spray drying of large batches of dispersion vehicle can be a long process performed over a number of hours. The zeta potential can be used as an indication of dispersion stability. Particles in suspension can form aggregates, which may settle out due to gravity (flocculate). According to DVLO theory, the stability of particles in a suspension is dependent on its total potential energy function, which is a balance of three factors: (i) the potential energy due to the solvent (minor contribution), (ii) the attractive (van der Waals) forces, and (iii) repulsive (electrical double layer) forces. The attractive and repulsive forces (dotted lines in Figure 1.5) are summed to obtain the net energy (solid line).

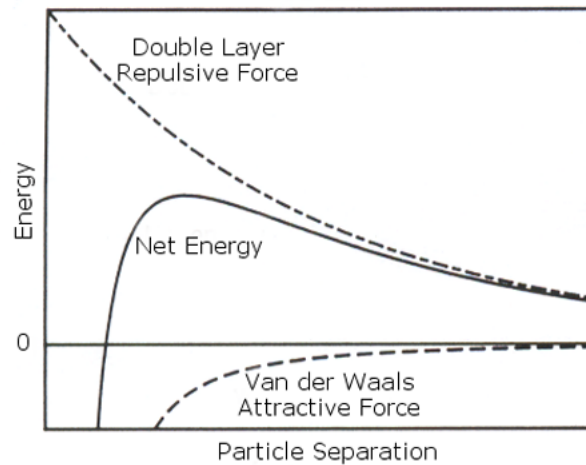


Figure 1.5 Schematic of free energy with particle separation according to DVLO theory [123].

The theory proposes that particles initially separated cannot approach each other due to the repulsive force, but if particles are forced with sufficient energy to overcome the repulsion (net energy peak), then the attractive force will pull them together. Particles with sufficiently high repulsion, high zeta potential values (further from zero, positive or negative) will resist flocculation resulting in a stable system. The zeta potential provides a good index of the magnitude of interaction between particles and can be used as a measure of dispersion stability.

The generally accepted dividing line between stable and unstable suspensions is ± 30 mV, so particles with zeta potential values more positive than +30 mV or more negative than -30 mV are considered stable [123]. The surface charge is dependent on the nature of the particle and its surrounding medium, on the acidic or basic strengths of the surface groups (resulting in negatively or positively charged surfaces, respectively), and on the pH of the solution.

Sirsi et al. [124] determined the zeta potential (ζ) of Survanta[®] at different pH values (Figure 1.6), which revealed that the commercial suspension is highly negatively charged over the pH range of 4 to 12, with an isoelectric point at approximately pH 3.

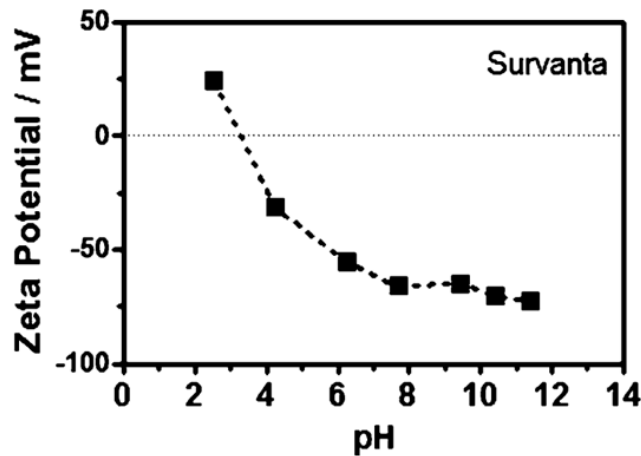


Figure 1.6 Zeta potential of Survanta (1 mg/mL phospholipids) as a function of pH [124].

1.10 Objectives

This research focuses on the reformulation of commercial surfactants using the EEG approach for aerosolized delivery coupled to administration with novel devices to achieve improved delivery to the infant lungs. The delivery of a dry powder surfactant during nasal CPAP will allow for rapid surfactant delivery to the lungs of infants at risk or suffering from RDS. In addition, the use of a nebulized surfactant-EEG formulation to be delivered as supplemental treatment during HFNC therapy for bronchiolitis would help to facilitate mucociliary clearance.

CHAPTER 2 HYPOTHESIS AND SPECIFIC AIMS

The overall aim of this research project was to develop surfactant dry powder formulations and devices for efficient delivery of aerosol formulations to infants using the excipient enhanced growth (EEG) approach. The development of novel formulations used in combination with novel inline delivery devices would allow for more efficient treatment of infants suffering from neonatal respiratory distress syndrome (RDS) and viral bronchiolitis. The research goals were achieved by addressing the following hypotheses and specific aims:

Hypothesis 1: The excipient enhanced growth (EEG) approach can be applied to dipalmitoylphosphatidylcholine (DPPC) to produce spray dried powders.

Specific aim 1-1: Develop methods to reproducibly produce micrometer sized spray dried DPPC-EEG powders suitable for inhalation.

Specific aim 1-2: Investigate the influence of spray drying and formulation variables on the primary particle size, aerosol performance, and surface tension activity of a range of spray dried DPPC-EEG powders.

Hypothesis 2: Optimization of the spray drying and formulation variables will improve dispersibility of EEG powders prepared with commercial replacement surfactants.

Specific aim 2-1: Produce EEG formulations with a commercially available exogenous surfactant using dry powder dispersion enhancers of different aqueous solubility in spray vehicles with different ethanol concentrations.

Specific aim 2-2: Investigate the influence of the dispersion enhancer on the feed dispersions, powder characteristics, and particle size distributions at different dispersion pressures.

Specific aim 2-3: Determine the influence of dispersion feed composition on the aerosol performance of spray dried powders using a novel dry powder inhaler.

Specific aim 2-4: Evaluate the presence of the surfactant proteins (SP-B and SP-C) following formulation processing and spray drying.

Hypothesis 3: Optimization of the design of a novel low dispersion air volume dose-containment unit dry powder inhaler will improve the delivery and dispersion of spray dried surfactant-EEG powders.

Specific aim 3-1: Investigate the influence of a series of design modifications to the low dispersion air volume dose-containment unit dry powder inhaler on the emitted mass and particle size of EEG-surfactant powders.

Specific aim 3-2: Determine the influence of fill mass on the emitted mass and particle size of surfactant-EEG powders with the dose-containment unit dry powder inhaler.

Hypothesis 4: Methods to reduce nebulized droplet size and synchronized aerosol delivery can be employed to improve the delivery of aerosols to a realistic infant model during *in vitro* testing of surfactant excipient enhanced growth formulations.

Specific aim 4-1: Perform experiments under steady state inhalation conditions with a novel low-volume mixer-heater device designed to deliver a micrometer sized aerosol and compare aerosol deposition and delivery efficiency with the standard of care methods using a nebulized albuterol sulfate formulation.

Specific aim 4-2: Using realistic *in vitro* test methods, determine the optimal breath synchronization and nebulization duration settings to achieve the maximum estimated lung dose using a novel low-volume mixer-heater device.

Specific aim 4-3: Determine the aerosol performance of surfactant-EEG formulations with the modified very low-volume mixer-heater device with the optimized breath synchronization conditions.

CHAPTER 3
ASSESSMENT OF THE EFFECT OF SPRAY DRYING PROCESS PARAMETERS
AND FORMULATION FACTORS ON POWDER CHARACTERISTICS AND
AEROSOL PERFORMANCE OF DPPC-EEG POWDERS

3.1 Introduction

The use of aerosolized surfactant has been explored as a potential delivery method to treat respiratory distress syndrome (RDS) as it can be administered by non-invasive means and has possible superiority over liquid instillation [10, 85-87]. Nebulization to generate surfactant aerosols for non-invasive administration has been studied extensively; however, administration challenges such as poor delivery efficiency to the alveolar region of the lungs, long delivery times, and insufficient evidence of efficacy have limited the use of surfactant as an aerosol therapy [10, 89]. The development of a dry powder surfactant formulation, using the excipient enhanced growth (EEG) application, administered via novel delivery devices and ventilation components, designed for minimal depositional losses, is hypothesized to provide a high lung delivery combination that will overcome the challenges of aerosolized surfactant therapy.

The delivery of dry powder surfactants has advantages over liquid formulations, such as the ability to deliver larger doses since there is no need for dilution of the surfactant suspension to enable nebulization, and delivery can be performed over a much shorter time frame. Dry powder surfactant preparations that have been investigated for the treatment of RDS include synthetic mixtures of DPPC with phosphatidylglycerol [125, 126], micronized powder formulations consisting of recombinant SP-C-based surfactant protein [88], and spray dried recombinant SP-C

surfactant protein [89]. Preparations of dry powder surfactants that utilize its low surface tension characteristics for applications as a drug delivery-carrier have also been attempted [127]. These formulations have all been synthetic in nature and a dry powder formulation prepared from naturally derived surfactant has yet to be studied.

Commercially available naturally derived replacement surfactant formulations in the United States include Curosurf[®] (poractant), Infasurf[®] (calfactant), and Survanta[®] (beractant). The formulations differ in the composition of proteins and lipids, but are similar in that dipalmitoylphosphatidylcholine (DPPC) is present as the dominant lipid component [30-32]. Given the high cost of each single-use vial of drug, which ranges from \$400-800 per vial, development studies to reliably produce a dry powder surfactant formulation were carried out with the main lipid component, DPPC.

Spray drying of DPPC has been explored for a number of applications including drug encapsulation [128] for protein stabilization [129], as a permeation enhancer to increase protein bioavailability [130], and as an excipient to produce low density powders [131]. In this study, DPPC was used as a model drug in spray drying experiments to minimize development costs with the intention of applying the developed methods to commercial surfactant formulations.

The aim of this study was to develop methods to reliably produce DPPC-EEG powders and use the developed methods to investigate the influence of spray drying process parameters and formulation factors on the mass median aerodynamic diameter (MMAD), fine particle fraction less than 1 μm and less than 5 μm of DPPC-EEG dry powder aerosol formulations using a full factorial design of experiments. The formulation factors included the percent solids concentration, the percentage of hygroscopic excipients, and the percent ethanol concentration in the feed dispersion. The process parameters studied were spray mesh size and inlet drying temperature. The levels

selected for the factors studied were based on the limits of the operating parameters as determined in preliminary studies. The developed methods were then applied to commercial surfactant formulations to produce dry powder formulations for the treatment of neonatal RDS.

3.2 Materials and methods

3.2.1 Materials

DPPC was purchased from Avanti Polar Lipids, Inc. (Alabaster, AL). L-leucine was purchased from Sigma-Aldrich Chemical Co. (St. Louis, MO). Pearlitol[®] PF-mannitol was donated from Roquette Pharma (Lestrem, France). Sodium chloride and all other reagents were purchased from Fisher Scientific Co. (Hanover Park, IL). Size 3 hydroxypropyl methylcellulose (HPMC) capsules were donated from Capsugel (Morristown, NJ) and Qualicaps, Inc. (Whitsett, NC). Molycote[®] 316 silicone spray was purchased from Dow Corning Corporation (Midland, MI). Curosurf[®] (poractant), Infasurf[®] (calfactant), and Survanta[®] (beractant) intratracheal suspensions was purchased from Cardinal Health, Inc. (Greensboro, NC) and stored at 2-8 °C.

3.2.2 Development of methods to produce DPPC-EEG feed dispersions for spray drying

Preliminary experiments were performed to assess the feasibility of adapting methods developed using water soluble albuterol sulfate as the active ingredient in EEG powders [76] to produce EEG spray dried formulations with DPPC which has a low water solubility (< 5 µg/mL). Experiments explored formulation combinations of varying concentrations of DPPC, mannitol, sodium chloride and trehalose; leucine was included in all formulations at a concentration of 20% w/w. Feed dispersions for spray drying were prepared in 20% v/v ethanol in water, in which DPPC was dissolved in ethanol and the excipients in water, then combined. The nominal composition of

the initial eleven feed dispersions and spray dried powders are listed as Formulations P1-P11 in Table 3.3. The percentage of solids concentration for these studies was 0.125% w/v.

3.2.2.1 Spray dried powder formation

Feed dispersions were spray dried using the Büchi Nano Spray Dryer B-90 (Büchi Labortechnik AG, Flawil, Switzerland) in the open-loop configuration. Parameters used for spray drying were based on methods for albuterol sulfate EEG preparation: size 4 µm spray mesh, inlet drying temperature of 70 °C (outlet temperature ranged from 38 to 41 °C), drying airflow of 120 L/min, and liquid feed rate of 100%. Powders were collected from the electrostatic particle collector into a tared vial. Powders were stored in a desiccator in a refrigerator (2-8 °C) when not in use. The percent powder yield was calculated from the mass of powder collected as a percentage of the mass of solids weighed in the feed dispersion using Equation 3.1.

$$\text{Powder yield, \%} = \frac{\text{powder mass collected, mg}}{\text{conc solids in dispersion, } \frac{\text{mg}}{\text{mL}} * \text{volume of dispersion spray dried, mL}} \times 100$$

Equation 3.1

3.2.2.2 Aerodynamic particle size characterization in ambient conditions

The aerosolization properties of the spray dried powders were determined following conventional cascade impaction methods using the Next Generation Impactor (NGI, MSP Co., Shoreline, MN) and an Aerolizer[®] dry powder inhaler (Novartis Pharmaceuticals, Basel, Switzerland). Approximately 1 to 2 mg of powder was filled into size 3 HPMC capsules and placed into the dry powder inhaler. The NGI collection cups and pre-separator were coated with Molycote[®] 316 silicone release spray (Dow Corning, Midland, MI) to minimize particle bounce.

The NGI was fitted with the pre-separator and positioned in an upright position to permit the use of the Aerolizer[®] in its horizontal orientation held in place with a mouthpiece adapter made from RTV (room temperature vulcanizing) silicone mold rubber (Micro-mark Ten-to-One, Berkeley Heights, NJ). Powder was released into the NGI at 80 L/min for 3 s. The flow rate was selected based on previous studies performed with albuterol sulfate EEG powder and the Aerolizer[®] [76].

Powder was extracted from the pre-separator, collection cups and filter using 100% methanol. DPPC was quantitatively analyzed using an LC-MS method to determine the emitted dose, the MMAD and particle fraction less than 1 μm and less than 5 μm at ambient temperature.

$$\text{Emitted dose, \%} = \frac{\text{mass of drug emitted from inhaler, mg}}{\text{nominal drug dose, mg}} \times 100 \quad \text{Equation 3.2}$$

$$\text{Particle fraction, \%} = \frac{\text{mass of drug < stated size, mg}}{\text{emitted drug mass, mg}} \times 100 \quad \text{Equation 3.3}$$

$$GSD = \sqrt{\frac{\text{size at cumulative count of 84.13\%}}{\text{size at cumulative count of 15.87\%}}} \quad \text{Equation 3.4}$$

MMAD values were directly calculated as the size associated with a cumulative count of 50% based on mass percentages calculated relative to the impactor dose.

3.2.2.3 Liquid chromatography-mass spectrometry for DPPC

DPPC detection was performed with positive electrospray ionization mass spectrometry. Quantification was performed following a liquid chromatography-mass spectrometry (LC-MS)

method adapted from Li et al. [132]. The system consisted of a tandem quadrupole mass spectrometer, Waters Micromass Quattro *micro*[™], linked to an Alliance 2695 Separations Module with MassLynx software v4.1 (Waters Corporation, Milford, MA). A Waters Atlantis hydrophilic interaction liquid chromatography (HILIC) silica column (1.0 mm x 50 mm, 5 μm) was used for the separation. The isocratic mobile phase, which consisted of 85% acetonitrile and 15% 5 mM ammonium formate in water with 0.1% formic acid, was eluted at a flow rate of 0.5 mL/min. A volume of 2 μL was injected for each sample. The mass spectrometer was used in positive electrospray ionization mode with the following settings: capillary, 4 kV; cone, 35 V; source temperature, 120 °C; desolvation temperature, 300 °C; desolvation gas flow, 420 L/h; cone gas flow, 35 L/h. The mass spectrometer was operated in selected ion monitoring (SIM) mode for *m/z* 734.6 (exact mass of DPPC is 733.56 Da).

For powder content analysis, approximately 1.3 mg of spray dried powder were dissolved in 100 mL of methanol by sonication for 30 s. Percent DPPC content was calculated by measuring the amount of drug in the spray dried powder by LC-MS and using Equation 3.5.

$$DPPC \text{ content, \%} = \frac{\text{assayed amount of DPPC in spray dried powder, mg}}{\text{mass of spray dried powder in sample, mg}} \times 100 \quad \text{Equation 3.5}$$

3.2.2.4 Thermogravimetric analysis

Thermogravimetric analysis (TGA) was performed on samples using the Pyris 1 TGA (PerkinElmer, Covina, CA) with TAC 7/DX Thermal Analysis Controller. Weight loss was determined from 1 to 2 mg samples of powder that were heated from 25 °C to 100 °C at a rate of

10 °C/min and then held at 100 °C for 45 minutes while under a nitrogen purge at 40 mL/min. The percent weight loss % following the isothermal hold corresponds to loss of water of hydration.

3.2.3 Development of methods for surface tension sample preparation and measurement

The aim of this task was to develop a sample preparation method for surface tension measurements to study the dynamic adsorption behavior of DPPC following spray drying. Surface tension measurements were necessary to ensure that the spray dried powders maintained their surface tension reduction properties with the understanding that DPPC would be chemically stable following processing, but possible conformational changes due to interactions with excipients in the formulation may affect its surface activity. A bubble pressure tensiometer (BP2, Krüss, Hamburg, Germany) was used to determine the dynamic surface tension of a liquid by measuring the maximum internal pressure of a gas bubble formed in a liquid from a capillary of known diameter. Using the Young-Laplace equation (Equation 3.6), the dynamic surface tension, γ , can be determined from the maximum pressure.

$$\gamma = \frac{1}{2}(P_{max} - P_0)r_c \quad \text{Equation 3.6}$$

Where P_{max} is the maximum bubble pressure, P_0 is the hydrostatic pressure in the capillary of known inner radius, r_c . Surface tension measurements of the DPPC dispersions were performed with the tensiometer connected to a recirculating water bath (Lauda-Brinkmann M3, Delran, NJ) that allowed for temperature-controlled measurements. Measurement settings were as follows: start at surface age of 0.5 to 10 s, stop at surface age of 50 s, stop quickscan at 5 s, linear acquisition, and 30 values were collected for each measurement.

A reference tensiogram for the surface activity of the commercial Survanta[®] formulation at 37 °C with a phospholipid concentration of 0.75 mg/mL is shown in Figure 3.1 [133]. At the young surface age of 0.01 s, the surface tension was approximately 70 mN/m, similar to that of saline [105], the solvent for the commercial surfactant formulation. At a surface age of 30 s, the dynamic surface tension was determined to be 45 mN/m; the extrapolated equilibrium surface tension was determined to be 37 mN/m [133].

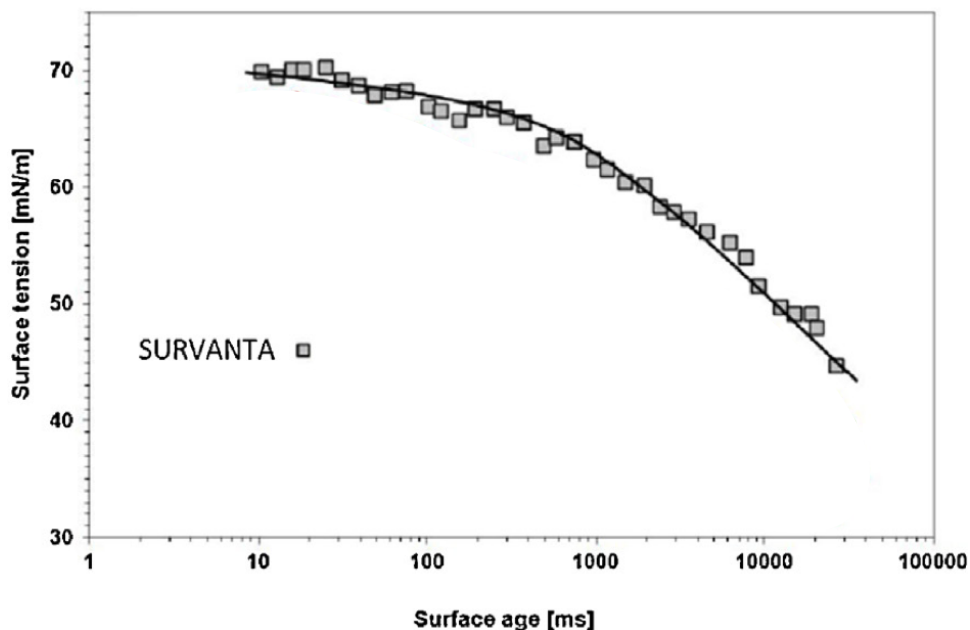


Figure 3.1 Dynamic tensiogram for the commercial Survanta formulation (0.75 mg/mL phospholipids) at 37 °C [133].

Dispersion preparation methods were explored using heat and sonication. Indirect sonication was performed with a bath sonicator (Bransonic[®] 5510R-MT, Branson Ultrasonics, Danbury, CT) and direct sonication was employed with a probe sonicator (Q700 with 1/8” microtip probe part no. 4418, Qsonica; Newtown, CT). The effect of sample preparation method,

measurement temperature and DPPC concentration on the dynamic surface tension of DPPC spray dried powders were studied.

3.2.4 Full factorial design of experiment (DOE) to assess selected formulation factors and spray drying parameters

The preliminary experiments described above were performed to develop processing and analytical methods and to identify the main factors that influence DPPC-EEG feed dispersions and spray dried powder performance. Factors and levels that were studied are shown in Table 3.1. Weight of solids and solvent volumes were dependent on the solids concentration, the ratio of the hygroscopic excipients and the ethanol concentration in the spray vehicle (Table 3.2). The nominal composition of sixteen feed dispersions and spray dried powders are listed as Formulations 1-16 in Table 3.9.

Table 3.1 Factors and levels for full factorial DOE assessment of DPPC-EEG formulation optimization.

Factors	Levels	
Solids in feed dispersion, % w/v	0.125	0.250
Ratio of mannitol-to-sodium chloride	3:1	15:1
Ethanol in feed dispersion, % v/v	0	5
Spray mesh size, μm	4	7
Inlet drying temperature, $^{\circ}\text{C}$	70	80

Table 3.2 Weight and volume amounts used for the formulation factors studied.

Weights	Mannitol-to-sodium chloride	3:1		15:1	
	Mannitol, mg	60		75	
	Sodium chloride, mg	20		5	
	solids, % w/v	0.125		0.250	
Volumes	ethanol, % v/v	0	5	0	5
	Water, mL	160	152	80	76
	Ethanol, mL	0	8	0	4

*Total solids weight of 200 mg; DPPC and leucine kept constant at 80 and 40 mg, respectively

Initial experiments with the spray mesh size of 7 μm resulted in consistently low yields (mean \pm standard deviation yields of $1.33 \pm 1.37\%$) and therefore removed as a study factor. A full factorial DOE approach was used to test the remaining four factors. Sixteen spray dried powders were studied with the aim of studying the effects of the different parameters on emitted dose, MMAD and particle fraction less than 1 μm and less than 5 μm .

3.2.4.1 Particle size determination

The primary particle size of each formulation was determined by laser diffraction using the Sympatec HELOS (submicron R1 lens with 20 mm focal length) with RODOS/M disperser and ASPIROS sample feeder (Sympatec GmbH, Clausthal-Zellerfeld, Germany). Sample vials were filled with 3 to 4 mg of powder, capped and placed into the ASPIROS sample feeder set to 60 mm/sec. The RODOS/M used compressed air set to 3.0 bar to disperse the powders. The minimum optical concentration (C_{opt}) was set to 2.1%. Data were collected over a measurement duration of 10 s. All measurements were performed in triplicate. Volume-based size distributions were calculated by WINDOX software using the Fraunhofer theory: the particle size below which 10%, 50% and 90% of the spray lies ($D_{\text{v}10}$, $D_{\text{v}50}$, and $D_{\text{v}90}$, respectively). The span of the particle size

distribution (PSD), indication of the width of the distribution, was calculated following Equation 3.7. The percentage of particles having a diameter less than 1 μm and 5 μm ($Dv < 1 \mu\text{m}$ and $Dv < 5 \mu\text{m}$, respectively) was obtained from the Sympatec software.

$$\text{Span} = \frac{Dv90 - Dv10}{Dv50} \quad \text{Equation 3.7}$$

3.2.5 Statistical analysis

Data analysis was performed using JMP[®] Pro software version 12.0 (SAS Institute Inc., Cary, NC). For DOE analysis, response was based on the powder characteristics, the powder aerosol performance and surface activity. The influence of each factor and two factor interactions on the response was performed using full factorial analysis of variance (ANOVA). For responses with no significant interactions, the effects of the main factors were assessed individually by Student's t-test. The Pearson correlation coefficient was determined to quantify the strength of linear relationships. A flat line (weakest correlation) would be indicated by a Pearson correlation equal to 0 while the strongest correlation occurs when the coefficient is equal to the absolute value of 1. The significance (*p*-value) indicates whether the correlation is different from a flat line. One-way ANOVA followed by Dunnett's method was used to determine the significant differences of powder characteristics of EEG formulations produced with commercial surfactant compared to the optimal DPPC-EEG formulation. *P* values less than 0.05 were considered as statistically significant.

3.3 Results and discussion

3.3.1 Development of methods to produce DPPC-EEG feed dispersions for spray drying

Previous EEG formulations have been prepared with relatively high aqueous solubility drugs (albuterol sulfate, terbutaline sulfate, azithromycin, tobramycin) and excipients. In contrast, DPPC is nearly insoluble in water. Feed dispersions in these initial experiments were prepared by dissolving the water-soluble excipients in the aqueous phase (80% v/v of the feed dispersion) and the DPPC in ethanol (20% v/v of the feed dispersion). These were then combined to produce the feed dispersion for spray drying. It should be noted that a coarse dispersion of DPPC was produced by precipitation of DPPC when the two phases were combined.

3.3.1.1 Preliminary studies on the effect of formulation excipients on powder yield

For the eleven feed dispersions prepared, leucine was kept at a concentration of 20% w/w while varying the concentrations of DPPC and mannitol. The percent solids concentration was 0.125% w/v. Low powder yields were observed, preliminary formulations P1-P3 in Table 3.3, which led to exploration of other excipients. The use of trehalose, a non-reducing sugar similar to mannitol in that it does not undergo Maillard reaction, did not improve powder yield (preliminary formulation P4, Table 3.3). Sodium chloride, however, was found to more than triple the percent powder yield when included as the hygroscopic excipient when compared to formulations with mannitol or trehalose (preliminary formulation P5 vs preliminary formulation P1 or P4, Table 3.3). The addition of sodium chloride to the formulation increased the transition temperature of the system enabling particle formation. Sodium chloride is highly hygroscopic, therefore not an ideal excipient for aerosol powder formulation as it may cause high particle agglomeration. Since mannitol is known to be hygroscopic at higher RH conditions, ~80% RH at 25 °C [106, 134],

varying compositions of mannitol and sodium chloride were explored as excipients for DPPC-EEG formulations (preliminary formulations P6-P11, Table 3.3).

The estimated moisture content in the spray dried powders was determined by measuring the total weight loss by heating. The powders were found to have low estimated moisture contents of < 4% w/w (Table 3.3). The highest powder yields were achieved with formulations containing 2.5-40% w/w sodium chloride, and therefore, explored further.

Table 3.3 Effect of formulation excipients on spray dried powder yield and DPPC content of DPPC-EEG powders.

Formulation	Formulation components, % w/w*				Powder yield, % w/w	Water content, % w/w	DPPC content, % w/w [#]
	DPPC	Mannitol	Trehalose	NaCl			
P1	40	40	0	0	18	.	.
P2	60	20	0	0	5	.	.
P3	20	60	0	0	16	.	.
P4	40	0	40	0	18	.	.
P5	40	0	0	40	63	2.4	30.1 (2.6)
P6	40	20	0	20	46	2.2	31.3 (1.6)
P7	40	30	0	10	62	2.6	29.5 (0.7)
P8	40	35	0	5.0	59	3.8	35.2 (3.6)
P9	40	37.5	0	2.5	63	2.4	30.8 (2.2)
P10	40	39.0	0	1.0	38	2.6	32.8 (0.4)
P11	40	39.5	0	0.5	32	2.3	26.9 (1.4)

*Leucine included in all formulations at a concentration of 20% w/w

[#]Values are mean (SD), n=3

3.3.1.2 Preliminary studies on the effect of mannitol-to-sodium chloride ratio on aerosol performance

The aerosol performance of the formulations with the highest powder yields (preliminary formulations P6-P9) were determined using the NGI and Aerolizer[®] DPI (Table 3.4). Formulations P6 and P7, with mannitol-to-sodium chloride ratios of 1:1 and 3:1, respectively, were observed to have more than 50% of the impactor dose deposited on stage 1 of the impactor, therefore MMAD values could not be determined and the aerosol performance was reflective of a poorly dispersed formulation. Formulation P9 was found to have the best aerosol performance with the smallest MMAD of 2.3 μm and highest particle fractions less than 1 μm and 5 μm of 22.8% and 60.3%, respectively. Formulation P9 was shown to have the best deaggregation corresponding to the lowest amount of sodium chloride (mannitol-to-sodium chloride ratio of 15:1); decreasing the mass of sodium chloride in the DPPC-EEG formulations appeared to reduce particle agglomeration and improve aerosol dispersion performance.

Table 3.4 Aerosol performance with the Aerolizer[®] of DPPC-EEG spray dried formulations using mannitol, sodium chloride and leucine as excipients.

Formulation	Excipients, % w/w*			MMAD, μm	Particle fraction, %	
	Mannitol	NaCl	Mannitol-to-NaCl		<1 μm	<5 μm
P6	20	20	1:1	n/a	6.9	19.7
P7	30	10	3:1	n/a	7.8	27.2
P8	35	5	7:1	5.2	10.6	29.9
P9	37.5	2.5	15:1	2.3	22.8	60.3

*DPPC and leucine included at concentrations of 40% w/w and 20% w/w, respectively.

3.3.1.3 Preliminary studies on the effect of feed dispersion preparation method on DPPC content

The main challenge with spray drying feed dispersions containing the poorly soluble hydrophobic DPPC with hydrophilic excipients in a mainly aqueous vehicle (80/20% v/v water/ethanol) was ensuring the production of powders with DPPC content that was close to the nominal or expected content of DPPC in the spray dried powder. The nominal concentration of DPPC in the preliminary formulations was 40% w/w. Analysis of the DPPC content in a series of spray dried powder samples revealed that DPPC was present at concentrations of between 26.9-35.2% w/w (Table 3.3), which was between 62-87% of the expected DPPC concentration. During spray drying, excessive foaming was observed and the presence of solids remaining at the end of the spray drying process was observed, suggesting that the feed dispersion was not homogeneous over the duration of the spray drying process (5-8 hours), which likely caused the lower than expected DPPC content.

The use of direct sonication was explored to prepare a homogenous and stable feed dispersion for spray drying following a method adapted from Gugliotti et al. [17]. Dispersions were prepared with the understanding that above its transition temperature of 41 °C, DPPC forms fluid liposomes (multilamellar), which when sonicated, tend to form stable vesicles (unilamellar) with an aqueous core [17, 135], which may or may not contain the hydrophilic excipients. The Qsonica model Q700 (Qsonica, Newtown, CT) with standard probe (12.7 mm tip diameter, part no. 4219) was used to disperse DPPC in water. The temperature was maintained below 60 °C using a water jacketed vessel attached to a recirculating water bath (Fisher Scientific model 9505, Waltham, MA) set to 45 °C. Sonication was performed at an amplitude of 35 for 15 minutes. After sonication, the dispersions were centrifuged (Beckman Coulter Avanti J-E centrifuge with JS-5.3 rotor, Pasadena, CA) at 6100×g for 20 minutes at 40 °C to remove titanium particles left behind

from the probe. Ethanol was added to the dispersion prior to spray drying. The maximum amount of ethanol that could be added without noticeable foaming was 5% v/v. Feed dispersions containing the excipient composition of preliminary formulation P9 were prepared in water/ethanol mixtures of 95/5 and 100/0% v/v, then spray dried as described above. The feed dispersions were assayed for DPPC content after sonication and at the end of spray drying. The DPPC content was also determined in the spray dried powders and compared to the nominal DPPC content (Table 3.5).

The expected DPPC content in the feed dispersion was maintained through feed dispersion preparation and powder formation when probe sonication was employed, indicating that a uniform feed dispersion was spray dried and that it was close to the nominal value. In both water and water/ethanol spray vehicles, the DPPC content remained > 90% of the nominal (Table 3.5). Assay of the spray dried powder determined DPPC contents of 37 and 40% w/w (92 and 99% of the nominal) for powders prepared in water/ethanol and 100% water, respectively. Both spray vehicles were explored further in the full factorial DOE.

Table 3.5 DPPC content of feed dispersions (nominal concentration = 20% w/w) prepared by probe sonication and resultant spray dried powder (nominal concentration = 40% w/w). Values are mean (SD), n=3.

	Dispersion feed vehicle (water/ethanol), % v/v			
	95/5		100/0	
	DPPC, % w/w	DPPC, % nominal	DPPC, % w/w	DPPC, % nominal
Feed dispersion				
After sonication	18.8 (1.6)	92.1 (7.7)	18.9 (0.6)	93.6 (3.0)
End of spray drying	20.3 (4.1)	99.6 (20.1)	18.8 (1.1)	96.5 (6.9)
Spray dried powder	37.4 (2.4)	92.3 (2.0)	39.8 (5.0)	99.4 (12.5)

3.3.2 Development of methods for surface tension measurements of DPPC-EEG powders

3.3.2.1 Effect of sample preparation and measurement temperature on DPPC surface activity measurements

The surface activity of DPPC-EEG powders was assessed to determine if the surfactant activity was maintained after spray drying. Following a sample preparation method adapted from Wen and Franses [136] (method 1), unprocessed DPPC (1.2 mg/mL) was dispersed in normal saline (154 mM sodium chloride) and heated for 30 min in a 55-60 °C water bath, then bath sonicated for 2 hours at 55 °C. The dynamic surface tension was measured at room temperature and found to have a final surface tension of 72 mN/m at a surface age of 50 s, which was similar to that of 154 mM NaCl measured under the same conditions (Figure 3.2). Increasing the study temperature had no effect on the initial surface tension compared to their respective temperature vehicle controls. At room temperature and 37 °C, there was no surface activity observed in the final surface tension measurements with a surface age of 50 s compared to the respective temperature controls or the initial surface tension measurement. However, there was a small reduction in the final surface tension measurement with a surface age of 50 s for the study performed at 50 °C. At the elevated temperature of 50 °C, the final surface tension was 65 mN/m (Figure 3.2). The increased activity observed is due to the increased fluidity of DPPC lipid layers at temperatures above its transition temperature, which allow DPPC particles to migrate to the newly formed air-liquid interfaces at an increased rate. Future analysis would be performed at 50 °C. It was hypothesized that at the lower temperatures the absence of any effect was due to insufficient time for the DPPC to orient at the newly created surface.

Surface tension measurements of unprocessed DPPC in water was also studied. Following the same procedure described above, DPPC was prepared in water instead of normal saline and

analyzed. At 37 °C, the sample in water was found to reach a final surface temperature of 69 mN/m, similar to the surface tension observed for the sample prepared in normal saline, indicating that the presence of sodium chloride in the sample had no effect on the surface tension activity of DPPC.

Surface tension values using method 1 for DPPC were higher than reported in the literature for equivalent concentrations (dispersions of 1.3 mg/mL DPPC in 154 mM NaCl resulting in surface tensions as low as 34 mN/m at 37 °C [136]). A second method for preparing lipid dispersions was studied. Method 2 was adapted from Kim and Franses [135]. Unprocessed DPPC (1.0 mg/mL) in water was heated for 30 minutes at 55-60 °C, stirred with a magnetic stir bar for 1 hour at 55-60 °C, then bath sonicated until clear (~7 hours) to decrease the size of the liposomes as much as possible. Determination of the sample surface tension after 6 hours of sonication at a measurement temperature of 50 °C revealed a final surface tension value of 62 mN/m. Further sonication yielded further reductions in the surface tension, with 17.5 hours of sonication resulting in a final surface tension value of 43 mN/m (Table 3.6). The increased sonication times produced a corresponding increase in surface activity as indicated by higher surface tension reduction rates (0.10, 0.15, and 0.47 mN/m/s for the 6, 12.5 and 17.5 h sonication times, respectively). It is believed that the increased sonication times produced increasingly smaller liposomes and vesicles that were able to adsorb more extensively and faster at the surface.

The sample preparation time of method 2 was not conducive to efficient analysis of repeat samples, therefore a third preparation method was studied. Direct sonication methods for sample preparation as described by Gugliotti et al. [17] were followed. Unprocessed DPPC (1.0 mg/mL) was dispersed in 1 mM NaCl using a microtip probe sonicator. The use of a 1 mM NaCl vehicle was assumed to have no effect on the surface tension activity of DPPC as the NaCl concentration

was within the range previously studied – 0 (water) and 154 mM NaCl – both of which were shown not to influence the surface tension measurements. The sample was held in place in a water jacket vessel connected to a recirculating water bath set to 41 °C. Sonication was performed at an amplitude of 35 for 15 minutes with the temperature monitored (Fisher Scientific Traceable Double Thermometer with Type K thermocouple, Waltham, MA) to ensure it remained below 60 °C. At a measurement temperature of 50 °C, the final surface tension of the sample was 43 mN/m, similar to that observed for the 17.5 h sample prepared by method 2. The two samples were also observed to have similar surface tension reduction rates of 0.46 mN/m/s and 0.47 mN/m/s for method 3 and method 2, respectively. With direct sonication, the total energy released from the probe was transferred to the sample; whereas with bath sonication, the energy is diluted by the water it must travel through to reach the sample vessel. A plot of the surface tension measurements for the three methods studied is shown in Figure 3.3. Surface tension measurements would be performed using samples prepared by probe sonication following method 3 in future studies.

Table 3.6 Comparison of surface activity of unprocessed DPPC following different preparation methods.

Preparation method	Sonication method	DPPC concentration, mg/mL	Solvent	Sonication time, h	Measurement temperature, °C	Surface age, s	Final surface tension, mN/m	Surface tension reduction rate, mN/m/s*
Wen et al. [136] (method 1)	bath	1.2	154 mM NaCl	2.0	RT	50.2	72.4	0
					37	52.4	70.7	0
					50	133.0	64.7	0.03
			water	2.0	37	50.1	69.3	0.02
Kim et al. [135] (method 2)	bath	1.0	water	6.0	50	56.0	62.1	0.10
				12.5	50	52.0	60.9	0.15
				17.5	50	50.6	43.3	0.47
Gugliotti et al. [17] (method 3)	probe	1.0	1 mM NaCl	0.25	50	55.7	43.0	0.46

*Negative values indicated as zero

RT=room temperature

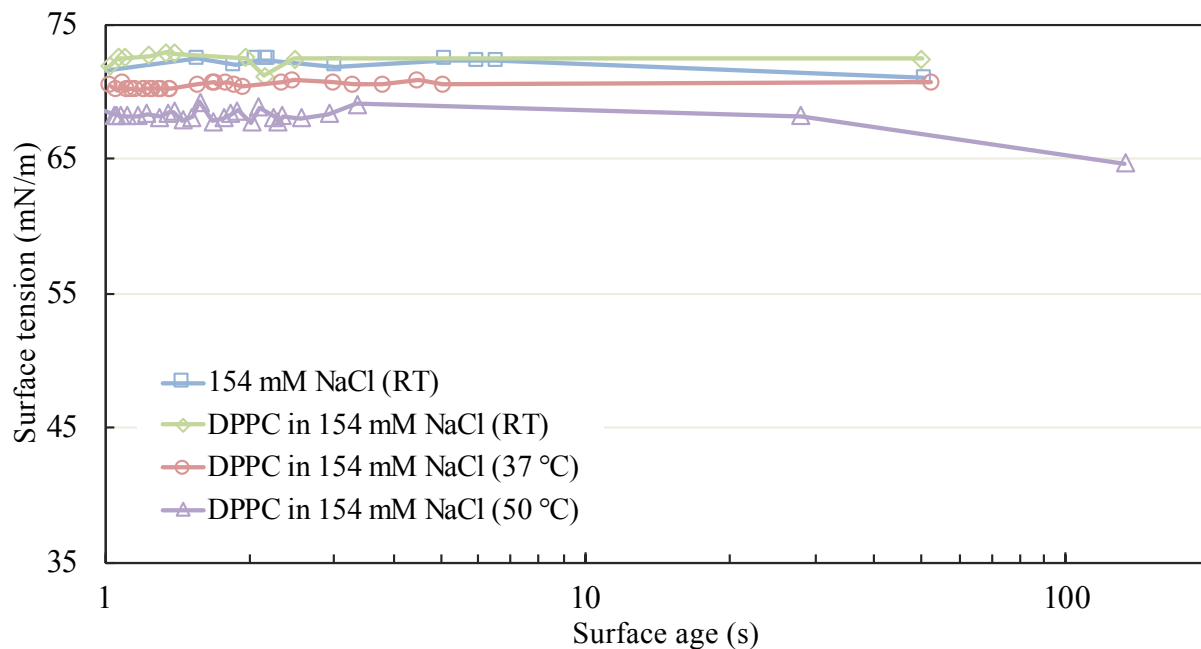


Figure 3.2 Effect of sample temperature on surface activity of 1.2 mg/mL dispersion of unprocessed DPPC in 154 mM NaCl vehicle performed using method 1. The surface activity of 154 mM NaCl solution is also shown for comparison. Markers represent individual values. RT=room temperature.

and a coefficient of determination of $R^2 = 0.8455$. The scatterplot correlation is shown in Figure 3.4. The higher the concentration of DPPC, the more surface-active particles there are available to reach the air-liquid interface to lower the surface tension; however, at DPPC concentrations above its critical micelle concentration, the surface activity will plateau as the interface becomes saturated. This correlation can be used to determine the DPPC concentration required to reach a desired surface tension within the range of concentrations studied.

To minimize the amount of powder necessary to prepare samples for surface tension measurements, a target concentration of 0.86 mg/mL of DPPC was selected for future measurements as it was the intermediate surface tension value of the concentrations studied, 55 mN/m, and a provided a measurable reduction in surface tension.

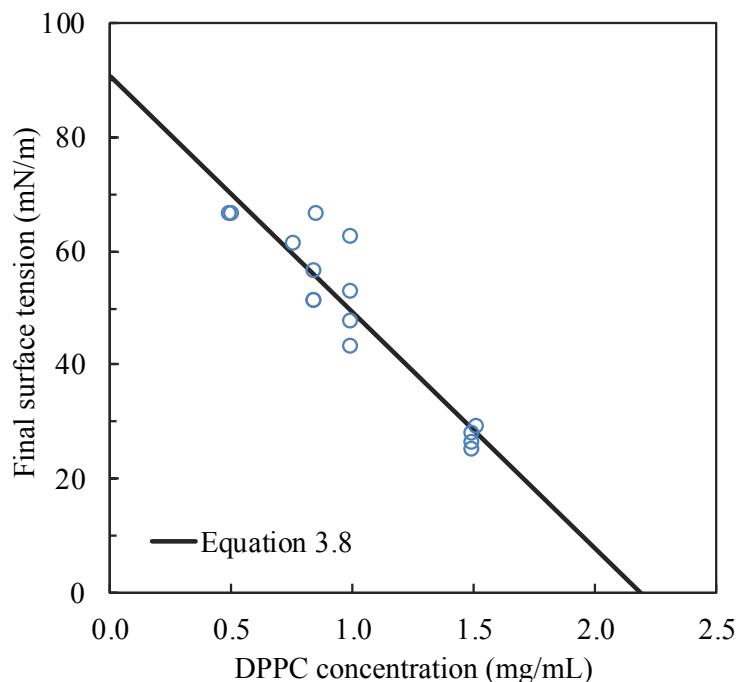


Figure 3.4 Correlation of final surface tension values with DPPC concentration for samples measured at 50 °C using method 3. Markers represent individual values.

3.3.2.3 Surface tension measurements with preliminary spray dried DPPC-EEG powders

The method developed for determining the surface tension of DPPC powders was applied to DPPC-EEG preliminary formulation P9. Powders were dispersed in 1 mM NaCl using the microtip probe sonicator at an amplitude of 35 for 15 minutes. The concentration of DPPC in the sample was 0.86 mg/mL. Surface tension measurements were performed at 50 °C. The mean \pm SD final surface tension value for preliminary formulation P9 was 56.6 ± 4.0 mN/m, not significantly different from the expected final surface tension value of 55.1 mN/m calculated from Equation 3.8.

Samples were compared to unprocessed DPPC powders analyzed using the same methods, Table 3.7. There were no significant differences observed in the surface age, final surface tension values and surface tension reduction rates for preliminary formulation P9 powders when compared to unprocessed DPPC, indicating that the surfactant activity of DPPC was not significantly affected by formulation excipients following spray drying. A comparison of unprocessed DPPC and preliminary formulation P9 surface tensiograms is shown in Figure 3.5.

Table 3.7 Comparison of surfactant activity for unprocessed DPPC and spray dried formulation P9 at a nominal DPPC concentration of 0.86 mg/mL dispersed in 1 mM NaCl measured at 50 °C using method 3. Values are mean (SD), n=3.

Powder sample	Surface age, s	Final surface tension, mN/m	Surface tension reduction rate, mN/m/s
Unprocessed DPPC	51.0 (0.4)	52.7 (3.0)	0.31 (0.06)
Formulation P9	54.6 (3.8)	56.6 (4.0)	0.35 (0.07)

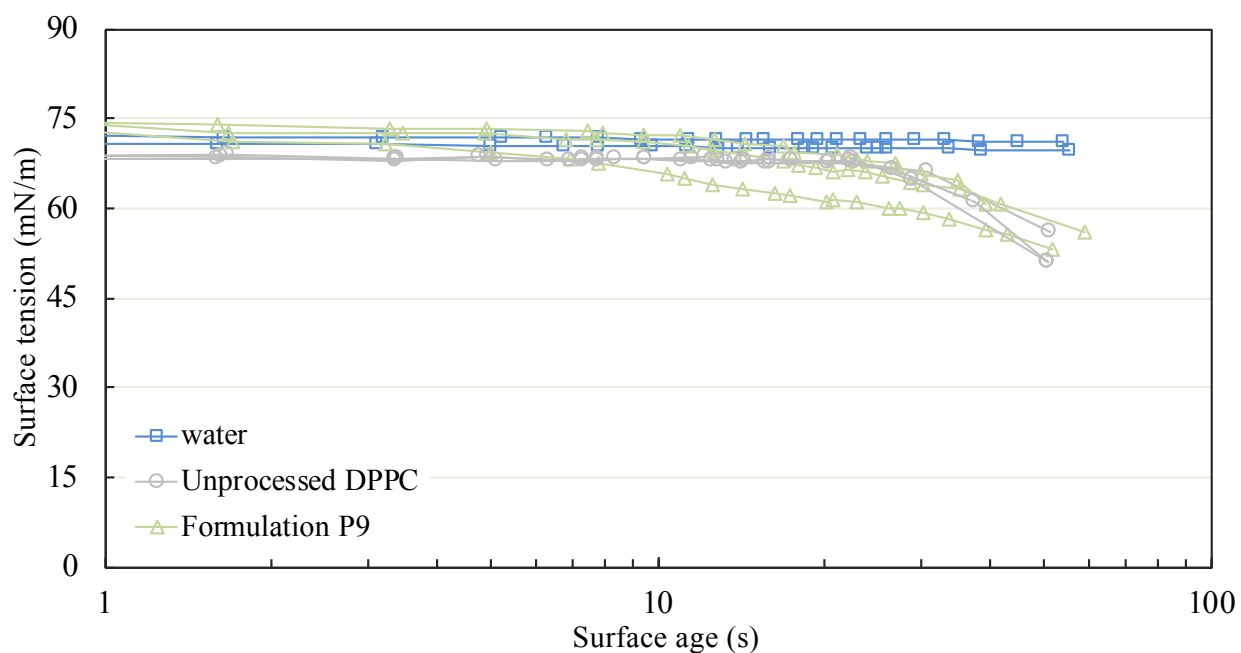


Figure 3.5 Surface tension activity comparison of unprocessed DPPC and spray dried formulation P9 with a nominal DPPC concentration of 0.86 mg/mL measured at 50 °C using method 3. The surface activity of water is also shown for comparison. Markers represent individual values.

3.3.2.4 Effect of powder age on DPPC surface activity measurements

A fresh batch of preliminary formulation P9 powder was prepared to determine the effect of powder age on surface tension activity. Measurements of surface activity of this powder batch was performed using the developed methods as described in the previous section and measured at intervals over 14 days. Powders were stored in the refrigerator (2-8 °C) between measurements. Surface tension measurement results are shown in Table 3.8. The measured surface tension was observed to be lowest when the powders were measured immediately after spray drying on day 0 and the measured surface activity of the powders was observed to decrease with increasing powder age. The highest surface activity, as indicated by the surface tension reduction rate, was observed with the freshly prepared powders, 0.49 mN/m/s. The surface activity decreased with increasing

powder age, which appeared to level off between 7 and 14 days after the powder was prepared. The largest change from the surface activity of freshly prepared powder was observed 7 days after powders were prepared, indicating that surface tension measurements should be performed within the first few days after powder preparation. The decrease in surface tension is not a concern for reasons other than performing accurate comparisons between DPPC-EEG formulations since these initial studies are focused on developing methods to be applied for EEG formulations with commercial surfactant.

Table 3.8 Surfactant activity characteristics of preliminary formulation P9 when stored at 2-8 °C for 14 days. Values are mean (SD), n=3.

Powder age, days	Surface age, s	Final surface tension, mN/m	Surface tension reduction rate, mN/m/s	Surface tension difference from day 0, mN/m
0	53.2 (2.7)	24.4 (0.5)	0.49 (0.03)	n/a
1	55.6 (5.0)	28.1 (2.5)	0.44 (0.09)	3.7
7	53.6 (2.5)	44.8 (1.8)	0.31 (0.02)	20.4
14	61.4 (2.1)	43.3 (3.4)	0.31 (0.04)	18.9

3.3.3 Full factorial design of experiment (DOE) to assess select formulation factors and spray drying parameters

The effects of four factors on the aerosol characteristics of spray dried DPPC-EEG formulations were investigated. The studied factors included percent solids in the feed dispersion, the ratio of mannitol-to-sodium chloride, percentage ethanol in the feed dispersion and the inlet drying temperature of the spray dryer. Each factor was studied at two levels and the preliminary studies described above were used to guide the factor selections.

Preliminary studies were performed with a percent solids concentration in the feed dispersion of 0.125% w/v. The formulation with the best aerosol performance had the highest ratio of mannitol-to-sodium chloride (15:1) and resulted in micrometer sized primary particles with an aerosol MMAD of 2.3 μm . The use of probe sonication to prepare uniform feed dispersions was employed since spray drying of feed dispersions prepared without sonication resulted in low DPPC content in the spray dried powders. The percent ethanol in the aqueous feed dispersion was reduced from 20% v/v to 0-5% v/v to minimize the amount of visible foaming.

A full factorial DOE was performed to determine if the factors affect each other with changing levels. The effect of the main factors and two-way interactions on the powder characteristics, the powder aerosol performance and surface activity were considered in the analysis. If no significance was determined with the interactions of the factors, then effects of the main factors were assessed individually.

3.3.3.1 Effect of formulation factors and spray drying parameters on powder yield and DPPC content of DPPC-EEG formulations

The powder characteristics (powder yield, moisture content and DPPC content) for the sixteen spray dried powders with the studied factors and levels are shown in Table 3.9. The powder yield ranged from 47-71%. ANOVA with main factors and their interactions did not identify any significant effects on powder yield. When examined separately, a significant effect of ethanol concentration was observed on powder yield where the higher concentration of ethanol resulted in higher powder yields (0% ethanol: $56 \pm 5\%$ yield, 5% ethanol: $64 \pm 6\%$ yield, $p=0.0149$; Student's t-test). Higher ethanol concentrations in the feed dispersion promote more efficient drying of the droplets exiting the nozzle of the spray dryer since it has a lower boiling point compared to that of water (78 °C vs 100 °C). There were no significant differences observed with percent solids in the

feed dispersion, the ratio of mannitol-to-sodium chloride and the inlet drying temperature on the percent yield when the effects were examined separately.

The DPPC content in the powders were observed to range from 35 to 44% (88-109% of the nominal value of 40% w/w) for the different powder formulations. No significant interactions were revealed with ANOVA. When examined separately, the percent solids concentration was observed to have a significant effect on the DPPC content where the higher solids content of 0.250% w/v resulted in higher DPPC content (0.125% w/v solids: $38 \pm 2\%$ DPPC, 0.250% w/v solids: $40 \pm 2\%$ DPPC, $p=0.0076$; Student's t-test). There were no significant differences observed with the other main factors when they were examined separately.

The spray dried powders were observed to have low moisture content, $< 3\%$ w/w; no significant effects were observed with the main factors on the moisture content of the spray dried powders.

Table 3.9 Effect of formulation factors and spray drying parameters on the powder characteristics of spray dried DPPC-EEG powders.

Expt	Run order	Solids in feed dispersion,		Ethanol in feed	Inlet drying temperature, °C	Powder yield, % w/w	Water content (SD), % w/w	DPPC content (SD), % w/w
		% w/v	Mannitol-to-NaCl	dispersion, % v/v				
1	1	0.125	3:1	0	70	57.0	1.0	41.4 (0.3)
2	16	0.125	3:1	0	80	58.1	1.0 (0.5)	38.0 (2.5)
3	13	0.125	3:1	5	70	62.0	1.1 (0.6)	35.9 (1.2)
4	14	0.125	3:1	5	80	63.9	1.6 (1.0)	36.9 (2.0)
5	11	0.250	3:1	0	70	63.0	2.1 (1.2)	39.0 (0.4)
6	8	0.250	3:1	0	80	55.8	1.9	38.3 (0.5)
7	10	0.250	3:1	5	70	71.3	0.7 (0.1)	38.4 (1.3)
8	3	0.250	3:1	5	80	62.3	0.9	42.4 (0.9)
9	5	0.125	15:1	0	70	54.1	1.4	38.3 (3.0)
10	12	0.125	15:1	0	80	61.3	1.5 (1.3)	36.9 (1.6)
11	2	0.125	15:1	5	70	55.2	0.8	35.8 (7.4)
12	9	0.125	15:1	5	80	57.3	1.8 (0.1)	35.1 (0.5)
13	6	0.250	15:1	0	70	46.6	0.8	38.7 (1.5)
14	4	0.250	15:1	0	80	53.9	0.6	43.0 (0.5)
15	15	0.250	15:1	5	70	68.7	1.5 (0.7)	43.5 (1.1)
16	7	0.250	15:1	5	80	69.0	1.5	40.6 (0.7)

3.3.3.2 Effect of formulation factors and spray drying parameters on the primary particle size distribution of DPPC-EEG formulations

The primary particle size values, particle fractions and span for the sixteen spray dried powders determined using the Sympatec HELOS with RODOS/M disperser are shown in Table 3.10. Overall, the powders were observed to be approximately one micrometer in size with small span values of < 2 . The particle fraction less than $1\ \mu\text{m}$ and $5\ \mu\text{m}$ was $> 33\%$ and $> 97\%$, respectively.

Analysis of the main factors and their two-way interactions on primary particle size, the particle fraction less than $1\ \mu\text{m}$ and $5\ \mu\text{m}$ and the span revealed no significant effects with their interactions. A summary of the mean values for primary particle size for the sixteen spray dried powder lots are shown in Table 3.11 by study factor. When examined separately, the percent solids content was found to have a significant effect on the primary particle size with the lower concentration of solids producing smaller primary particles ($p=0.0003$; Student's t-test). No other significant effects were observed on the primary particle size.

The particle fraction less than $1\ \mu\text{m}$ for the sixteen formulations were shown to be significantly affected by the percent solids concentration with the lower solids concentration resulting in a higher fraction of particles less than $1\ \mu\text{m}$ ($p=0.0001$; Student's t-test). No other significant effects were observed on the fractions of particles less than $1\ \mu\text{m}$. Analysis of the fraction of particles less than $5\ \mu\text{m}$ and the span revealed there were no significant effects of main factors when examined separately.

Table 3.10 Primary particle size measurements and aerosol properties of spray dried DPPC-EEG powders for each experiment varying formulation factors and spray drying parameters. Values are mean (SD), n=3.

Expt	Primary particle				Aerosol properties				
	Dv50, μm	Particle fraction, %		Span	Emitted dose, %	MMAD, μm	Particle fraction, %		GSD
		<1 μm	<5 μm				<1 μm	<5 μm	
1	0.99 (0.01)	50.8 (0.5)	100 (0.0)	1.5 (0.0)	62.9 (8.1)	1.44 (0.04)	20.9 (2.0)	77.5 (3.8)	1.8 (0.0)
2	1.06 (0.01)	46.3 (0.2)	98.8 (0.2)	1.5 (0.0)	73.1 (1.8)	1.70 (0.06)	8.8 (1.7)	50.2 (3.6)	1.9 (0.1)
3	1.03 (0.02)	47.9 (1.4)	99.7 (0.4)	1.5 (0.0)	68.2 (2.0)	1.61 (0.02)	12.2 (0.2)	60.4 (0.4)	1.8 (0.0)
4	1.07 (0.01)	45.1 (0.1)	98.2 (0.2)	1.6 (0.0)	70.6 (0.4)	1.75 (0.04)	8.6 (0.7)	54.1 (3.8)	1.9 (0.1)
5	1.31 (0.03)	33.9 (0.9)	97.1 (0.7)	1.8 (0.1)	67.7 (1.8)	2.08 (0.03)	4.0 (0.3)	49.0 (2.2)	1.9 (0.0)
6	1.13 (0.01)	42.2 (0.2)	99.4 (0.4)	1.6 (0.0)	65.2 (2.5)	1.73 (0.01)	10.9 (0.7)	68.1 (2.9)	1.8 (0.0)
7	1.12 (0.01)	42.2 (0.7)	99.8 (0.2)	1.5 (0.0)	62.3 (4.2)	1.58 (0.03)	15.4 (0.9)	76.0 (2.3)	1.7 (0.0)
8	1.14 (0.01)	41.6 (0.6)	99.9 (0.0)	1.6 (0.0)	66.2 (3.8)	1.60 (0.02)	16.7 (0.4)	82.7 (0.7)	1.3 (0.1)
9	0.94 (0.01)	55.3 (0.6)	100 (0.0)	1.5 (0.0)	59.1 (0.8)	1.50 (0.02)	18.7 (1.2)	74.2 (2.8)	1.8 (0.0)
10	1.01 (0.01)	49.1 (0.9)	100 (0.0)	1.5 (0.0)	68.1 (1.1)	1.62 (0.03)	12.4 (0.7)	69.5 (4.5)	1.7 (0.1)
11	0.96 (0.01)	52.7 (0.2)	100 (0.0)	1.5 (0.0)	51.0 (3.2)	1.42 (0.00)	21.7 (0.7)	76.0 (2.0)	1.5 (0.1)
12	1.01 (0.01)	49.6 (0.5)	99.9 (0.1)	1.4 (0.0)	69.3 (0.9)	1.52 (0.01)	14.8 (0.8)	63.3 (2.4)	1.8 (0.0)
13	1.09 (0.01)	44.3 (0.6)	99.9 (0.0)	1.6 (0.0)	54.2 (4.3)	1.66 (0.04)	14.9 (2.0)	79.9 (6.8)	1.7 (0.0)
14	1.12 (0.01)	42.8 (0.4)	99.9 (0.0)	1.7 (0.0)	56.4 (5.1)	1.69 (0.03)	13.1 (1.7)	76.1 (5.2)	1.7 (0.1)
15	1.15 (0.01)	40.8 (0.4)	99.5 (0.5)	1.6 (0.0)	73.3 (4.0)	1.81 (0.02)	7.8 (0.2)	57.1 (2.0)	1.8 (0.0)
16	1.12 (0.01)	42.3 (0.2)	99.9 (0.1)	1.6 (0.0)	59.6 (1.6)	1.67 (0.01)	13.0 (0.4)	77.1 (2.9)	1.7 (0.0)

Table 3.11 Summary of primary particle size of spray dried DPPC-EEG powders by study factor. Values are mean (SD), n=8.

Study factor (level)	Dv50, µm	Particle fraction, %		Span
		<1 µm	<5 µm	
Solids (0.125% w/v)	1.01 (0.05)	49.6 (3.3)	99.6 (0.7)	1.5 (0.1)
Solids (0.250% w/v)	1.15 (0.07)*	41.3 (3.1)*	99.4 (1.0)	1.6 (0.1)
Mannitol-to-NaCl (3:1)	1.11 (0.10)	43.8 (5.1)	99.1 (1.0)	1.6 (0.1)
Mannitol-to-NaCl (15:1)	1.05 (0.08)	47.1 (5.3)	99.9 (0.2)	1.5 (0.1)
Ethanol (0% v/v)	1.08 (0.11)	45.6 (6.5)	99.4 (1.0)	1.6 (0.1)
Ethanol (5% v/v)	1.08 (0.07)	45.3 (4.4)	99.6 (0.6)	1.5 (0.1)
Inlet temperature (70 °C)	1.07 (0.12)	46.0 (7.1)	99.5 (1.0)	1.6 (0.1)
Inlet temperature (80 °C)	1.08 (0.05)	44.9 (3.2)	99.5 (0.7)	1.6 (0.1)

*Significant difference from 0.125% w/v solids; Student's t-test, $p < 0.05$

3.3.3.3 Effect on aerosol performance

The aerosol performance of the spray dried powders was determined using the NGI and an Aerolizer DPI operating a flow rate of 80 L/min. Overall, the powders demonstrated moderate aerosolization properties with the Aerolizer with emitted doses of 51-73% of the loaded mass. The MMAD of the powders were 1-2 µm in size with small span values of < 2. The fine particle fraction less than 1 µm and 5 µm were greater than 7% and 49% of the emitted dose, respectively. Aerosol performance data for each experiment are shown in Table 3.10.

Analysis of the main factors and their two-way interactions on the MMAD, the aerosol particle fraction less than 1 µm and 5 µm and the GSD revealed no significant effects with their interactions. A summary of the mean values of the aerosol properties for the sixteen spray dried powder lots are shown in Table 3.12 by study factor. The percent solids content was found to have a significant effect on the MMAD with the lower concentration of solids producing smaller

MMAD values ($p=0.0424$; Student's t-test). No other significant effects were observed on the MMAD. Analysis of the fraction of particles less than 1 μm and less than 5 μm and the GSD revealed there were no significant effects of main factors when examined separately.

Table 3.12 Summary of aerosol properties of spray dried DPPC-EEG powders by study factor. Values are mean (SD), $n=8$.

Study factor (level)	MMAD, μm	Particle fraction, %		GSD
		<1 μm	<5 μm	
Solids (0.125% w/v)	1.57 (0.12)	14.6 (5.5)	65.7 (10.3)	1.8 (0.1)
Solids (0.250% w/v)	1.73 (0.16)*	12.0 (4.3)	70.8 (11.9)	1.7 (0.2)
Mannitol-to-NaCl (3:1)	1.69 (0.19)	12.2 (5.3)	64.8 (13.2)	1.8 (0.2)
Mannitol-to-NaCl (15:1)	1.61 (0.12)	14.6 (4.2)	71.7 (7.8)	1.7 (0.1)
Ethanol (0% v/v)	1.68 (0.19)	12.8 (5.6)	68.1 (12.0)	1.8 (0.1)
Ethanol (5% v/v)	1.62 (0.12)	13.8 (4.5)	68.3 (10.8)	1.7 (0.2)
Inlet temperature (70 °C)	1.64 (0.22)	14.5 (6.2)	68.8 (11.5)	1.8 (0.1)
Inlet temperature (80 °C)	1.66 (0.08)	12.1 (3.1)	68.6 (11.3)	1.7 (0.2)

*Significant difference from 0.125% w/v solids; Student's t-test, $p<0.05$

The plot in Figure 3.6 shows the primary particle Dv_{50} values ordered in increasing size on the primary y-axis with combined study factors on the x-axis. The corresponding aerosol MMAD values are plotted on the secondary y-axis. A significant positive correlation was observed between MMAD values and Dv_{50} values, where higher Dv_{50} values resulted in larger MMAD values ($r = 0.8766$, $p<.0001$; Pearson correlation) with the following relationship,

$$\text{MMAD, } \mu\text{m} = -0.003289 + 1.532 * Dv_{50}, \mu\text{m}$$

Equation 3.9

and a coefficient of determination of $R^2 = 0.7685$. The scatterplot is shown in Figure 3.7. The strong correlation between MMAD and Dv_{50} reveals the good dispersion efficiency of the powders. In terms of particle size, the powder formulations, relative to each other, performed similarly with the Aerolizer DPI at a pressure drop of 4 kPa as with the RODOS dispersion unit operating at a dispersion pressure 75x that of the DPI. The correlation could be used to estimate the aerodynamic size of spray dried DPPC-EEG powders, which would minimize having to perform time-consuming cascade impaction experiments.

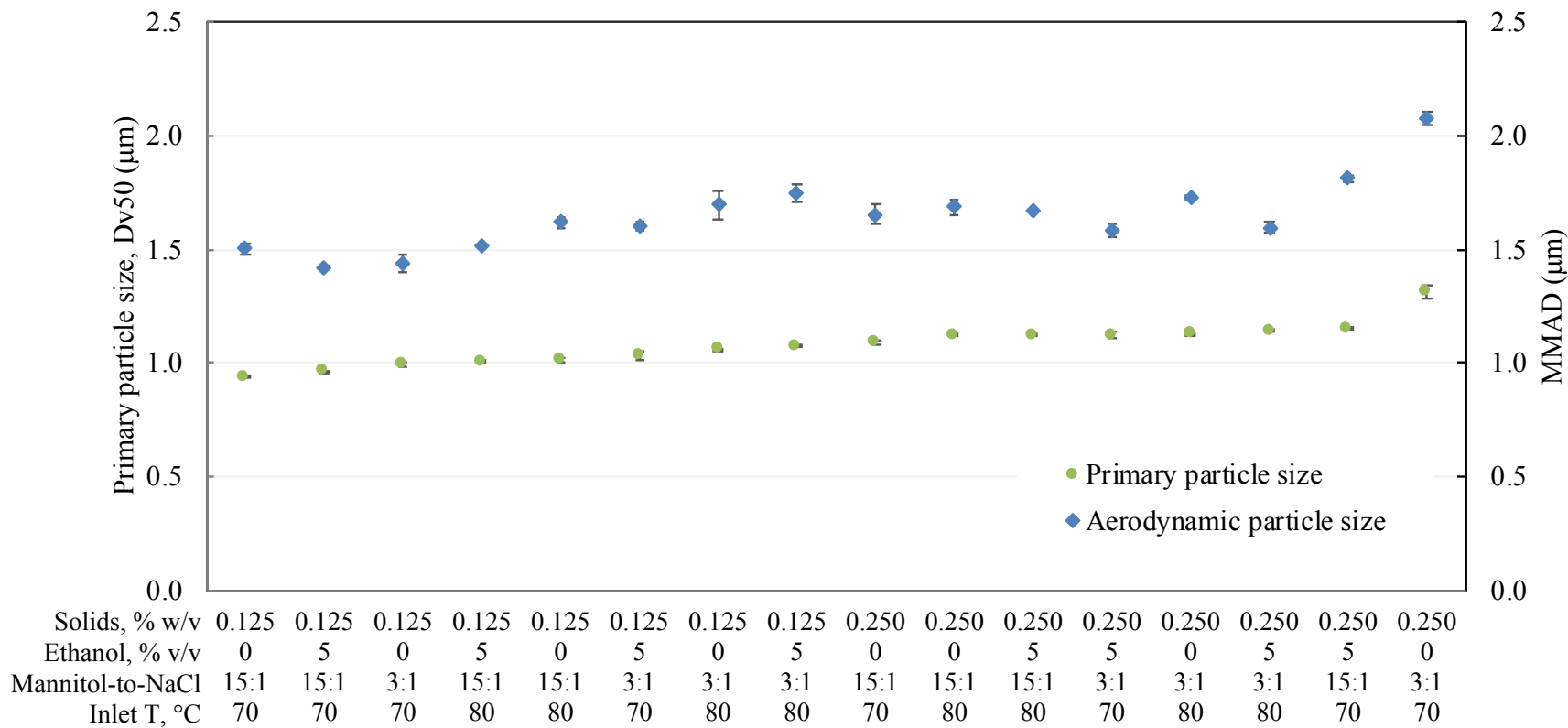


Figure 3.6 Combined study factors ordered by increasing primary particle size (primary y-axis) with corresponding MMAD values on the secondary y-axis. Markers represent the mean, error bars represent the SD, n=3.

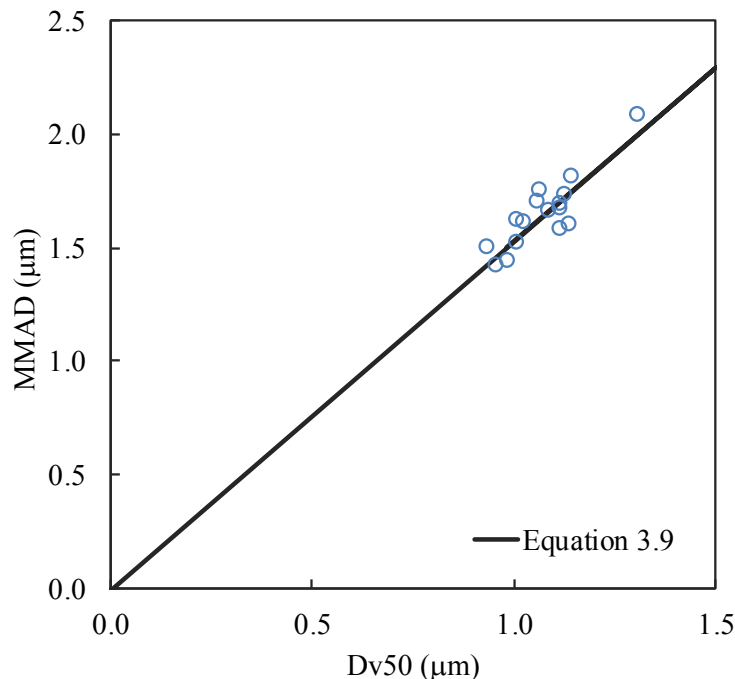


Figure 3.7 Correlation of MMAD with Dv50 values for DPPC-EEG powders. Markers represent mean values, n=3.

3.3.3.4 Effect of formulation factors and spray drying parameters on the surface tension of DPPC-EEG formulations

The surface tension of the spray dried DPPC-EEG powders was determined using the Krüss Bubble Pressure Tensiometer - BP2 on samples prepared by probe sonication (method 3). Samples were prepared with a nominal DPPC concentration of 0.86 mg/mL. The surface tension values determined for the different powder formulations are shown in Table 3.13. The final surface tension values ranged from 34 to 64 mN/m, comparable to the surface tension of unprocessed DPPC of 53 mN/m. The calculated surface tension reduction rates were 0.11 to 0.62 mN/m/s, indicating that the powders demonstrated retention of surface activity functionality.

Analysis of the main factors and their two-way interactions on the final surface tension values and surface tension reduction rates showed no significant effects with their interactions.

Examining each of the factors separately revealed that the ratio of mannitol-to-sodium chloride was observed to significantly affect the final surface tension values of the spray dried powders. The mannitol-to-sodium chloride ratio of 3:1 resulted in significantly lower final surface tension values, 43.4 ± 7.2 mN/m, compared to the mannitol-to-sodium chloride ratio of 15:1, 52.7 ± 9.8 mN/m ($p=0.477$; Student's t-test). The mannitol-to-sodium chloride ratio was also observed to have a significant effect on the surface tension reduction rates with the mannitol-to-sodium chloride ratio of 3:1 resulting in higher reduction rates (0.45 ± 0.13 mN/m/s) than that of the mannitol-to-sodium chloride ratio of 15:1, 0.28 ± 0.17 mN/m/s ($p=0.0427$; Student's t-test). Sodium chloride is known to reduce the electrokinetic repulsion between surfactant molecules allowing them to pack closer together, promoting adsorption of surfactants to the interface and thereby reducing the surface tension [137]. The higher amount of sodium chloride in the formulations with a mannitol-to-sodium chloride ratio of 3:1 compared to a ratio of 15:1 had a greater influence on surfactant adsorption leading to the observed outcome of lower final surface tension values and higher surface tension reduction rates with the mannitol-to-sodium chloride ratio of 3:1. Analysis of the other main factors (percent solids in the feed dispersion, percent of ethanol in the feed dispersion and the inlet drying temperature) revealed no significant effects on the final surface tension values and the surface tension reduction rates.

Table 3.13 Effect of formulation factors and spray drying parameters on the surface tension for spray dried DPPC-EEG powder with DPPC concentration of 0.86 mg/mL dispersed in 1 mM NaCl at 50 °C. Values are mean (SD), n=3.

Experiment	Surface age, s	Final surface tension, mN/m	Surface tension reduction rate, mN/m/s
1	54.9 (1.8)	42.0 (2.4)	0.49 (0.06)
2	55.4 (3.2)	44.1 (1.1)	0.42 (0.06)
3	51.5 (1.8)	37.3 (0.84)	0.62 (0.03)
4	58.1 (5.2)	36.3 (2.9)	0.53 (0.04)
5	56.2 (6.8)	51.1 (1.8)	0.33 (0.03)
6	55.8 (3.6)	48.8 (4.4)	0.33 (0.10)
7	60.5 (13.2)	53.4 (2.0)	0.27 (0.03)
8	59.7 (7.6)	34.2 (2.0)	0.57 (0.07)
9	54.5 (1.0)	61.8 (3.7)	0.12 (0.08)
10	52.9 (0.2)	43.7 (1.7)	0.45 (0.02)
11	54.7 (2.5)	35.3 (3.1)	0.57 (0.07)
12	56.1 (2.6)	63.7 (2.8)	0.11 (0.05)
13	53.8 (2.9)	57.9 (5.3)	0.21 (0.11)
14	53.6 (0.5)	47.1 (7.9)	0.39 (0.15)
15	66.5 (3.8)	55.1 (0.57)	0.20 (0.02)
16	58.3 (6.2)	57.4 (2.1)	0.17 (0.05)

Only a few significant effects were observed, which may have resulted from narrow high/low values of the levels that were able to be investigated in these studies. The values were selected based on results from preliminary experiments and the limitation of the spray dryer. The high level for the percent solids concentration was selected by doubling the solids concentration that was studied in preliminary experiments, 0.125% w/v. The ratio of mannitol-to-sodium chloride was selected based on the best performing powders in preliminary experiments. The high/low levels for the percent ethanol concentration were selected to minimize foaming of the feed dispersion. The high level for the inlet temperature was selected as it resulted in outlet

temperatures at the transition temperature of DPPC (41 °C), which would have resulted in more cohesive powders if exceeded. These experiments did reveal that the main factors studied have no significant interactions and also the relatively wide range of operating conditions that can be employed in which DPPC-EEG powders can be prepared with similar properties and aerosol performance.

Based on the significant effects observed with the main factors, the optimal DPPC-EEG formulation was determined to be formulation 3 with an MMAD of 1.6 μm , particle fraction <1 μm of 12%, and particle fraction <5 μm of 60%. Formulation 3 was produced with the following parameters: 0.125% w/v solids in the feed dispersion, mannitol-to-sodium chloride ratio of 3:1, 5% v/v ethanol in water in the feed dispersion and inlet drying temperature of 70 °C. The described parameters were used to prepare EEG formulations with commercial surfactant.

3.3.4 Preliminary assessment of EEG formulations with commercial surfactants

The parameters specified from the results of the full factorial DOE were applied to the preparation of EEG formulations with commercial surfactants Curosurf[®] (poractant), Infasurf[®] (calfactant), and Survanta[®] (beractant). All commercial formulations are supplied as suspensions in 0.9% w/v sodium chloride.

3.3.4.1 Feed dispersion preparation and powder formation of commercial surfactant-EEG formulations

Feed dispersions were prepared based on the solids concentration of the commercial formulations with the goal of including the highest mass of phospholipids in the formulation while maintaining a feed dispersion solids concentration of 0.125% w/v. The solids concentration in the commercial formulations were determined by drying. For each commercial formulation, a syringe

was used to accurately transfer 20 μL of the suspension to a TGA sample pan and then allowed to dry in the TGA, which was programmed for an isothermal hold at 50 $^{\circ}\text{C}$, until a stable weight was reached. DPPC content was also determined using accurately measured aliquots of the commercial formulations that were dissolved in methanol and assayed for DPPC using LC-MS as described previously. Table 3.14 shows the formulation characteristics.

Excipients (mannitol, sodium chloride, leucine) were dissolved in water followed by addition of the commercial surfactant at the volume specified in Table 3.14. The amount of sodium chloride in the commercial formulations were calculated and supplemental sodium chloride was added to reach the mannitol-to-sodium chloride ratio of 3:1. Ethanol was added to the dispersions, then probe sonicated and centrifuged as described above (method 3). Dispersions were spray dried using the size 4 μm spray mesh with an inlet temperature of 70 $^{\circ}\text{C}$ and feed rate of 100%.

Powders were collected from the electrostatic particle collector and the powder yield for each formulation was determined using Equation 3.1. Estimated moisture content of the surfactant-EEG powders was determined using the TGA and DPPC content was assessed using LC-MS. The three formulations had decent powder yields of 62-69% w/w and low moisture contents, < 3% w/w. The DPPC content for the formulations were determined to be 10-12% w/w, which was 77-85% of the expected DPPC content based on assay results of each commercial formulation for DPPC.

The commercial surfactant-EEG formulation contents are shown in Table 3.15. The mannitol-to-sodium chloride ratio and leucine content was kept constant at 3:1 and 20% w/w, respectively, for all formulations. The phospholipid content was estimated for each EEG formulation based on the label claim and the DPPC content determined from LC-MS assay (shown in Table 3.14). As prepared, the Curosurf-EEG and Infasurf-EEG formulations were able to

include a higher mass of phospholipids in the spray dried formulations compared to the Survanta-EEG formulation. This is due to the higher concentration of phospholipids present in the commercial Curosurf[®] and Infasurf[®] suspensions compared to Survanta[®]. The protein content for each formulation was estimated based on the label claim, with all formulations having a protein content < 2% w/w. The remaining components consisted of neutral lipids, palmitic acid and tripalmitin, depending on the commercial formulation used. The percent content of the remaining components was determined by summing up the known and estimated component contents and subtracting from 100%.

Table 3.14 Characteristics of EEG formulations prepared with commercial surfactant. Values are mean (SD), n=3.

Formulation	Commercial formulation			Powder characteristics		
	Solids concentration, mg/mL	DPPC content, mg/mL	Volume in feed dispersion, mL	Powder yield, % w/w	Water content, % w/w	DPPC content, % w/w
Curosurf-EEG	95 (4)	25.5 (1.7)	0.9	62	2.4 (0.9)	10.4 (0.3)
Infasurf-EEG	43 (1)	13.7 (0.6)	2	63	2.2 (0.7)	11.5 (0.1)
Survanta-EEG	40 (3)	11.9 (0.1)	2	69	1.8 (1.1)	10.7 (0.1)

Table 3.15 Commercial surfactant-EEG formulation contents.

Formulation	Mannitol, % w/w	NaCl, % w/w	Mannitol-to-NaCl	Leucine, % w/w	Estimated from label claim, % w/w		other components in commercial formulation, % w/w
					Total PL content [#]	Protein content	
Curosurf-EEG	29.9	9.8	3:1	20.0	30.3	0.47	9.5
Infasurf-EEG	31.9	10.8	3:1	21.4	32.1	1.02	2.8
Survanta-EEG	33.0	10.9	3:1	22.0	24.5	<1.09	8.5

[#]Includes DPPC content

PL=phospholipids

3.3.4.2 Evaluation of the primary particle size of commercial surfactant-EEG formulations

The primary particle size of the commercial surfactant-EEG formulations was determined using the Sympatec HELOS and compared with that determined for the optimal DPPC-EEG powder formulation. Overall, the powders prepared with the commercial surfactant formulations were found to have larger mean Dv50 values, lower percent particle fractions <1 μm and <5 μm and larger span values compared to the DPPC-EEG powders (Table 3.16).

One-way ANOVA revealed significant differences in the primary particle size, particle fractions less than 1 μm and 5 μm and the span values for the different commercial surfactant EEG formulations ($p < .0001$). Using Dunnett's method for post-hoc analysis, the formulations prepared with Curosurf[®], Infasurf[®] and Survanta[®] were determined to have significantly larger Dv50 values compared to the optimal DPPC-EEG formulation ($p < .0001$, $p < .0001$, and $p = 0.0349$, respectively). The particle fraction less than 1 μm for the three commercial surfactant formulations were determined to be significantly lower compared to the DPPC-EEG formulation ($p < .0001$; Dunnett's method). The particle fraction less than 5 μm was also determined to be significantly lower for the commercial surfactant formulations compared to the DPPC-EEG formulation (Curosurf[®]: $p < .0001$, Infasurf[®]: $p = 0.0006$, Survanta[®]: $p = 0.0077$; Dunnett's method). The span values for the commercial surfactant formulations were all observed to be significantly larger compared to the span of the DPPC-EEG formulation (Curosurf[®]: $p < .0001$, Infasurf[®]: $p = 0.0022$, Survanta[®]: $p = 0.0032$; Dunnett's method).

The particle size distributions are plotted in Figure 3.8. There is a clear difference in the particle size distributions of the EEG formulations prepared with commercial surfactant compared to the DPPC-EEG formulation, indicating that the primary particle size of the spray dried commercial surfactant EEG powders or the aggregation properties are determined by formulation

factors rather than the spray drying conditions that were held constant. The differences observed between the commercial surfactant-EEG formulations can be attributed to the variable lipid-protein compositions that make up the commercial suspensions. It was observed that Curosurf-EEG showed the most deviation from DPPC-EEG powders as it was shifted the furthest right (increased particle size). The Curosurf-EEG powders also showed a bimodal profile, which was suggested by the larger observed span (Table 3.16). The Survanta-EEG formulation was found to be the most comparable to the DPPC-EEG formulation.

Since the commercial surfactant-EEG formulations were observed to have larger Dv50 values and lower particle fractions compared to the DPPC-EEG formulation, the commercial-EEG formulations were not expected to exhibit similar aerosol performance. Therefore, aerosol performance was only determined for the best and worst commercial-EEG formulations, Survanta-EEG and Curosurf-EEG, respectively.

Table 3.16 Comparison of primary particle size characteristics of DPPC-EEG formulation with commercial surfactant-EEG formulations. Values are mean (SD), n=3.

Formulation [‡]	Dv50, µm	Particle fraction, %		Span
		<1 µm	<5 µm	
DPPC-EEG, formulation 3	1.03 (0.02)	47.9 (1.4)	99.7 (0.4)	1.5 (0.0)
Curosurf-EEG	1.82 (0.12)*	24.3 (1.7)*	87.1 (1.7)*	2.9 (0.2)*
Infasurf-EEG	1.60 (0.00)*	26.5 (0.1)*	95.3 (1.0)*	2.0 (0.1)*
Survanta-EEG	1.19 (0.01)*	39.3 (0.3)*	96.2 (0.5)*	1.9 (0.0)*

[‡]Statistically significant effect of formulation; one-way ANOVA, $p < 0.05$

*Significant difference compared to DPPC-EEG formulation 3; Dunnett's method, $p < 0.05$

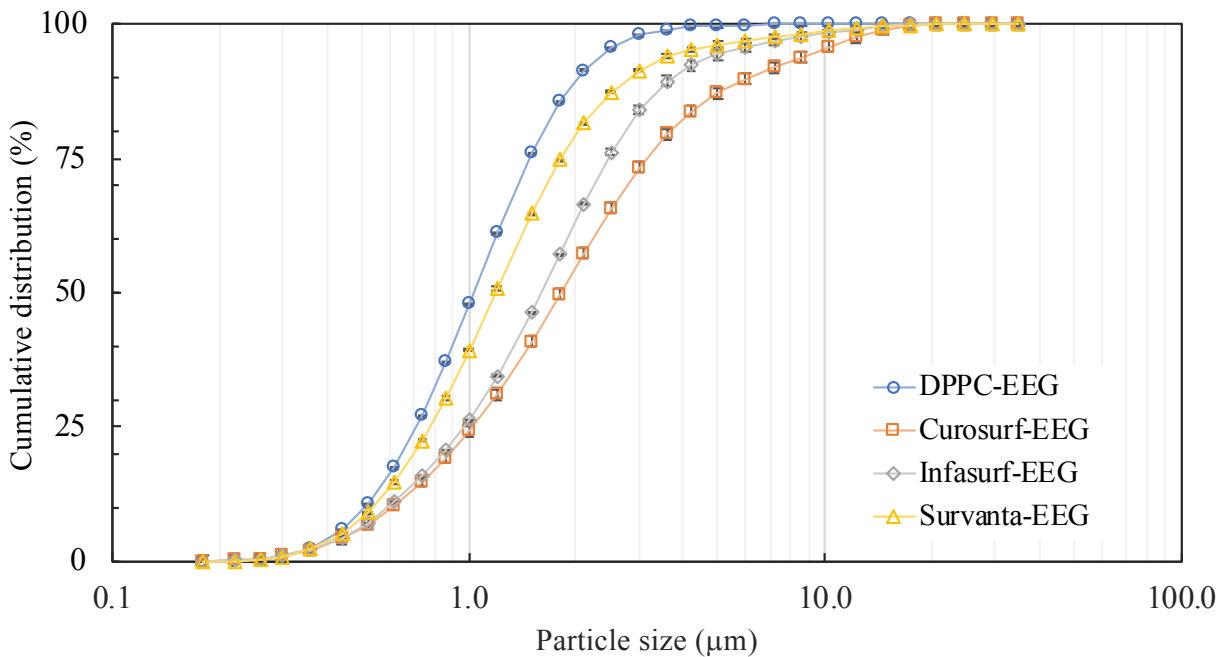
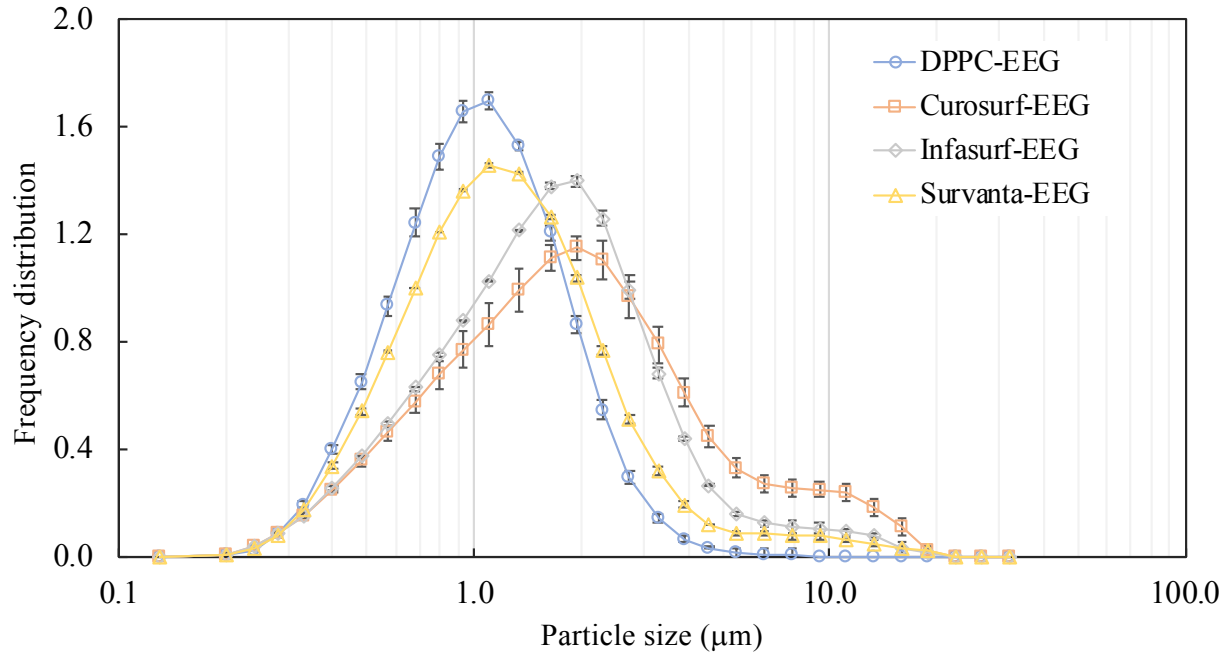


Figure 3.8 Particle size distribution comparisons for commercial surfactant-EEG powders with DPPC-EEG formulation 3 determined on the Sympatec HELOS with RODOS dispersion pressure of 3.0 bar. Markers represent the mean value, error bars represent the SD, n=3.

3.3.4.3 Aerosol performance of commercial surfactant-EEG formulations

The aerosolization properties of Curosurf-EEG and Survanta-EEG powders were determined using the NGI and an Aerolizer DPI operating a flow rate of 80 L/min for 3 s. The aerosol characteristics are shown in Table 3.17 with the optimal DPPC-EEG formulation for comparison. Although the EEG formulations prepared with commercial surfactant showed good emptying, emitted dose values of greater than 80% of the nominal dose, the MMAD values were larger and the particle fractions were lower than those observed with the optimal DPPC-EEG formulation.

One-way ANOVA revealed significant differences in the MMAD particle fractions less than 1 μm and 5 μm ($p=0.0003$, $p<.0001$, $p<.0001$, respectively). Dunnett's method for post-hoc analysis determined that the Curosurf-EEG formulation resulted in a significantly larger MMAD compared to the DPPC-EEG formulation ($p=0.0003$). The MMAD for the Survanta-EEG formulation was not significantly different from the DPPC-EEG formulation. Both spray dried commercial surfactant formulations were observed to have significantly lower particle fractions less than 1 μm when compared to DPPC-EEG powders (Curosurf-EEG: $p<.0001$, Survanta-EEG: $p=0.0003$; Dunnett's method). Similarly, the particle fractions less than 5 μm for Curosurf-EEG and Survanta-EEG powders were observed to be significantly lower when compared to DPPC-EEG powders ($p<.0001$ and $p=0.0030$, respectively; Dunnett's method). No differences were found in the GSD values for the three formulations.

Table 3.17 Comparison of aerosol performance of DPPC-EEG formulation with spray dried commercial surfactant-EEG powders. Values are mean (SD), n=3.

Formulation [‡]	Emitted dose, %	MMAD, μm	Particle fraction, %		
			<1 μm	<5 μm	GSD
DPPC-EEG, formulation 3	68.2 (2.0)	1.61 (0.02)	12.2 (0.2)	60.4 (0.4)	1.8 (0.0)
Curosurf-EEG	80.0 (13.0)	3.32 (0.43)*	0.5 (0.0)*	16.0 (0.6)*	1.9 (0.1)
Survanta-EEG	81.4 (2.6)	1.91 (0.04)	7.0 (1.0)*	49.6 (4.2)*	2.0 (0.0)

[‡]Statistically significant effect of formulation; one-way ANOVA, $p < 0.05$

*Significant difference compared to DPPC-EEG formulation 3; Dunnett's method, $p < 0.05$

3.3.4.4 Surface tension of commercial surfactant-EEG formulations

Surface tension measurements of Curosurf-EEG and Survanta-EEG powders were performed with a target phospholipid concentration of 1.5 mg/mL to obtain a measurable decrease in surface tension. Measurements were also performed on the original commercial suspension formulations for comparison. The surface activity data are shown in Table 3.18. The mean \pm SD final surface tension of Curosurf-EEG powders was determined to be 31.4 ± 2.1 mN/m, which was determined to be significantly higher than the final surface tension of the commercial Curosurf[®] formulation of 23.2 ± 0.3 mN/m ($p = 0.0023$; Student's t-test). However, the surface tension reduction rates of the two formulations were not significantly different, an indication that the surfactant activity was retained following formulation processing.

For Survanta-EEG powders and the Survanta[®] commercial formulation, the mean \pm SD final surface tension values were 33.0 ± 1.5 mN/m and 29.9 ± 5.5 mN/m, respectively. The surface tension reduction rates were 0.73 ± 0.16 and 0.58 ± 0.07 mN/m/s for Survanta[®] and Survanta-EEG formulations, respectively. There were no significant differences observed between the Survanta formulations, which indicate that the surface tension reduction properties were retained following formulation processing.

Table 3.18 Comparison of surfactant activity for EEG formulations prepared with commercial surfactant with nominal DPPC content of 1.5 mg/mL measured at 50 °C using method 3. Values are mean (SD), n=3.

Formulation	Surface age, s	Final surface tension, mN/m	Surface tension reduction rate, mN/m/s
Curosurf [®]	61.7 (6.5)	23.2 (0.3)	0.63 (0.10)
Curosurf-EEG	57.2 (6.1)	31.4 (2.1)*	0.57 (0.07)
Survanta [®]	59.0 (13.1)	29.9 (5.5)	0.73 (0.16)
Survanta-EEG	65.6 (1.3)	33.0 (1.5)	0.58 (0.07)

*Significant difference compared to Curosurf[®]; Student's t-test, $p < 0.05$

Comparisons of the tensiograms for the EEG powder formulations with the commercial replacement suspension formulations are shown in Figure 3.9. The profiles for all formulations show a decrease in surface tension with increasing surface age. Curosurf[®] was observed to reach lower surface tension values at younger surface ages compared to Survanta[®], which may be due to the higher concentration of lipids and proteins in Curosurf[®]; at a concentration of 1.5 mg/mL DPPC, an estimated 3.8 mg of phospholipids were present in the Curosurf[®] sample compared to 2.8 mg of phospholipids in Survanta[®] sample based on the label claim. The shape of the Survanta[®] surface tension profile was observed to be similar to that found in literature (Figure 3.1), which had an estimated surface tension reduction rate of 0.83 mN/m/s.

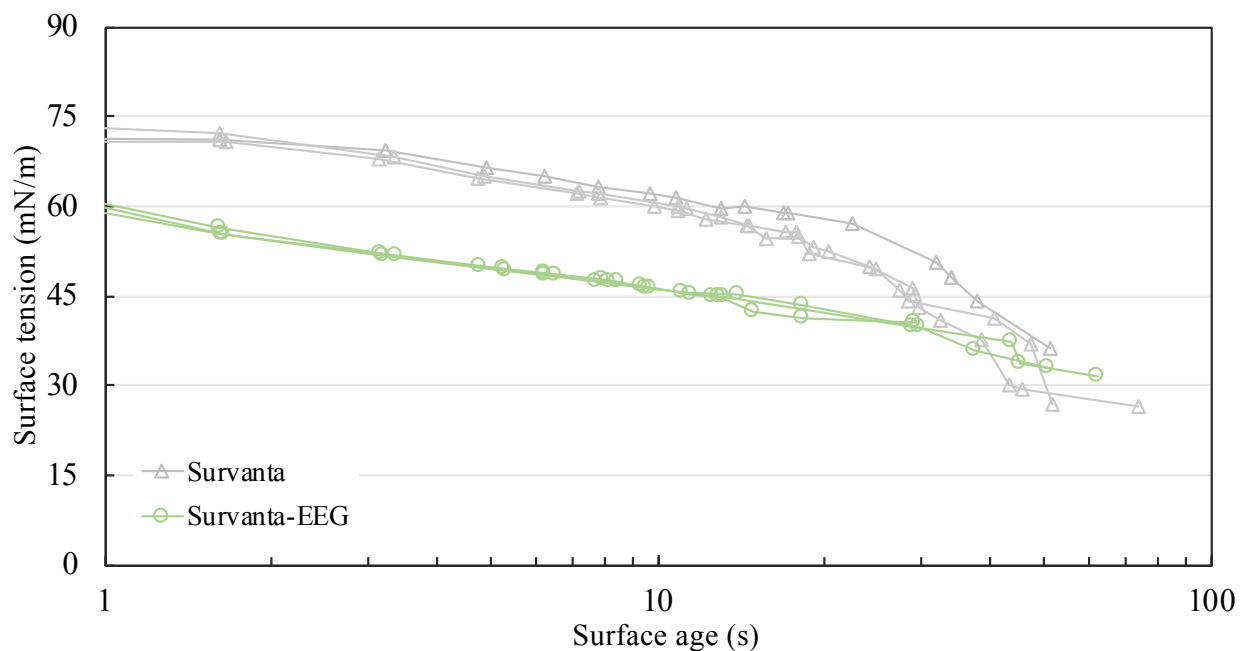
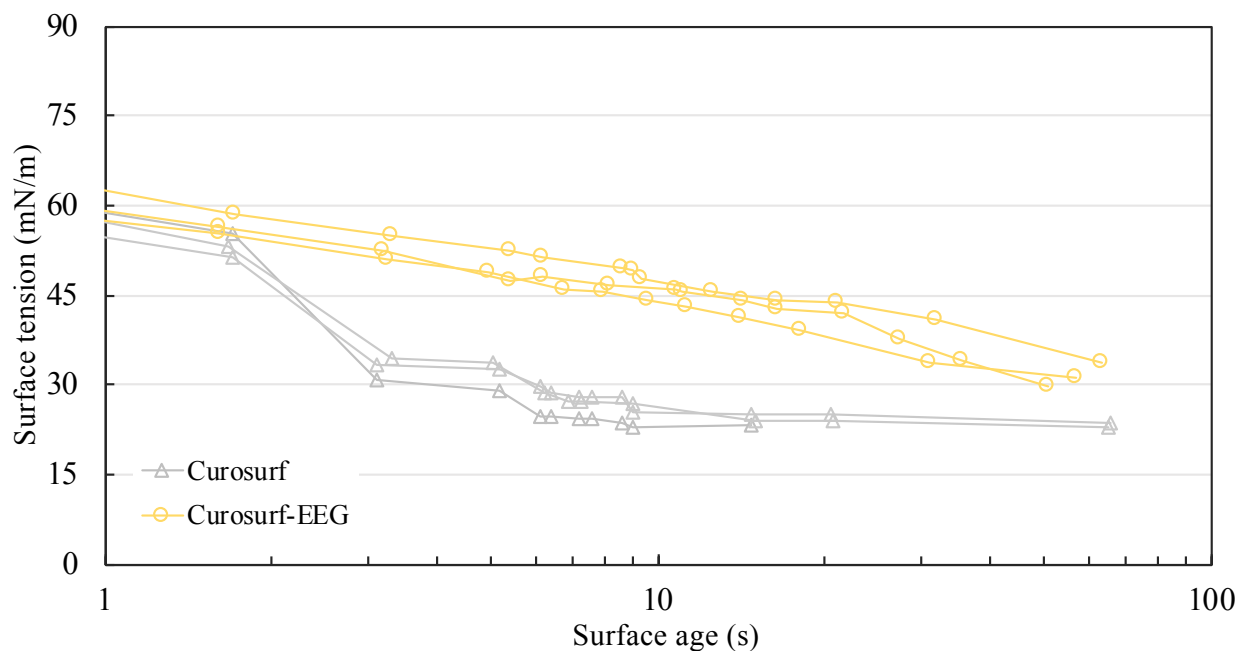


Figure 3.9. Surface tension activity comparison of commercial replacement surfactant formulations with EEG powder formulations of Curosurf[®] (top) and Survanta[®] (bottom) with nominal DPPC content of 1.5 mg/mL measured at 50 °C using method 3. Markers represent individual values.

The surface tension values determined for the different formulations were in agreement with the predictions made from Equation 3.8 (predicted surface tension of 28.5 mN/m with 1.5 mg/mL DPPC), based upon the changes expected for DPPC alone in the spray dried formulation as the surface-active agent, despite the presence of other formulation lipids and proteins. However, the commercial surfactant EEG formulations were observed to have different tensiometer profiles than observed for the DPPC-EEG formulations (Figure 3.10). The surface tension activity in both commercial surfactant EEG formulations were observed to be higher (lower surface tension values) at younger surface ages than those observed with unprocessed DPPC, likely due to the presence of proteins and other lipids in the formulation of the commercial surfactants. An evaluation of the integrity of the surfactant proteins in the spray dried formulation was performed and is described in Chapter 7.

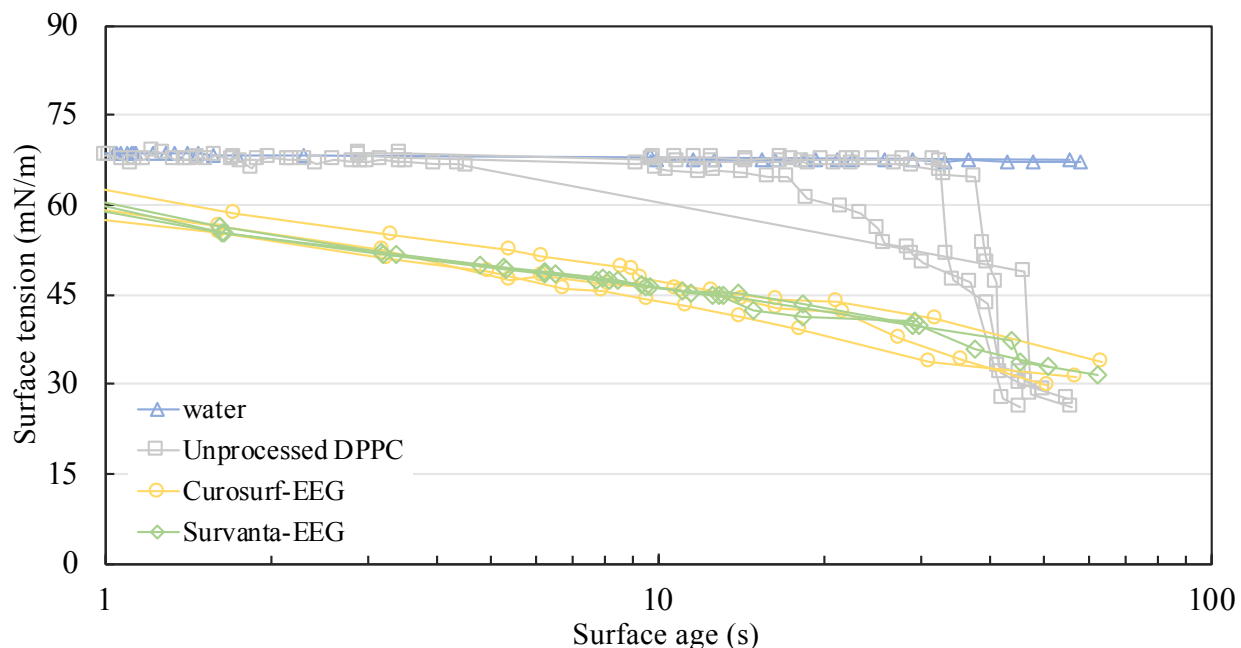


Figure 3.10 Surface tension activity comparison of unprocessed DPPC (squares) with commercial surfactant EEG powder formulations of Curosurf (circles) and Survanta (diamonds) with nominal DPPC content of 1.5 mg/mL measured at 50 °C using method 3. The surface activity of water is also shown for comparison. Markers represent individual values.

3.4 Conclusions

This study developed methods to reliably produce DPPC-EEG formulations (Specific aim 1-1), which were used to investigate the effect of spray drying factors (percent solids concentration in the feed dispersion, ratio of hygroscopic excipients, percent of ethanol in the feed dispersion and inlet drying temperature of the spray dryer) on the powder characteristics, the aerosol performance and the surfactant activity (Specific aim 1-2). DPPC-EEG spray dried powders were observed to be most influenced by the percent solids concentration in the feed dispersion, where the lower solids concentration of 0.125% w/v resulted in a smaller primary particle size, a higher primary particle fraction less than 1 μm , and a smaller MMAD than powders produced with a solids concentration of 0.250% w/v. The optimal processing parameters to produce DPPC-EEG powders were determined as follows: a percent solids concentration of 0.125% w/v in the feed dispersion, a ratio of mannitol-to-sodium chloride of 3:1, a percent ethanol concentration of 5% v/v in the feed dispersion and an inlet drying temperature of 70 $^{\circ}\text{C}$.

The parameters determined for optimal DPPC-EEG powder production were employed for EEG formulations with commercial replacement surfactants. Overall, the commercial surfactant EEG formulations were found to have a larger primary particle size, lower primary particle fraction less than 1 μm and 5 μm , and larger span. Aerosol performance of the commercial surfactant-EEG formulations revealed poorer performance (larger MMAD, lower particle fractions less than 1 μm and 5 μm) compared to that of the DPPC-EEG formulation. The commercial surfactant-EEG formulations were, however, shown to maintain surfactant activity following feed dispersion preparation and spray drying (Specific aim 5-1).

This study demonstrated that although optimal formulation factors and spray drying parameters were determined for production of EEG powders prepared with DPPC, the

predominant lipid component in commercial surfactants, the parameters when applied to produce EEG formulations with commercial surfactants did not produce powders with similar characteristics or aerosol performance across the range of commercial surfactant formulations evaluated. While the particle size of DPPC-EEG powders was observed to be largely influenced by the percent solids concentration in the feed dispersion, the particle size or dispersibility of the commercial surfactant-EEG formulations were determined by other formulation factors. The formulation factors and spray drying parameters determined for the production of DPPC-EEG powders provided only a basis for the development of EEG formulations with commercial surfactants, as the complex mixture of lipids and proteins of the replacement formulations require additional optimization. The Survanta-EEG formulation was observed to be most comparable to the DPPC-EEG formulation with respect to powder characteristics and aerosol performance, therefore further optimization with this formulation was studied as described in the following chapter.

CHAPTER 4
DETERMINATION OF THE EFFECT OF DISPERSION ENHANCERS AND
SPRAY VEHICLE ALCOHOL CONCENTRATION ON THE DISPERSIBILITY OF
EEG POWDERS PREPARED WITH COMMERCIAL REPLACEMENT
SURFACTANTS

4.1 Introduction

The previous chapter described methods developed for the reliable production of EEG powders with DPPC. The developed methods were applied to commercial surfactant formulations but were found to not perform as well as the DPPC-EEG powders; the commercial surfactant EEG formulations had larger MMAD values and higher fine particle fractions. EEG powders produced with the commercial surfactant formulation Survanta[®] were observed to perform most comparable to the DPPC-EEG powder and thus selected for further optimization.

When developing a drug formulation for inhalation, a primary consideration is ensuring that the aerosol generated has particles in the 1 to 5 micrometer size range to ensure deposition in the small airways and alveoli of the lungs. Powder formulations produced by spray drying are capable of generating particles in this size range, but the small size of the particles results in increased cohesive forces leading to agglomeration of the powder that requires effective dispersion to a primary particle aerosol during drug delivery. The need to generate a well dispersed aerosol for effective drug delivery is the main obstacle with delivering dry powders for inhalation.

Particle dispersion efficiency is affected by many factors, mainly, powder formulation and DPI design. These factors can be controlled to optimize powder dispersion for enhanced drug delivery to the lungs. For the powder formulation, the incorporation of excipients can be used to

improve the dispersion. Leucine and trileucine have been shown to reduce agglomeration of spray dried powders, therefore effectively enhancing dispersibility of the powder formulations [95, 138, 139]. The surface-active nature and low solubility of leucine and trileucine in ethanol/water co-solvent systems is hypothesized to produce corrugated shells that encapsulate the other components in the formulation [95]. The corrugated surface of the dried particles reduces the surface area available for particle-particle interaction and thus, reduces agglomeration.

In this study, the aim was to develop and characterize dry powder pulmonary surfactant formulations that would be used for the treatment of neonatal RDS during non-invasive ventilation. The specific objectives included exploring the use of leucine or trileucine as the dry powder dispersion enhancer combined with the commercially available natural surfactant formulation, Survanta[®] intratracheal suspension, to produce spray dried powders using the EEG application, and evaluation of the aerosol performance of the EEG powders with a novel DPI. Survanta[®] intratracheal suspension is a natural bovine lung extract suspended in 0.9% sodium chloride with 25 mg/mL of phospholipids – dipalmitoylphosphatidylcholine (DPPC) and 1-palmitoyl-2-oleoyl-*sn*-glycero-3-phosphoglycerol (POPG) are the two main lipid components, making up 44-62% and 13-45% of the total formulation, respectively [30, 100]. Mannitol was selected as the hygroscopic excipient in addition to the sodium chloride present in the commercial surfactant formulation.

4.2 Materials and methods

4.2.1 Materials

Survanta[®] (beractant) intratracheal suspension was purchased from Cardinal Health, Inc. (Greensboro, NC) and stored at 2-8 °C. Pearlitol[®] PF-mannitol was donated from Roquette Pharma (Lestrem, France). L-leucine was purchased from Sigma Chemical Co. (St Louis, MO). Trileucine was purchased from Fisher Scientific Co. (Hanover Park, IL) and stored at -20 °C.

4.2.2 Feed dispersion preparation

The previous chapter described the use of probe sonication to prepare DPPC-EEG dispersions for spray drying. Direct sonication of samples results in higher effective energy output into the suspension and consequently shorter preparation time, however this requires an additional processing step. During direct sonication titanium particles are detached from the probe tip and contaminate the feed dispersion. An additional centrifugation step following sonication was employed, however it did not adequately separate the titanium particles, therefore, dispersions with Survanta[®] were prepared via indirect sonication methods.

Feed dispersions for spray drying were prepared by heated bath sonication (Fisher Scientific[™] CPXH, Hanover Park, IL) with the aim of producing homogenous dispersions to ensure uniform spray dried particles. All formulations contained mannitol and sodium chloride in a 3:1 ratio with a dry powder dispersion enhancer (leucine or trileucine) at a concentration of 20% w/w. Approximately 27% w/w of phospholipids (including approximately 14% w/w DPPC) were included in each formulation based on the Survanta[®] label claim [30] as 0.014 mL of Survanta was added per mL of dispersion feed solution.

Excipients (mannitol and leucine/trileucine) were accurately weighed and dissolved in the spray vehicle (5 or 20 % v/v ethanol in water) followed by addition of Survanta[®] resulting in a total solids concentration of 0.125% w/v. Feed dispersions were sonicated for a minimum of 40 minutes. The water bath was set to 60 °C, which resulted in a feed dispersion temperature of 55-58 °C. This elevated temperature was used to ensure that sonication was performed >10 °C above the transition temperature of Survanta[®] to disrupt the order of the lipid bilayers, ideally allowing for homogenous incorporation of the added excipients, then reorganization of the bilayers, which theoretically occurs when the temperature returns below the main transition temperature [17, 100].

4.2.2.1 Stability of feed dispersions

The zeta potentials of the feed dispersions were measured to assess its suspension stability. High absolute zeta potential values lead to repulsion between particles, which can prevent aggregation and is thus used as a measure of dispersion stability. The zeta potentials (ζ) of the feed dispersions were determined using dynamic light scattering (Zetasizer Nano S, Malvern Instruments, Ltd., Worcestershire, UK). The mean particle sizes (z-Ave) and estimates of the width of the distribution (polydispersity index, PDI) were also determined by dynamic light scattering.

For zeta potential and sizing analysis, appropriate cuvettes were filled with approximately 0.5-1.0 mL of the prepared feed dispersion. All measurements were performed at 25 °C with the helium-neon laser operating at 633 nm set for backscatter detection. The test material was set as phospholipids (refractive index: 1.450, absorption coefficient: 0.001) and the dispersant set as water (refractive index: 1.330, viscosity: 0.887 cP, dielectric constant: 78.5). Zeta potential values were calculated using the Smoluchowski approximation for samples in aqueous media. Intensity-weighted mean particle sizes and polydispersity values were estimated from cumulants analysis. All measurements were performed in triplicate.

4.2.3 Spray dried powder formation

Powders were formed using the Nano Spray Dryer B-90 HP (Büchi Labortechnik AG, Flawil, Switzerland) using the open-loop configuration for aqueous applications. The HP model incorporates a modified spray head for use with redesigned atomizers for more efficient spray drying compared to the spray meshes in the previous design (Nano Spray Dryer B-90), which were used to prepare the DPPC-EEG formulations described in the previous chapter. More efficient spray drying was reported to be achieved with an increased spray mesh diameter and an increased

spray frequency; the previous design operated at a fixed frequency of around 60 kHz [140] whereas the HP model has a controllable range of 80-140 kHz [96]. The spray drying parameters are listed in Table 4.1.

Table 4.1 Spray drying parameters to produce Survanta-EEG powders.

Spray drying parameter	Setting
Inlet temperature	70 °C (outlet temperatures of 37-41 °C)
Drying gas flow	120 L/min (chamber pressure of 40-42 mbar)
Spray frequency	120 kHz
Pump speed	3%
Spray percentage	80%

A characteristic feature to the Nano Spray Dryer allowed for bypass flow in the spray head. Any excess feed dispersion that was not atomized by the spray mesh could be collected in a separate vessel or recycled back into the original feed stock container. In general, recycling of the surfactant feed dispersions was avoided to ensure uniform dispersion feed concentrations were maintained throughout the spray drying process. Preliminary studies with the HP model spray dryer found that a pump speed of 3% and a spray setting of 80% were ideal to prevent excess dispersion feed being presented to the spray head and therefore minimized amount of feed dispersion that was bypassed without considerably extending the spray drying time. During spray drying, feed dispersions were continuously mixed using a stir bar and stir plate and kept cool with ice packs. Preparations were spray dried in small batches of feed dispersion with the remainder kept in a refrigerator (2-8 °C). The feed dispersion bypass volume and total spray drying time was recorded for each run.

Powders were collected from the electrostatic precipitator and stored in tared glass vials. Percent powder yield was calculated from the mass of powder collected using Equation 4.1. Powders were stored in a desiccator in the refrigerator when not in use.

$$\text{Powder yield, \%} = \frac{\text{powder mass collected, mg}}{\text{conc solids in dispersion, } \frac{\text{mg}}{\text{mL}} * \text{volume of dispersion spray dried, mL}} \times 100$$

Equation 4.1

4.2.4 Particle size characterization

The primary particle size distribution of each formulation was determined by laser diffraction using the Sympatec HELOS with RODOS/M disperser and ASPIROS sample feeder as described in the previous chapter. Sample vials were filled with 3 to 4 mg of powder, capped and placed into the ASPIROS sample feeder set to 60 mm/sec. The RODOS/M used compressed air to disperse the powders which for these studies was set to either 1.0 and 4.5 bar. The minimum C_{opt} was set to 2.1%. Data were collected over a measurement duration of 10 seconds. All measurements were performed in triplicate. Volume-based size distributions for each of the dispersion pressures (1.0 and 4.5 bar) were calculated by WINDOX software using the Fraunhofer theory. The particle size below which 10%, 50% and 90% of the powder distribution lies (D_{v10} , D_{v50} , and D_{v90} , respectively) was determined. The span of the PSD was calculated using Equation 4.2. The percent of particles having a diameter less than 1 μm and 5 μm ($D_{v<1 \mu\text{m}}$ and $D_{v<5 \mu\text{m}}$, respectively) was obtained from the Sympatec software.

$$Span = \frac{Dv90 - Dv10}{Dv50} \quad \text{Equation 4.2}$$

4.2.5 DPPC content analysis

The DPPC concentration was determined by LC-MS as described in the previous chapter. For DPPC content analysis of feed dispersions, 250 μ L of the dispersion was aliquoted into a 10 mL volumetric flask and then Q.S. to volume with methanol. For the spray dried formulations, approximately 1.1 mg of spray dried powder was dissolved in 25 mL of methanol using sonication for 20 seconds. The percent DPPC content was calculated by assessing the amount of drug in the spray dried powder and using Equation 4.3.

$$DPPC \text{ content, \%} = \frac{\text{Assayed amount of DPPC in spray dried powder, mg}}{\text{Mass of spray dried powder for assay sample, mg}} \times 100 \quad \text{Equation 4.3}$$

4.2.6 Aerosol performance of leucine powder formulation

4.2.6.1 Modified low-volume dry powder inhaler

A DPI designed to use a low volume of air (10 mL) to deaggregate and deliver dry powder aerosol was developed at the VCU School of Engineering by Farkas et al. [141]. As described in the following chapter, the low air volume DPI (LV-DPI) was modified to operate for use with a smaller volume of air (3 mL) with the intention of using it for intratracheal administration of dry powder to small animal models and eventually for use in very low birth weight infants. The outlet of the modified LV-DPI used in this study attached directly to a 12.7 mm long, 14-gauge catheter which could be inserted through an incision in the trachea. The device consists of two parts: 1) an inlet body that contains three 0.60 mm holes with a commercial luer lock connection, and 2) an

outlet body, that contains a 0.89 mm hole extending to a 19 gauge extra-thin-walled capillary needle (internal diameter = 0.89 mm) with a length of 55 mm (extended to the end of the catheter) when measured from the outer o-ring of the device (Figure 4.1). The DPI was constructed using rapid prototyping (Object24 printer, Stratasys Ltd., Eden Prairie, MN) with a rigid opaque photopolymer, VeroWhitePlus (RGD835). When assembled, the interior volume (dose containment unit or powder chamber) of the device measures 0.21 mL.

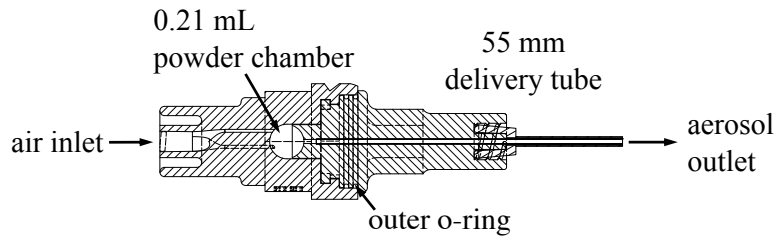


Figure 4.1 Axial cross-section view of the assembled modified containment unit DPI with 55 mm delivery tube length. Inlet body (▨) and outlet body (▩) portions differentiated by fill pattern.

4.2.6.2 Malvern Spraytec[®] aerosol characterization

The particle size distribution of the aerosol exiting the device was determined by laser diffraction using a Malvern Spraytec[®] (Malvern Instruments, Ltd., Worcestershire, UK). All measurements were performed using the 100 mm focal length lens, which has a Dv50 size range of 0.5-200 μm , with the following settings: 98% transmission (2% obscuration), media refractive index of $1.00 + 0.00i$ (air) and particulate refractive index of $1.50 + 0.50i$ (opaque). A background reading was taken prior to each measurement. Applying Mie scattering theory, the RTSizer software reported data as Dv50, the 50% cumulative volume undersize. The particle fraction data

was calculated from the Spraytec[®] size results based on the percent of particles having a diameter less than 1 μm and 5 μm .

A representative time history profile plot of the transmission and Dv50 values of the aerosol plume captured by the Spraytec[®] is shown in Figure 4.2. The % transmission gives an indication of the density of the aerosol plume, with a lower transmission indicating a denser plume as less of the laser light source is able to reach the detector. The % transmission is measured every 0.4 ms and is plotted as a function of time. Similarly, a particle size distribution measurement was also made every 0.4 ms and the measured median volume diameter at each time point was plotted and labelled as Dv50 in Figure 4.2. For data analysis the average Dv50 is calculated over the entire run. Figure 4.2 shows an approximately 500 ms spray duration.

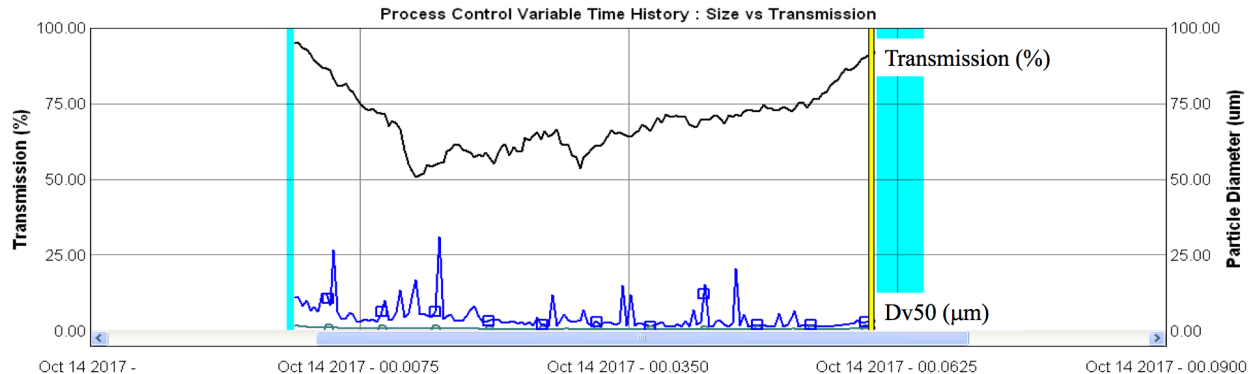


Figure 4.2 Representative time history plot for the aerosol plume of Survanta-EEG powder generated with the modified containment unit DPI using 3 mL volume of dispersion air as captured by the Malvern Spraytec[®].

4.2.6.3 Emitted mass determination

The emitted mass for the modified containment unit DPI was determined by gravimetric analysis. Powder was first weighed to determine the initial powder fill mass and then manually

filled into the inlet body of the device. Once assembled, the device with powder was weighed to determine mass of loaded device. A 5 mL syringe was filled with room air to 3 mL and connected to the luer-lock inlet of the DPI. The device with syringe was mounted in a horizontal position to a fixed stand so that the tip of the device outlet was 5 cm from the middle of the laser beam. The powders were dispersed by manual compression of the syringe, which occurred in approximately 0.12 ± 0.01 seconds, as determined using a Photron PCI R2 high-speed camera to capture images at 1000 frames per second with Photron FASTCAM Viewer software to analyze the images. This results in a short burst at an airflow rate of approximately 1.6 L/min. The syringe was then disconnected from the DPI and the device was reweighed to determine the mass of device after actuation. Measurements were repeated for up to three actuations. The percent of powder mass emitted was calculated from the initial mass loaded into the device using Equation 4.4.

$$\text{Emitted mass, \%} = \frac{(\text{mass of loaded device} - \text{mass of device after actuation}), \text{ mg}}{\text{initial powder fill mass, mg}} \times 100$$

Equation 4.4

4.2.7 Spray dried powder analysis

4.2.7.1 Scanning electron microscopy

The morphology of the powders was examined using a scanning electron microscope, SEM (Carl ZEISS EVO 50XVP, Carl Zeiss AG, Germany). Samples were prepared on SEM specimen mounts using double-sided tape and then coated with gold grain in a sputter coater (EMS550X, Electron Microscopy Sciences, Hatfield, PA). Samples were viewed under high vacuum mode and an accelerating voltage of 15 kV at magnifications of 19,000 to 21,000 with a specimen working distance of 9 mm.

4.2.7.2 Solid state powder characteristics

Spray drying produces powders with low-moisture content, which was verified by TGA. TGA was performed using the Pyris 1 TGA with TAC 7/DX Thermal Analysis Controller as described in the previous chapter. Powder samples weighing 1 to 2 mg were heated from 25 °C to 100 °C while under a nitrogen purge at 40 mL/min. The % moisture content was determined by the stable weight loss (%) following an isothermal hold at 100 °C.

The main transition temperature of the spray dried powders was determined by differential scanning calorimetry (DSC) using the DSC 7 (PerkinElmer, Covina, CA) with a TAC 7/DX Thermal Analysis Controller. Sample masses of 1 to 2 mg of spray dried powder were filled into tared aluminum DSC pans and hermetically sealed. In addition, the commercial suspension was also dried in a sample pan in an oven set to 50 °C to obtain 1 to 2 mg of sample. These samples were analyzed by heating from 25 °C to 100 °C at a rate of 5 °C/min with a 20 mL/min nitrogen purge gas.

4.2.8 Statistical analysis

Data analysis was performed using JMP[®] Pro software version 12.0 (SAS Institute Inc., Cary, NC). Student's t-statistic or one-way analysis of variance (ANOVA) followed by Tukey's HSD was performed to determine statistically significant differences in the data obtained. The Pearson correlation coefficient was determined to quantify the strength of linear relationships. *P* values less than 0.05 were considered as statistically significant.

4.3 Results and discussion

4.3.1 Effect of bypass flow on feed dispersion DPPC content

Preliminary experiments studied the effect of feed dispersion recycling on its DPPC content. Feed dispersions were prepared with Survanta[®], mannitol and trileucine in a 5% v/v ethanol in water spray vehicle and sonicated for 40 minutes. The spray drying bypass dispersion was collected into a separate vessel following each pass across the spray head and assayed for DPPC (Figure 4.3). HPLC analysis of the DPPC content of the Survanta formulation allowed an estimated DPPC content in the feed dispersion following the addition of Survanta to be made of 0.16 mg/mL DPPC. Analysis and assay of the initial feed dispersion revealed that the mean \pm SD measured DPPC content was 0.17 ± 0.01 mg/mL. From the initial concentration to the third bypass cycle, there is a gradual increase in the DPPC content in the feed dispersion with each pass across the spray head; the mean \pm SD DPPC concentration after the third cycle was 0.20 ± 0.01 mg/mL. This gradual increase is likely due to the evaporation of the spray vehicle, concentrating the remaining solids. Due to the inability to control the relative proportions of feed dispersion that were bypassed and were sprayed, dispersions for spray drying were not recycled in order to ensure that a uniform feed dispersion was introduced to the spray head throughout the spray drying process.

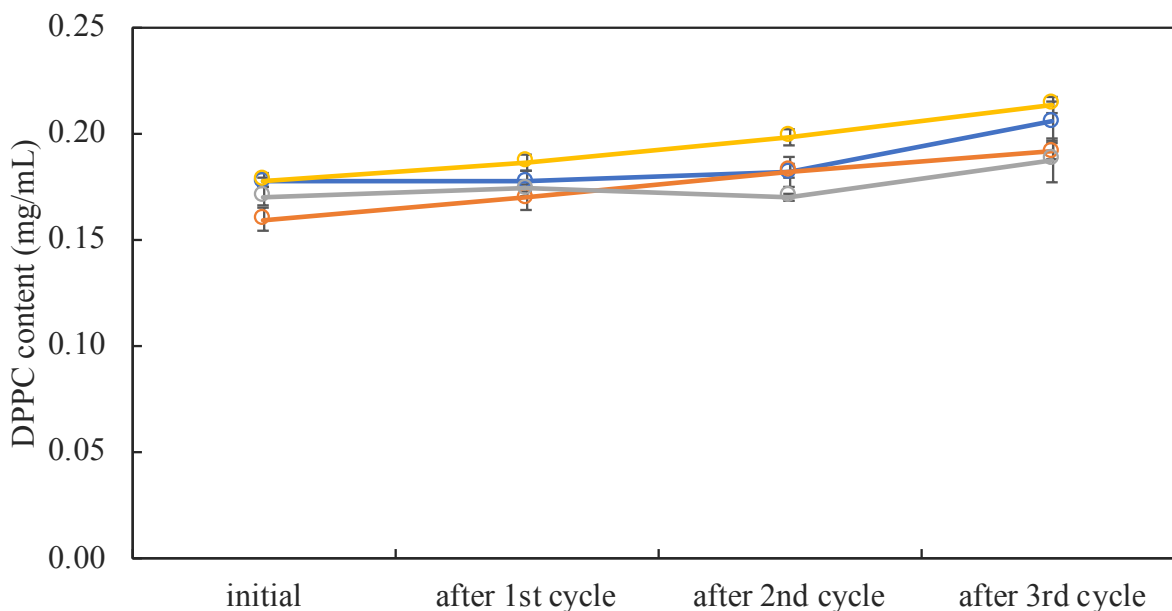


Figure 4.3 DPPC content in replicate runs of recycled dispersions of Survanta-EEG formulations with trileucine in 5% v/v ethanol in water spray vehicle. Markers represent the mean value, error bars represent the SD, n=3.

4.3.2 Effect of sonication time on feed dispersion and spray dried powder characteristics

The effect of sonication time on feed dispersion characteristics and the particle size distribution of the spray dried powders were explored (Table 4.2). Feed dispersions with Survanta[®], mannitol and trileucine in a 5% v/v ethanol in water spray vehicle were sonicated for 40, 75 and 100 minutes. Feed dispersion characteristics were determined with the Malvern Zetasizer. The dispersions produced at the different sonication times were all shown to have zeta potential values more negative than -30 mV, the threshold value for stability, indicating stable dispersions. Determination of the Pearson correlation coefficient found that there was a significant positive correlation of sonication time with the zeta potential of the feed dispersion ($r = 0.8650$, $p=0.0026$, $R^2 = 0.7481$), where an increase in sonication time resulted in more stable dispersions.

Spray drying of the feed dispersions resulted in spray rates of 0.23-0.29 mL/min and powder yields of 65-69%. Assay of the DPPC content in the Survanta[®] formulation allowed the calculation of a theoretical DPPC concentration of $12.5 \pm 1.4\%$ w/w in the powder formulation. The experimental DPPC content in the spray dried powders was determined to be 12.2-13.8% w/w for the spray dried powders, 98-110% of the theoretical value. Sonication time was not found to have an effect on the primary particle size characteristics or DPPC content of the spray dried powders. Although the sonication time was found to have a significant correlation with the stability of the feed dispersion, this was not reflected in the content uniformity data of the spray dried powders; powders produced following 40 minutes of sonication were found to be less variable than powders produced following 100 minutes of sonication (Table 4.2). All powders were observed to have a mean volume diameter of about 1 μm with over 40% of the particles $<1 \mu\text{m}$. Future studies prepared feed dispersions with 40 minutes of sonication to minimize preparation time.

4.3.3 Effect of spray atomizer size on particle size distribution

The redesigned spray atomizers used in the Nano Spray Dryer B-90 HP were produced in three sizes: small, medium and large. The effect of the spray atomizer size on the particle size of surfactant powders was studied. Feed dispersions for spray drying were prepared with Survanta[®], mannitol and trileucine in a 5% v/v ethanol in water spray vehicle. The powder yields ranged from 64-70% w/w. As expected, the spray rate increased with increasing atomizer size – 0.26, 0.34 and 0.44 mL/min for the small, medium and large spray atomizer sizes, respectively (Table 4.3). The primary particle size of each powder formulation was determined by laser diffraction using the Sympatec HELOS with RODOS dispersion pressure of 4.5 bar. The mean primary particle D_{v50} values and the fraction of particles $<1 \mu\text{m}$ were not affected by the spray atomizer size; however,

the span and fraction of particles $<5 \mu\text{m}$ were significantly affected by the spray atomizer size ($p=0.0296$ and $p=0.0338$, respectively; one-way ANOVA). The powders prepared with the large spray atomizer had a significantly smaller span ($p=0.0248$; Tukey's HSD) and significantly higher fraction of particles $<5 \mu\text{m}$ ($p=0.0343$; Tukey's HSD) compared to the powders prepared with the small spray atomizer.

The modified containment unit DPI (Figure 4.1) was used to determine the aerosol performance of the spray dried powders produced from the different spray atomizer sizes. A nominal fill mass of 5 mg of spray dried powder was used and the aerosol performance was determined using the Malvern Spraytec[®]. The mean aerosol $Dv50$ values, particle fraction $<1 \mu\text{m}$ and particle fraction $<5 \mu\text{m}$ were not found to be significantly affected by the spray atomizer size; however the powders produced with the medium size spray atomizer were observed to have the smallest aerosol $Dv50$ value ($2.6 \mu\text{m}$) with the highest particle fractions (28% $<1 \mu\text{m}$ and 57% $<5 \mu\text{m}$, Table 4.3). Thus, powder formulations were prepared using the size medium spray atomizer in future studies.

Table 4.2 Effect of sonication time on feed dispersion characteristics (Malvern Zetasizer) and primary particle size characteristics (Sympatec HELOS with RODOS dispersion pressure of 4.5 bar). Values are mean (SD), $n \geq 3$.

Sonication time, min	Feed dispersion			Spray dried powder				
	z-Ave, nm	PdI	ζ , mV [‡]	Primary particle Dv50, μm	Span	Particle fraction, %		DPPC content, % w/w
						<1 μm	<5 μm	
40	154 (3)	0.36 (0.04)	-32 (1)	1.11 (0.06)	1.8 (0.3)	43.6 (2.5)	96.8 (2.8)	13.8 (0.1)
75	118 (4)	0.38 (0.01)	-35 (2)	1.07 (0.04)	1.5 (0.2)	45.7 (2.5)	99.1 (1.6)	12.2 (0.5)
100	171 (4)	0.42 (0.04)	-40 (3)	1.10 (0.06)	1.7 (0.3)	44.1 (2.6)	97.0 (2.6)	12.8 (1.0)

ζ = zeta potential

[‡]Significant correlation with sonication time; Pearson correlation, $p < 0.05$

Table 4.3 Effect of spray atomizer size on particle size characteristics: primary particle size determined on the Sympatec HELOS with RODOS dispersion pressure of 4.5 bar, aerosol performance determined on Malvern Spraytec® with the modified containment unit DPI using 5 mg powder fill mass and 3 mL volume dispersion air. Values are mean (SD), n≥3.

Spray atomizer size	Spray rate, mL/min	Primary particle size				Aerosol performance		
		Primary particle Dv50, μm	Span [‡]	Particle fraction, %		Aerosol Dv50, μm	Particle fraction, %	
				<1 μm	<5 μm [‡]		<1 μm	<5 μm
small	0.26	1.11 (0.06)	2.1 (0.3)	43.9 (1.8)	95.3 (1.4)	3.1 (0.8)	25.4 (1.8)	57.1 (3.8)
medium	0.34	1.07 (0.04)	1.9 (0.2)	41.9 (3.1)	96.6 (2.2)	2.6 (0.3)	27.9 (1.6)	57.1 (1.7)
large	0.44	1.10 (0.06)	1.5 (0.2)*	41.8 (2.2)	99.4 (1.3)*	3.3 (0.6)	24.1 (2.2)	55.7 (3.2)

[‡]Statistically significant effect of spray atomizer size; one-way ANOVA, $p < 0.05$

*Significant difference compared to small spray atomizer size, Tukey's HSD, $p < 0.05$

4.3.4 Selection of dispersion enhancer

4.3.4.1 Effect of dispersion enhancer on feed dispersion characteristics

Table 4.4 summarizes the spray drying feed dispersion characteristics determined by dynamic light scattering for the studied formulations. For the feed dispersions in 5% v/v ethanol in water, the presence of leucine resulted in significantly more stable dispersions ($\zeta = -40$ mV, $p=0.0365$; Student's t-test) than feed dispersions prepared with trileucine ($\zeta = -36$ mV). Feed dispersions prepared with leucine were also observed to have a significantly smaller mean particle size ($z\text{-Ave} = 125$ nm, $p<.0001$; Student's t-test) with higher polydispersity ($PdI = 0.48$, $p=0.0250$; Student's t-test) than the feed dispersions containing trileucine.

As with the 5% v/v ethanol in water feed dispersion, the polydispersity index was significantly higher for feed dispersions prepared with leucine than trileucine (0.60 vs 0.41) at the 20% v/v ethanol concentration ($p<.0001$; Student's t-test); however, there were no significant differences observed in the dispersion stability and mean particle size of the feed dispersions prepared in 20% v/v ethanol between the two dispersion enhancers. Dispersions prepared with a higher ethanol concentration were observed to have decreased dispersion stability (lower zeta potential values). This was expected since short-chain alcohols are known to disturb the natural microstructure of the lipid membrane by residing in the headgroup region resulting in the observed increase in disorder [142].

Table 4.4 Effect of dispersion enhancer on the zeta potential (ζ), particle size (z-Ave), and polydispersity index (Pdl) of the spray drying dispersion. Values are mean (SD), $n \geq 3$.

Ethanol concentration, % v/v	Dispersion enhancer	ζ , mV	z-Ave, nm	PdI
5	leucine	-40 (1)*	125 (2)*	0.48 (0.06)*
5	trileucine	-36 (4)	162 (10)	0.39 (0.05)
20	leucine	-22 (1)	176 (15)	0.60 (0.05)#
20	trileucine	-21 (1)	188 (9)	0.41 (0.04)

* Significant difference compared to trileucine at 5% v/v ethanol in water concentration; Student's t-test, $p < 0.05$

Significant difference compared to trileucine at 20% v/v ethanol in water concentration; Student's t-test, $p < 0.05$

4.3.4.2 Effect of dispersion enhancer on primary particle size distribution

The spray dried powders were determined to have powder yields ranging from 65 to 76 % w/w. The DPPC content of the spray dried powders were determined to range from 11 to 14 % w/w which represented values of 85 to 110% of the theoretical content assessed based on assay of DPPC content in the stock commercial surfactant, Survanta[®].

A summary of the mean particle size characteristics (Dv10, Dv50 and Dv90) of the spray dried Survanta-EEG powders are shown in Figure 4.4. Overall, the particle size of the powders was observed to be dependent on the air dispersion pressure (4.5 vs 1.0 bar) used during the primary particle analysis, with greater dispersion at the higher air dispersion pressure – the average primary particle Dv50 was approximately 0.3 μm smaller at 4.5 bar than 1.0 bar. Assuming that the results obtained at 4.5 bar represent the primary particle characteristics, the median particle diameter (Dv50) of the powders at this higher pressure are all approximately 1 μm . At the lower air dispersion pressure of 1.0 bar, powders prepared with leucine appeared to have less aggregates (low Dv90) at both ethanol concentrations compared to powders prepared with trileucine (gray

wavy fill pattern bar vs gray solid fill pattern bar in second cluster of data, Figure 4.4), although this was most pronounced at the 5% v/v ethanol in water concentration (gray solid fill bar vs gray diagonal fill pattern bar in the first cluster of data, Figure 4.4). This difference was not anticipated as trileucine has been shown to have improved dispersibility compared to leucine [143]. This unexpected observation may be explained by the presence of other surface-active components in the formulation (phospholipids in the commercial formulation) that compete for space at the air-liquid interface of the droplets exiting the spray atomizer during the spray drying process. In this scenario, the surface of the dried particle may then be more enriched with phospholipids than the dispersion enhancer and the difference observed between the dispersion enhancers is not as expected and becomes difficult to predict.

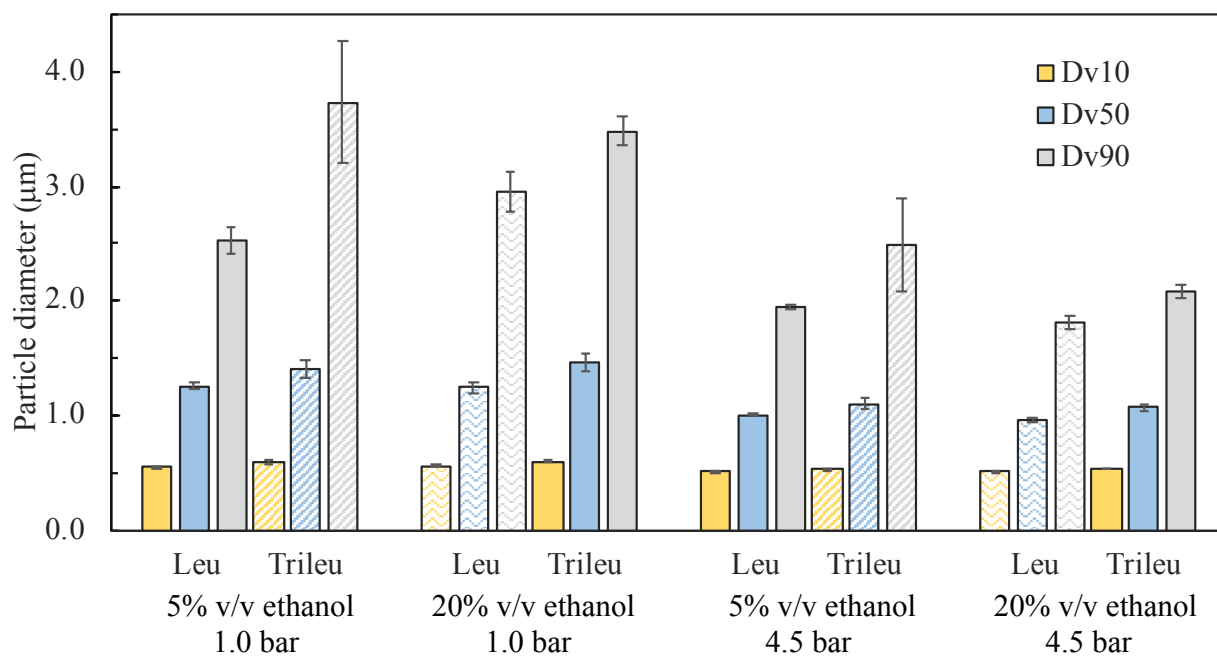


Figure 4.4 Primary particle size characteristics of spray dried Survanta-EEG powders determined on the Sympatec HELOS with RODOS dispersion pressures of 1.0 and 4.5 bar. Bars represent the mean value, error bars represent the SD, $n \geq 3$.

The choice of dispersion enhancer was shown to have a significant effect on the primary particle size (Dv10, Dv50, and Dv90), the span, and the fraction of particles less than 1 μm and 5 μm (Table 4.5). For the 5% v/v ethanol in water feed dispersions, powders prepared with leucine were observed to show a significantly lower median primary particle size (Dv50) compared to those prepared with trileucine ($p=0.0005$; Student's t-test) when characterized using 4.5 bar air dispersion pressure. However, this difference in particle size was relatively small ($\sim 0.1 \mu\text{m}$). Similarly, significant differences were also seen with other particle characterization parameters, Dv10 and Dv90 ($p=0.0002$ and $p=0.0079$, respectively; Student's t-test). Leucine powders had a smaller span (1.4 vs 1.8, $p=0.0159$; Student's t-test), a higher fraction of submicrometer particles (50 vs 44%, $p=0.0003$; Student's t-test), and a higher fraction of particles $<5 \mu\text{m}$ (100 vs 98%, $p=0.0440$; Student's t-test) when compared to trileucine powders.

Similarly, leucine powders prepared in 20% v/v ethanol in water were shown to produce significantly smaller particles (0.96 vs 1.07 μm , $p<.0001$; Student's t-test), a smaller span (1.4 vs 1.5, $p=0.0022$; Student's t-test), and a higher submicrometer particle fraction (53 vs 46%, $p=0.0001$; Student's t-test) than the powders prepared with trileucine when characterized at 4.5 bar air dispersion pressure.

Similar effects were observed when characterizing the spray dried powders at the air dispersion pressure of 1.0 bar (Table 4.6). At the 5% v/v ethanol in water concentration, powders produced with leucine were shown to have a significantly smaller median particle size compared to powders prepared with trileucine (1.26 vs 1.41 μm , $p=0.0035$; Student's t-test). The leucine powders had a smaller span (1.57 vs 2.23, $p=0.0005$; Student's t-test), a higher fraction of submicrometer particles (36.2 vs 31.8%, $p=0.0041$; Student's t-test), and a higher fraction of particles $<5 \mu\text{m}$ (99.7 vs 94.0%, $p=0.0005$; Student's t-test) when compared to trileucine powders.

At the 20% v/v ethanol in water concentration, powders produced with leucine were shown to have a significantly smaller median particle size (1.25 vs 1.46 μm , $p=0.0001$; Student's t-test) and a higher fraction of submicrometer particles (36.9 vs 30.5%, $p=0.0001$; Student's t-test) compared to powders prepared with trileucine. There was no significant difference observed in the span values and the fraction of particles $<5 \mu\text{m}$ of the leucine and trileucine powders at the 20% v/v ethanol in water concentration, 1.91 vs 1.98 and 96.7 vs 96.4%, respectively.

Dispersibility of the powders were studied by comparing the Dv90 results at RODOS dispersion pressures of 1.0 bar vs 4.5 bar for each dispersion enhancer-ethanol concentration combination. For the leucine powders prepared at 5% v/v ethanol in water concentration (solid gray bars in first and third cluster of data, Figure 4.4), the leucine powders prepared at 20% v/v ethanol in water concentration (gray bars with wavy fill pattern in second and fourth cluster of data, Figure 4.4), and the trileucine powders prepared at 20% v/v ethanol concentration (solid gray bars in second and fourth cluster of data, Figure 4.4), the Dv90 values at 4.5 bar dispersion pressure were found to be significantly smaller than the Dv90 values at 1.0 bar dispersion pressure with a p -value of $<.0001$ using Student's t-test. For trileucine powders prepared at 5% v/v ethanol in water concentration (gray bars with diagonal fill pattern in first and third cluster of data, Figure 4.4), the Dv90 value at 4.5 bar dispersion pressure was also found to be significantly smaller than the Dv90 value at 1.0 bar dispersion pressure, however the p -value showed lower significance ($p=0.0061$; Student's t-test), indicating that the trileucine powders prepared at 5% v/v ethanol in water concentration had poorer dispersion of aggregates compared to the other three dispersion enhancer-ethanol concentration powder combinations.

Table 4.5 Effect of dispersion enhancer on the primary particle size characteristics, span and particle fractions of the spray dried powders determined using the Sympatec HELOS with RODOS dispersion pressure of 4.5 bar. Values are mean (SD), n=3.

Ethanol concentration, % v/v	Dispersion enhancer	Primary particle, μm				Particle fraction, %	
		Dv10	Dv50	Dv90	Span	<1 μm	<5 μm
5	leucine	0.51 (0.00)	1.00 (0.01)	1.95 (0.02)	1.44 (0.01)	50.0 (0.5)	100 (0.0)
5	trileucine	0.53 (0.01)*	1.10 (0.05)*	2.49 (0.41)*	1.76 (0.28)*	43.8 (2.9)*	97.7 (2.5)*
20	leucine	0.51 (0.01)	0.96 (0.03)^	1.82 (0.06)^	1.36 (0.03)^	53.3 (2.5)^	100 (0.0)
20	trileucine	0.53 (0.00)#	1.07 (0.03)#	2.08 (0.06)#	1.45 (0.04)#	45.6 (1.9)#	100 (0.0)

*Significant difference compared to leucine at 5% v/v ethanol in water concentration; Student's t-test, $p < 0.05$

#Significant difference compared to leucine at 20% v/v ethanol in water concentration; Student's t-test, $p < 0.05$

^Significant difference compared to leucine at 5% v/v ethanol in water concentration; Student's t-test, $p < 0.05$

Table 4.6 Effect of dispersion enhancer on the primary particle size characteristics, span and particle fractions of the spray dried powders determined using the Sympatec HELOS with RODOS dispersion pressure of 1.0 bar. Values are mean (SD), n=3.

Ethanol concentration, % v/v	Dispersion enhancer	Primary particle, μm				Particle fraction, %	
		Dv10	Dv50	Dv90	Span	<1 μm	<5 μm
5	leucine	0.56 (0.00)	1.26 (0.03)	2.53 (0.12)	1.57 (0.07)	36.2 (0.9)	99.7 (0.6)
5	trileucine	0.59 (0.02)*	1.41 (0.08)*	3.74 (0.53)*	2.23 (0.24)*	31.8 (2.1)*	94.0 (2.1)*
20	leucine	0.56 (0.01)	1.25 (0.05)	2.96 (0.17)^	1.91 (0.07)^	36.9 (1.9)	96.7 (1.1)^
20	trileucine	0.60 (0.01)#	1.46 (0.07)#	3.49 (0.12)#	1.98 (0.09)	30.5 (1.7)#	96.5 (1.0)

*Significant difference compared to leucine at 5% v/v ethanol in water concentration; Student's t-test, $p < 0.05$

#Significant difference compared to leucine at 20% v/v ethanol in water concentration; Student's t-test, $p < 0.05$

^Significant difference compared to leucine at 5% v/v ethanol in water concentration; Student's t-test, $p < 0.05$

4.3.5 Evaluation of leucine formulation

Further analysis was performed on the leucine powder formulation since the results at both dispersion pressures showed smaller PSDs, smaller spans, and higher submicrometer particles for leucine powders compared to trileucine powders. The aerosol performance of the leucine formulation prepared at both ethanol concentrations were evaluated using the modified containment unit DPI at a fill mass of 10 mg using 3 mL volumes of dispersion air.

4.3.5.1 Effect of ethanol concentration in feed dispersion on the primary particle size distribution

The ethanol concentration was shown to have a small, but significant effect on the primary particle size Dv_{50} and Dv_{90} values, the span, and the fraction of particles less than 1 μm (Table 4.5). The leucine powders prepared in 20% v/v ethanol in water concentration were observed to have significantly smaller Dv_{50} and Dv_{90} values compared to leucine powders prepared in 5% v/v ethanol in water concentration ($p=0.0044$ and $p=0.0006$, respectively; Student's t-test). The powders prepared in 20% v/v ethanol in water concentration were observed to have a smaller span ($p=0.0007$; Student's t-test), and a higher fraction of submicrometer particles ($p=0.0089$; Student's t-test) compared to leucine powders prepared at the 5% v/v ethanol in water concentration.

At the lower RODOS dispersion pressure of 1.0 bar, the ethanol concentration was observed to have small, but significant effect on the Dv_{90} , span and fraction of particles less than 5 μm (Table 4.6). The leucine powders prepared in 20% v/v ethanol in water concentration were observed to have significantly larger Dv_{90} and larger span values ($p=0.0005$ and $p<.0001$, respectively; Student's t-test) indicating poorer dispersibility at the lower pressure given that the Dv_{90} and span values at the 4.5 bar pressure were smaller compared to the powders prepared at 5% v/v ethanol in water concentration. The fraction of particles less than 5 μm were observed to

be lower for powders prepared at 20% v/v ethanol in water concentration ($p=0.0002$; Student's t-test) compared to leucine powder prepared at 5% v/v ethanol in water concentration where there was no difference observed in the two formulations at the higher pressure.

4.3.5.2 Effect of ethanol concentration in feed dispersion on DPI emitted mass

The cumulative emitted mass data from the modified containment unit DPI are plotted as a percentage of the nominal mass in Figure 4.5 (primary y-axis, circles) for each actuation. Overall, the powders were shown to have good aerosolization properties with $\geq 88\%$ of the nominal mass emitted after 3 actuations for both leucine powder formulations. The mass emitted on the first actuation (as a percentage of the nominal mass) was observed to be significantly higher for powders prepared with 5% v/v ethanol in water compared to powders prepared with 20% v/v ethanol in water (63.8 vs 53.8%, $p=0.0485$; Student's t-test). However, overall performance was observed to be similar between the two formulations in the subsequent actuations. On the third actuation, the cumulative mass emitted (% nominal mass) was observed to be 90.3% and 89.5% for the 5% and 20% v/v ethanol in water feed dispersions, respectively, indicating that it was possible to efficiently empty the 10 mg surfactant formulation using only three-3 mL actuations.

The mass emitted for each actuation as a percentage of the mass remaining in the device, calculated from the difference in the nominal mass and the mass emitted in the previous actuation(s), is plotted on the secondary y-axis in Figure 4.5 (triangle markers). For the 5% v/v ethanol in water feed dispersion, a lower percentage of powder was emitted with each successive actuation (64, 60, and 34% of the mass remaining for actuations 1, 2, and 3, respectively). However, more consistent and reproducible percent powder masses per actuation were observed with the 20% v/v ethanol in water feed dispersion (54, 56, and 47% of remaining for actuations 1, 2, and 3, respectively).

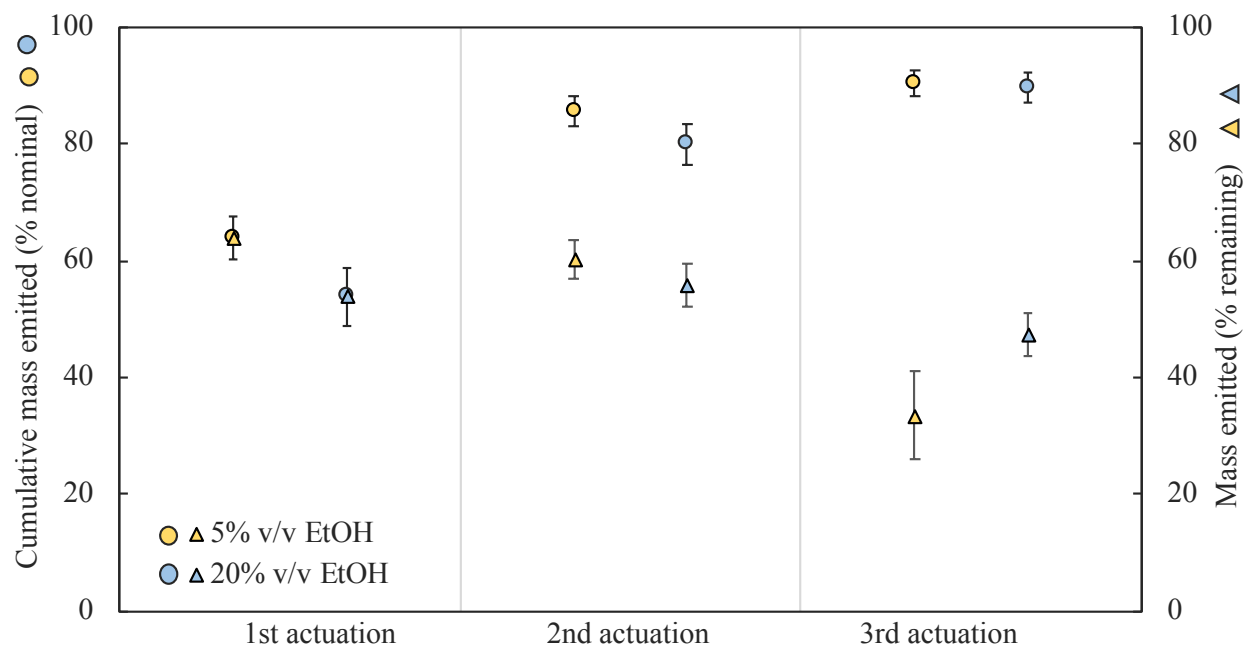


Figure 4.5 Cumulative mass emitted (% nominal, circles) and mass emitted (% remaining, triangles) for leucine-Survanta-EEG powders with the modified containment unit DPI with 10 mg powder fill mass using 3 mL pulses of dispersion air. Markers represent the mean value, error bars represent the SD, n=3; EtOH=ethanol.

4.3.5.3 Effect of ethanol concentration in feed dispersion on aerosol characteristics

Table 4.7 lists the aerosol characteristics for the leucine-Survanta-EEG powders. The aerosol Dv50 values for the 5% v/v ethanol in water feed dispersion was observed to decrease with each successive actuation of 3 mL dispersion air, whereas the aerosol Dv50 values for the 20% v/v ethanol in water feed dispersion was observed to decrease from the first actuation to the second actuation and then level off on the third actuation. The particle fractions for the 5% v/v ethanol in water feed dispersion increased with each successive actuation, whereas the 20% v/v ethanol in water feed dispersion showed more consistent and reproducible particle fractions between actuations. Figure 4.6 shows the relationship between the mass of formulation emitted during each actuation (primary y-axis, square markers) and the measured aerosol Dv50 (secondary y-axis, circle markers).

diamond markers). Despite differences in the emitted mass, there were no significant differences observed between the formulations at each actuation.

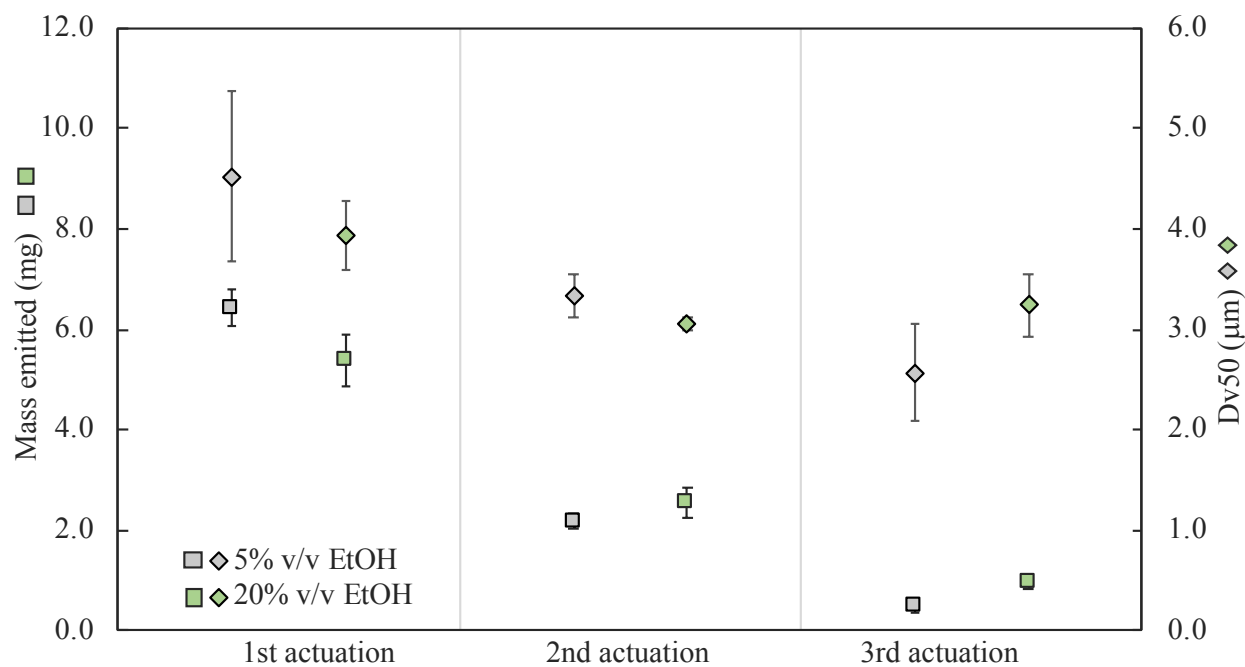


Figure 4.6 Mass emitted (mg, squares) and Dv50 (μm , diamonds) values for leucine-Survanta-EEG powders with the modified containment unit DPI with 10 mg powder fill mass using 3 mL pulses of dispersion air. Markers represent the mean value, error bars represent the SD, $n=3$; EtOH=ethanol.

The aerosol plume durations were determined from exported Spraytec[®] files and defined as the time duration (in milliseconds, ms) in which data collection occurred (Table 4.7). The first actuation for both spray dried formulations had similar aerosol plume durations, 90.4 and 91.1 ms for the 5% v/v and 20% v/v ethanol in water concentrations, respectively. Successive actuations resulted in shorter plume durations; the second actuation was not significantly different between the two formulations, while the third actuation showed a significantly longer plume duration for the 20% v/v ethanol in water formulation compared to the powders prepared with 5% v/v ethanol in water (72.3 vs 46.0 ms, $p=0.0003$; Student's t-test).

Table 4.7 Aerosol characteristics of leucine-Survanta-EEG spray dried powders using the modified containment unit DPI with 10 mg powder fill mass and 3 mL pulses of dispersion air. Values are mean (SD), n=3.

Ethanol in spray vehicle, % v/v	Mass emitted, mg	Aerosol Dv50, μm	Particle fraction, %		Aerosol plume duration, ms [^]	Maximum obscuration, % [^]	Obscuration >20% duration, ms [^]
			<1 μm	<5 μm			
1 st actuation							
5	6.42 (0.37)	4.5 (0.8)	19.6 (1.1)	51.7 (2.6)	90.4 (12.7)	91.6 (0.9)*	61.1 (0.5)*
20	5.38 (0.51)	3.9 (0.4)	18.1 (1.1)	54.6 (2.2)	91.1 (6.4)	86.7 (1.0)	73.3 (3.6)
2 nd actuation							
5	2.18 (0.14)	3.3 (0.2)	21.6 (1.3)	56.4 (0.8) [#]	66.7 (9.5)	71.8 (4.2)	52.0 (4.4) [#]
20	2.57 (0.30)	3.1 (0.1)	20.6 (0.2)	60.0 (0.7)	85.2 (10.6)	71.3 (5.6)	65.1 (3.1)
3 rd actuation							
5	0.48 (0.10)	2.6 (0.5)	25.5 (2.7)	61.7 (4.4)	46.0 (3.7) [‡]	34.6 (5.7) [‡]	17.5 (5.1) [‡]
20	0.96 (0.12)	3.2 (0.3)	20.6 (1.8)	57.8 (2.6)	72.3 (1.0)	45.4 (3.3)	38.7 (7.1)

*Significant difference compared to 20% v/v ethanol in water concentration for the 1st actuation; Student's t-test, $p < 0.05$

[#]Significant difference compared to 20% v/v ethanol in water concentration for the 2nd actuation; Student's t-test, $p < 0.05$

[‡]Significant difference compared to 20% v/v ethanol in water concentration for the 3rd actuation; Student's t-test, $p < 0.05$

[^]Significant correlation with mass emitted; Pearson correlation, $p < 0.05$

Light obscuration values were determined by subtracting the average % transmission values from 100 for each measurement time point for the powder formulations evaluated. The obscuration values were plotted to study the time course of the aerosol plumes (Figure 4.7). Profiles appeared similar for the two ethanol concentrations with a distinct onset in plume formation, a stable phase of aerosol formation followed by a decline in the density of the aerosol plume. Maximum obscurations were determined by finding the peak obscuration value for each aerosol plume, with higher obscurations indicating denser aerosol clouds. The duration of the steady state period of aerosol generation was characterized by determining the duration of time that obscuration of the laser was greater than 20%.

For the first actuation, the powders prepared with 5% v/v ethanol in water were found to reach a higher maximum obscuration of 91.6% compared to the powders prepared with 20% v/v ethanol in water, 86.7%, ($p=0.0029$; Student's t-test). A shift is seen for the subsequent actuations; the maximum obscurations for the two formulations were similar in the second actuation and in the third actuation, the 20% v/v ethanol in water formulation had a significantly higher maximum obscuration than the 5% v/v ethanol in water formulation (45.4 vs 34.6%, $p=0.0472$; Student's t-test). This shift is expected since the maximum obscuration values were observed to have a strong positive correlation with powder mass emitted.

Significant correlations of powder mass emitted was observed with aerosol plume duration, maximum obscuration and the duration of obscuration above 20% (Pearson correlation, $p<0.05$). Strong positive correlations were observed between emitted mass values and aerosol plume durations for the 5% v/v and 20% v/v ethanol in water formulations ($r = 0.8911$, $p=0.0013$, $R^2 = 0.7940$ and $r = 0.7801$, $p=0.0131$, $R^2 = 0.6085$, respectively; Pearson correlation), indicating that longer plume durations were observed for increasing emitted mass values. Higher maximum

obscurations values (denser aerosol clouds) were observed for increasing emitted mass values as indicated by the strong negative correlations observed between emitted mass values and maximum obscuration values for the 5% v/v and 20% v/v ethanol in water formulations ($r = -0.8441$, $p=0.0042$, $R^2 = 0.7124$ and $r = -0.8955$, $p=0.0011$, $R^2 = 0.8019$, respectively; Pearson correlation).

Observations of the duration of the steady state aerosol (obscurations values greater than 20%, which was selected based on the lower obscuration values observed in profiles of the third actuation, Figure 4.7c) revealed that powders prepared with 20% v/v ethanol in water were significantly longer for all three actuations compared to powders prepared with 5% v/v ethanol in water concentration (1st: $p=0.0042$; 2nd: $p=0.0137$, 3rd: $p=0.0137$; Student's t-test). Negative correlations were observed between emitted mass values and the duration of obscuration > 20% for the 5% v/v and 20% v/v ethanol in water formulations ($r = -0.7531$, $p=0.0192$, $R^2 = 0.5671$ and $r = -0.8289$, $p=0.0057$, $R^2 = 0.6871$, respectively; Pearson correlation), indicating that longer plume durations with obscuration values > 20% were observed for increasing emitted mass values.

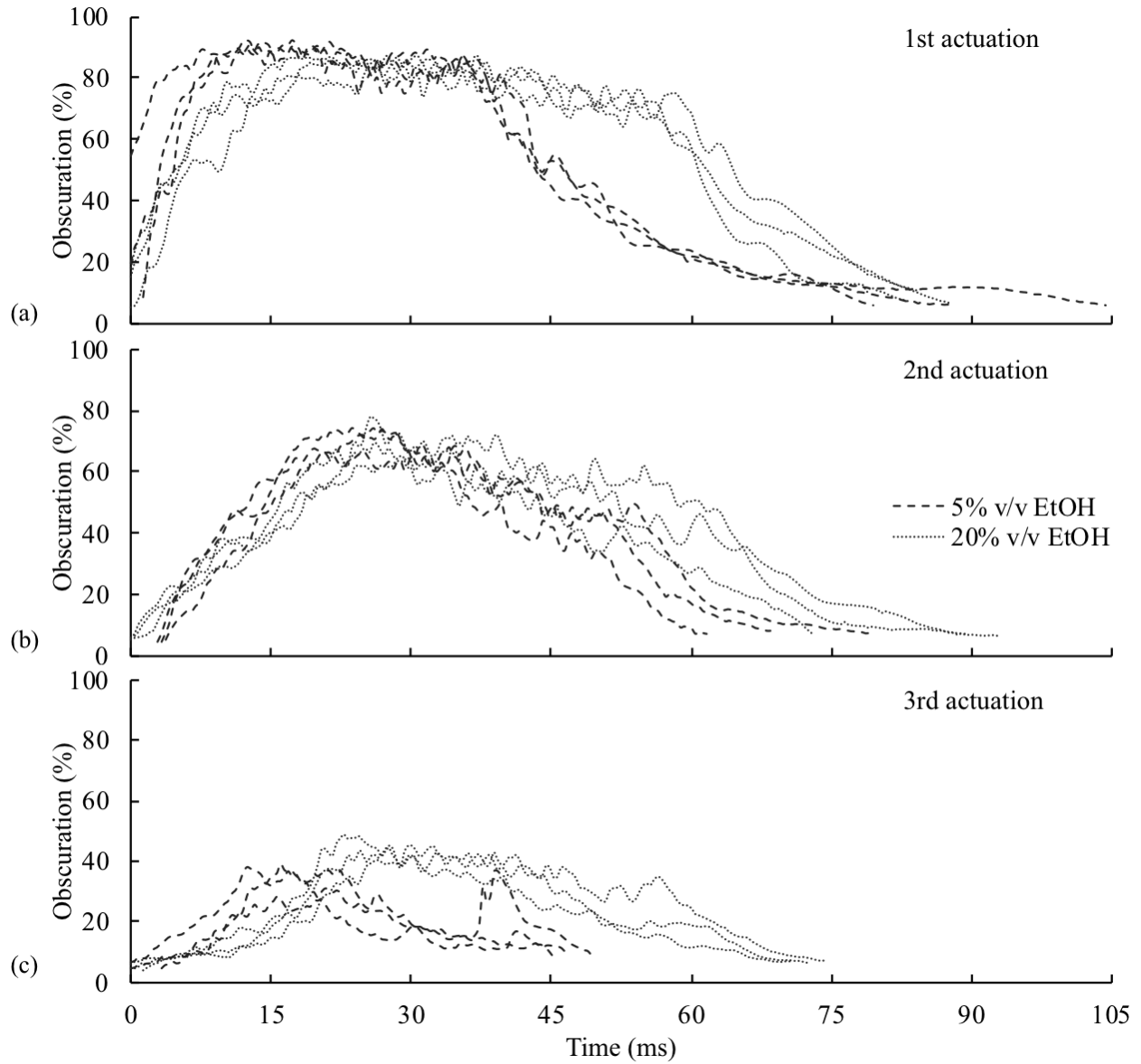


Figure 4.7 Obscuration-time profiles for the (a) first actuation, (b) second actuation, and (c) third actuation replicate aerosol plumes from the modified containment unit DPI filled with 10 mg of leucine-Survanta-EEG powders dispersed with 3 mL volume of dispersion air, EtOH=ethanol.

The size distribution profiles plotted as mean volume fraction/ μm are shown in Figure 4.8 plotted on a log-linear scale. As observed with the emitted mass values, aerosol plume durations and obscuration parameters, the size distributions of the powders prepared with 20% v/v ethanol in water concentration showed less variability between the three actuations compared to powders prepared with 5% v/v ethanol in water. For both of the powders, a high aerosol submicrometer fraction was observed demonstrating the efficiency of the combination of the modified containment unit DPI and leucine-Survanta-EEG formulation to achieve a respirable aerosol with a very low dispersion air volume (3mL) suitable for both small animal administration and delivery to low body weight infants.

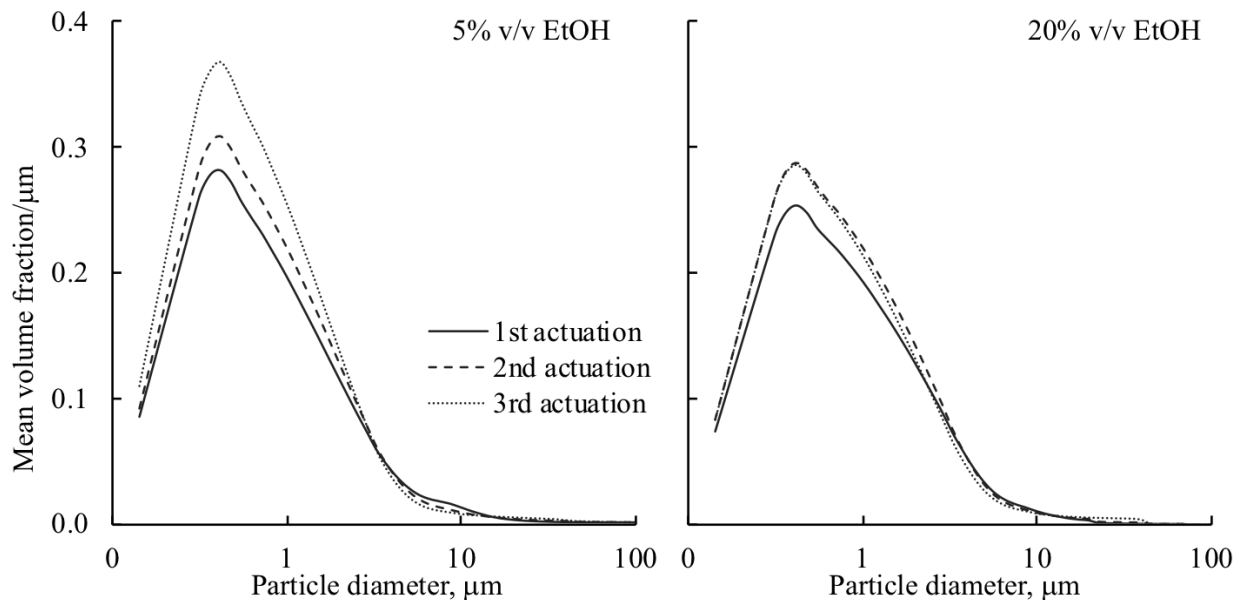


Figure 4.8 Log-linear plots showing comparisons of mean volume fraction/ μm distributions for each actuation of Survanta-EEG formulations prepared with 5% and 20% v/v ethanol in water concentrations; EtOH=ethanol.

Overall, the leucine powders prepared with 20% v/v ethanol in water were found to produce more consistent aerosols across the three actuations in regards to emitted mass values, aerosol plume durations, obscuration parameters and size distributions when compared to powders prepared with 5% v/v ethanol in water. Leucine has a higher solubility in water than in ethanol; the converse is true for phospholipids. Dispersions with higher ethanol concentration possibly allowed leucine to precipitate sooner in the drying process resulting in higher concentrations of the dispersion enhancer on the surface of the spray dried particles; therefore, resulting in less cohesive powders and consequently more consistent aerosols.

4.3.5.4 Effect of ethanol concentration in feed dispersion on solid state powder characteristics

The size and surface morphology of the spray dried powders was visualized using SEM. Leucine-Survanta-EEG powders prepared in the different feed dispersions are shown in Figure 4.9. The powder morphology appeared similar and the size range was observed to be approximately 1 to 2 μm , as was expected according to the laser diffraction data. The samples were sputter coated 3 times to prevent sample degradation during analysis, which may have obscured the fine details on the surface of the particles.

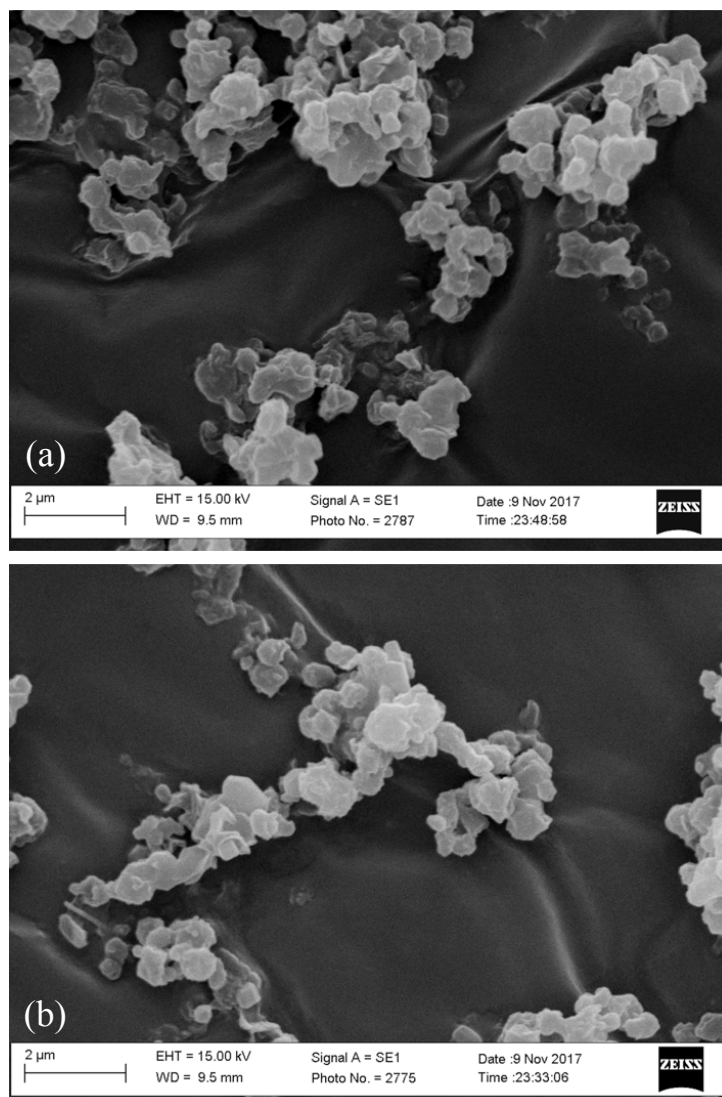


Figure 4.9 SEM images of leucine-Survanta-EEG spray dried powder formulations prepared in (a) 5% v/v ethanol in water, and (b) 20% v/v ethanol in water feed dispersions.

The total weight loss by heating was used to determine the moisture content in the spray dried powders. As expected, the spray dried powders were found to have low moisture contents of < 3% w/w (Figure 4.10a). Powders produced with a higher organic concentration were expected to have lower moisture content considering the preferential drying of organic solvents during the spray drying process. However, no significant differences were observed at the different ethanol

concentrations for the studied formulations with mean \pm SD percent weight losses of $2.5 \pm 0.7\%$ and $2.2 \pm 0.2\%$, respectively for the 5% v/v and 20% v/v ethanol in water feed dispersions.

The Tg of the commercial Survanta[®] formulation was determined to be 37 °C (Figure 4.10b). The observed transition temperature of the spray dried leucine-Survanta-EEG formulations of 34 to 36 °C is as expected since the formulation components mannitol and leucine tend to maintain their crystallized form when spray dried [95, 138], therefore would not contribute to a change in the Tg of the system. No recrystallization or melting transitions were observed in the spray dried powders over the range of 25 to 100 °C, however, a broad melting range between 50 to 80 °C (above Tg) was observed in the commercial Survanta[®] formulation, which may indicate relaxing, or loss in chain order, of the acyl chains of the phospholipid structure.

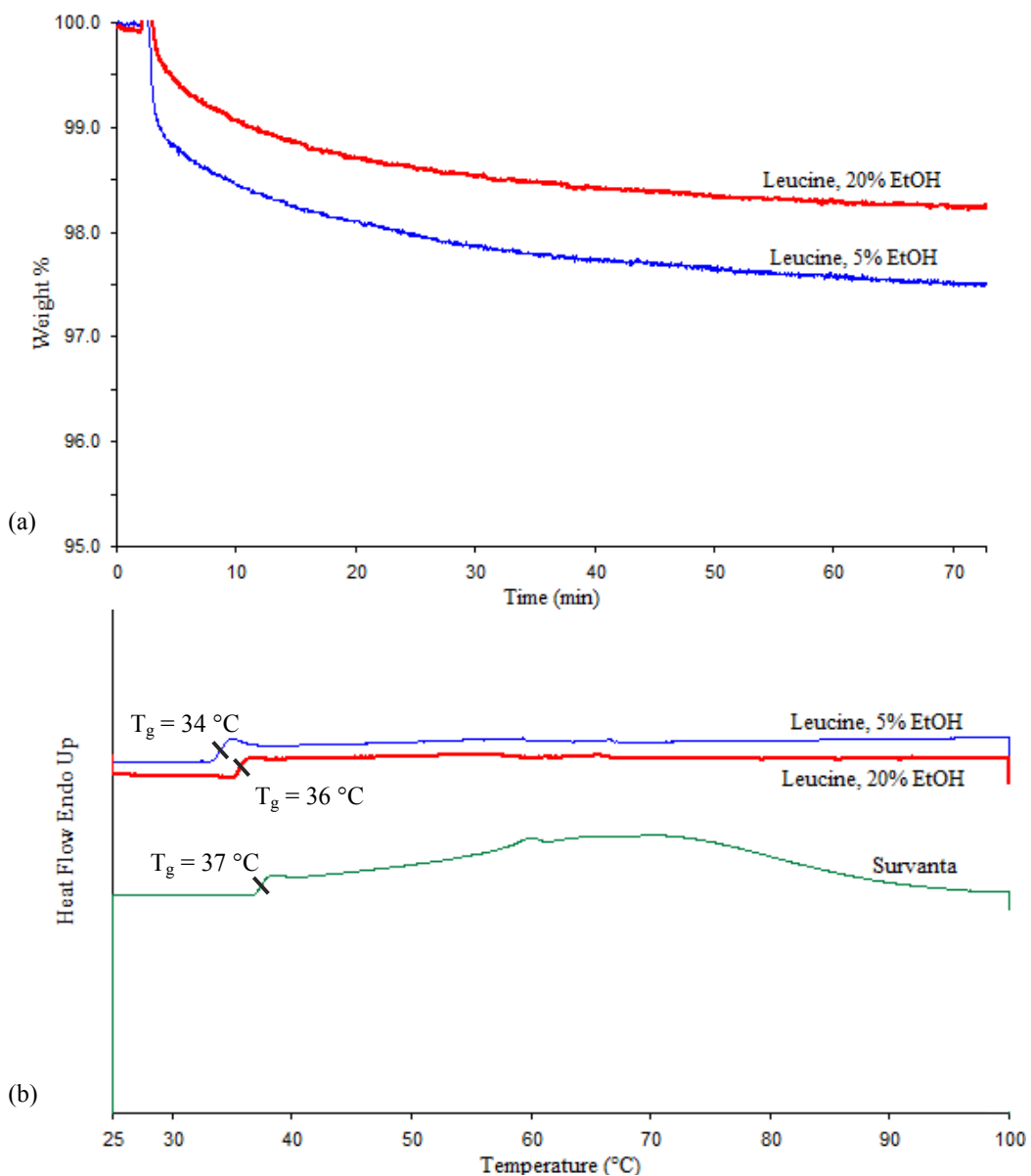


Figure 4.10 Characteristic plots showing (a) thermogravimetric analyzer profiles with isothermal hold at 100 °C and (b) dynamic scanning calorimetry thermograms heated from 25 to 100 °C at a rate of 5 °C/min for spray dried leucine-Survanta-EEG formulations.

4.4 Conclusions

The objective of this study was to produce surfactant powders with leucine and trileucine (Specific aim 2-1) and study the effects of the dry powder dispersion enhancers on feed dispersions, powder characteristics, and primary particle size distributions (Specific aim 2-2). The aerosol performance of powders prepared with leucine using different feed dispersion alcohol concentrations were evaluated using a novel DPI designed to utilize 3 mL of dispersion air to deliver fine particle aerosols (Specific aim 2-3). Powders were engineered using the EEG application to produce submicrometer particles for high delivery efficiency to the lungs. Survanta[®] intratracheal suspension was the selected commercial surfactant formulation used in this study and mannitol was selected as the hygroscopic excipient included in addition to the sodium chloride present in the commercial suspension.

Investigation of the two dispersion enhancers revealed that powders produced with leucine resulted in smaller primary particles, smaller spans, and higher fractions of submicrometer particles compared to powders prepared with trileucine at both ethanol concentrations studied. These findings can be attributed to the presence of other surface-active components in the formulation that compete for space at the air-liquid interface of droplets formed in the spray dryer resulting in a powder surface possibly more enriched with phospholipids rather than the dispersion enhancer resulting in powder dispersion characteristics that are difficult to predict.

Aerosol performance of powders produced with leucine in the 20% v/v ethanol in water feed dispersion resulted in more consistent emitted mass values, size distributions, aerosol plume durations and obscuration parameters over three actuations that were less variable compared to leucine powders prepared in the 5% v/v ethanol in water feed dispersion. Leucine powders were

spray dried to a low moisture content of < 3% w/w with transition temperatures close to that of the commercial surfactant formulation.

A potential issue with the methods employed in this research lies in the spray drying process. The inlet of the spray dryer was set to a temperature of 70 °C, which resulted in outlet temperatures of 37 to 41 °C. These outlet temperatures are approximately the same as the transition temperature of the produced powders, which may negatively impact powder formation and dispersibility of the resulting powders. Lower inlet temperatures of 40 to 60 °C (resulting outlet temperatures of 33 to 39 °C) were explored, but significantly lower powder yields of 30 to 40% were obtained. Other factors that largely influence the outlet temperature of the spray dryer are: (i) the spray rate intensity, increasing would decrease the outlet temperature; (ii) the drying gas flow rate, decreasing would decrease the outlet temperature; and (iii) the spray vehicle, higher water content results in lower outlet temperatures [94]. The spray rate intensity is influenced by the spray and pump percentage. For this research, the spray percentage was set to the highest manufacturer suggested rate of 80%, and the pump setting of 3% was selected to minimize dispersion bypass, so changing the pump setting would result in lower powder yield. With regards to the second factor, decreasing the drying gas flow rate would risk producing powders that are not fully dried. Lastly, aqueous spray vehicles were studied in this research, with one consisting of 95% water, which does not offer much room for improvement. The inclusion of high transition temperature excipients may be worthwhile to revisit since preliminary work done in this area was with DPPC and not with the commercial surfactant formulation.

CHAPTER 5
ASSESSMENT OF THE EFFECTS OF DESIGN MODIFICATIONS TO A LOW AIR
VOLUME ACTUATED DRY POWDER INHALER ON AEROSOL
PERFORMANCE CHARACTERISTICS

5.1 Introduction

The delivery of dry powder surfactant formulations during non-invasive ventilation offers a number of advantages over the current method of replacement surfactant delivery; in particular, it would avoid the need for invasive intubation and does not require the patient to be taken off ventilation to be treated.

Effective powder aerosol delivery to the lungs is dependent on several factors including the powder formulation and device design. DPIs used to deliver powder formulations are categorized as either passive or active devices. Passive DPIs depend on patient inspiratory effort, while active DPIs provide an external energy source to aerosolize and deliver the powder, which reduces dependence on proper patient use. This characteristic of active DPIs make them useful in situations such as delivery to pediatric patients with low inhalation flow rates [144], inline during non-invasive ventilation [145], and for aerosol delivery to test animals [146].

The previous chapter described the development of a novel pulmonary surfactant aerosol formulation as a spray dried powder using the excipient enhanced growth approach. Feasibility of dry powder surfactant administration must first be assessed for therapeutic efficacy and safety in small animal models. Efficient delivery of powder aerosols to small animals present unique challenges, such as how to produce efficient powder dispersion and delivery in animal models with

very small tidal volumes (0.2-0.3 mL for mice, 2-3 mL for rats [147-149]). Insufflation is a common method for the delivery of dry powder with the Dry Powder Insufflator™ DP-4 (Penn-Century, Inc, Philadelphia, PA) being one of the most frequently used devices [150]. No longer commercially available, the DP-4-R was designed for use with rats in which a small amount of dry powder (1-5 mg) was manually filled into the device and the powder was dispersed using small “puffs” of air (2 mL) via an air-filled plastic syringe [151]. Initial studies using the DP-4-R device with spray dried surfactant formulations resulted in poor powder dispersion; therefore, it was found necessary to develop a novel device capable of efficiently aerosolizing and delivering powder surfactant-EEG formulations to animal models, as a highly challenging delivery scenario. This developed device should also be suitable and adaptable for use in delivering surfactant-EEG aerosols during non-invasive ventilation such as high flow nasal cannula therapy to very low birth weight infants.

The aim of this research was to develop an optimal DPI that is capable of delivering surfactant-EEG formulations with high efficiency using a very low volume of dispersion air (3 mL). High efficiency is determined by an emitted mass that is sufficient to theoretically elicit an effect in a rat surfactant depletion model. When delivered as an aerosol, as low as ~2 mg/kg of lipids has been shown to induce physiological changes in preterm lambs [83]. For the surfactant-EEG formulation, delivery of 2-10 mg doses of spray dried powder will be required to assess therapeutic efficacy and safety in small animal models. This dose would ideally be delivered in the least number of actuations possible to minimize the amount of time the animal spends without assisted ventilation.

5.2 Materials and methods

5.2.1 Spray dried powder formulations

Surfactant-EEG spray dried powders were prepared as described in the previous chapter. Dispersions containing Survanta[®], mannitol and leucine in a ratio of 45:33:22 % w/w in a 5% ethanol in water mixture with a solids concentration of 0.125% w/v were spray dried using the Büchi Nano Spray Dryer B-90 HP (Büchi Labortechnik AG, Flawil, Switzerland). Spray drying parameters were as follows: 70 °C inlet temperature (outlet temperatures of 37-41 °C), pump speed of 3%, spray intensity of 80%, and a gas inlet flow of 120 L/min (drying chamber pressure of 40-42 mbar). Powders were collected from the electrostatic particle collector into vials and stored in a desiccator in a fridge (2-8 °C) when not in use.

The primary particle size distribution of the spray dried surfactant-EEG powders was determined by laser diffraction using the Sympatec HELOS. A total of ten spray dried powder batches were used in this study. The powders were observed to be monodisperse with an overall mean \pm SD Dv50 of $1.3 \pm 0.07 \mu\text{m}$ and $1.0 \pm 0.04 \mu\text{m}$ for 1.0 and 4.5 bar dispersion pressures, respectively. This resulted in coefficients of variation of $< 6\%$ across the ten batches, indicating good reproducibility of the spray drying process. The particle size distribution profiles at the 4.5 bar dispersion pressure are shown in Figure 5.1. The span was determined to be 1.4 ± 0.1 at 4.5 bar dispersion pressure with percent particle fractions of $50.1 \pm 2.6\%$ and $99.9 \pm 0.3\%$ for Dv $<1 \mu\text{m}$ and Dv $<5 \mu\text{m}$, respectively.

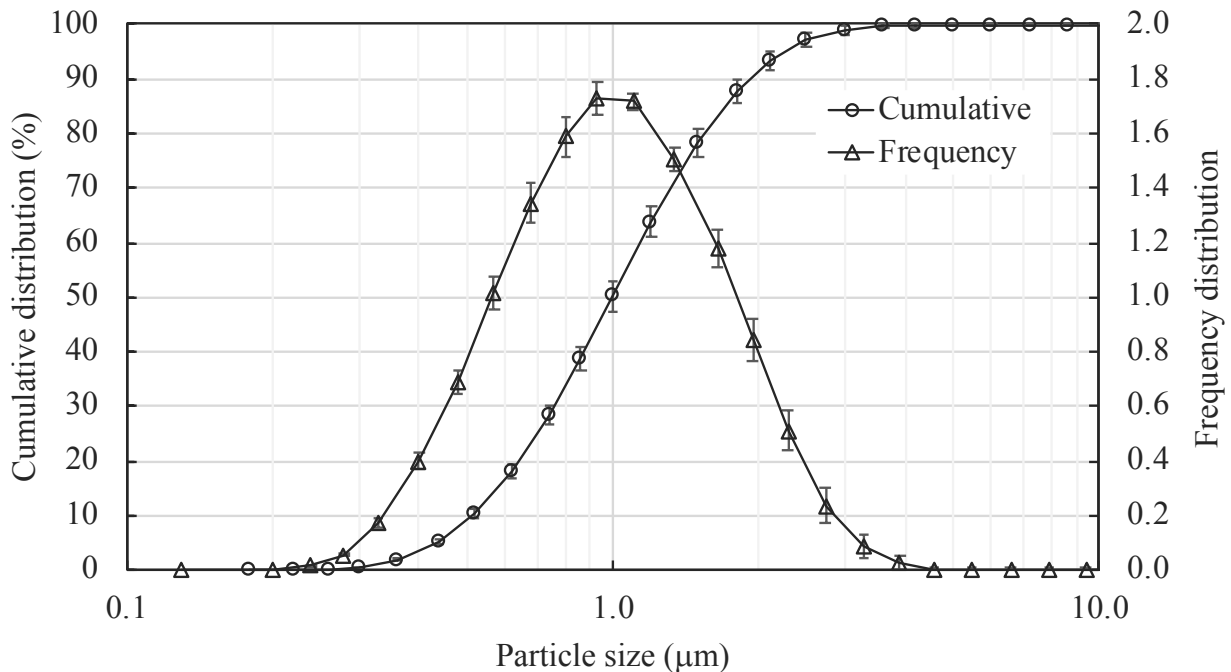


Figure 5.1 Particle size cumulative distribution (primary y-axis) and frequency distribution (secondary y-axis) of the spray dried surfactant-EEG powder batches determined using the Sympatec RODOS dispersion pressure of 4.5 bar. Markers represent the mean value, error bars represent the SD, n=10.

5.2.2 Low dispersion air volume actuation dry powder inhalers

A device developed to use a low dispersion air volume to aerosolize dry powders was design by Farkas et al. [141]. The low air volume DPI (LV-DPI), developed to deliver powder aerosol with a dispersion air volume of 10 mL per actuation, consists of two halves that when assembled, pierces a size 0 capsule housed in the chamber of the device. The capsule is pierced by two hollow capillaries: 1) the inlet capillary with an internal diameter (ID) of 0.60 mm and 2) an outlet capillary with an ID of 0.89 mm. Dispersion air is introduced into the device using a disposable syringe via a standard luer lock connection to the inlet. Their single sided (SS) design (Figure 5.2), referring to the inlet and outlet capillaries configured on the same side of the capsule,

was observed to have a high emitted dose (84.8% of loaded dose) with a mass median aerodynamic diameter of 2.13 μm and a fine particle fraction less than 5 μm of the emitted dose of 89.3% [141].

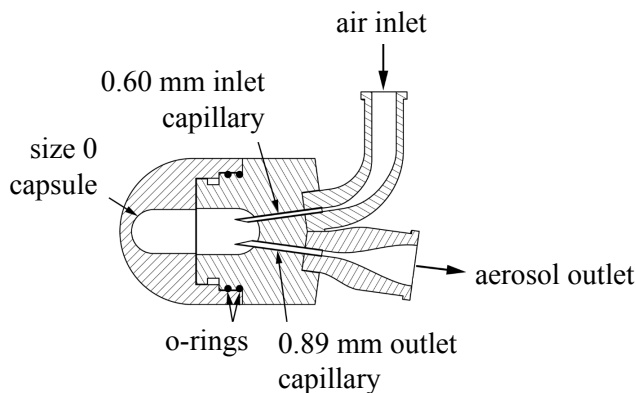


Figure 5.2 Axial cross-section of assembled single side device showing the inlet and outlet capillaries inside the capsule.

For delivery of surfactant-EEG powder formulations using very low volume dispersion air, the lead LV-DPI design was initially modified with an extended length outlet delivery tube of 90 mm when measured from the outer o-ring of the device (Figure 5.3a). The delivery tube was extended with the intention of developing a device for oral tracheal intubation of small animal models and the length was selected based on the delivery tube of the Penn Century Dry Powder Insufflator. A series of design modifications were then made in an effort to maximize aerosol performance – high emitted mass with good powder dispersion for the surfactant-EEG formulation with a dispersion air volume suitable for small animal administration.

The first design modification made with the extended delivery tube device was removal of the capsule and replacement with an integral dose containment chamber into which the formulation was loaded. Initial studies investigated the effects of a reduction of the powder chamber volume in the dose containment unit. The volume was reduced from 0.68 mL to 0.21 mL (~30% of the

original volume) to account for the chamber dead space that becomes a concern when decreasing the dispersion air volume from 10 mL to 3 mL (30% of the original volume). Incorporation of a dose containment unit eliminated the need of protruding inlet and outlet capillaries for capsule piercing, therefore the capillaries were retracted from the powder chamber as shown in Figure 5.3b.

The smaller powder chamber with non-protruding inlet and outlet capillaries was carried into the next design modification which focused on the airflow pathway in the dose containment unit. Instead of the near 180-degree turn in the airflow path of the SS design, a straight through (ST) airflow path configuration was explored. In this configuration, the airflow path travels in a single direction where the aerosol exits out the opposite end of the powder chamber from where the air enters (Figure 5.3c). Farkas et al. studied this design configuration with multiple inlet designs – using a size 0 capsule and 10 mL volume of dispersion air – and found that an inlet design with four-0.60 mm inlet capillaries (clustered together around the longitudinal axis of the capsule) resulted in the best aerosol performance with good dispersion (MMAD of 1.6 μm , fine particle fraction less than 5 μm of the emitted dose of 95.2%), but poorer emitted dose (61.9%) when compared to the SS design [152].

The next design change that was studied explored the number of air inlet holes. The previous designs consisted of one-0.60 mm air inlet hole; in an effort to reduce powder adherence on the walls of the powder chamber, an inlet with three-0.60 mm holes spaced equidistant along the longitudinal axis of the device was designed and tested with the reduced powder chamber volume device in the ST configuration (Figure 5.3d).

Having extensively studied the delivery tube ID of 0.89 mm, delivery tube IDs smaller and larger (0.60 mm and 1.17 mm, respectively, Figure 5.3e) were studied to determine the effect of

delivery tube ID on aerosol performance of the surfactant-EEG powders. The device configuration resulting in the best aerosol performance was determined as that having the smallest Dv50 with the highest emitted mass on the first actuation.

The final device design change explored different delivery tube lengths with the delivery tube internal diameter of 0.89 mm. All previous design changes were studied at the delivery tube length of 90 mm. The effect of delivery tube length on aerosol performance was studied for shorter delivery tube lengths – 55, 45, 30 and 7 mm – with the 55 mm tube length being the minimum length required for *in vivo* studies as dictated by the length of the catheter that would be used with the surfactant-depleted small animal models.

All DPIs were constructed using rapid prototyping (Object24 printer, Stratasys Ltd., Eden Prairie, MN) with a rigid opaque photopolymer, VeroWhitePlus (RGD835). The outlet delivery tubes were custom cut from stainless steel (SAE 304) tubing and secured in place with water resistant epoxy.

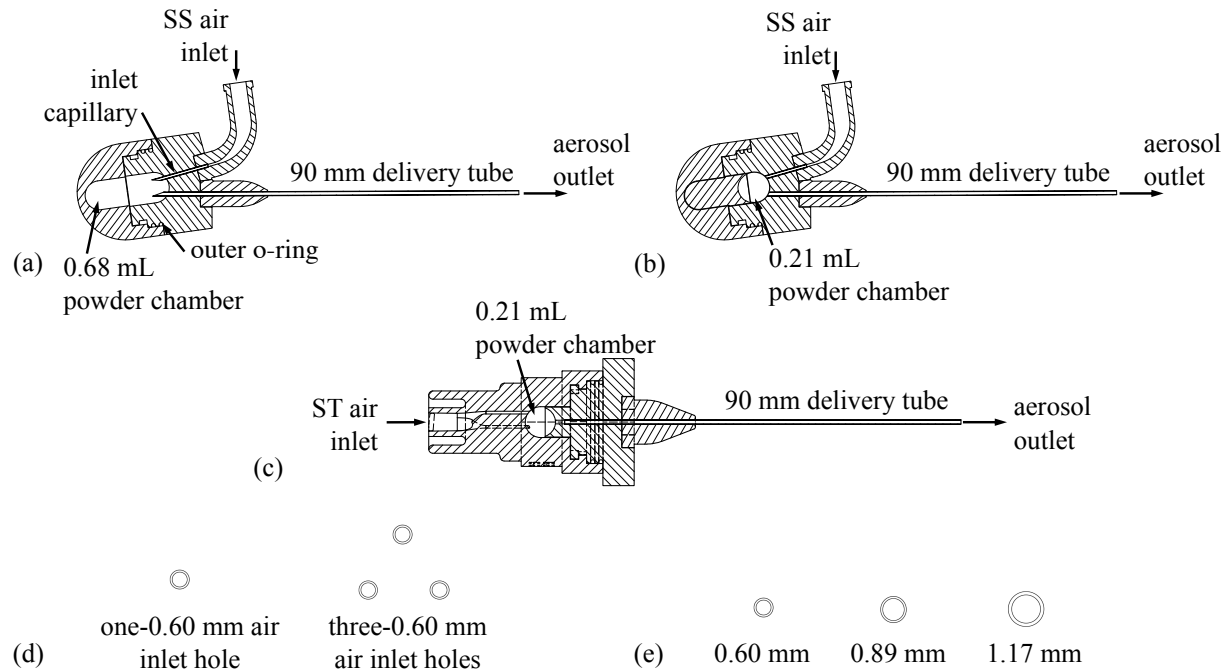


Figure 5.3 Axial cross-section of assembled containment unit DPIs: (a) SS with 0.68 mL powder chamber, (b) SS with 0.21 mL powder chamber, (c) ST with 90 mm delivery tube. Open powder chamber view of studied air inlets (d) and delivery tube internal diameters (e); SS: single side, ST: straight through.

5.2.3 Aerosol performance of modified containment unit DPIs

The emitted mass and particle size of the aerosols exiting the modified containment unit DPIs were studied. As described in the previous chapter, the emitted mass was determined by gravimetric analysis and the particle size distribution of the aerosol exiting the device was determined by laser diffraction using a Malvern Spraytec[®] (Malvern Instruments, Ltd., Worcestershire, UK). Powder was weighed and manually filled into one half of the device containment unit (or capsule for the DPI depicted in Figure 5.3a). Once assembled, the device with powder was weighed to determine the pre-actuation weight. A 5 mL syringe was filled with room air to 3 mL and connected to the luer-lock inlet of the DPI. The device and syringe were mounted in a horizontal position on a fixed stand to ensure a consistent position at a distance 3 cm from the

laser light was maintained for replicate runs. The powders were deaggregated by manual compression of the syringe. The syringe was then disconnected from the device and the device was reweighed to determine the post-actuation weight. Particle size measurements were repeated for up to three actuations. The different parameters explored in this study are listed in Table 5.1.

Table 5.1 Device design parameters explored for the modified containment unit DPI with 3 mL volume of dispersion air.

Experiment	Powder chamber volume, mL	Device configuration	Air inlet holes	Delivery tube ID, mm	Delivery tube length, mm	Powder fill mass, mg
1	0.68	SS	1	0.89	90	3
2	0.21	SS	1	0.89	90	3
3	0.21	ST	1	0.89	90	3
4	0.21	ST	3	0.89	90	3, 5, 10
5	0.21	ST	3	0.60	90	3
6	0.21	ST	3	1.17	90	3
7	0.21	ST	3	0.89	55	3, 5, 10
8	0.21	ST	3	0.89	45	3, 5, 10
9	0.21	ST	3	0.89	30	5
10	0.21	ST	3	0.89	7	5

SS = Single side, ST = Straight through, ID = internal diameter.

5.2.4 Aerosol performance with micronized powder

The aerosol performance of micronized albuterol sulfate with the ST device was studied to determine if powders prepared by a method other than spray drying could be dispersed and delivered with the modified containment unit DPI using 3 mL volumes of dispersion air. Micronized albuterol sulfate USP was purchased from Letco Medical, LLC (Decatur, AL). The micronized powder was first evaluated using the Sympatec HELOS with RODOS dispersion unit

to determine the particle size at two dispersion pressures. The particle size distribution profiles at the 4.5 bar dispersion pressure are shown in Figure 5.4. The micronized powder was observed to be larger in size, have a larger span and a smaller submicrometer particle fraction compared to the spray dried surfactant powders. The micronized powder had mean \pm SD Dv50 of $1.7 \pm 0.02 \mu\text{m}$ and $1.3 \pm 0.05 \mu\text{m}$ for 1.0 and 4.5 bar dispersion pressures, respectively. The span was determined to be 1.9 ± 0.1 at the 4.5 bar dispersion pressure with percent particle fractions of $34.8 \pm 1.4\%$ and $99.9 \pm 1.0\%$ for $D_v < 1 \mu\text{m}$ and $D_v < 5 \mu\text{m}$, respectively. A powder fill mass of 10 mg was used when assessing aerosol performance.

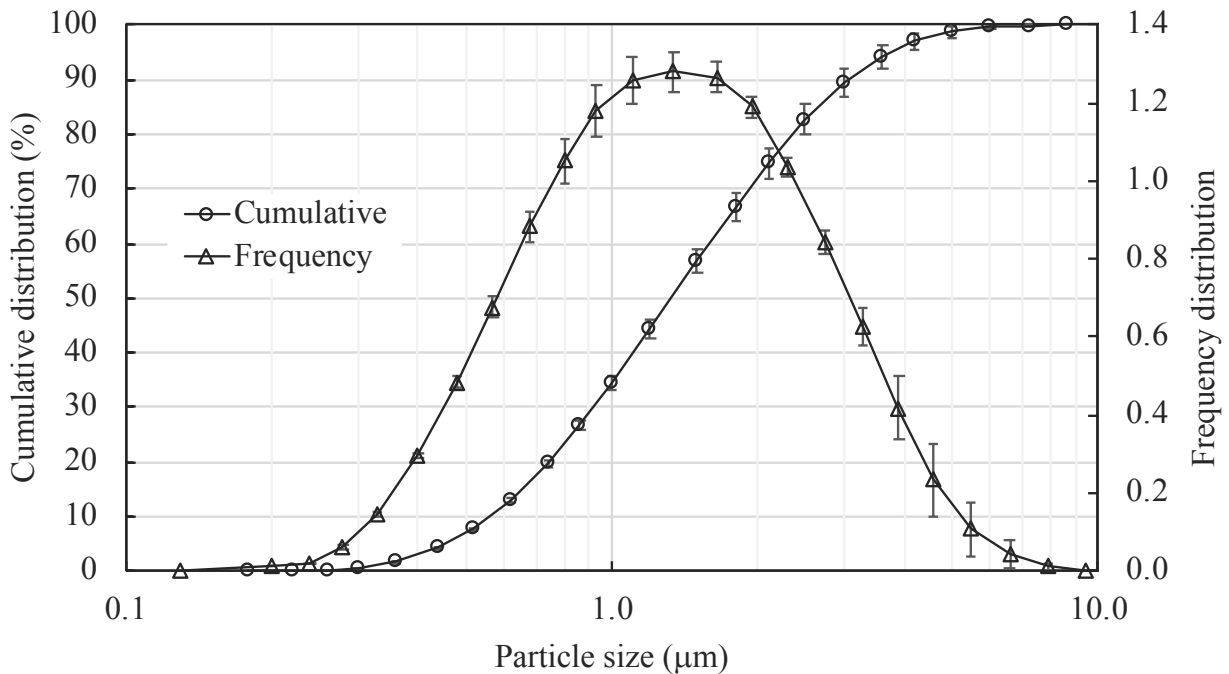


Figure 5.4 Particle size cumulative distribution (primary y-axis) and frequency distribution (secondary y-axis) of the micronized albuterol sulfate powder determined using the Sympatec RODOS dispersion pressure of 4.5 bar. Markers represent the mean value, error bars represent the SD, n=4.

5.2.5 Statistical analysis

Data analysis was performed using JMP[®] Pro software version 12.0 (SAS Institute Inc., Cary, NC). Student's t-statistic or one-way analysis of variance (ANOVA) followed by Dunnett's method or Tukey's HSD was performed to determine statistically significant differences in the data obtained. The Pearson correlation coefficient was determined to quantify the strength of linear relationships. *P* values less than 0.05 were considered as statistically significant.

5.3 Results and discussion

5.3.1 Effect of powder chamber volume, design configuration, and number of air inlet holes

At a powder fill mass of 3 mg, the unmodified SS LV-DPI with the extended outlet capillary (90 mm delivery tube) was observed to have an emitted mass of 20.2 ± 3.6 % on the first 3 mL actuation of air. After the third 3 mL actuation of air, a cumulative emitted mass of 43.6 ± 4.4 % was observed (Table 5.2, Expt 1). In this first experiment with the delivery tube and powder chamber oriented horizontally, the low fill mass formed a shallow powder bed that resided below the outlet capillary resulting in powder losses under the outlet capillary and consequently low emitted mass values.

Rotating the device so the delivery tube pointed vertically upwards showed no improvement in the emitted mass (18.7 ± 8.1 %) after the first 3 mL actuation of air. Changing the orientation of the DPI would affect the position of the formulation powder bed within the inhaler with the powder bed in the direct path of the inlet airflow, but in this case revealed that orientation had no effect on the dose emission likely due to the low volume of dispersion air into the larger powder chamber.

Reducing the powder chamber volume from 0.68 mL to 0.21 mL and removing inlet and outlet capillary protrusion in the powder chamber significantly doubled the percent emitted mass after one actuation ($p=0.0048$; Student's t-test) and generated an aerosol with a mean \pm SD Dv_{50} of $2.5 \pm 0.6 \mu\text{m}$. Decreasing the powder chamber volume was expected to increase the emitted mass as the dead space in the original design was removed enabling the lower volume of dispersion air to empty the powder chamber more efficiently. In addition, removing the outlet capillary protrusion in the powder chamber eliminated the powder loss that was observed around the base of the capillary, therefore contributing to the higher observed emitted mass. The particle fraction less than $1 \mu\text{m}$ and $5 \mu\text{m}$ was $28.8 \pm 3.8\%$ and $60.1 \pm 4.4\%$, respectively. After three 3 mL actuations, the cumulative emitted mass was 77.1% of the nominal fill mass (Table 5.2, Expt 2).

The next design modification explored the design configuration in which the dispersion airflow path travels straight through the dose containment unit. In this case, rather than directing the dispersion air directly at the powder bed, the air flow is directed over the top of the powder. The simpler ST design significantly increased the emitted mass after the first actuation to 55.5% of the nominal fill mass compared to the SS design (40.4%, $p=0.0109$; Student's t-test) without having a significant effect on the Dv_{50} (2.7 vs $2.5 \mu\text{m}$, $p=0.6016$; Student's t-test). Insignificant changes were observed in the fine particle fraction data, with a decrease in the submicrometer particle fraction (23.3%, $p=0.0618$; Student's t-test) and an increase in the particle fraction $<5 \mu\text{m}$ (62.5%, $p=0.7163$; Student's t-test) compared to 28.8% and 60.1%, respectively for the SS design (Table 5.2, Expt 3 compared to Expt 2). The larger outlet diameter of 0.89 mm relative to the inlet diameter of 0.60 mm, caused a deceleration in the inlet airflow and an increase in secondary velocities in the containment unit. The secondary velocities generated from the difference in inlet/outlet diameters were responsible for aerosolization of the powder bed. The total mass

emitted following three 3 mL actuations with the ST design configuration was 83% of the nominal fill mass.

The observed results imply that the inlet airflow path had a larger influence on the emitted mass than on powder dispersion. The SS design directed the inlet airflow path at the powder bed, which may have created turbulent forces that caused the aerosolized powder to impact on the walls of the containment unit, which resulted in a lower emitted mass. Since the ST design directed the inlet airflow path to travel in a single direction over the powder bed within the containment unit, it reduced the chance of creating turbulent forces, which resulted in more powder exiting the device.

An inlet design with three-0.6 mm holes, spaced evenly apart, was also studied (Expt 4). The inlet was designed to have three jets of air make contact with the powder with the intention of reducing the amount of powder remaining in the containment unit after actuation. Incorporation of three air inlet holes in the ST design significantly increased the emitted mass to 70.9% from 55.5% of the nominal fill mass ($p=0.0040$; Student's t-test) while the Dv_{50} remained unaffected at 2.7 μm . The total cross-sectional area of the inlet (1.8 mm) was greater than the single outlet diameter of 0.89 mm, providing an inlet jet that enabled better emptying of the dose containment unit. An insignificant increase in the submicrometer particle fraction to 26.8% ($p=0.1437$; Student's t-test) and insignificant decrease in the particle fraction $<5 \mu\text{m}$ to 57.5% ($p=0.4587$; Student's t-test) was observed. The total emitted mass after the third 3 mL actuation was 92% (Table 5.2, Expt 4). Given the significant increase in emitted mass without an observed change in the Dv_{50} value, the three air inlet hole design with ST device configuration was explored further.

Table 5.2 Effect of powder chamber volume, design configuration, number of air inlet holes, and delivery tube internal diameter on aerosol performance of surfactant-EEG spray dried powders (fill mass: 3 mg, values are mean (SD), $n \geq 3$).

Expt	Powder chamber volume, mL	Device config	Air inlet holes	Delivery tube ID, mm [†]	1 st actuation					Cumulative mass emitted on 3 rd actuation, % nominal mass
					Mass emitted, mg	Mass emitted, % nominal mass	Dv50, μ m	Particle fraction, %		
								<1 μ m	<5 μ m	
1	0.68	SS	1	0.89	0.62 (0.12)	20.2 (3.6)	.	.	.	43.6 (4.4)
2	0.21	SS	1	0.89	1.23 (0.22)*	40.4 (7.5)*	2.5 (0.6)	28.8 (3.8)	60.1 (4.4)	77.1 (13.7)
3	0.21	ST	1	0.89	1.67 (0.16) [‡]	55.5 (5.7) [‡]	2.7 (0.6)	23.3 (3.4)	62.5 (10.5)	83.1 (7.9)
4	0.21	ST	3	0.89	2.12 (0.12) [#]	70.9 (3.7) [#]	2.7 (0.2)	26.9 (2.1)	57.5 (2.6)	92.4 (1.9)
5	0.21	ST	3	0.60	1.05 (0.03) [^]	33.9 (0.3) [^]	1.7 (0.1) [^]	32.6 (0.2) [^]	73.5 (5.7) [^]	70.8 (2.6)
6	0.21	ST	3	1.17	2.26 (0.13)	74.2 (4.7)	6.8 (0.1) [^]	12.0 (1.1) [^]	44.7 (0.7) [^]	98.2 (3.6)

*Significant difference compared to 0.68 mL powder chamber volume; Student's t-test, $p < 0.05$

[‡]Significant difference compared to SS device configuration; Student's t-test, $p < 0.05$

[#]Significant difference compared to one-0.60 mm air inlet hole; Student's t-test, $p < 0.05$

[†]Statistically significant effect of delivery tube internal diameter comparing expts 4-6; one-way ANOVA, $p < 0.05$

[^]Significant difference compared to 0.89 mm delivery tube internal diameter; Dunnett's method, $p < 0.05$

5.3.2 Effect of outlet delivery tube internal diameter on aerosol performance

To determine the effect of the internal diameter (ID) of the outlet delivery tube on the aerosol performance of the best performing containment unit DPI (Expt 4), additional devices of the ST design were manufactured with internal diameters of 0.60 mm and 1.17 mm. Table 5.2 (Expt 4, 5, 6) summarizes the emitted mass data (after one actuation, cumulative mass after three actuations) and particle size data (aerosol Dv50, particle fractions <1 μm and <5 μm) for the different devices.

The 0.89 mm ID device was shown to be a good compromise between device emptying and aerosol performance in regard to particle size characteristics (Expt 4). One-way ANOVA revealed significant differences in the emitted mass and particle size data of the different ID devices ($p<.0001$). Using Dunnett's method for post-hoc analysis, the 0.60 mm ID device was observed to empty significantly less powder on the first actuation compared to the 0.89 mm ID device (33.9 vs 70.7% of the nominal fill mass, $p<.0001$). During testing, powder was noticeably clumped at the outlet hole of the 0.60 mm ID device partially blocking the exit resulting in the poor emptying. No difference was seen in the percent mass emitted for the 1.17 mm ID device compared to the 0.89 mm ID device.

The aerosol Dv50 values were observed to increase with increasing ID, which corresponded to decreasing submicrometer particle fraction values. The mean Dv50 value for the 0.89 mm ID device was 2.7 μm , significantly larger than the Dv50 of 1.7 μm for the 0.60 mm ID device ($p<.0001$) and significantly smaller in size than 6.8 μm for the 1.17 mm ID device ($p=0.0032$). For all three outlet delivery tube devices, the total cross-sectional area of the inlet (1.8 mm) was greater than the diameter of the outlet (0.60, 0.89 or 1.17 mm), indicating that the hydrodynamic force needed to deaggregate that powder was in the form of an inlet jet. The outlet

diameter of 0.60 mm had the highest pressure at the outlet and consequently had more dispersed powders but resulted in poor emptying. The delivery tube with a larger ID of 1.17 mm had the lowest pressure at the outlet of the three IDs studied and therefore had the poorest dispersion. The submicrometer particle fraction for the 0.89 mm ID device was 26.8%, which was found to be significantly lower compared to the 0.60 mm ID device ($p=0.0036$), but significantly higher than that of the 1.17 mm ID device ($p<.0001$).

Pearson correlation coefficients were determined to assess the relationship of outlet delivery tube ID with aerosol performance characteristics. The correlation statistics are listed in Table 5.3. All correlations studied had strong significant relationships with the delivery tube ID; the absolute value of correlation coefficients for all relationships were > 0.85 with p -values <0.05 . The mass emitted in the first actuation and the cumulative mass emitted on the third actuation were found to have positive correlations with the outlet delivery tube ID; higher emitted fractions with larger outlet delivery tube internal diameters. A positive correlation was observed between the Dv_{50} values with the outlet delivery tube ID, increasing outlet delivery tube ID resulted in larger Dv_{50} values. The particle fractions $<1 \mu\text{m}$ and $<5 \mu\text{m}$ were found to have strong negative correlations with the outlet delivery tube ID, increasing outlet delivery tube ID resulted in decreasing particle fraction values. The design modifications investigated revealed that the ST device with a three air inlet hole design and a 0.89 mm ID outlet delivery tube offered the optimum performance in terms of delivered dose and aerosol performance and was used for further studies described below.

Table 5.3 Correlation statistics of outlet delivery tube internal diameter with aerosol performance characteristics.

Characteristic	Correlation coefficient, <i>r</i>	Significance, <i>p</i> -value	Coefficient of determination, <i>R</i> ²
Mass emitted on 1 st actuation	0.8622	0.0028*	0.7434
Dv50 values	0.9369	0.0002*	0.8777
Particle fraction <1 μm	-0.9576	<.0001*	0.9170
Particle fraction <5 μm	-0.9654	<.0001*	0.9320
Cumulative mass emitted on 3 rd actuation	0.9353	0.0002*	0.8747

*Significant; Pearson correlation, *p*<0.05

5.3.3 Effect of outlet delivery tube length and fill mass on powder performance

Three outlet delivery tube lengths (90, 55 and 45 mm lengths) were studied. The volume of the delivery tubes were determined to be 0.056, 0.034 and 0.028 mL for the 90, 55, and 45 mm tube lengths, respectively. Time durations for manual compression of the syringe was determined using a Photron PCI R2 high-speed camera to capture images at 1000 frames per second with Photron FASTCAM Viewer software to analyze the images. The 90 mm delivery tube length device was observed to take 0.14 ± 0.00 s to deliver 3 mL of actuation air, while both the 55 mm and 45 mm delivery tube lengths were observed to take 0.12 ± 0.01 s to deliver 3 mL of actuation air. This resulted in a short burst of 1.3 L/min for the 90 mm delivery tube length device and 1.6 L/min for the two shorter delivery tube length devices. The slower flow rate observed for the longest delivery tube length device was expected considering the larger internal volume of this device compared to the two shorter delivery tube devices (total volume for 90 mm delivery tube

length device 0.27 mL compared to 0.25 mL and 0.24 mL for 55 mm and 45 mm delivery tube length devices, respectively).

The effect of delivery tube length on aerosol performance was studied at three powder fill masses: 3, 5 and 10 mg in the best performing containment unit DPI as described previously. The data are shown in Table 5.4. Overall, it was observed that increasing the fill mass of the surfactant-EEG formulation increased the delivered powder mass from the modified containment unit DPI using each of the three delivery tube lengths on the first actuation and after 3 actuations. The highest percent emitted masses (expressed as % nominal mass) following the first actuation were observed at the lowest fill mass of 3 mg for each of the delivery tube lengths (> 66% of nominal). The cumulative mass emitted was $\geq 77\%$ of the nominal fill mass after 3 actuations for all runs. The mean \pm SD total mass emitted after 3 actuations for the 90 mm delivery tube length at 3, 5 and 10 mg fill masses were 2.77 ± 0.05 , 4.77 ± 0.13 and 8.63 ± 0.23 mg, respectively. Similar values for the 55 mm delivery tube were 2.76 ± 0.16 , 4.39 ± 0.10 and 9.08 ± 0.22 mg and the 45 mm delivery tube were 2.69 ± 0.13 , 3.89 ± 0.04 and 8.05 ± 0.57 mg.

Considering the emitted mass for the 90 mm delivery tube device, one-way ANOVA determined that fill mass had a significant effect on the percent emitted mass on the first actuation ($p=0.0036$). Tukey's HSD determined that at the 3 mg fill mass, the percent mass emitted after the first actuation was significantly higher than at the 5 mg ($p=0.0120$) and 10 mg fill masses ($p=0.0038$), but the two higher fill masses were not significantly different ($p=0.5194$). After three actuations, there was a significant effect of fill mass on the cumulative mass emitted ($p=0.0130$; one-way ANOVA). The total percent mass emitted at the 3 and 5 mg fill masses were significantly higher than the 10 mg fill mass ($p=0.0457$ and $p=0.0125$; Tukey's HSD, respectively), but the two lower fill masses were not significantly different ($p=0.5365$; Tukey's HSD).

Powder dispersion efficiency during the first actuation was independent of fill mass for the 90 mm delivery tube when considering the volume median diameter with an aerosol Dv50 of 2.7 μm for each of the three fill masses. There was a significant effect of fill mass on the particle fractions $<1 \mu\text{m}$ and $<5 \mu\text{m}$ ($p=0.0281$ and $p=0.0168$; one-way ANOVA, respectively) for the first actuation. The submicrometer particle fraction at the 5 mg fill mass was significantly higher than at the 10 mg fill mass (29.3% vs 24.6%, $p=0.0233$; Tukey's HSD), whereas the particle fraction $<5 \mu\text{m}$ at the 10 mg fill mass was significantly higher than at the 5 mg fill mass (61.8% vs 55.0%, $p=0.0145$; Tukey's HSD). Correlations of powder dispersion characteristics with fill mass were determined for the 90 mm delivery tube after the first actuation (Table 5.5), which confirmed that dispersion efficiency was independent of fill mass as poor correlation coefficients were observed with the Dv50 and submicrometer particle fractions. The particle fraction $<5 \mu\text{m}$ had a correlation coefficient of 0.68 with p -value of 0.042.

For the 55 mm delivery tube device, the powder fill mass had a significant effect on the percent emitted mass after the first actuation, the Dv50, and the submicrometer particle fraction ($p=0.0027$, $p=0.0272$, and $p=0.0151$; one-way ANOVA, respectively). The 3 mg fill mass resulted in significantly higher percent emitted mass than the 5 mg and 10 mg fill masses ($p=0.0022$ and $p=0.0447$; Tukey's HSD, respectively) after the first actuation. The 10 mg fill mass resulted in an aerosol Dv50 value of 4.5 μm , which was significantly larger than the Dv50 of 3.0 μm observed with the 3 mg fill mass ($p=0.0331$; Tukey's HSD) after the first actuation. The submicrometer particle fraction at the 3 mg and 5 mg fill masses were significantly higher than that of the 10 mg powder fill mass ($p=0.0349$ and $p=0.0173$; Tukey's HSD, respectively).

Significant Pearson correlation coefficients indicated that powder dispersion on the first actuation was dependent on fill mass with the 55 mm delivery tube. Aerosol Dv50 values showed

a strong positive relationship with powder fill mass; increasing fill mass resulted in increased Dv50 values (increasingly poor dispersion) with the first actuation. The particle fractions $<1\ \mu\text{m}$ and $<5\ \mu\text{m}$ were observed to have strong negative correlations with powder fill mass; increasing fill mass resulted in decreased particle fraction values.

With the shortest delivery tube of 45 mm, the fill mass had a significant effect on all parameters studied (the percent emitted mass after the first actuation, the cumulative mass emitted after the third actuation, and the powder dispersion characteristics). There was a significant effect on the percent emitted mass after the first actuation ($p=0.0365$; one-way ANOVA) with the 3 mg fill mass having a significantly higher emitted mass than the 10 mg fill mass ($p=0.0403$; Tukey's HSD). The cumulative mass emitted after the third actuation was significantly affected by fill mass ($p=0.0306$; one-way ANOVA) with the 3 mg fill mass having a higher emitted mass than the 5 mg fill mass ($p=0.0290$; Tukey's HSD).

For powder dispersion characteristics, the Dv50 values for the first actuation were significantly affected by fill mass ($p=0.0015$; one-way ANOVA) with the 3 mg fill mass being significantly smaller than the Dv50 values at the 5 and 10 mg fill masses ($p=0.0013$ and $p=0.0079$; Tukey's HSD, respectively). Fill mass had a significant effect on the submicrometer particle fraction for the first actuation ($p=0.0214$; one-way ANOVA) with the 3 mg fill mass having a significantly higher submicrometer fraction than the 10 mg fill mass ($p=0.0218$; Tukey's HSD). For the particle fraction $<5\ \mu\text{m}$, there was a significant effect of fill mass ($p=0.0186$; one-way ANOVA) with the 3 mg fill mass having a significantly higher particle fraction than the 5 and 10 mg fill masses ($p=0.0202$ and $p=0.0466$; Tukey's HSD, respectively).

Correlation analysis of the powder characteristics at the 45 mm delivery tube length found significant relationships of Dv50, the particle fraction $<1\ \mu\text{m}$ and $<5\ \mu\text{m}$ with fill mass (Table 5.5)

for the first actuation. Dv50 was found to be positively correlated with fill mass; increased fill mass resulted in increased Dv50 values. As with the 55 mm delivery tube length, the particle fractions $<1\ \mu\text{m}$ and $<5\ \mu\text{m}$ for the 45 mm delivery tube length for the first actuation were observed to have strong negative correlations with fill mass; increasing fill mass resulted in decreased particle fraction values.

For the three delivery tube length devices studied, particle deaggregation was expected to be from an inlet jet as the cross-sectional area of the inlet (1.8 mm) was greater than the diameter of the outlet (0.89 mm). At the low fill mass of 3 mg, the powder bed was likely outside of the direct inlet airflow path, which enabled good emptying for all three delivery tube lengths. However, at the higher fill masses of 5 mg and 10 mg, it is likely that the powder bed was in the direct inlet airflow path, possibly creating turbulent flows and causing powder to impact on the walls of the containment unit, which resulted in the observed poorer emptying compared to the lower fill mass of 3 mg (Table 5.4). Powder dispersion was independent of device configuration at the low fill mass of 3 mg; the Dv50 values for all three delivery tube length devices were $2.7\ \mu\text{m}$. However, at the higher fill masses of 5 and 10 mg, the volume of the delivery tube likely played a role in dispersion of the powders, with the larger volume of the 90 mm delivery tube length device providing better dispersion of the powders compared to the 55 mm and 45 mm delivery tube length devices. The longer length and therefore larger volume of the 90 mm delivery tube length device allowed the particles to interact with more surfaces that may have enabled better deaggregation.

When comparing the three delivery tube lengths at the 10 mg fill mass, the 55 mm delivery tube had the highest emitted mass (although not significantly) on the first actuation at 63.8% compared to that for the 90 and 45 mm delivery tube devices (52.3 and 54.7%, respectively). With

a lipid concentration of ~27% in the powder formulation, the 55 mm delivery tube device was able to deliver 1.7 mg of lipids in the first actuation, nearly 3 times the theoretical minimum of 0.60 mg of lipids needed to elicit a physiological change in a 300 g surfactant depleted rodent model. The aerosol Dv50 and submicrometer particle fraction for the first actuation were determined to be 4.5 μm and 19.5%, respectively (Table 5.4). For the 90 mm delivery tube device, 1.4 mg of lipids was delivered in the first actuation, which is more than double the theoretical minimum expected to elicit an effect. While the shorter length device emitted more powder in the one actuation, the smaller aerosol Dv50 of 2.7 μm and higher submicrometer particle fraction of 24.6%, compared to the 55 mm delivery tube device, makes the longer delivery tube device a better candidate for delivery of dry powder surfactant aerosols to surfactant depleted rodent models.

Table 5.4 Effect of delivery tube length and fill mass on aerosol performance of surfactant-EEG spray dried powders. Values are mean (SD), n=3.

Delivery tube length, mm	Fill mass, mg [‡]	1 st actuation					Cumulative mass emitted after 3 actuations, % nominal mass
		Mass emitted, mg	Mass emitted, % nominal mass	Dv50, µm	Particle fraction, %		
					<1 µm	<5 µm	
90	3	2.12 (0.12)	70.9 (3.7) ^{*#}	2.7 (0.4)	26.9 (2.1)	57.5 (2.6)	92.4 (1.9) [#]
90	5	2.83 (0.19)	56.2 (4.4)	2.7 (0.2)	29.3 (1.2) [#]	55.0 (0.7) [#]	94.8 (3.1) [#]
90	10	5.28 (0.43)	52.3 (4.4)	2.7 (0.2)	24.6 (1.2)	61.8 (2.2)	85.4 (3.0)
55	3	2.15 (0.09)	73.6 (3.5) ^{*#}	3.0 (0.3) [#]	23.7 (1.6) [#]	57.1 (2.2)	94.5 (6.0)
55	5	2.73 (0.23)	54.9 (4.2)	3.2 (0.3)	24.5 (1.8) [#]	54.7 (1.1)	87.8 (2.7)
55	10	6.42 (0.37)	63.8 (3.6)	4.5 (0.8)	19.6 (1.1)	51.7 (2.6)	90.3 (2.2)
45	3	2.03 (0.15)	66.8 (4.4) [#]	2.7 (0.6) ^{*#}	21.4 (4.3) [#]	65.3 (13.5) ^{*#}	88.3 (3.5) [*]
45	5	2.88 (0.13)	56.7 (2.5)	7.2 (1.8)	15.2 (1.3)	44.5 (3.7)	76.5 (0.8)
45	10	5.51 (0.61)	54.7 (6.2)	9.1 (0.7)	13.4 (0.2)	39.8 (1.4)	79.8 (6.1)

[‡]Statistically significant effect of fill mass; one-way ANOVA, $p < 0.05$.

^{*}Significant difference compared to 5 mg fill mass for the same delivery tube device; Tukey's HSD, $p < 0.05$.

[#]Significant difference compared to 10 mg fill mass for the same delivery tube device; Tukey's HSD, $p < 0.05$.

Table 5.5 Correlation statistics of powder fill mass with powder dispersion characteristics for the three delivery tube lengths during the first actuation.

Delivery tube length, mm	Characteristic	Correlation coefficient, r	Significance, p -value	Coefficient of determination, R^2
90	Dv50 values	-0.0286	0.9481	0.0008
90	Particle fraction <1 μm	-0.5701	0.1090	0.3250
90	Particle fraction <5 μm	0.6843	0.0420*	0.4682
55	Dv50 values	0.8228	0.0065*	0.6770
55	Particle fraction <1 μm	-0.7914	0.0111*	0.6263
55	Particle fraction <5 μm	-0.7784	0.0135*	0.6059
45	Dv50 values	0.8371	0.0049*	0.7007
45	Particle fraction <1 μm	-0.7257	0.0269*	0.5266
45	Particle fraction <5 μm	-0.7115	0.0316*	0.5063

*Significant; Pearson correlation, $p < 0.05$

A plot depicting the cumulative percent mass emitted after each actuation for each fill mass and delivery tube length is shown in Figure 5.5. Overall, the different delivery tube lengths demonstrated good powder emptying with >74% and $\geq 77\%$ emitted after the second and third actuations of 3 mL of dispersion air, respectively. For all three fill masses, the cumulative mass emitted was lowest for the 45 mm delivery tube length.

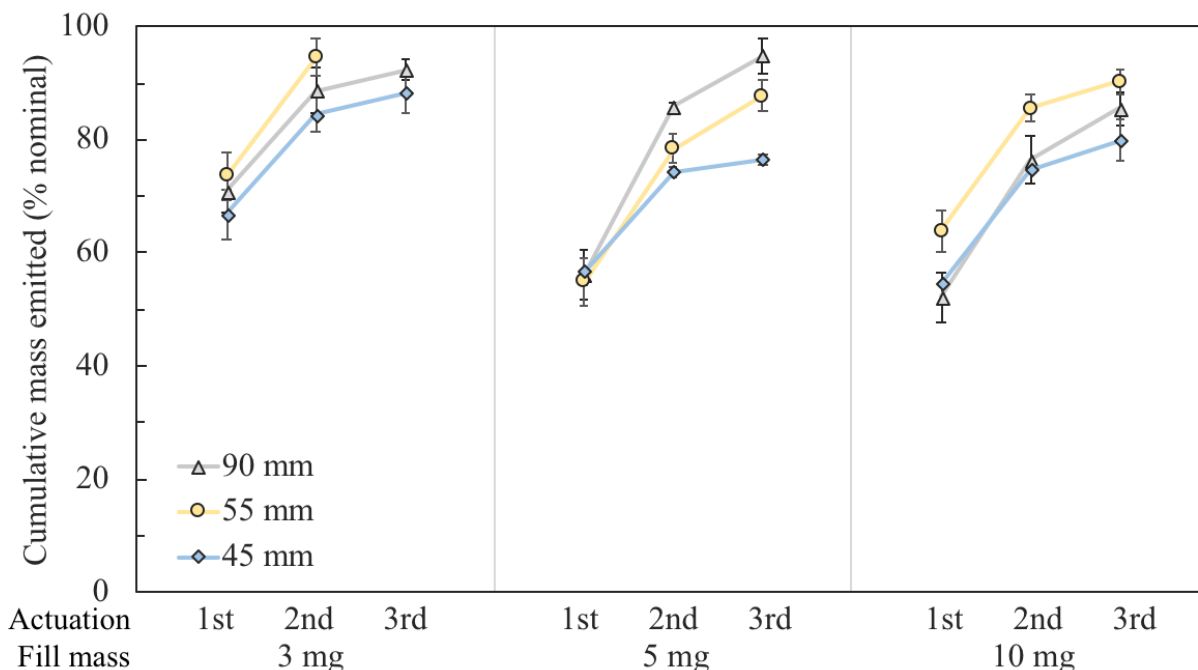


Figure 5.5 Cumulative mass emitted (% nominal) for each actuation by delivery tube length and fill mass. Markers represent the mean value, error bars represent the SD, n=3.

5.3.4 Aerosol plume characteristics

The use of laser diffraction allowed for real time measurement of aerosol plumes exiting the modified containment unit DPIs. The aerosol plume characteristics of the first actuation were studied for the three delivery tube lengths at the different fill masses (Table 5.6).

The light obscuration values were determined by subtracting the average % transmission values from 100 for each measurement time point for the powder lots evaluated. The obscuration values were plotted to study the time course of the aerosol plumes during the first spray actuation (Figure 5.6). All profiles appeared to have an initial increase in obscuration, a steady state with relatively stable obscuration values followed by a decline in the obscuration values.

Table 5.6 Aerosol plume characteristics of the first actuation of surfactant-EEG spray dried powders delivered with the optimized containment unit DPI. Values are mean (SD), n=3.

Delivery tube length, mm	Fill mass, mg	Mass emitted, mg	Aerosol plume duration, ms	Maximum obscuration, %	Obscuration >20%	
					Duration, ms	% Aerosol plume duration
90	3	2.12 (0.12)	53.6 (5.8)	47.8 (4.5)	44.3 (3.9)	82.9 (5.1)
90	5	2.83 (0.19)	63.1 (6.0)	57.4 (3.4)	47.3 (3.1)	75.4 (7.4)
90	10	5.28 (0.43)	84.2 (11.6)	79.2 (5.2)	65.5 (4.1)	78.2 (5.9)
55	3	2.15 (0.09)	53.1 (4.9)	46.2 (0.9)	42.0 (2.4)	79.4 (5.0)
55	5	2.73 (0.23)	63.6 (3.4)	72.5 (2.2)	50.6 (3.1)	79.6 (1.7)
55	10	6.42 (0.37)	90.4 (12.7)	91.6 (0.9)	61.1 (0.5)	68.4 (9.6)
45	3	2.03 (0.15)	51.1 (5.7)	63.7 (6.6)	40.7 (7.0)	79.5 (5.5)
45	5	2.88 (0.13)	72.0 (10.0)	86.0 (1.5)	51.1 (4.0)	71.8 (10.2)
45	10	5.51 (0.61)	108.7 (6.6)	94.7 (1.2)	84.5 (9.5)	77.6 (4.3)

With increasing fill mass, the aerosol plume profiles of the first actuation were observed to develop more distinguishable steady state aerosols. Aerosol plume duration increased with increasing fill mass for each delivery tube length. Of the three delivery tube lengths, the 90 mm length was observed to have the least variability in aerosol plume duration across fill masses (65 ± 14 ms) compared to the 55 mm and 45 mm delivery tube lengths (69 ± 18 ms and 77 ± 26 ms, respectively), further indicating that powder dispersion during the first actuation is independent of fill mass at the longer length.

The maximum obscuration was determined by finding the peak obscuration value for each aerosol plume. At each delivery tube length, it was observed that there is an increase in the percent maximum obscuration indicating progressively denser aerosol plumes with increased fill mass for the first actuation. The relative steady state portion of the profiles was studied by determining the duration above 20% obscuration. For each delivery tube length, an increase in the aerosol time with obscuration values $>20\%$ was observed with increasing fill mass during the first actuation. The obscuration $>20\%$ as a percent of the total aerosol plume duration for each replicate was determined to normalize the data for comparison across fill masses and delivery tube lengths. There were no significant differences observed across fill masses and delivery tube lengths, during the first actuation indicating that the duration of the steady state portion of the aerosol plume is a function of the total aerosol plume duration.

At the 3 mg fill mass, the aerosol plume duration for the first actuation is comparable across the three delivery tube lengths with similar maximum obscuration values for the 90 mm and 55 mm delivery tube devices. The 45 mm delivery tube device had a significantly denser aerosol plume indicated by the maximum obscuration value of 64% compared to the 55 mm and 90 mm delivery tube lengths ($p=0.0087$ and $p=0.0134$; Tukey's HSD, respectively) despite having a

similar mass emitted on the first actuation (Table 5.4). Increasing the fill mass to 5 mg, the aerosol durations remained comparable for the 90 mm and 55 mm delivery tube lengths, but the 45 mm delivery tube length was higher at 72 ms, although not significantly. The maximum obscuration was significantly affected by delivery tube length ($p < .0001$; one-way ANOVA) with significant differences between all pairs ($p < 0.05$; Tukey's HSD). At the 10 mg fill mass, the aerosol plumes generated from the 45 mm delivery tube length appeared to be longer in duration and reach higher obscuration values, indicating denser aerosol clouds than those produced from the 55 mm and 90 mm delivery tube lengths (Figure 5.6).

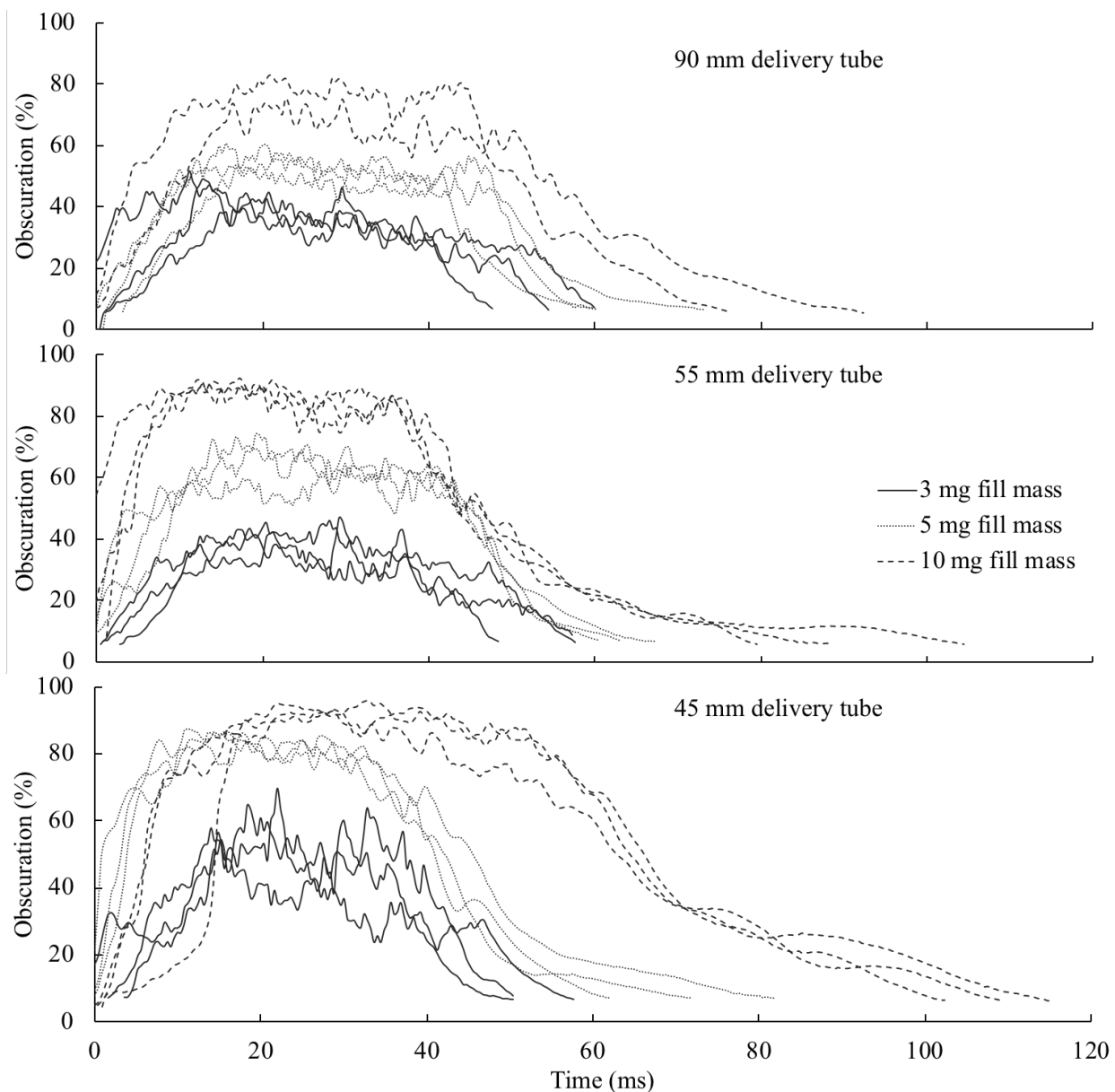


Figure 5.6 Replicate obscuration-time profiles for different fill masses of surfactant-EEG powder studied with the (a) 90 mm (b) 55 mm, and (c) 45 mm delivery tube lengths of the optimized containment unit DPI on the first 3 mL actuation of dispersion air, n=3.

The aerosol performance of the optimized containment unit DPI with delivery tube lengths of 30 mm and 7 mm were also tested at the 5 mg fill mass (Table 5.7). Pearson correlation coefficients were determined to assess the strength of the relationships between the delivery tube length and the powder dispersion characteristics for the aerosol plume emitted during the first actuation (Dv50 and the particle fractions less than 1 μm and 5 μm). A strong negative correlation was observed where longer delivery tube lengths resulted in smaller Dv50 values ($r = -0.8777$, $p < .0001$) with the following relationship,

$$\text{Dv50, } \mu\text{m} = 15.48 - 0.1604 * \text{delivery tube length, mm} \quad \text{Equation 5.1}$$

with a coefficient of determination of $R^2 = 0.7706$. A strong positive correlation was observed where the particle fraction less than 1 μm was found to increase with increasing delivery tube length ($r = 0.9290$, $p < .0001$) with the following relationship,

$$\text{Particle fraction } < 1 \mu\text{m, \%} = 7.861 + 0.2410 * \text{delivery tube length, mm} \quad \text{Equation 5.2}$$

with a $R^2 = 0.8631$. A strong positive correlation was also observed between the particle fraction less than 5 μm and the delivery tube length ($r = 0.8868$, $p < .0001$),

$$\text{Particle fraction } < 5 \mu\text{m, \%} = 26.98 + 0.3547 * \text{delivery tube length, mm} \quad \text{Equation 5.3}$$

with a $R^2 = 0.7863$. The scatterplot correlations are shown in Figure 5.7.

Table 5.7 Effect of delivery tube length on aerosol performance of surfactant-EEG spray dried powders (fill mass: 5 mg, values are mean (SD), n=3).

Delivery tube length, mm	1 st actuation					Cumulative mass emitted on 3 rd actuation, % nominal
	Mass emitted, mg	Mass emitted, % nominal mass	Dv50, μm	Particle fraction, %		
				<1 μm	<5 μm	
30	2.73 (0.04)	54.1 (0.6)	13.5 (1.7)	14.8 (3.1)	32.1 (2.5)	72.4 (3.7)
7	3.46 (0.30)	68.1 (6.4)	14.3 (1.0)	10.2 (0.7)	29.2 (1.0)	88.0 (5.7)

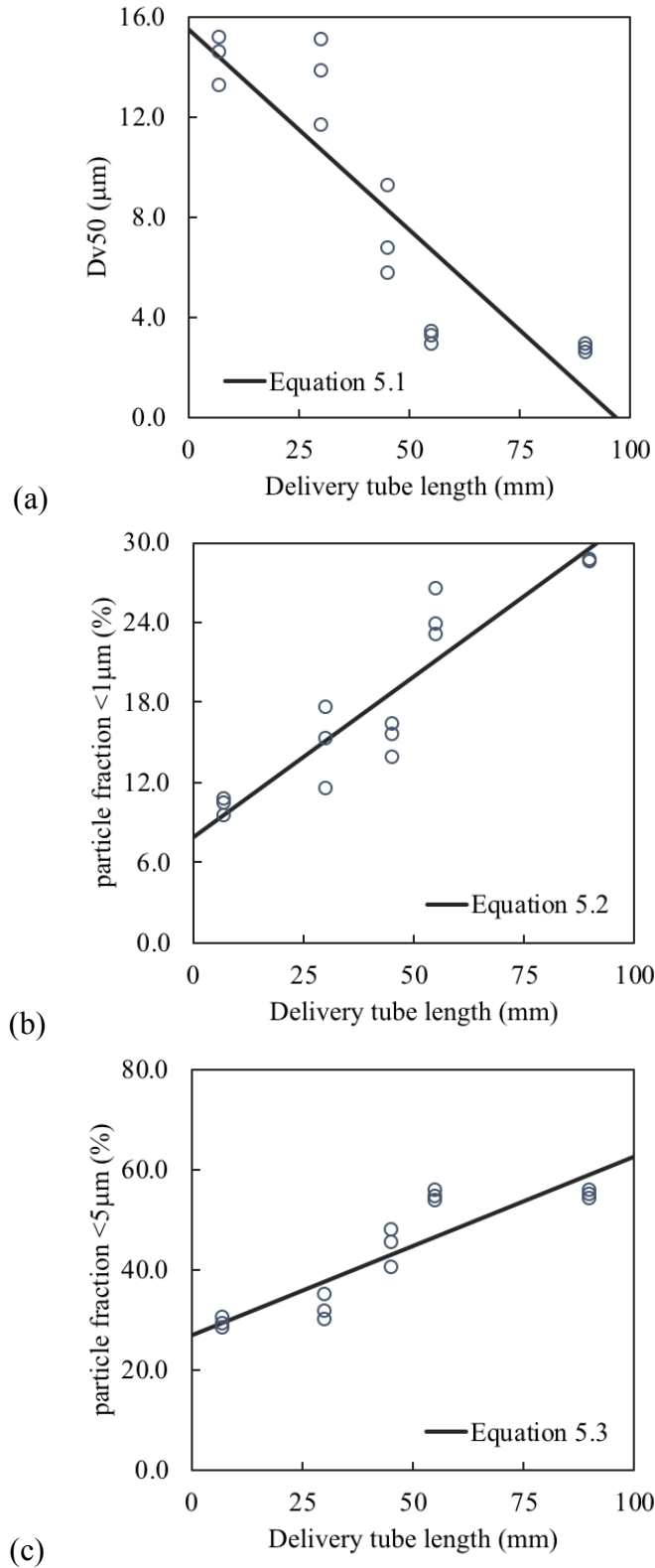


Figure 5.7 Correlation of delivery tube length of the optimized containment unit DPI with a) Dv50, b) particle fraction <1 µm, and c) particle fraction <5 µm of surfactant-EEG powders on the first 3 mL actuation of air with 5 mg powder fill mass. Markers represent individual values.

5.3.5 Aerosol performance with micronized powder

A fill mass of 10 mg was used to determine the aerosol performance of the micronized albuterol sulfate with the 90 mm and 55 mm delivery tube length devices. The data are shown in Table 5.8. The optimized containment unit DPI was shown to deliver > 70% of the nominal fill mass on the first actuation for both delivery tube lengths. This resulted in Dv50 values of 5.8 and 5.3 μm for the 90 and 55 mm delivery tube lengths, respectively. The larger Dv50 values and lower submicrometer particle fraction values for the micronized powder compared to the spray dried powder was expected as the primary particle size distributions were larger for the micronized powder (Figure 5.4 vs Figure 5.1).

Table 5.8 Aerosol performance of micronized albuterol sulfate powder with the optimized containment unit DPI (fill mass: 10 mg, values are mean (SD), $n \geq 3$).

Delivery tube length, mm	1 st actuation					Cumulative mass emitted on 3 rd actuation, % nominal mass
	Mass emitted, mg	Mass emitted, % nominal mass	Dv50, μm	Particle fraction, %		
				<1 μm	<5 μm	
90	7.22 (0.36)	72.8 (3.1)	5.8 (1.8)	13.2 (2.0)	48.6 (7.4)	94.4 (0.5)
55	7.35 (0.35)	72.5 (3.0)	5.3 (1.8)	9.4 (3.0)	51.8 (9.3)	90.3 (2.2)

5.4 Conclusions

The objective of this study was to develop an optimized dry powder inhaler for the delivery of spray dried surfactant powders by determining the influence of a series of design modifications and powder fill mass on aerosol performance (Specific aims 3-1 and 3-2). The inhaler was required to disperse relatively high powder masses (3-10 mg) with very low volumes of dispersion air for applications of delivering drugs as aerosols to small rodent animal models and being suitable for delivery of aerosols to low birth weight infants. Challenges to the design optimization included (i) being restricted to a low dispersion air volume (~3 mL), and (ii) a preference of delivering the dose in one actuation. The low volume of dispersion air was restricted by the low tidal volume of the selected animal model. Delivering the dose in one actuation was preferred to minimize the time that the animal spent off the ventilator following lung lavage and surfactant administration. The aim was to develop a device that was capable of delivering ≥ 2 mg/kg of lipids in one 3 mL actuation of air. For the surfactant-EEG formulation, this translates to approximately 2.2 mg of spray dried powder for a 300 g rodent. Design modifications made to an active DPI prototype enabled delivery of > 2 mg of spray dried powder using one 3 mL actuation of dispersion air with 3-10 mg powder fill masses.

Studying the effects of delivery tube length and fill mass on aerosol performance revealed an optimal device with powder dispersion characteristics independent of fill mass (3-10 mg) with good powder emptying in one actuation. With a powder fill mass of 10 mg, the lead design was able to deliver 5.3 mg of surfactant powder with an aerosol Dv_{50} of 2.7 μm in a single 3 mL actuation of dispersion air.

The device developed in this research can be adapted for use in the treatment of infants on non-invasive ventilation. A low volume of air, as is used to disperse the powder formulations in

the optimized containment unit DPI, is vital when dealing with preterm infants with tidal volumes as low as 4 mL/kg [81]. The optimized containment unit DPI was also shown to perform well with micronized drug (7.2 mg emitted from 10 mg fill mass with aerosol Dv50 of 5.8 μm), indicating that the device has potential for use in other applications.

A possible issue with the optimized containment unit DPI is the difficulty in controlling the density of the aerosol plume exiting the device. Too dense of a cloud has the potential of impacting along the trachea and bronchi of the rodent airways (or delivery tubing in the case of treatment to infants on non-invasive ventilation) decreasing the amount of aerosol available to reach the alveoli of the lung. The aerosol cloud was noticeably less dense at lower fill masses as indicated by the obscuration profiles presented in Figure 5.7, which could be a method to explore in order to control the aerosol cloud exiting the device.

CHAPTER 6
EVALUATION OF THE *IN VITRO* AEROSOL DELIVERY EFFICIENCY OF
SURFACTANT-EEG FORMULATIONS USING NOVEL LOW-VOLUME MIXER-
HEATERS

6.1 Introduction

Viral bronchiolitis, a common cause of lower respiratory tract infection in infants, is characterized by wheezing and mucus plugging, often leading to airway obstruction [45, 153]. Conventional treatments include supplemental oxygen and respiratory support. The administration of bronchodilators have been studied, but have not shown effectiveness in symptomatic management of the disease [154] and are not recommended for use [49]. The use of high flow nasal cannula (HFNC) therapy has been indicated to be feasible and well tolerated in infants with bronchiolitis [53] and delivery of a surfactant aerosol during HFNC therapy could possibly hasten the resolution of symptoms. Heated and humidified inspiration gas delivered during HFNC therapy enables delivery of higher inspired gas flow rates (up to 12 L/min in infants and 30 L/min in older children) than those typically seen with dry gas delivery (maximum of 2 L/min) [53].

Efficient delivery of inhaled drugs via the nasal route is important for the infant population as they are preferential nasal breathers. Lung deposition of < 4% has been reported in spontaneously breathing infants using a jet nebulizer with a face mask interface [103, 155]. An *in vitro* study found that the most efficient interface for aerosol delivery to a realistic seven-month-old model was nebulization via a front-loaded mask, which produced delivered doses of 1.52% and 0.71% of the nominal dose, using jet and vibrating mesh nebulizers, respectively [156]. The

low delivery efficiencies of inhaled aerosols to infants using this standard of care system suggests the need for the development of more efficient methods for the delivery of high dose medications and to avoid drug waste.

An aerosol mixer system, developed at Virginia Commonwealth University (VCU), was designed for use with vibrating mesh nebulizers to generate submicrometer excipient enhanced growth (EEG) aerosols [157]. The unit consisted of a large mixing region (aerosol reservoir) where aerosol generated from the commercial vibrating mesh nebulizer was mixed with recirculating heated air then entrained to pass a narrow heat-transfer region. The entrained drug aerosol would be delivered to the patient via connective tubing and a nasal cannula interface. The mixer-heater system was shown to achieve *in vitro* lung delivery efficiencies > 70% of the nebulized dose at conventional high flows (~30 L/min) when using adult breathing conditions and a deep tidal volume of 930 mL [158]. The first-generation mixer-heater system has been modified to provide HFNC therapy together with aerosol drug delivery. The newly modified mixer-heater system has a reduced chamber volume and can be operated at lower flows, which enables its use with the infant population.

The aim of this study was to determine the *in vitro* particle size and delivery efficiency of a dispersion of commercial surfactant containing EEG excipients, sodium chloride and mannitol, using a commercial vibrating mesh nebulizer and newly modified VCU low-volume mixer-heater systems with a streamlined nasal cannula (VCU Department of Engineering). Performance of the novel delivery system was compared to the performance of a front-loaded infant face mask standard of care system. Also tested was a high flow therapy system that utilized a commercial infant high flow nasal cannula interface.

6.2 Materials and methods

6.2.1 VCU mixer-heater systems

6.2.1.1 Low-volume mixer-heater design

The low-volume mixer heater system has been described by Spence et al. [159]. As with the original mixer-heater design [157], the reservoir-based system is designed to produce submicrometer pharmaceutical aerosols from vibrating mesh nebulizers. The new design enables use of the mixer-heater during high flow nasal cannula (HFNC) therapy (Figure 6.1). The VCU low-volume mixer heater has a volume of 61.6 mL, from the midplane of the nebulizer to the outlet plane, which is reduced from the first-generation mixer-heater that had a volume of 576 mL just in the mixing region. The VCU low-volume mixer-heater was designed to utilize two nebulizers – one for the drug formulation and one for saline – but only one nebulizer was used for this study with a stopper placed in the second nebulizer opening. Standard infant ventilator tubing with an internal diameter of 10 mm was used to connect the mixer-heater device to a novel streamlined nasal cannula. Room temperature ventilation gas at a rate of 6 L/min was introduced into the VCU low-volume mixer-heater with the heating element set to 60 °C, which resulted in an exit aerosol temperature of 35 °C at the exit of the nasal cannula. The device was produced using rapid prototyping (Object 24 printer, Stratasys Inc., Eden Prairie, MN) with VeroWhitePlus™ (RGD835, Stratasys Inc., Eden Prairie, MN) material.

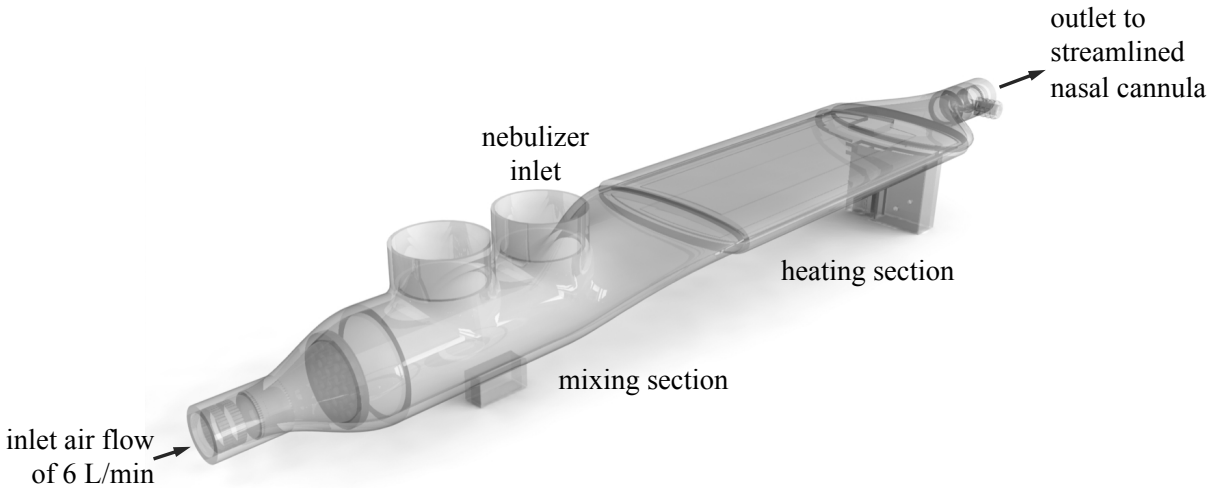


Figure 6.1 Computer aided design rendered image of the VCU low-volume mixer-heater.

6.2.1.2 Very low-volume mixer-heater design

Design changes were made to the VCU low-volume mixer-heater to further reduce the volume of the system to improve its efficiency and minimize respiration losses [160]. The main design change was removal of the heating element and incorporation of an external heat source to provide warm ventilation gas (43 °C) into the system at a rate of 6 L/min to mix with the aerosolized drug (Figure 6.2). This resulted in an exit aerosol temperature of 25 °C from the 23 cm length of tubing (Tygon® B-44-4X with 5 mm ID, Saint-Gobain, Courbevoie, France) that was used to connect the streamlined cannula. The optimized device had a reduced volume of 2.66 mL (from the centerline of the nebulizer inlet plane to the outlet plane) in comparison to the previous low-volume mixer-heater configuration (61.6 mL), resulting in a greater than 20-fold reduction in volume. The VCU very low-volume mixer-heater was designed for use with a modified Aerogen® Solo (Aerogen, Galway, Republic of Ireland), which eliminated the dead space at the outlet of the

nebulizer to further reduce the total volume of the delivery system (Figure 6.2). As with the previous design, the device was produced using rapid prototyping.

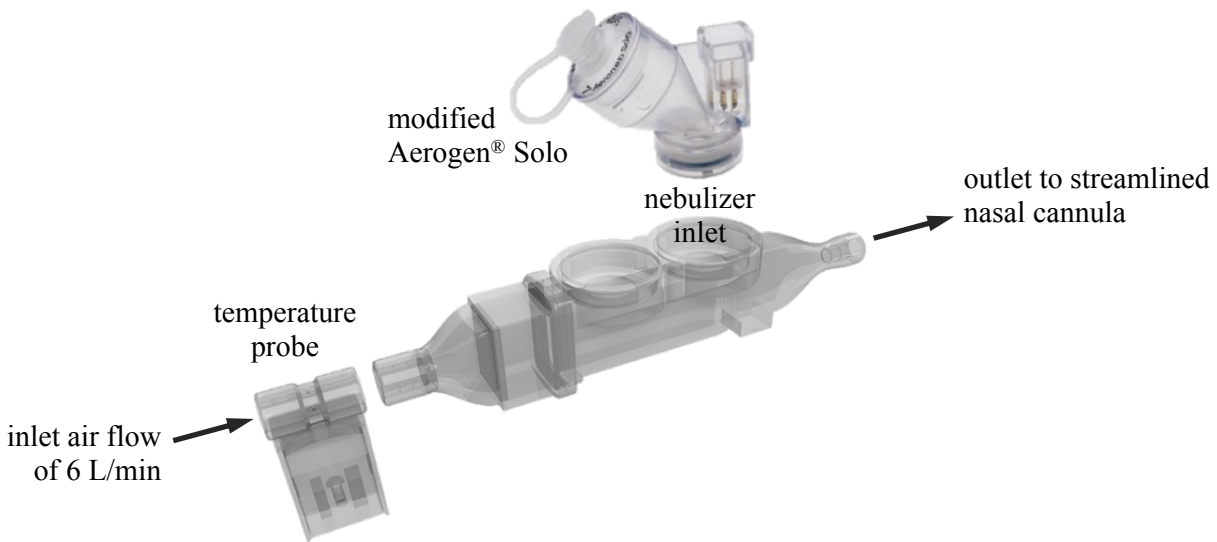


Figure 6.2 Computer aided design rendered image of VCU very low-volume mixer-heater and modified Aerogen® Solo.

6.2.2 Realistic infant nose-throat model

In vitro aerosol deposition experiments were performed with a realistic nose-throat model based on computed tomography (CT) scans of a 20-week-old male infant weighing 7.7 kg. The realistic model was constructed using Mimics® (Materialize, Ann Arbor, MI) image segmentation software and constructed using rapid prototyping (Object 24 printer, Stratasys Inc., Eden Prairie, MN) with a rigid opaque photopolymer (VeroWhitePlus™, RGD835, Stratasys Inc., Eden Prairie, MN). The model anatomy includes nostrils, turbinates, nasopharynx, larynx and a portion of the trachea and is segmented into three portions: (i) the anterior nose, (ii) the middle passage, and (iii) the nasopharynx, larynx and trachea (Figure 6.3).

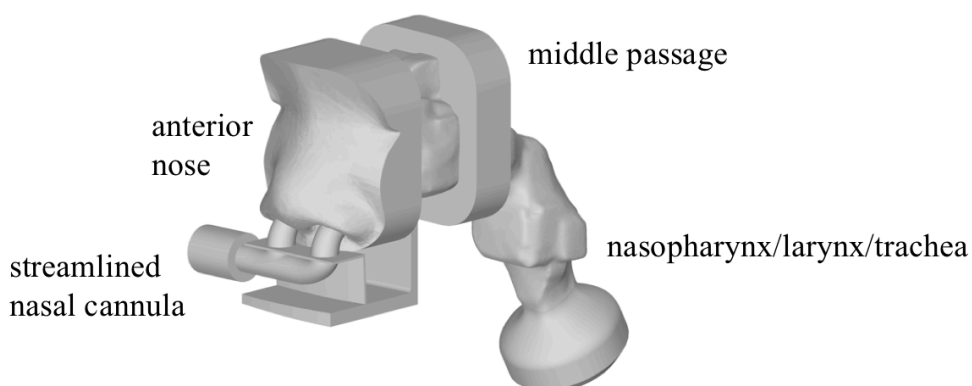


Figure 6.3 Infant nose-throat model, based on the computed tomography scans of a 20-week-old male infant weighing 7.7 kg, with streamlined infant nasal cannula.

6.2.3 *In vitro* nasal delivery experimental set up

Initial studies were performed with albuterol sulfate as the drug in the nebulization studies, due to the challenges of routinely assaying the surfactant-EEG formulation via quantification of DPPC using LC-MS. These studies were focused on mixer-heater optimization, which would be applicable for all nebulizer formulations. Optimization experiments were performed with 0.5% w/v albuterol sulfate in water solution prepared by dissolving albuterol sulfate USP (Letco Medical, LLC, Decatur, AL) in water. For all initial testing, an Aerogen[®] Pro nebulizer (Aerogen, Galway, Republic of Ireland) was used; the nebulizer was filled with 3.5 mL of the nebulizer formulation and weighed prior to and following nebulization for each run to determine the nominal dose by mass – the amount of drug emitted by nebulizer. A solution density of 1 g/mL was assumed and the mass difference before and after nebulization was multiplied by the albuterol sulfate (AS) concentration (Equation 6.1) to determine the nominal dose (Equation 6.2) of albuterol sulfate nebulized.

$$AS \text{ soln conc, mg/mL} = \frac{\text{assayed amount of AS in drug solution, mg}}{\text{volume of drug solution in assay sample, mL}} \quad \text{Equation 6.1}$$

$$\text{Nominal dose, mg} = \frac{(\text{filled weight} - \text{final weight}), \text{ g}}{\text{density of AS, } \frac{\text{g}}{\text{mL}}} \times AS \text{ soln conc, } \frac{\text{mg}}{\text{mL}} \quad \text{Equation 6.2}$$

6.2.3.1 VCU low-volume mixer-heater with streamlined infant nasal cannula

Reducing the volume of the mixer-heater and using the low ventilation gas flow rates required for infant delivery presented a significant challenge for efficient drying of the nebulizer aerosol output to produce the required submicrometer aerosol. To ensure adequate drying of the aerosol, a modified nebulizer controller was used to reduce the nebulizer output following procedures developed by Holbrook et al. [161]. The modified controller was set to operate the nebulizer at the same frequency as the commercial controller (128 kHz), while the amplitude of the applied sinusoidal operating voltage was reduced to produce approximately one-fourth of the aerosol output by mass from the vibrating mesh nebulizer, from 50 V_{rms} to 14.1 V_{rms} . A function waveform generator (Agilent Technologies model 33120A, Santa Clara, CA) was used to generate the desired signal, which was amplified using a modulated power supply (TS200 Option 5B, Accel Instruments, Irvine, CA).

The modified reduced output controller was used to operate the vibrating mesh nebulizer in the experimental setup with the low-volume mixer-heater delivery system as shown in Figure 6.4. Ventilation gas (air) was delivered through the system at a constant flow rate of 6 L/min (100 mL/s). The VCU low-volume mixer-heater operating temperature was set to a nominal value of 60 °C, which resulted in an exit aerosol temperature from the streamlined cannula of 35 °C.

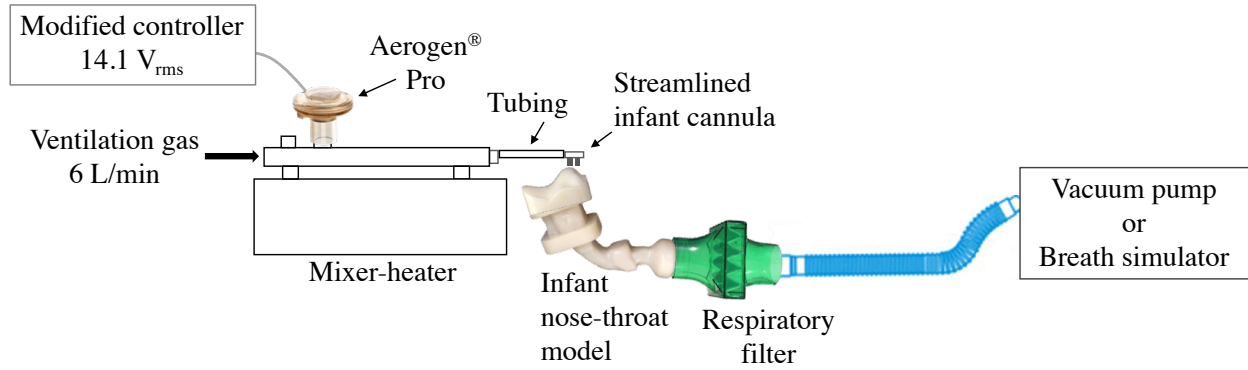


Figure 6.4 Experimental setup for the VCU low-volume mixer-heater system with streamlined infant nasal cannula.

6.2.3.2 Face mask standard of care system

The face mask standard of care system experimental test setup is depicted in Figure 6.5. A front-loading face mask based on Bubbles the Fish II® pediatric mask (Pari Respiratory Equipment Inc., Midlothian, VA) was tightly fitted to the infant model. The Aerogen® Pro nebulizer was connected to the infant mask using an adapter designed to connect the mask and nebulizer; the nebulizer was operated using the commercial Aerogen® controller in continuous mode.

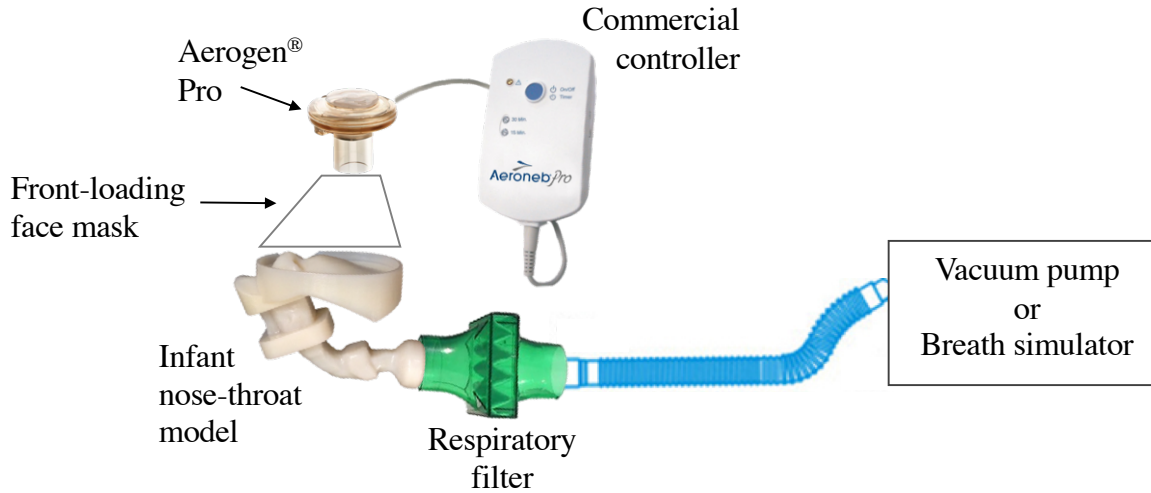


Figure 6.5 Face mask standard of care system experimental setup

6.2.3.3 High flow nasal cannula standard of care system

A high flow therapy device, Vapotherm model 2000i, (Vapotherm, Exeter, NH) was set to 37 °C and used to provide high flow heated and humidified air at a rate of 6 L/min (100 mL/s) to the experimental setup as shown in Figure 6.6. The mesh nebulizer was positioned in a porous walled T-piece (Aeroneb[®] Aerosol Adapter, Vapotherm[®], Stevensville, MD), which was attached to the Vapotherm[®] infant nasal cannula and infant model. The commercial Aerogen[®] controller was used to operate the mesh nebulizer in continuous mode.

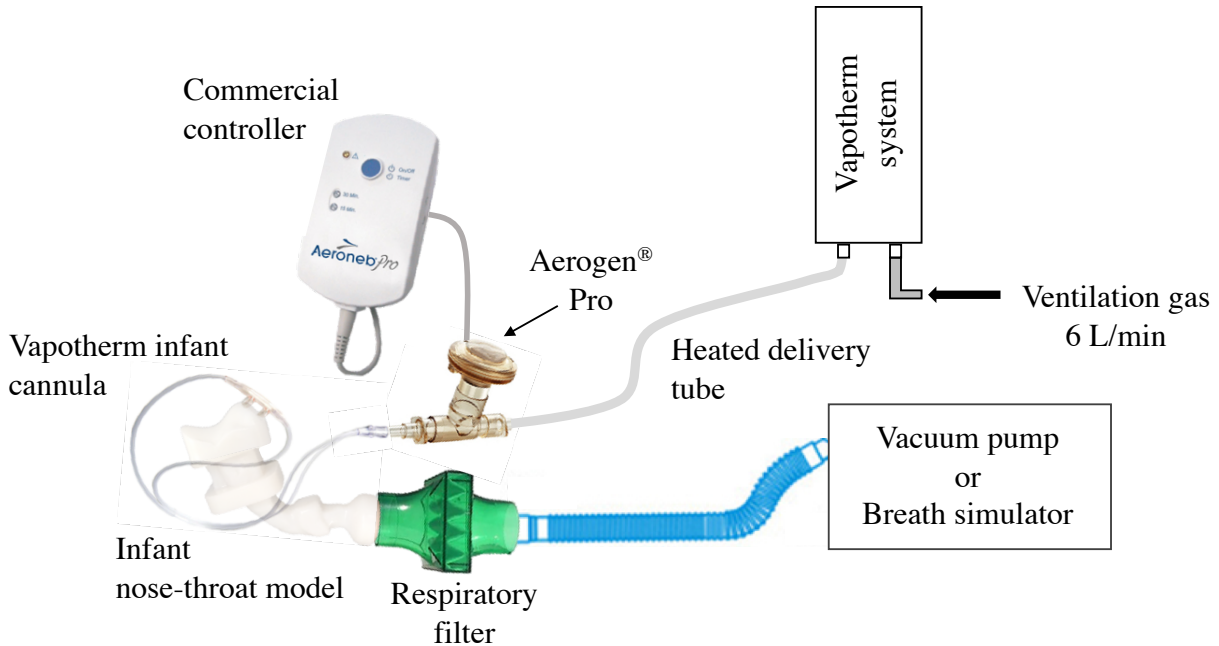


Figure 6.6 High flow nasal cannula standard of care system experimental setup.

6.2.4 Breathing conditions

Experiments were performed under two breathing conditions: (i) steady state inhalation flow conditions (without an exhalation cycle) and (ii) realistic breathing cycle (with both inhalation and exhalation cycles). The steady state inhalation flow utilized a vacuum pump to draw air through the experimental setups at a constant flow of 7 L/min (117 mL/s). The realistic breathing cycle was generated by a breath simulator (ASL 5000, IngMar Medical, Pittsburgh, PA) based on the breathing profile of an 8 kg infant [81]. The breathing profile (Figure 6.7) is a sinusoidal waveform with a peak inspiratory flow rate of 10.5 L/min (175 mL/s), a tidal volume of 56 mL, 40 breaths per minute and an inspiratory-expiratory ratio of 1:2. The inhalation and exhalation durations were 0.5 s and 1.0 s, respectively.

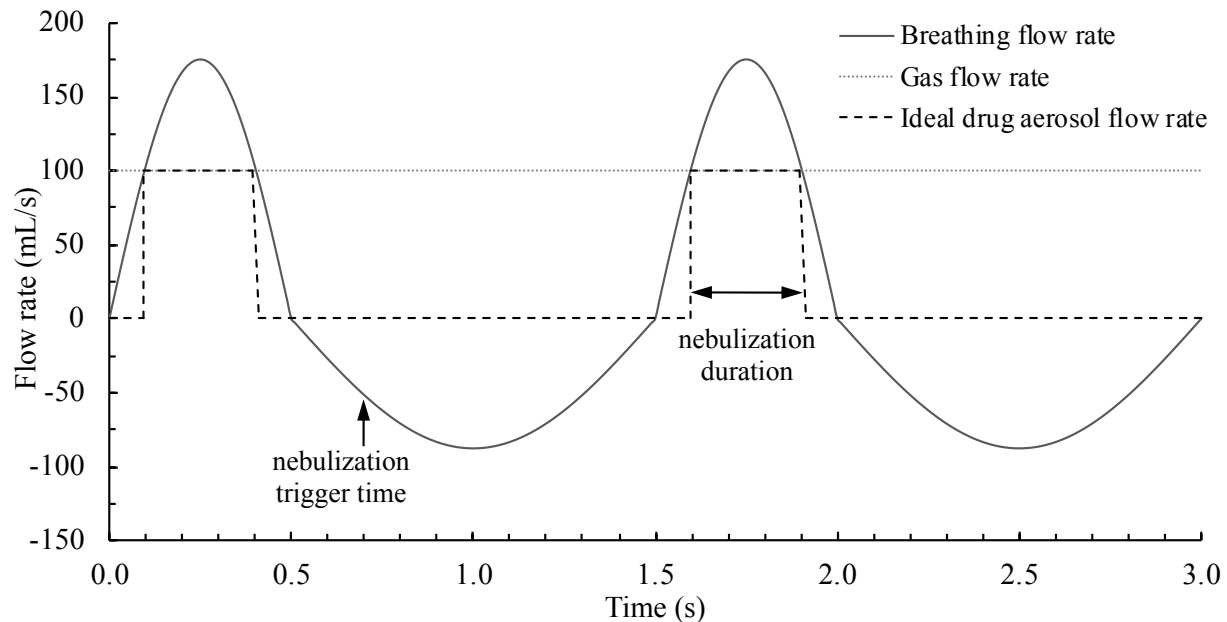


Figure 6.7 Two cycles of a realistic breathing profile based on an 8 kg infant. The ventilation gas flow rate is 100 mL/s (6 L/min) delivered continuously. Ideally, drug aerosol is delivered to the patient in the ventilation gas flow only during inhalation and the delivery time should be synchronized such that delivery occurs when the inhalation flow rate is greater than the ventilation gas flow as shown by the nebulization duration. To achieve this delivery through the low-volume mixer heater, nebulization must be triggered during the exhalation cycle, as shown by the nebulization trigger time. In this example, the nebulization trigger time was 0.8 s before the next breath and the nebulization duration was 0.3 s.

6.2.4.1 Optimization of breath synchronized aerosol drug delivery

To reduce drug losses, the use of breath-actuated nebulization was studied. A relay timer (Time Delay Relay TD-88122, Macromatic Industrial Controls, Inc., Menomonee Falls, WI) was used to trigger the modified reduced output controller to actuate the nebulizer for a set time duration. The optimal setting for two parameters were determined: (i) nebulization trigger time – the time at which the nebulizer was triggered during the exhalation cycle relative to the start of the next inhalation phase of the breathing cycle, and (ii) the nebulization duration – the amount of time the nebulizer was set to operate during the cycle.

Based on the volume of the VCU low-volume mixer-heater device (from the centerline of the nebulizer inlet plane to the outlet plane, 61.6 mL), the volume of the ventilator tubing connecting the mixer-heater to the streamlined cannula (9.4 mL), and the ventilation gas air flow entrained through the system (100 mL/s), the theoretical delivery time for the aerosol generated by the nebulizer to reach the infant cannula was calculated to be 0.71 s. From the realistic breathing profile, the time in which the inspiratory flow was greater than the ventilation gas air flow of 6 L/min (100 mL/s in Figure 6.7) was determined to be 0.3 s out of a total inhalation time of 0.5 s.

Starting conditions for the nebulization trigger time and the nebulization time were selected as 0.8 s prior to the start of inhalation and 0.3 s, respectively. For all experiments, the nebulizer was filled with 3.5 mL of 0.5% w/v AS in water solution and allowed to run for 20 minutes. The filter component, the estimated % lung dose, was analyzed in the optimization experiments.

6.2.5 Droplet sizing experiments with the Andersen Cascade Impactor

Sizing experiments were performed using the Andersen Cascade Impactor (ACI, Copley Scientific, Nottingham, UK) placed in an environmental chamber (Espec, Hudsonville, MI) set to 99% relative humidity (RH) to minimize effects of evaporative size changes during sizing measurements. A vacuum pump was used to draw air through the impactor at a flow rate of 28.3 L/min as monitored with a mass flow meter (TopTrak[®] 822, Sierra Instruments, Monterey, CA) placed between the impactor and vacuum pump. Aerosol delivery experiments were performed with 0.5% w/v AS in water solution. The Aerogen[®] Pro nebulizer was filled with 3.5 mL of nebulizer formulation and weighed prior to and following nebulization for each run to determine the nominal dose by mass (Equation 6.1). A solution density of 1 g/mL was assumed and the mass difference before and after nebulization was multiplied by the albuterol sulfate concentration to

determine the nominal dose of albuterol sulfate nebulized. In order to obtain similar emitted masses, the nebulizer was allowed to run for 5 minutes and 20 minutes for experiments performed with the commercial controller and the modified reduced output controller, respectively.

Drug was extracted from the impactor stages and filter to determine the emitted dose, the mass median aerodynamic diameter (MMAD), the geometric standard deviation (GSD) and particle mass fraction less than 1 μm and less than 5 μm . MMAD, GSD, and particle fractions were determined by linear interpolation. MMAD values were directly calculated as the size associated with a cumulative count of 50% based on mass percentages calculated relative to the impactor dose. GSD values were calculated following Equation 6.3. Particle mass fractions were calculated as the cumulative mass fraction frequency associated with sizes of 1 μm and 5 μm , respectively. Each measurement was performed a minimum of three times.

$$GSD = \sqrt{\frac{\text{size at cumulative count of 84.13\%}}{\text{size at cumulative count of 15.87\%}}} \quad \text{Equation 6.3}$$

6.2.6 High performance liquid chromatography assay

Drug was recovered from the components using known volumes of water and analyzed using an isocratic high-performance liquid chromatography (HPLC) assay method. The mobile phase consisted of 30% ammonium formate buffer (20 mM, pH 3.4) and 70% methanol. A Restek™ Allure™ pentafluorophenyl column (150 mm x 3.0 mm, particle diameter 5 μm) was used to separate AS at 0.75 mL/min with an injection volume of 100 μL on a Waters 2695

Separations Module and detection performed at 276 nm using a Waters 2475 fluorescence detector (Waters Corporation, Milford, MA).

6.2.7 Statistical analysis

Data analysis was performed using JMP[®] Pro software version 12.0 (SAS Institute Inc., Cary, NC). Student's t-statistic or one-way analysis of variance (ANOVA) followed by Dunnett's method or Tukey's HSD was performed to determine statistically significant differences in the data obtained. The Pearson correlation coefficient was determined to quantify the strength of linear relationships. *P* values less than 0.05 were considered as statistically significant.

6.3 Results and discussion

6.3.1 Droplet aerosol sizing experiments with the ACI

6.3.1.1 Effect of modified controller on nebulizer initial aerosol droplet size

The effect of the nebulizer controller amplitude on initial droplet size was determined by comparing the size of the aerosol at the exit of the mesh nebulizer generated from the commercial Aerogen[®] controller with the aerosol size generated using the modified controller (driving amplitude of one-fourth of the commercial controller, 14.1 V_{rms} vs 50 V_{rms}). Experiments were performed at 25 °C and 99% RH in the environmental chamber. Bimodal size distributions were observed for both controller configurations (Figure 6.8, top). The droplets generated with the commercial controller were determined to have a mean ± SD MMAD of 5.0 ± 0.1 μm and GSD of 1.8 ± 0.04. The droplets generated with the modified controller were determined to be significantly smaller with a mean ± SD MMAD of 3.8 ± 0.6 μm compared to the commercial controller (*p*=0.0087; Student's t-test). The controller amplitude was found to have a significant effect on the particle fraction less than 5 μm, with higher particle fractions observed with the

modified controller compared to the commercial controller (69.8 % vs 50.8 %, $p=0.0011$; Student's t-test). No differences were observed in the GSD values of the particle size distributions and the submicrometer particle fractions between the two controllers. Results are shown in Table 6.1.

Reducing the driving amplitude to one-fourth that of the commercial controller resulted in a proportional decrease in output from the nebulizer, from 300 $\mu\text{L}/\text{min}$ for the commercial controller to 72 $\mu\text{L}/\text{min}$ for the modified controller (Table 6.1). The significantly smaller MMAD values observed with the modified controller were due to the decreased output from the nebulizer; since less droplets were exiting the nebulizer at a given time (lower aerosol concentration at the exit of the nebulizer), this resulted in less interactions between droplets and therefore reduced droplet coagulation. MMAD values from the nebulizer were observed to have a positive correlation with the output rate from the nebulizer ($r = 0.7805$, $p=0.0046$, $R^2 = 0.6092$; Pearson correlation), where an increase in output rates resulted in larger median droplet diameters.

6.3.1.2 Effect of mixer-heater on nebulizer aerosol droplet size

The size of the aerosol at the exit of the streamlined infant nasal cannula was also determined following generation and drying in the VCU low-volume mixer-heater operating at 60 $^{\circ}\text{C}$. Studies were similarly performed in a controlled temperature and humidity environment. Experiments were performed at 35 $^{\circ}\text{C}$, the temperature of the exit aerosol from the streamlined cannula, and 99% RH in the environmental chamber. The modified controller was used to power the vibrating mesh nebulizer to produce aerosol that mixed with ventilation gas introduced into the VCU low-volume mixer-heater at 6 L/min . The size of the aerosol exiting the nasal cannula was compared to the size determined at the exit of the nebulizer. The aerosol exiting the streamlined cannula of the VCU low-volume mixer-heater delivery system was determined to have a mean \pm

SD MMAD of $1.4 \pm 0.1 \mu\text{m}$ and a GSD of 1.4 ± 0.0 . This resulted in a significantly smaller MMAD and GSD compared to the aerosol exiting the nebulizer ($p < .0001$ and $p = 0.0306$, respectively; Student's t-test). The particle fractions were significantly affected by the use of the VCU low-volume mixer-heater with a higher percent of particles less than $1 \mu\text{m}$ and less than $5 \mu\text{m}$ compared to the aerosol exiting the nebulizer ($p = 0.0052$ and $p < .0001$, respectively; Student's t-test).

The use of the VCU low-volume mixer-heater enabled drying of the droplets exiting the nebulizer; the aerosol was mixed with dry ventilation gas and then further dried as the nebulizer aerosol-ventilation gas mixture was heated. This resulted in particles that were more monodisperse (top plot of Figure 6.8, square vs diamond markers) and less variable (smaller standard deviation values obtained for MMAD calculations, Table 6.1).

Considering the solids concentration of the nebulizer formulation, the initial droplet size of $3.8 \mu\text{m}$, and the density of albuterol sulfate of 1.34 g/cm^3 , the predicted dry particle size of a 0.5% w/v solution of AS is estimated to be $0.68 \mu\text{m}$, which indicates that the particles exiting the streamlined cannula are likely not completely dry. The larger than predicted particle size suggests that the VCU low volume mixer-heater system can still be optimized as ensuring complete drying of the droplets from the mixer-heater would possibly allow for improved delivery efficiency of aerosols to the infant lungs.

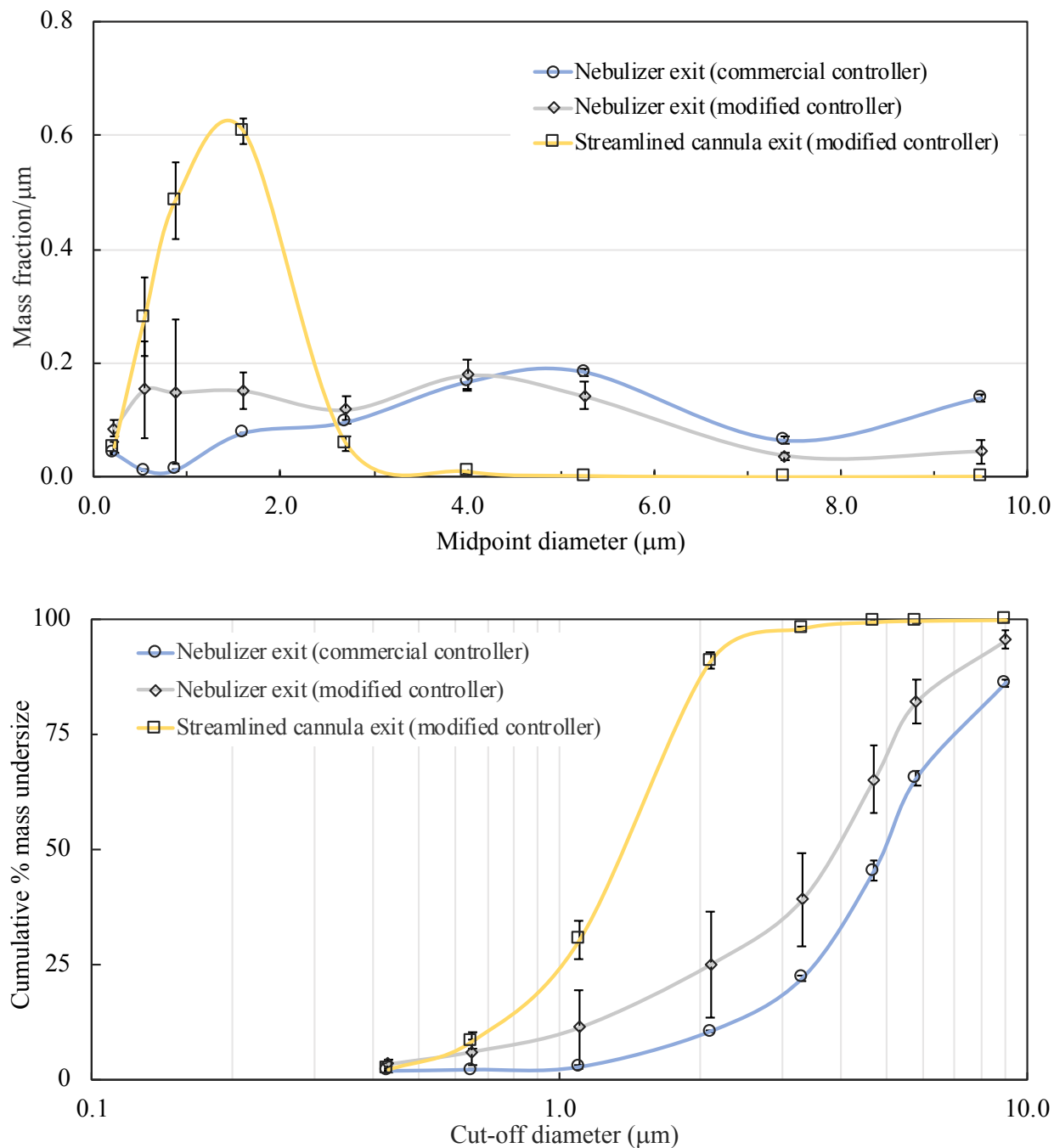


Figure 6.8 Droplet size distributions of mass fraction/ μm (top) and cumulative percent mass undersize (bottom) of 0.5% w/v albuterol sulfate in water from the Aeroneb[®] Pro nebulizer determined by cascade impaction with the ACI in an environmental chamber set to 99% RH. Aerosol size was determined at the nebulizer exit using the (i) commercial controller and (ii) modified controller, together with (iii) the aerosol size at the streamlined cannula exit following aerosol generation into the VCU low-volume mixer-heater. Markers represent the mean value, error bars represent the SD, $n \geq 3$.

Table 6.1 Droplet size characteristics of 0.5% w/v albuterol sulfate in water from the Aeroneb[®] Pro nebulizer determined by cascade impaction with the ACI. Aerosol size was determined at the nebulizer exit using the (i) commercial controller and (ii) modified controller, together with (iii) the aerosol size at the streamlined cannula exit following aerosol generation into the VCU low-volume mixer-heater. Values are mean (SD), n≥3.

Controller (amplitude voltage)	Droplet size measurement position	Output rate, μL/min	MMAD, μm	GSD	Particle fraction, %	
					<1 μm	<5 μm
Commercial (50 V _{rms})	nebulizer exit	300 (10)	5.0 (0.1)	1.8 (0.0)	2.5 (0.1)	50.8 (1.9)
Modified (14.1 V _{rms})	nebulizer exit	72 (10)	3.8 (0.6)*	1.7 (0.2)	10.1 (6.8)*	69.8 (6.7)*
Modified (14.1 V _{rms})	streamlined cannula exit	101 (3)	1.4 (0.1)#	1.4 (0.0)#	25.5 (3.5)#	99.5 (0.0)#

*Significant difference compared to commercial controller; Student's t-test, $p < 0.05$

#Significant difference compared to exit of nebulizer with modified controller; Student's t-test, $p < 0.05$

6.3.2 *In vitro* aerosol deposition with a realistic infant nose-throat model

6.3.2.1 Effect of aerosol delivery system on *in vitro* drug deposition

The drug deposition results comparing the face mask standard of care delivery system with the VCU low-volume mixer-heater system using steady state inhalation flow conditions (7 L/min) and continuous nebulization are shown in Figure 6.9. The mean \pm SD emitted dose from the patient interface (amount of drug available to enter the nose-throat model) was significantly higher in the VCU low-volume mixer-heater system, $97.5 \pm 0.5\%$, compared to the face mask standard of care system, $78.6 \pm 0.9\%$ ($p < .0001$; Student's t-test). For the face mask standard of care system, a majority of the drug deposition was on the nose-throat model, $73.9 \pm 8.5\%$ of the nominal dose, compared to $3.9 \pm 1.0\%$ that was observed with the VCU low-volume mixer-heater system ($p = 0.0001$; Student's t-test). For the VCU low-volume mixer-heater system, a majority of the drug deposition was observed on the filter (the estimated % lung dose), $76.2 \pm 2.9\%$, which was significantly higher than that observed for the face mask standard of care system ($p < .0001$; Student's t-test).

The smaller droplets introduced to the *in vitro* infant nose-throat airway using the VCU low-volume mixer-heater system compared to the face mask standard of care system, $1.4 \mu\text{m}$ vs the $5.0 \mu\text{m}$, resulted in improved aerosol drug delivery efficiency through the realistic airway; the smaller droplets were able to traverse the narrow airways of the model more efficiently than the larger droplets. Aerosol drug deposition on the delivery device (nebulizer outlet) was higher for the face mask standard of care system compared to the VCU low-volume mixer-heater system. Similarly, deposition on the patient interface (face mask) was also higher for the standard of care aerosol delivery method compared to the VCU low-volume mixer-heater system (Figure 6.9). Table 6.2 shows the total and regional (italicized) deposition for the different components. These

results clearly indicate the advantages of the smaller aerosol droplet size generated using the VCU low-volume mixer-heater which produced minimal drug deposition losses in the delivery device and cannula and maximizes the amount of drug aerosol able to penetrate the nasal passages of the infant and be delivered to the patient airways, as shown by the estimated % lung dose of 76 %.

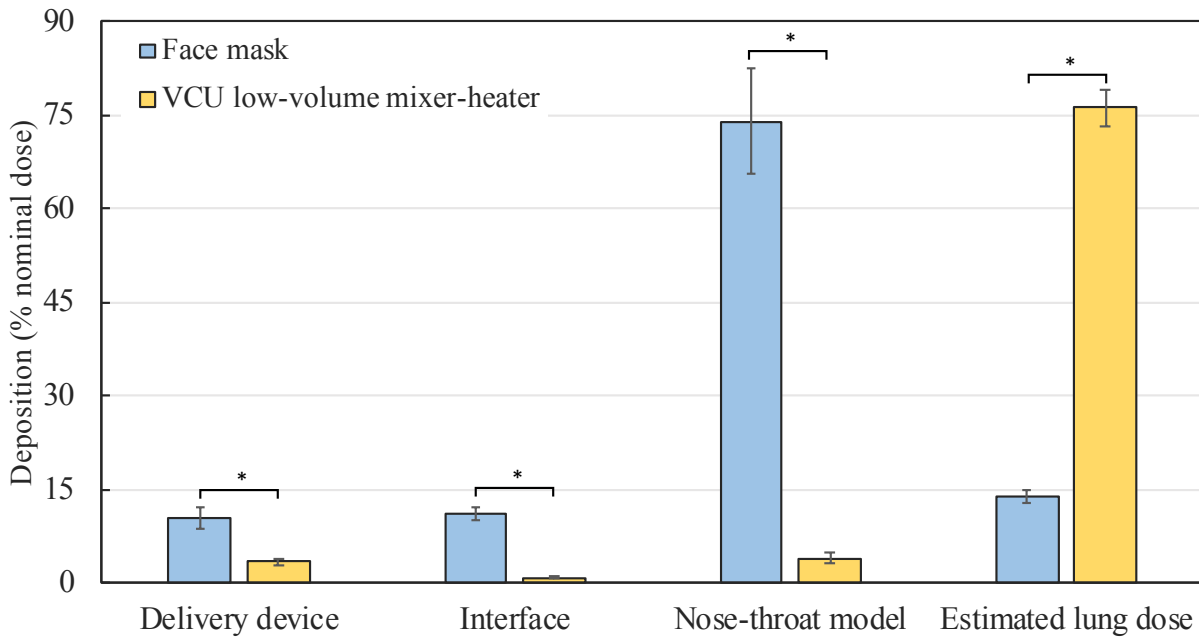


Figure 6.9 Aerosol drug deposition comparison for the face mask standard of care system and the VCU low-volume mixer-heater system using steady state inhalation conditions. Delivery device: face mask system = nebulizer outlet; mixer-heater system = nebulizer outlet, mixer-heater, tubing. Bars represent the mean value, error bars represent SD, n=3. *Significant difference; Student's t-test, $p < 0.05$.

Table 6.2 Total and regional aerosol drug deposition comparison for the standard of care systems with the VCU mixer-heater delivery system using steady state inhalation conditions. Values are mean (SD), n=3.

Component	Face mask standard of care system	VCU low-volume mixer-heater system	HFNC standard of care system
Delivery device			
<i>Nebulizer outlet</i>	10.3 (1.6)	0.2 (0.1)	4.0 (1.8)
<i>Mixer-heater</i>	n/a	2.1 (0.6)	n/a
<i>Tubing</i>	n/a	1.0 (0.1)	n/a
<i>T-piece</i>	n/a	n/a	57.0 (2.4)
Total	10.3 (1.6)	3.3 (0.6) [#]	61.0 (4.1)
Interface*	11.0 (0.9)	0.8 (0.2) [#]	2.3 (0.3)
Nose-throat model			
<i>Anterior nose</i>	.	0.9 (0.2)	2.5 (0.4)
<i>Middle passage</i>	.	1.2 (0.3)	10.7 (2.5)
<i>Nasopharynx</i>	.	1.8 (0.9)	20.0 (1.5)
Total	73.9 (8.5)	3.9 (1.0) [#]	33.1 (4.2)
Estimated lung dose	13.9 (1.0)	76.2 (2.9) [#]	1.3 (0.2)

*Face mask system: face mask; mixer-heater system: streamlined nasal cannula; HFNC system: commercial infant nasal cannula

[#]Significant difference compared to face mask standard of care system; Student's t-test, p<0.05

The high flow therapy system with HFNC was also tested to determine the drug deposition in the realistic infant nose-throat model with a commercial system while humidity is incorporated. In this system, the delivery device, which consisted of the nebulizer outlet and the T-piece, had the highest drug deposition at 61% of the nominal dose with a mean \pm SD emitted dose from the interface of $36.7 \pm 4.1\%$ of the nominal dose. This resulted in 33% deposition in the nose-throat model and only 1.3% of the nominal dose reaching the filter. The high deposition in the T-piece is likely due to two related factors: 1) the high rate of aerosol exiting the nebulizer, and 2) the larger

sized aerosols generated from the nebulizer with the commercial controller. With entrained air at a flow rate of 6 L/min, deposition in the T-piece is due to impaction losses from both the high rate of aerosol at the exit of the nebulizer and to impaction of the particles entrained in the turbulent flow. The presence of humidity in the system prevented aerosol evaporation and drying which maintained the size of the aerosol droplets as they exited the nebulizer. There was significant deposition of the 5 μm aerosol in the passageways of the delivery system and nose-throat model due to inertial impaction and sedimentation resulting in the observed poor estimated % lung dose of 1.3% of nominal dose.

6.3.2.2 Effect of a realistic breath cycle on *in vitro* aerosol deposition

The effect of incorporating realistic breathing conditions on drug deposition was studied using continuous aerosol generation from the nebulizer. For the VCU low-volume mixer-heater system the estimated % lung dose was decreased significantly when an exhalation cycle was incorporated into the breathing cycle, from $76.3 \pm 2.9\%$ to $12.0 \pm 0.8\%$ of the nominal dose ($p < .0001$; Student's t-test). No significant differences in drug deposition were observed in the other device components (delivery device or patient interface) or the nose-throat model. Similarly, incorporating the exhalation cycle found significant decreases in the estimated % lung dose with the face mask standard of care delivery system, from $13.9 \pm 1.0\%$ to $5.2 \pm 0.30\%$ of the nominal dose ($p < .0001$; Student's t-test). There were significant differences seen in aerosol drug deposition on the other components of the standard of care delivery system; increases in drug deposition were observed for the delivery device and interface components ($p = 0.0168$ and $p = 0.0482$, respectively; Student's t-test), while a decrease in deposition was observed in the nose-throat model ($p = 0.0017$; Student's t-test).

For the VCU low-volume mixer-heater system, the mean \pm SD emitted dose from the interface of $95.2 \pm 0.6\%$ was not different from steady state inhalation flow conditions ($95.7 \pm 0.5\%$ of the nominal dose), but significantly higher than the emitted dose from the interface for the face mask standard of care system ($63.3 \pm 1.8\%$, $p < .0001$; Student's t-test). A comparison of the estimated % lung dose in the two delivery systems when realistic breathing conditions were employed found that the VCU low-volume mixer-heater system had a significantly higher estimated % lung dose compared to the face mask standard of care system ($p < .0001$; Student's t-test). Deposition in the delivery device, interface, and nose-throat model were all significantly lower in the mixer-heater system compared to the face mask standard of care system (Table 6.3, $p < 0.05$; Student's t-test). The decrease in estimated % lung dose observed in both systems was attributed to exhalation losses due to constant nebulization throughout the breath cycle.

Table 6.3 Deposition comparison of standard of care systems with the VCU low-volume mixer-heater delivery system with realistic breathing conditions and constant nebulization. Values are mean (SD), n=4.

Component	Face mask standard of care system	VCU low-volume mixer-heater system
Delivery device	17.8 (3.4)	3.7 (0.5) [#]
Interface*	18.9 (5.0)	1.0 (0.2) [#]
Nose-throat model	46.5 (4.1)	2.6 (0.7) [#]
Estimated lung dose	5.2 (0.3)	12.0 (0.8) [#]

*Face mask system: face mask; mixer-heater system: streamlined nasal cannula

[#]Significant difference compared face mask standard of care system; Student's t-test, $p < 0.05$

6.3.3 Optimization of aerosol delivery synchronization with realistic breathing cycle

In order to minimize drug losses and increase the estimated % lung dose, the use of aerosol delivery synchronization with the breathing cycle was explored to ensure that aerosol was delivered to the airways only during inhalation. Experiments were performed with realistic breathing conditions in which nebulization was synchronized with the patients simulated breathing pattern in this highly controlled laboratory environment to investigate the critical variables controlling efficient aerosol delivery. The effect of the nebulizer aerosol output rate, the nebulization trigger time within the breathing cycle and the nebulization duration on the estimated % lung dose were each studied independently.

6.3.3.1 Effect of nebulizer aerosol output rate on *in vitro* aerosol deposition

In order to determine the effect of the output rate of the nebulizer with the VCU low-volume mixer-heater system on the estimated % lung dose, the modified controller driving amplitude was varied to produce lower nebulizer output rates as shown in Table 6.4. The nebulizer was triggered 0.3 s prior to the start of inhalation and the nebulization duration was 0.2 s for these studies to determine the effect of output rate on the estimated % lung dose. Data are shown in Table 6.4.

Due to the use of breath-synchronized nebulization, lower output rates (5-10 $\mu\text{L}/\text{min}$) were observed since the nebulizer was only triggered for 0.3 s of each 1.5 s breath cycle compared to the values observed during continuous nebulization (70-100 $\mu\text{L}/\text{min}$, Table 6.1). The output rate of the nebulizer was observed to have a strong positive correlation with the driving amplitude ($r = 0.8877$, $p < .0001$, $R^2 = 0.7881$; Pearson correlation); the output rate increased with increasing driving amplitude. This outcome was expected as the same trend was observed when comparing

output rates of the commercial controller with the modulated controller in earlier studies using continuous nebulization (Table 6.1).

The estimated % lung dose was observed to have a negative correlation with the output rate of the nebulizer ($r = -0.7253$, $p=0.0050$, $R^2 = 0.5260$; Pearson correlation); the estimated % lung dose as a percent of the nominal dose decreased with increasing output rate. From the droplet sizing experiments, it was observed that reducing the aerosol output from the nebulizer resulted in smaller droplet sizes, therefore, the negative correlation of estimated % lung dose with the aerosol output rate is likely due to higher deposition of the larger aerosol droplet in the other components in the system (delivery device, interface, and nose-throat model) at the higher output rates, resulting in the lower estimated % lung dose.

A strong positive correlation was observed with the mass of drug recovered from the filter component with the output rate of the nebulizer ($r = 0.8831$, $p<.0001$, $R^2 = 0.7798$; Pearson correlation); higher masses of drug were recovered with increasing aerosol output rate. Although the 5.1 $\mu\text{L}/\text{min}$ output rate provided more efficient delivery (higher estimated % lung dose as a percent of the nominal dose), the higher output rates of 9.4 and 11.1 $\mu\text{L}/\text{min}$ were able to deliver a higher mass of drug to the filter in the same delivery time of 20 minutes, with the output rate of 11.1 $\mu\text{L}/\text{min}$ delivering nearly twice as much drug compared to the output rate of 5.1 $\mu\text{L}/\text{min}$. Thus, future studies were performed with a driving amplitude of 4 Vpp and an output rate of ~ 11 $\mu\text{L}/\text{min}$.

Table 6.4 Comparison of nebulizer output rate of the modified controller on estimated % lung dose and total delivered lung dose. Values are mean (SD), $n \geq 3$.

Driving amplitude	Output rate, $\mu\text{L}/\text{min}^*$	Estimated lung dose, % nominal*	Total lung dose, μg^*
4 Vpp	11.1 (1.5)	29.2 (4.0)	329 (42)
3 Vpp	9.4 (1.0)	31.9 (1.2)	308 (40)
2 Vpp	5.1 (0.4)	36.0 (4.5)	188 (9.5)

*Significant correlation with driving amplitude; Pearson correlation, $p < 0.05$

6.3.3.2 Effect of nebulizer synchronization on *in vitro* aerosol deposition

To ensure maximal delivery of aerosol to the lungs, the aerosol should be delivered in the ventilation gas during inhalation when the inhalation flow rate is greater than the ventilation gas flow. For the realistic breathing profile, the time interval during which the inhalation flow is greater than the ventilation gas flow was determined to be 0.3 s (Figure 6.7). To study the synchronization of the nebulizer actuation to achieve the highest estimated % lung dose, the nebulization duration was held constant at 0.3 s. For these highly controlled *in vitro* studies, it was possible to investigate the time (trigger time) in the breathing cycle when the nebulizer should be actuated in order to maximize aerosol delivery. The results plotted in Figure 6.10 show the estimated % lung dose values as a function of the nebulization trigger time relative to the start of inhalation (top) and also when shown on the time axis of the breathing cycle (bottom). For these studies the output rates from the nebulizer ranged from 8 to 20 $\mu\text{L}/\text{min}$.

The nebulization trigger time with the highest estimated % lung dose (mean \pm SD of $32.0 \pm 2.7\%$ of the nominal dose) was determined to be 0.4 s prior to the start of inhalation phase of the breathing cycle. The nebulization trigger time of 0.4 s was also found to have the highest drug recovery for the different trigger times studied ($492 \pm 84 \mu\text{g}$, Table 6.5), indicating that the aerosol

from the nebulizer took approximately 0.4 s to travel to the exit of the streamlined cannula with entrained air flow of 6 L/min. The plot of estimated % lung doses at different trigger times when plotted on the same scale as the breathing profile had a similar profile to that of the inhalation flow (bottom plot of Figure 6.10), indicating that delivery of the nebulized aerosol is synchronized with the inhalation profile when offset by 0.4 s prior to the start of inhalation and that this was the optimal nebulization trigger time.

The lowest estimated % lung dose as a percent of the nominal dose and the lowest recovered drug dose ($4.1 \pm 0.9\%$ and $79 \pm 20 \mu\text{g}$, respectively) was observed when the nebulization trigger time was set to 1.0 s prior to the next inhalation. Since it has been determined that the aerosol takes 0.4 s to travel from the nebulizer to the exit of the streamlined cannula, then the aerosol generated at a trigger time of 1.0 s prior to the next inhalation would reach the nose-throat model near the peak of the exhalation cycle (bottom plot of Figure 6.10), consistent with the low lung and recovered drug doses observed at this trigger time.

The delivery time for the aerosolized drug to travel from the nebulizer to the nose-throat model was therefore determined as 0.4 s, future studies were performed with a fixed nebulization trigger time of 0.4 s prior to the next inhalation.

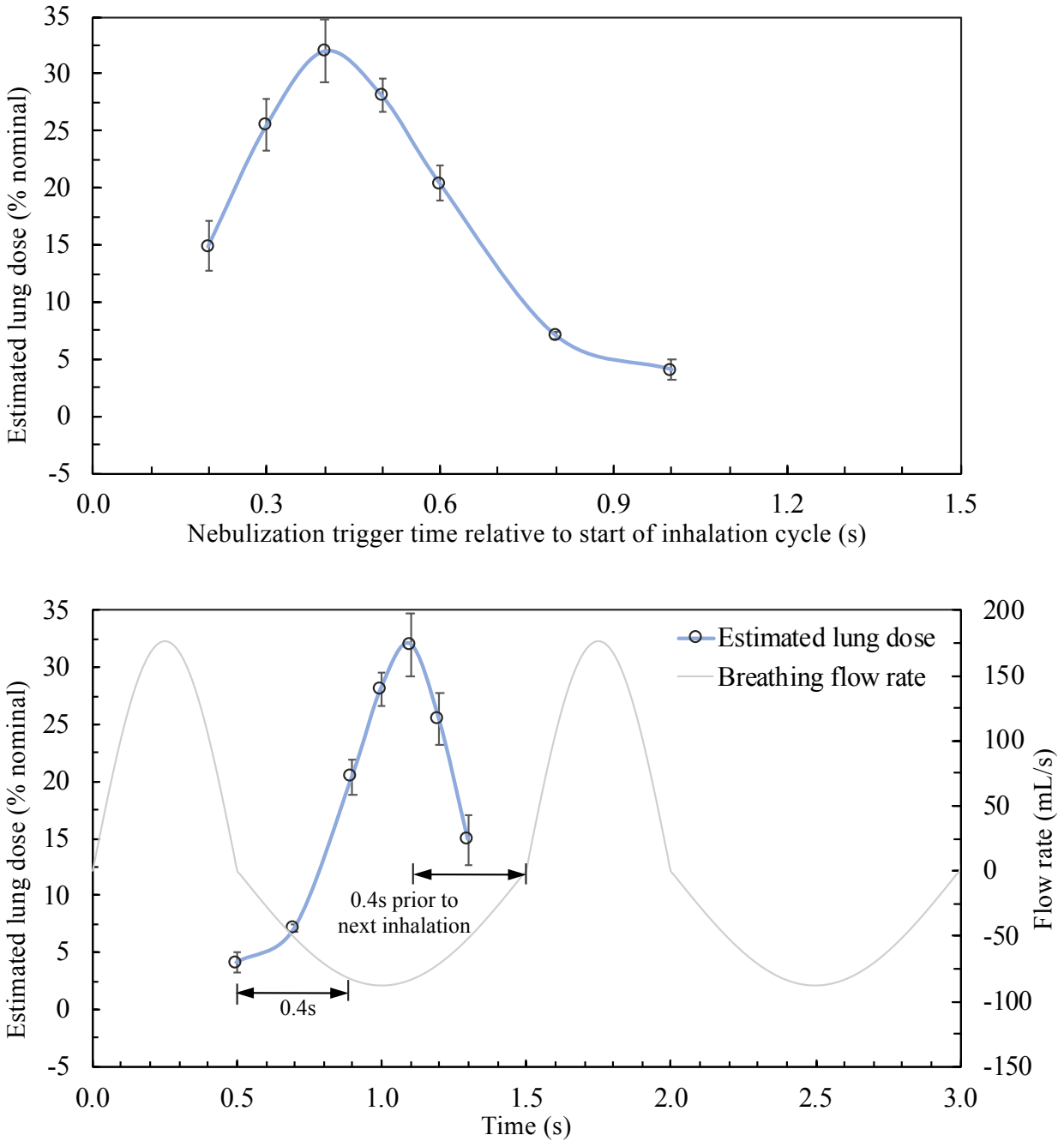


Figure 6.10 Estimated *in vitro* lung dose at different nebulization trigger times relative to the start of inhalation (top) and relative to the realistic breathing profile (bottom) with nebulization duration of 0.3 s. Markers represent the mean value, error bars represent the SD, n=3.

Table 6.5 Comparison of *in vitro* aerosol deposition for nebulization trigger times relative to the start of inhalation with a nebulization duration of 0.3 s and realistic breathing conditions. Values are mean (SD), n=3.

Nebulization trigger time relative to start of inhalation	Output rate, $\mu\text{L}/\text{min}$	Estimated lung dose, % nominal	Total recovered drug, μg
0.2 s	7.9 (1.0)	14.9 (2.2)	114 (14)
0.3 s	14.2 (3.7)	25.5 (2.3)	347 (59)
0.4 s	15.7 (1.7)	32.0 (2.8)	492 (84)
0.5 s	17.3 (3.6)	28.1 (1.5)	477 (120)
0.6 s	16.9 (5.8)	20.4 (1.5)	332 (84)
0.8 s	17.4 (3.9)	7.1 (0.4)	121 (30)
1.0 s	20.3 (5.6)	4.1 (0.9)	79 (20)

6.3.3.3 Effect of nebulization duration on *in vitro* aerosol deposition

Once the optimal point in the breathing cycle to synchronize delivery of the nebulized aerosol with the peak of the inhalation cycle was determined (0.4 s prior to the start of inhalation), the optimal nebulization duration was then studied. The nebulization durations of 0.1 s and 0.2 s were tested and compared to results obtained for the 0.3 s nebulization duration. At nebulization durations of 0.1 s and 0.2 s, the estimated % lung doses were determined to be $30.0 \pm 2.0\%$ and $35.0 \pm 1.5\%$ of the nominal dose, respectively. One-way ANOVA revealed a significant effect of nebulization duration on the estimated % lung dose, $p=0.0445$. A significant difference was revealed between 0.1 s and 0.2 s nebulization durations ($p=0.0397$; Tukey's HSD), both of which were not shown to be significantly different from the 0.3 s nebulization time ($p>0.05$; Tukey's HSD). In terms of total delivered dose of drug, the highest dose of AS was recovered when the nebulization duration was set to 0.3 s compared to the 0.2 s or 0.1 s nebulization time (492 vs 420 vs 154 μg), respectively. While the percentage drug delivery is important in terms estimating the

efficiency of the aerosol delivery process, the total delivered lung dose is also critical for applications where relatively large doses of drug are required for therapeutic efficacy.

The output rate and recovered drug dose were both found to have significant correlations with the nebulization duration at the 0.4 s nebulization trigger time. A positive correlation was observed between output rate and nebulization duration ($r = 0.8774$, $p=0.0009$, $R^2 = 0.7698$; Pearson correlation); longer nebulization durations resulted in higher output rates. The recovered drug dose was positively correlated with nebulization duration ($r = 0.8756$, $p=0.0009$, $R^2 = 0.7667$; Pearson correlation); increased nebulization durations resulted in higher recovered drug doses. These correlations were expected as longer nebulization durations allow for more drug to be nebulized, resulting in increased output rates and higher drug recovery.

Table 6.6 Comparison of *in vitro* aerosol deposition when varying the nebulization duration for nebulization trigger time of 0.4 s prior to the next inhalation with realistic breathing conditions. Values are mean (SD), $n \geq 3$.

Nebulization duration	Output rate, $\mu\text{L}/\text{min}^*$	Estimated lung dose, % nominal	Total recovered drug, μg^*
0.1 s	5.0 (0.2)	30.0 (2.0)	154 (8)
0.2 s	12.1 (2.7)	35.0 (1.5)	420 (71)
0.3 s	15.7 (1.7)	32.0 (2.8)	492 (84)

*Significant correlation with nebulization duration; Pearson correlation, $p < 0.05$

6.3.4 Optimized *in vitro* deposition with a realistic infant nose-throat airway model

The optimized breath-actuation conditions for maximizing *in vitro* aerosol delivery in a realistic infant nose-throat airway model were determined. The optimized conditions were as follows: driving amplitude of 4 Vpp, nebulization trigger time of 0.4 s prior to the start of

inhalation and nebulization duration of 0.2 s. The nebulizer was filled with 3.5 mL of 0.5% w/v AS and set to run for 20 minutes. Table 6.7 shows the full characterization of the regional aerosol deposition when tested using these conditions. As expected, the estimated % lung dose was 35% of the nominal dose. The mean \pm SD emitted dose from the interface was $84.1 \pm 0.6\%$, which was significantly lower than what was observed with continuous nebulization with realistic breathing conditions ($95.3 \pm 0.6\%$, $p < .0001$; Student's t-test). Significantly higher deposition was observed in the delivery device and nose-throat model when compared to continuous nebulization with realistic breathing conditions (Figure 6.11, $p < .0001$ and $p = 0.0032$, respectively).

It was assumed that any drug not recovered in the assay was due to respiration loss – drug loss due to aerosol generation during the exhalation portion of the breathing cycle and exhaled drug losses. Respiration losses were estimated by calculating the difference between the nominal dose and the recovered dose. A recovered dose of $61.5 \pm 3.2\%$ of the nominal dose was obtained for the optimized settings, resulting in an estimated respiration loss of $38.5 \pm 3.2\%$ of the nominal dose. To study the respiration loss in the system, the regional deposition experiment with the nose-throat model was repeated at the nebulization duration setting of 0.1 s as it was expected to have the lowest respiration loss since nebulization trigger time is less critical at lower nebulization duration times, thus increasing the chances of capturing the entire aerosol dose generated during each breath. Table 6.7 shows the deposition results for the components of the system.

The total mean \pm SD recovered dose was $76.3 \pm 7.0\%$, resulting in an estimated respiration loss of $23.7 \pm 7.0\%$ of the nominal dose. However, decreasing the respiration loss using the 0.1 s nebulization duration resulted in increased deposition in the delivery device. When compared with the 0.2 s nebulization duration and continuous nebulization, it was observed that increasing deposition was seen in the delivery device with decreasing nebulization duration (Figure 6.11, $r =$

-0.8706, $p=0.0005$, $R^2 = 0.7579$; Pearson correlation). It was observed that the shorter nebulization duration of 0.1 s resulted in inconsistent aerosol generation during the run, which may have caused the observed increased deposition in the delivery device.

The higher deposition in the delivery device resulted in an emitted dose from the interface for the 0.1 s nebulization duration that was significantly lower than what was observed with 0.2 s nebulization duration and with continuous nebulization with realistic breathing conditions ($69.2 \pm 4.1\%$, $p=0.0017$ and $p=0.0001$, respectively; Student's t-test). However, the estimated % lung dose with the 0.1 s nebulization duration was comparable to that of the 0.2 s nebulization duration when values were calculated as percent of the nominal dose (37% vs 35% of the nominal dose). When aerosol delivery was considered relative to the fraction of the aerosol that was emitted from the cannula (to normalize for losses within the delivery device), the estimated % lung dose for 0.1 s nebulization duration was significantly higher compared to that of the 0.2 s nebulization ($53.9 \pm 7.8\%$ vs $41.9 \pm 0.6\%$ of the interface dose, $p=0.0485$; Student's t-test) with similar nose-throat model deposition ($12.6 \pm 2.5\%$ vs $12.3 \pm 3.5\%$ of the interface dose, respectively). More of the aerosol from the shorter nebulization duration was captured on the filter as indicated by the higher estimated % lung dose when compared to the 0.2 s nebulization duration, which was the expected outcome with decreased nebulization duration.

Table 6.7 Comparison of *in vitro* aerosol deposition when varying the nebulization duration with breath-actuated nebulization with 0.4 s nebulization trigger time prior to the start of inhalation and realistic breathing conditions. Values are mean (SD) percent of nominal dose, $n \geq 3$.

Component	Nebulization duration	
	0.2 s	0.1 s
Delivery device	14.1 (1.6)	26.4 (4.0)
Streamlined cannula	1.9 (1.1)	4.4 (1.1)
Nose-throat model	10.3 (2.9)	8.4 (2.0)
Estimated % lung dose	35.2 (0.6)	37.1 (3.7)
Estimated respiratory loss	38.5 (3.2)	23.7 (7.0)

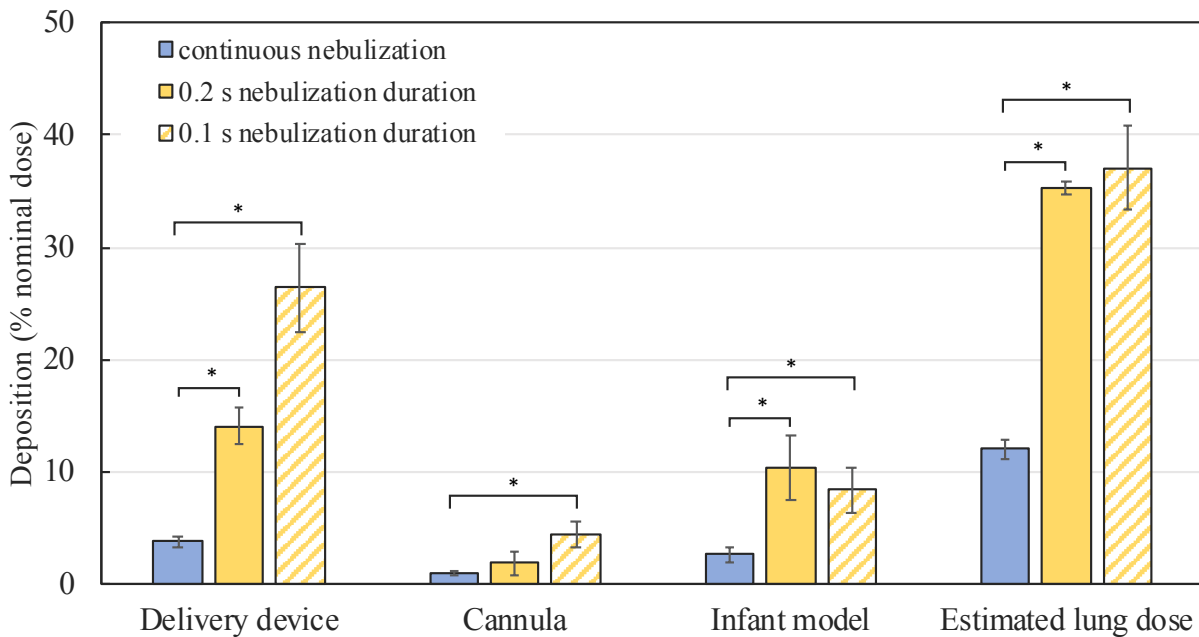


Figure 6.11 Comparison of *in vitro* aerosol deposition when varying the nebulization duration using the VCU low-volume mixer-heater. Bars represent the mean value, error bars represent the SD, $n \geq 3$. *Significant difference; Student's t-test, $p < 0.05$.

Although the lower nebulization duration of 0.1 s provided more efficient delivery, significantly less drug was delivered in 20 minutes at this nebulization duration when compared

to the 0.2 s nebulization duration setting ($162 \pm 27 \mu\text{g}$ vs $310 \pm 14 \mu\text{g}$ of AS, $p=0.0004$; Student's t-test). The estimated % lung dose achieved with the VCU low-volume mixer-heater at 0.2 s nebulization duration during realistic breathing conditions was 35% of the nominal dose, a significant improvement over the current methods of aerosol delivery to the lungs of infants which deliver < 4% of the nominal dose [156] using similar highly controlled *in vitro* testing conditions.

The *in vitro* testing conditions with a breathing simulator allowed for determination of the highest potential estimated % lung dose by utilizing a nebulization trigger time. Realistically, the use of a nebulization trigger time is not practical in a clinical environment as the breathing profile of infants with respiratory issues is erratic and nonuniform. The *in vitro* experiments demonstrated that a nebulization trigger time of 0.4 s resulted in the highest estimated lung dose, indicating the importance that timing of aerosol delivery has on ensuring inhalation of the drug aerosol in maximizing the dose that reaches the infant lung.

6.3.5 *In vitro* aerosol deposition with a realistic infant nose-throat airway model from the VCU very low-volume mixer-heater

Initial experiments were performed with the VCU very low-volume mixer-heater system and modified controller to aerosolize 0.5% w/v AS solution [160]. These studies showed that due to the very low volume of the mixer-heater, it was now possible to synchronize nebulization with the start of the inhalation cycle and eliminate the need of the nebulization trigger time prior to the start of inhalation while maintaining a high estimated % lung dose. In this section, studies were performed to investigate the aerosolization of a surfactant-EEG formulation using the optimized settings determined with AS solution.

6.3.5.1 Surfactant-EEG dispersion for nebulization

Surfactant-EEG nebulization formulations were produced by combining mannitol with Survanta[®] and water to produce a solids concentration of 0.5% w/v. The formulation was dispersed by sonication as described for preparation of feed dispersions for spray drying in Chapter 4 – indirect sonication for 40 minutes in a heated water bath sonicator set to 60 °C. The formulation had a final concentration of 54% phospholipids, 10% mannitol, and 20% sodium chloride, with the remaining 16% consisting of other components present in the commercial Survanta[®] suspension (triglycerides, fatty acids, and proteins). The solids concentration was verified by determining the weight of 2 mL of the surfactant-EEG dispersion allowed to dry overnight in an oven set to 80 °C; three replicates were performed with a mean \pm SD percent solids of $0.47 \pm 0.2\%$ w/v. Dispersion stability was determined by measuring the zeta potential (Zetasizer Nano S, Malvern Instruments, Ltd., Worcestershire, UK) and the DPPC content of the formulations was determined by LC-MS as described in Chapter 3. Zeta potential and percent DPPC content data are shown in Table 6.8.

The dispersions were observed to be stable for at least 20 days following preparation as indicated by the zeta potential absolute values greater than 30 mV. DPPC content was determined to be approximately 1.2 mg/mL for 7 days after preparation, which theoretically equates to 2.3 mg of phospholipids per mL according to the Survanta[®] label claim [30]. The dispersions could be reliably used for up to 7 days following preparation if stored in the refrigerator (2-8 °C) when not in use.

Table 6.8 Surfactant-EEG nebulizer formulation dispersion stability and DPPC content over time. Values are mean (SD), n≥3.

Measurement parameter	Day 1	Day 3	Day 7	Day 20
Zeta potential, mV	-32.4 (0.3)	-33.2 (1.2)	-	-42.4 (3.5)
DPPC content, mg/mL	1.23 (0.01)	1.18 (0.03)	1.19 (0.03)	-

6.3.5.2 Effect of nebulizer formulation composition on aerosol concentration

The effect of nebulizer formulation composition on the aerosol particle concentration was determined using a condensation particle counter comparing the AS nebulizer formulation with the surfactant-EEG formulation. For each formulation, aerosols were continuously generated from the modified Aerogen[®] Solo nebulizer using the modified controller into a T-piece that was connected to a condensation particle counter (CPC model 3022A, TSI Inc., Shoreview, MN). Dilution airflow was introduced into the T-piece to deliver aerosol to the CPC that was configured in high flow operation (1.5 L/min). The dilution gas flow rate was varied to produce flows of 3, 6, and 8 L/min. Measurements were performed for 300 s per run. There were differences in the aerosol particle concentration at the 3 L/min dilution gas flow, in which the AS solution had a higher aerosol particle concentration, but this difference was not observed at the higher gas flow rates, Figure 6.12. With similar particle concentration at both 6 and 8 L/min dilution flows (similar to the flows used in the mixer-heater system), the aerosols generated from the two formulations were deemed similar.

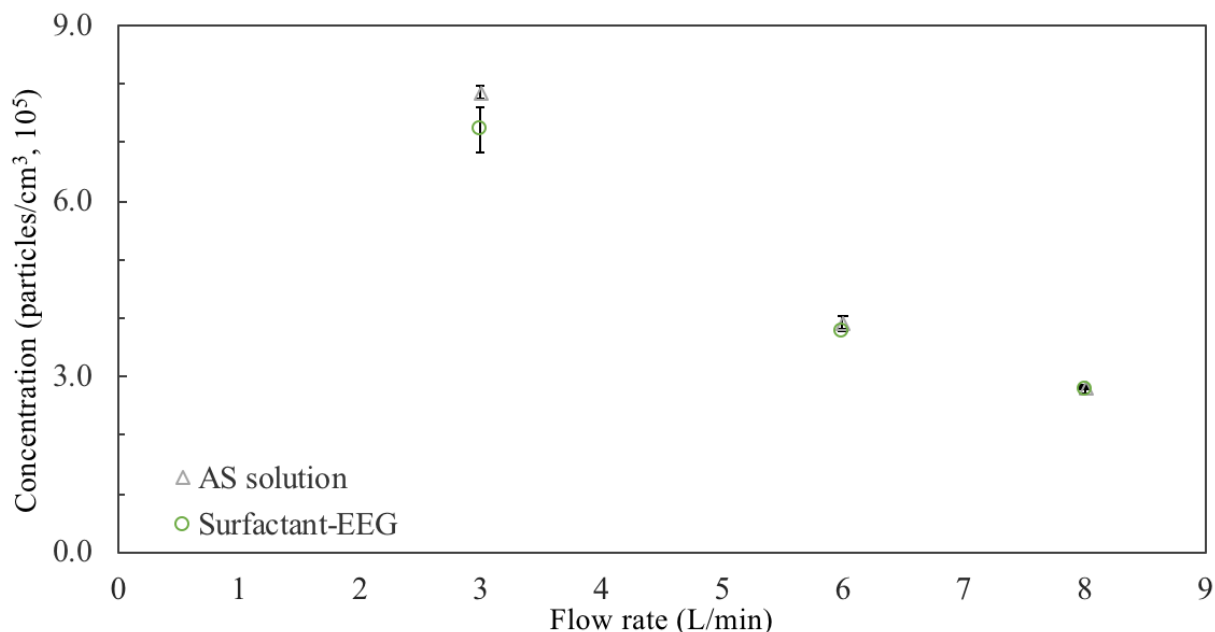


Figure 6.12 Aerosol particle concentration of albuterol sulfate and surfactant-EEG nebulizer formulation aerosols generated as a function of dilution gas flow rate measured using the condensation particle counter from aerosols generated by the modified Aerogen[®] Solo powered by the modified controller. Markers represent the mean value, error bars represent the SD, n=4.

6.3.5.3 VCU very low-volume mixer-heater with the modified controller

6.3.5.3.1 Effect of the VCU very low-volume mixer-heater on the aerosol droplet size

Sizing experiments with the ACI were performed with the modified controller to determine the particle size distribution of the surfactant-EEG formulation with the VCU very low-volume mixer-heater. The aerosol size distribution was measured at the exit of the nebulizer to evaluate the initial aerosol size. The droplet size distribution was then determined at the exit of the delivery tubing from the very low-volume mixer-heater system during continuous nebulization. The droplet size distributions are shown in Figure 6.13. Studies were performed in the environmental chamber which was set to 25 °C, the temperature of the aerosol exiting the nebulizer and VCU very low-

volume mixer-heater. Relative humidity in the chamber was maintained at 99% RH to minimize droplet evaporation during sizing measurements.

A bimodal droplet size distribution was observed for the aerosol exiting the nebulizer, which was less apparent when the aerosol was passed through the VCU very low-volume mixer-heater. The initial particle size of the droplets at the exit of the nebulizer was determined to have a mean \pm SD MMAD of $2.2 \pm 0.8 \mu\text{m}$, which was significantly reduced by the VCU very low-volume mixer-heater to droplets with an MMAD of $1.0 \pm 0.0 \mu\text{m}$ ($p=0.0356$; Student's t-test). The incorporation of the VCU very low-volume mixer-heater was found to have a significant effect on the particle fractions less than $1 \mu\text{m}$ and $5 \mu\text{m}$, with higher particle fractions observed with the VCU very low-volume mixer-heater compared to the nebulizer alone ($p=0.0006$ and $p=0.0003$, respectively; Student's t-test). No differences were observed in the GSD values of the particle size distributions with and without incorporation of the VCU very low-volume mixer-heater. Results are listed in Table 6.9.

As observed with the previous generation mixer-heater and AS nebulizer formulation, the use of the VCU very low-volume mixer-heater enabled efficient drying of the surfactant-EEG droplets that exited the nebulizer by mixing the aerosol with warmed ventilation gas. Replacing the heating zone of the mixer-heater with heated ventilation gas to reduce the volume of the delivery system was successfully implemented for this surfactant-EEG formulation. This resulted in aerosol particles that were smaller than the aerosols generated using the VCU low-volume mixer-heater (1.0 vs $1.4 \mu\text{m}$) with a higher fraction of particles less than $1 \mu\text{m}$ (51 vs 26 %).

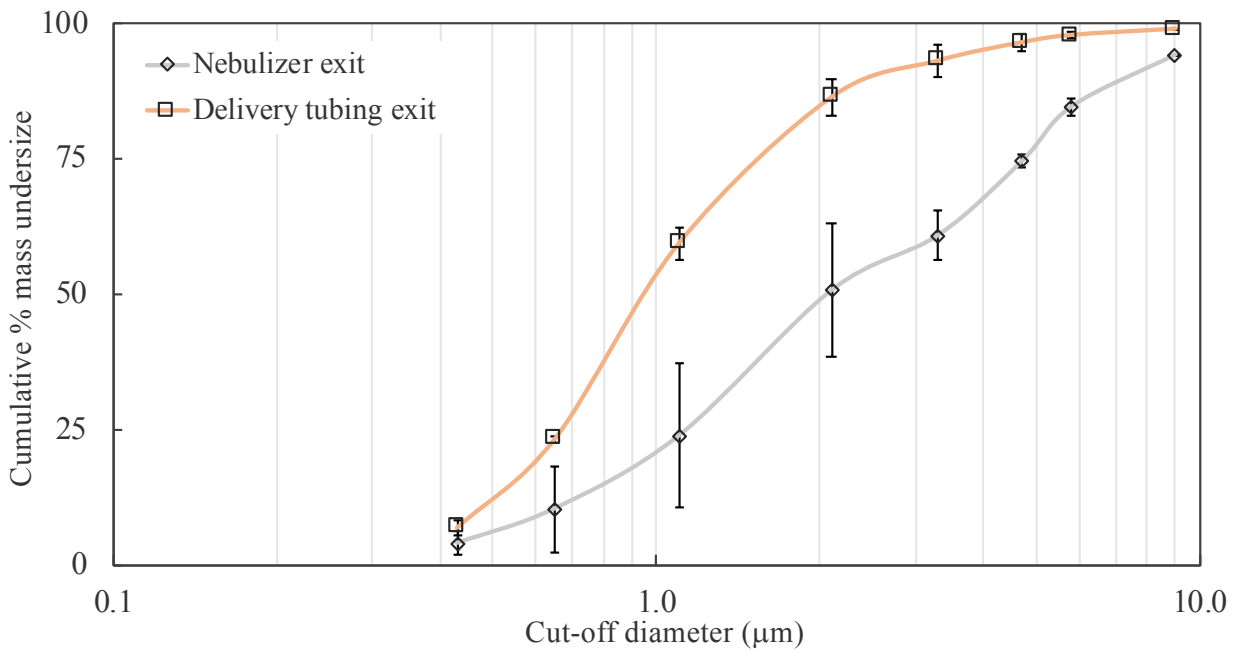
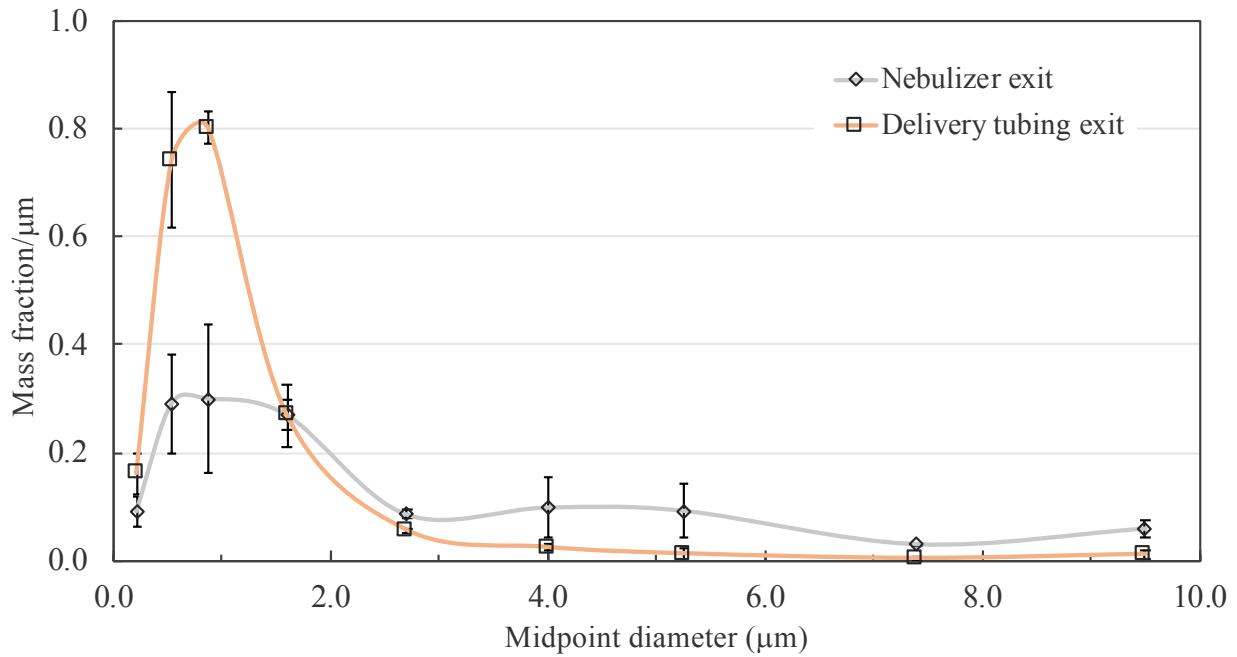


Figure 6.13 Aerosol droplet size distributions of the modified Aeroneb® Solo nebulizer output (nebulizer exit) and following delivery from the very low-volume mixer-heater (delivery tubing exit) of 0.5% w/v surfactant-EEG formulation generated by the Aerogen® Solo with the modified controller. Markers represent the mean value, error bars represent the SD, $n \geq 3$.

Table 6.9 Aerosol droplet size characteristics of the modified Aeroneb® Solo nebulizer output and following delivery from the very low-volume mixer-heater (delivery tubing exit) of 0.5% w/v surfactant-EEG formulation determined by cascade impaction with the ACI. Aerosols were generated using the modified and commercial Aerogen® controllers. Values are mean (SD), n≥3.

Controller (amplitude voltage)	Droplet size measurement position	MMAD, µm	GSD	Particle fraction, %	
				<1 µm	<5 µm
Modified (14.1 V _{rms})	Initial size at nebulizer exit	2.5 (0.9)	2.6 (1.0)	20.8 (6.6)	77.2 (3.0)
Modified (14.1 V _{rms})	Final size at delivery tubing exit	1.0 (0.0)*	2.1 (0.1)	51.3 (0.6)*	96.7 (0.6)*
Commercial (50 V _{rms})	Initial size at nebulizer exit	4.2 (0.3)‡	1.8 (0.1)	7.2 (2.8)‡	63.7 (5.7)‡
Commercial (50 V _{rms})	Final size at delivery tubing exit	2.0 (0.4)#^	2.3 (0.3)#	22.1 (7.0)#^	88.5 (1.9)#^

*Significant difference compared to initial size at nebulizer exit with the modified controller; Student's t-test, $p < 0.05$

#Significant difference compared to initial size at nebulizer exit with the commercial controller; Student's t-test, $p < 0.05$

‡Significant difference compared to the modified controller at the nebulizer exit; Student's t-test, $p < 0.05$

^Significant difference compared to the modified controller at the delivery tubing exit; Student's t-test, $p < 0.05$

6.3.5.3.2 Effect of the VCU very low-volume mixer-heater on *in vitro* regional aerosol deposition

The VCU very low-volume mixer-heater was evaluated using the *in vitro* aerosol deposition set up described previously with a realistic infant breathing profile and nose-throat infant airway model. Due to the reduced volume of the system, offset of the start of nebulization with the start of inhalation was no longer required to synchronize aerosol delivery with inhalation to the model. Therefore, nebulization was triggered at the start of each inhalation. Initial development studies with this device revealed that the VCU very low-volume mixer-heater using a nebulization duration of 0.3 s and the modified controller delivered 100 μL of 0.5% w/v AS solution in a total time of 14 minutes, with an estimated % lung dose of $48.1 \pm 2.3\%$ of the nominal dose [160]. This was shown to offer a significant improvement over the delivery of around 35% of the nominal dose observed with the VCU low-volume mixer heater.

The initial realistic deposition studies with albuterol sulfate were then performed using the 0.5% w/v surfactant-EEG nebulizer formulation. To ensure that an adequate amount of DPPC could be detected from the system components, a volume of 620 μL of the surfactant-EEG nebulizer formulation was used for the deposition studies. Complete nebulization (run to dryness) took approximately 40 minutes. An estimated % lung dose of $30.4 \pm 2.8\%$ of the nominal dose was observed. Minimal deposition was observed on the other components of the system, a total of $7.7 \pm 0.8\%$ of the nominal dose, indicating high respiration loss ($61.9 \pm 2.0\%$ of the nominal dose). Table 6.10 lists the deposition recovered on the different components in the system.

The deposition with a nebulization duration of 0.1 s was studied to determine if the respiration loss in the system could be decreased. A volume of 750 μL of surfactant-EEG formulation was filled into the nebulizer, which was allowed to run for 130 minutes. The estimated

% lung dose was found to be $52.1 \pm 1.7\%$ of the nominal dose, significantly higher than that observed with the nebulization duration of 0.3 s ($p=0.0003$; Student's t-test). The deposition in the other components were similar to that determined with 0.3 s nebulization duration, except for the cannula component, which was significantly higher with the shorter nebulization duration of 0.1 s ($p=0.0248$; Student's t-test), Figure 6.14. The respiration loss was estimated as $36.1 \pm 2.9\%$ of the nominal dose, an improvement over the longer nebulization duration, but higher than expected for the short nebulization duration used in this study; a respiration loss of $18.3 \pm 4.3\%$ of the nominal dose was observed for AS studies. An estimated % lung dose of 52.1% of the nominal dose equates to $430.7 \pm 16.5 \mu\text{g}$ of DPPC (or an estimated 813 μg of total phospholipids), which took over 2 hours to deliver. An increase in the output rate of the aerosol from the VCU low-volume mixer-heater was further studied to determine if delivery time of surfactants could be minimized while still maintaining the high delivery efficiency.

Table 6.10 Comparison of *in vitro* aerosol DPPC deposition when varying the nebulization duration using the VCU very low-volume mixer-heater with surfactant-EEG. The modified controller and commercial controller was used to initiate nebulization at the start of a realistic inhalation breathing cycle. Values are mean (SD) percent of nominal dose, n=3.

Controller	Component	Nebulization duration	
		0.3 s	0.1 s
Modified			
	Delivery device	2.7 (0.3)	3.1 (0.6)
	Streamlined cannula	3.8 (0.3)	7.2 (1.7)*
	Nose-throat model	1.2 (0.2)	1.5 (0.7)
	Estimated lung dose	30.4 (2.8)	52.1 (1.7)*
	Estimated respiratory loss	61.9 (2.0)	36.1 (2.9)
Commercial			
	Delivery device	7.5 (3.2)	6.1 (0.9)^
	Streamlined cannula	8.1 (1.8)‡	5.3 (1.4)
	Nose-throat model	5.2 (1.7)‡	0.8 (0.3)#
	Estimated lung dose	14.7 (0.3)‡	31.2 (0.4)#^
	Estimated respiratory loss	64.6 (3.1)	56.7 (0.4)

*Significant difference compared to nebulization duration of 0.3 s with modified controller; Student's t-test, $p < 0.05$

#Significant difference compared to nebulization duration of 0.3 s with commercial controller; Student's t-test, $p < 0.05$

‡Significant difference compared to modified controller at nebulization duration of 0.3 s; Student's t-test, $p < 0.05$

^Significant difference compared to modified controller at nebulization duration of 0.1 s; Student's t-test, $p < 0.05$

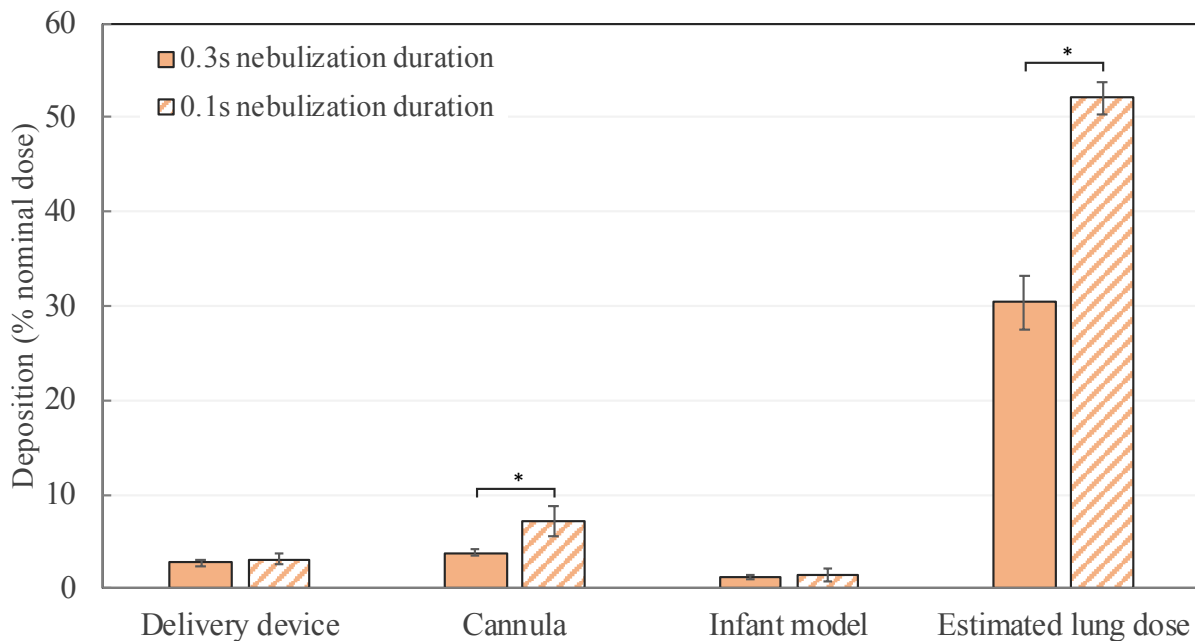


Figure 6.14 Comparison of *in vitro* aerosol DPPC deposition when varying the nebulization duration using the VCU very low-volume mixer-heater with surfactant-EEG and the modified controller initiating nebulization at the start of a realistic inhalation breathing cycle. Bars represent the mean value, error bars represent the SD, n=3. *Significant difference; Student's t-test, $p < 0.05$.

6.3.5.4 VCU very low-volume mixer-heater with the commercial controller

Using the modified controller, it was not possible to further increase the driving amplitude as it was operated at the maximum setting in previous studies. Therefore, in an attempt to increase the aerosol output from the VCU very low-volume mixer-heater, the commercial controller was used in a series of studies to operate the Aerogen® Solo. Aerosol deposition in the realistic infant airway model and delivery time with the surfactant-EEG formulation was studied to determine the delivery efficiency compared to the modified controller.

6.3.5.4.1 Effect of the commercial controller on the aerosol droplet size from the VCU very low-volume mixer-heater

The initial droplet aerosol size distribution of the surfactant-EEG aerosols exiting the nebulizer outlet and following passage through the VCU very low-volume mixer-heater at the tubing exit were determined following aerosol generation using the commercial controller. Size distribution measurements were performed in an environmental chamber set to 25 °C and 99% RH as previously described.

The initial size of the nebulized aerosol revealed large aerosol droplets exiting the nebulizer, with a mean \pm SD MMAD of $4.2 \pm 0.3 \mu\text{m}$ and GSD 1.8 ± 0.1 , compared to those generated with the modified controller (MMAD of $2.5 \mu\text{m}$). The aerosol produced following passage through the VCU very low-volume mixer-heater and exiting the delivery tubing was observed to have a significantly reduced MMAD of $2.0 \pm 0.4 \mu\text{m}$ ($p < .0001$; Student's t-test) compared to the droplets measured at the exit of the nebulizer. A bimodal distribution was observed for the aerosol exiting the VCU very low-volume mixer-heater, which was determined to be significantly more polydisperse than the initial aerosol generated by the nebulizer ($p = 0.0088$; Student's t-test). The bimodal distribution suggests that partial or incomplete drying may have occurred in the mixer-heater which had a final size of $2.0 \mu\text{m}$ compared to the MMAD of $1.0 \mu\text{m}$ observed with the modified controller. As observed with the modified controller, the use of the VCU very low-volume mixer-heater to generate an aerosol was found to have a significant effect on the particle fractions less than $1 \mu\text{m}$ and $5 \mu\text{m}$, with higher particle fractions observed with the VCU very low-volume mixer-heater compared to the nebulizer alone ($p = 0.0022$ and $p < .0001$, respectively; Student's t-test). Data are shown in Table 6.9 and plotted in Figure 6.15.

As expected, the droplets produced with the commercial controller were significantly larger when compared to those produced with the modified controller, both at the exit of the nebulizer and at the exit of the delivery tubing connected to the mixer-heater ($p=0.0039$ and $p=0.0027$, respectively; Student's t-test). The higher output from the nebulizer ($281 \pm 67 \mu\text{L}/\text{min}$), when operated by the commercial controller, resulted in less evaporation of the droplets as they exited the nebulizer due to the higher local concentration and therefore the larger observed droplet size compared to the modified controller which produced a lower output. The VCU very low-volume mixer-heater was not able to completely dry the higher output of larger droplets. The aerosol output with the commercial controller was observed to be significantly larger than the aerosol droplets exiting the VCU very low-volume mixer-heater that were produced using the modified controller. Aligned with the significantly larger aerosol size observed, there were significant differences in the particle fractions less than $1 \mu\text{m}$ and $5 \mu\text{m}$, with higher particle fractions observed with the modified controller compared to the commercial controller (nebulizer exit: $p=0.0040$ and $p=0.0038$, delivery tubing exit: $p=0.0004$ and $p=0.0018$, respectively; Student's t-test).

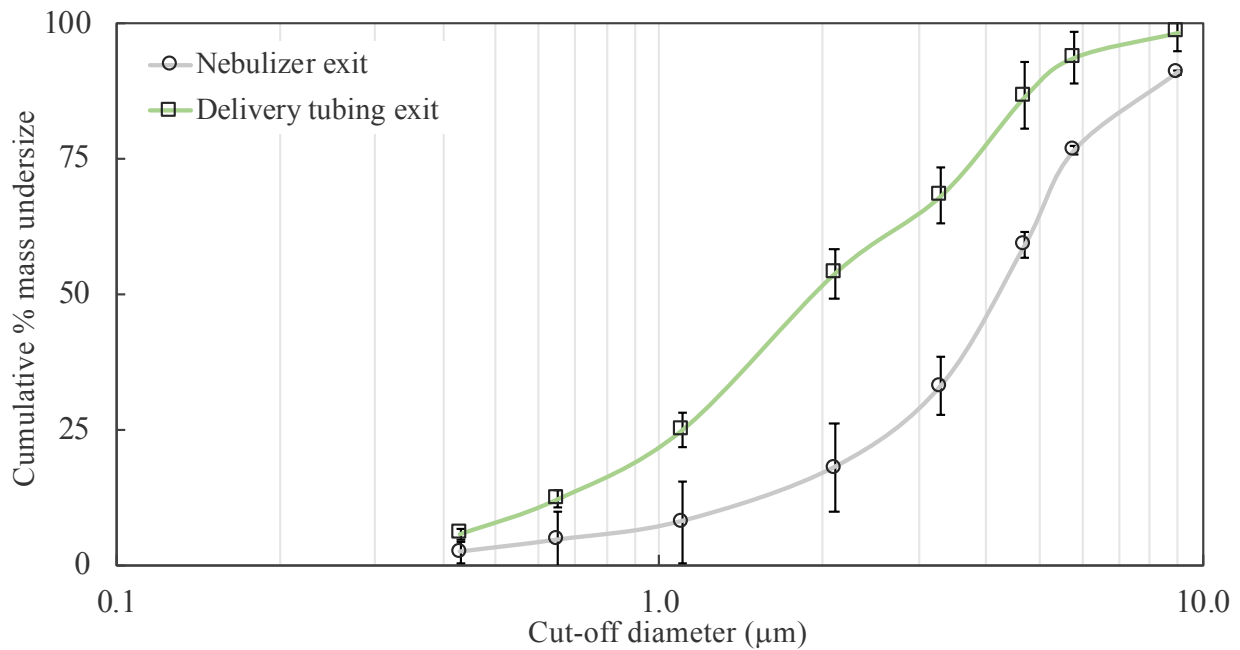
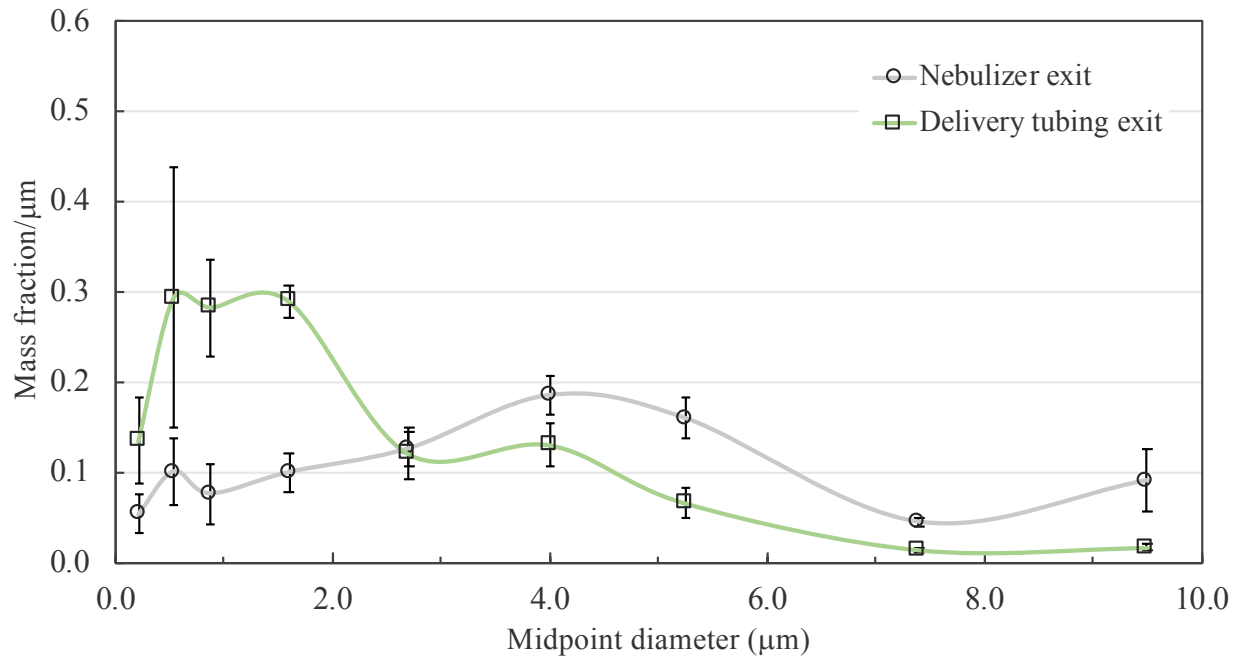


Figure 6.15 Aerosol droplet size distributions of the Aeroneb[®] Solo nebulizer output (nebulizer exit) and following delivery from the very low-volume mixer-heater (delivery tubing exit) of 0.5% w/v surfactant-EEG formulation generated by the Aerogen[®] Solo with the commercial controller. Markers represent the mean value, error bars represent the SD, n=5.

6.3.5.4.2 Effect of the commercial controller on the *in vitro* regional aerosol deposition from the VCU very low-volume mixer-heater

Deposition testing with the commercial controller was performed with the VCU very low-volume mixer-heater using nebulization durations of 0.3 s and 0.1 s. A volume of 750 μL of surfactant-EEG formulation was filled into the nebulizer and allowed to run to dryness, which took 8.4 ± 0.3 minutes and 25.7 ± 0.4 minutes for the 0.3 s and 0.1 s nebulization durations, respectively, and delivered 123.7 ± 3.1 and 263.8 ± 3.5 μg of DPPC (or an estimated 233 and 498 μg of total phospholipids). Table 6.10 shows the DPPC deposition of the emitted aerosol on the different components in for each nebulization duration.

Similar emitted doses from the nasal cannula were observed for the nebulization durations of 0.3 s and 0.1 s with the commercial controller ($84.5 \pm 4.6\%$ and $88.6 \pm 0.6\%$ of nominal dose, respectively). Figure 6.16 compares the DPPC deposition for two nebulization durations with the commercial controller. Significant differences were observed with deposition in the nose-throat model and the estimated % lung dose. The nebulization duration of 0.3 s was observed to have significantly higher deposition in the infant model compared to the nebulization duration of 0.1 s ($p=0.0123$; Student's t-test), which may be due to less deposition during exhalation with the shorter nebulization duration.

The shorter nebulization duration of 0.1 s resulted in a significantly higher estimated % lung dose of DPPC compared to the nebulization duration of 0.3 s ($p<.0001$; Student's t-test), however, the rate of drug delivery should also be considered. The nebulization of 750 μL of surfactant-EEG at the nebulization duration of 0.1 s took 26 minutes to deliver, which was more than 3 times longer than with the nebulization duration of 0.3 s. An estimated 715 μg of phospholipids would be delivered in 26 minutes if a nebulization duration of 0.3 s were to be used,

nearly 1.5x more phospholipids than with the 0.1 s nebulization duration (498 μg of total phospholipids). The delivery time of surfactants would be minimized at the higher nebulization duration but at the expense of delivery efficiency, which holds true when the results are compared with the modified controller.

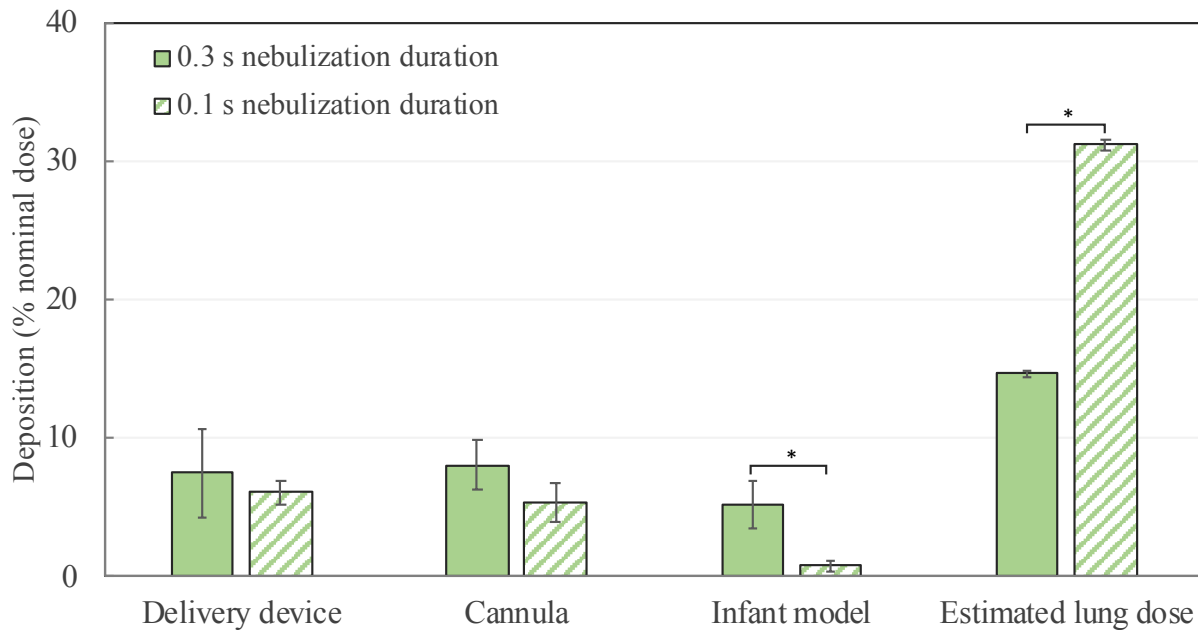


Figure 6.16 Comparison of *in vitro* aerosol DPPC deposition when varying the nebulization duration using the VCU very low-volume mixer-heater with surfactant-EEG and the commercial controller initiating nebulization at the start of a realistic inhalation breathing cycle. Bars represent the mean value, error bars represent the SD, n=3. *Significant difference; Student’s t-test, $p < 0.05$.

Use of the commercial controller resulted in a significantly lower estimated % lung dose of DPPC for both nebulization durations compared to those measured with the modified controller (0.3 s nebulization duration: $p=0.0006$, 0.1 s nebulization duration: $p<.0001$; Student’s t-test). For the 0.3 s nebulization duration, higher DPPC deposition was observed on all components using the commercial controller system compared to the modified controller system, with the cannula and

nose-throat model having significantly higher DPPC deposition ($p=0.0152$ and $p=0.0171$, respectively; Student's t-test). With the 0.1 s nebulization duration, the DPPC deposition in the delivery device was significantly higher using the commercial controller system compared to the modified controller system ($p=0.0086$; Student's t-test).

The drug delivery rate was compared for the different combinations of controller type and nebulization durations. The estimated % lung dose was used to determine the estimated amount of phospholipids delivered (based on recovered DPPC lung dose and the Survanta[®] label claim) and then used to determine the estimated delivery rate of phospholipids to normalize the results for delivery time. The results are shown in Table 6.11.

The modified controller with 0.1 s nebulization duration was shown to have the highest estimated % lung dose but the slowest estimated delivery rate for phospholipids. The commercial controller with 0.3 s nebulization duration was observed to have the highest delivery rate for phospholipids but the lowest estimated % lung dose. The other two controller-nebulization duration combinations (modified controller with 0.3 s nebulization duration, commercial controller with 0.1 s nebulization duration) had results that were somewhere in between. It appears that a balance between drug delivery rate and delivery efficiency needs to be determined for optimal delivery of surfactants using the VCU very low-volume mixer-heater.

The use of surfactant therapy as supplemental treatment for infants with bronchiolitis has only been proposed and the dose that would be needed to elicit an effect (hasten the resolution of symptoms) is not known. Dose estimates based on current treatment protocols for neonatal RDS with commercial replacement surfactant would likely result in an overestimate as delivery of a liquid bolus is known to be much less efficient than delivery in an aerosolized form when the target site is the peripheral region of the lungs. Aerosolized delivery of surfactants on animal models

have shown that as little as 2 mg of phospholipids per kg of body weight has been observed to show improved outcomes [83]. For an 8 kg infant, this would be delivery of 16 mg of phospholipids, which would take between 9.6 h to administer by the fastest, but least efficient method (commercial controller with 0.3 s nebulization duration) to 42.3 h (1.8 days) with the slowest, but most efficient method (modified controller with 0.1 s nebulization time). With the commercial controller and 0.1 s nebulization duration, 16 mg of phospholipids could be theoretically delivered in 13.7 hours, which is reasonable considering that treatment would be administered concomitantly with supplemental oxygen support, possibly alleviating symptoms in a shorter time than the typical 2 to 3 days that most children spend in the hospital when admitted for treatment for bronchiolitis [46].

Table 6.11 Comparison of estimated delivered doses and respiratory losses for the nebulization durations of 0.3 s and 0.1 s with the modified and commercial controllers using the VCU very low-volume mixer-heater. Values are mean (SD), n=3.

Controller, nebulization duration	Estimated lung dose, % nominal	Estimated PL delivery, μg	Estimated PL delivery, $\mu\text{g}/\text{min}$	Respiratory loss, % nominal
Modified, 0.3 s	30.4 (2.8)	397.8 (37.9)	9.9 (1.0)	61.9 (2.0)
Modified, 0.1 s	52.1 (1.7)	812.6 (31.2)	6.3 (0.2)	36.1 (2.9)
Commercial, 0.3 s	14.7 (0.2)	233.4 (5.8)	27.9 (0.4)	64.6 (3.1)
Commercial, 0.1 s	31.2 (0.4)	497.7 (6.5)	19.4 (0.2)	56.7 (0.4)

PL=phospholipids

Aerosolization with the commercial controller resulted in increased respiration loss for both nebulization durations, $64.6 \pm 3.1\%$ of nominal dose for nebulization duration of 0.3 s and $56.7 \pm 0.4\%$ of nominal dose for nebulization duration of 0.1 s, compared to the estimated losses with the modified controller. To study the unexpectedly high estimated respiration loss in the

system, the commercial controller with nebulization duration of 0.1 s was selected as it was shown to have the second highest estimated % lung dose, second lowest respiratory loss and second highest phospholipid delivery rate (Table 6.11).

6.3.5.4.3 Assessment of DPPC recovered dose using steady state inhalation flow with the very low-volume mixer-heater and the commercial controller

With the commercial controller and nebulization duration of 0.1 s, aerosol deposition studies were repeated with a total capture aerosol filter (replacing the infant airway model) placed at the exit of the nasal cannula in an attempt to determine the fate of the delivered aerosol. Steady state inhalation flow of 30 L/min was drawn through the filter to capture the aerosol exiting the cannula. Surfactant-EEG nebulizer formulation volumes of 750 μ L were filled into the nebulizer and allowed to run to dryness.

Table 6.12 and Figure 6.17 shows a comparison of the DPPC deposition and recovery for the steady state inhalation experiments compared with the previously described deposition and recovery observed using similar conditions and sampled with a realistic breathing cycle. The output rate measured during the steady state inhalation experiments was similar to previous experiments with the breathing cycle. Significantly higher deposition was observed in the delivery device and cannula components when compared to those observed with delivery using a realistic breathing profile ($p=0.0004$ and $p=0.0090$, respectively; Student's t-test). The mean \pm SD total recovered dose using a steady state inhalation flow of 30 L/min was $74.8 \pm 0.8\%$ of the nominal dose which was significantly higher than the recovery observed during realistic breathing (43.3%), due to the capture of the respiration losses. However, it was expected that the use of a steady state inhalation flow would allow capture of all of the emitted aerosol exiting the cannula and mass balance of DPPC would be observed compared to the nominal dose. However, approximately 25%

of the nominal dose was not accounted for during the steady state study. One hypothesis was that the DPPC stability was affected by the heating process during the aerosol drying. Small changes in the chemical structure would affect its molecular weight and therefore its quantitative analysis using the LC-MS method.

Table 6.12 Comparison of DPPC aerosol deposition and recovery from the very low-volume mixer heater captured using a realistic breathing cycle and a steady state inhalation flow of 30 L/ min. Steady state inhalation deposition experiments were performed using heated and room temperature ventilation gas flowing through the very low-volume mixer heater with the commercial controller with 0.1 s nebulization duration. Values are mean (SD), n=3.

Parameter	Realistic breathing cycle with nose-throat model	Steady state inhalation, heated gas	Steady state inhalation, room temp gas
Output rate, $\mu\text{L}/\text{min}$	28.6 (0.4)	27.3 (0.5)	22.1 (0.5)
Recovered dose, % nominal	43.3 (0.4)	74.8 (0.8)	79.3 (0.4)
Delivery device, % nominal	6.1 (0.9)	13.9 (0.8)*	7.8 (1.3)#
Cannula, % nominal	5.3 (1.4)	9.3 (0.4)*	22.1 (3.1)*#
Filter, % nominal	31.9 (0.2)	52.8 (1.7)	49.4 (1.5)

Statistical analysis only performed on delivery device and cannula components:

*Significant difference compared to experiments with exhalation; Student's t-test, $p < 0.05$

#Significant difference compared to constant inspiratory with heat; Student's t-test, $p < 0.05$

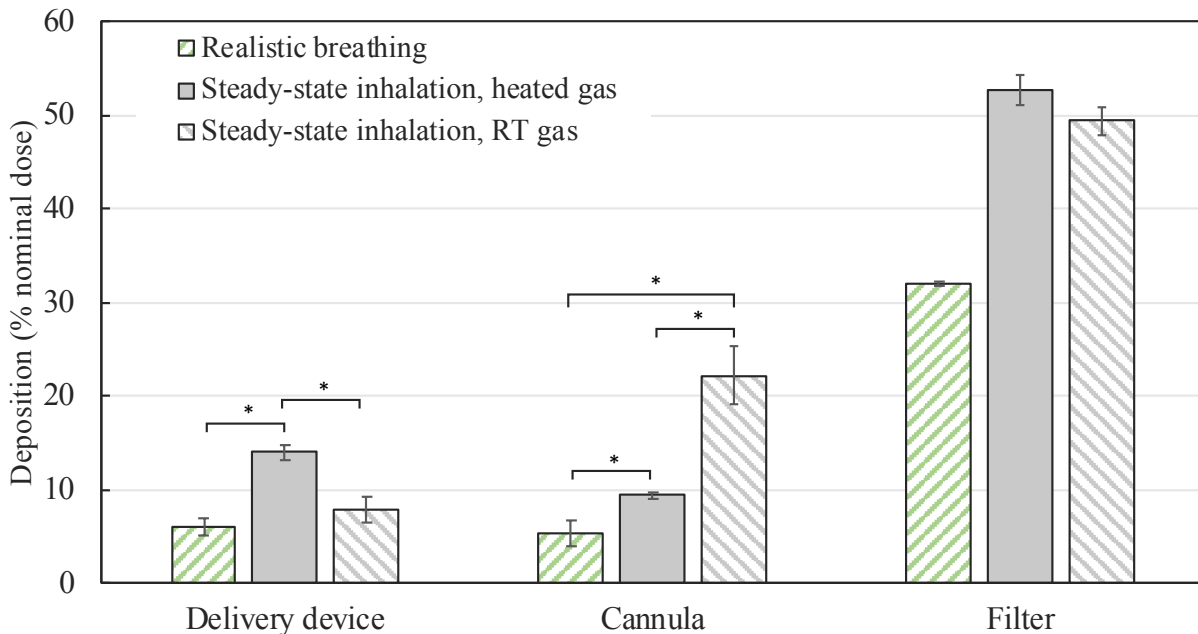


Figure 6.17 Comparison of DPPC aerosol deposition from the VCU very low-volume mixer heater captured using a realistic breathing cycle and a steady state inhalation flow of 30 L/ min. Steady state inhalation deposition experiments were performed using heated and room temperature ventilation gas flowing through the VCU very low-volume mixer heater with the commercial controller with 0.1 s nebulization duration. Bars represent the mean value, error bars represent the SD, n=3. *Significant difference; Student’s t-test, $p < 0.05$. RT=room temperature

6.3.5.4.4 Assessment of DPPC recovered dose using room temperature ventilation gas with using the very low-volume-mixer-heater and the commercial controller with steady state inhalation flow

The DPPC recovered dose was assessed using an aerosol generated from the VCU very low-volume mixer-heater using room temperature ventilation gas. Surfactant-EEG nebulizer formulation volumes of 750 μL were filled into the nebulizer and allowed to run to dryness.

The mean \pm SD total recovered dose for constant inspiratory flow was $79.3 \pm 0.4\%$ of the nominal dose using the room temperature ventilation gas which was not significantly different from the studies performed with the heated ventilation gas (74.8%) as shown in Table 6.12. There was also no significant difference observed in the filter deposition (Table 6.12 and Figure 6.17).

This suggests that heating the DPPC aerosol likely did not affect its stability with its observed total recovery remaining unchanged despite changes in its regional deposition due to its likely larger size when delivered using room temperature ventilation gas. Significantly higher deposition was observed in the cannula component using room temperature ventilation gas when compared to heated ventilation gas experiments with breathing or using state-steady inhalation flow ($p=0.0010$ and $p=0.0021$, respectively; Student's t-test). This was expected as the absence of heat resulted in aerosol that was incompletely dried when exiting the VCU very low-volume mixer-heater resulting in larger sized aerosol that deposited by impaction onto the cannula interface.

6.4 Conclusions

The objective of this study was to determine the delivery efficiency of novel low-volume mixer-heater systems in use with an EEG dispersion of commercial surfactant with sodium chloride and mannitol using a commercial vibrating mesh nebulizer. Albuterol sulfate solutions were used to perform studies to determine the efficiency of a novel delivery system, which was compared to the performance of a front-loaded infant face mask standard of care system (Specific aim 4-1). The optimal nebulization trigger time and nebulization duration settings were determined for the novel delivery system (Specific aim 4-2) using realistic breathing conditions and a realistic *in vitro* infant model. Following modifications to the novel low-volume mixer-heater system, the aerosol performance with a surfactant-EEG formulation was determined (Specific aim 4-3). An albuterol sulfate solution of 0.5% w/v was selected for use in optimization studies due to its established assay method and ease of extraction from sample components given its high solubility in water.

Comparison of steady state experiments with the novel low-volume mixer-heater and the face mask standard of care system revealed significant differences in deposition; highest

deposition with the low-volume mixer-heater system was an estimated % lung dose of 76% of nominal dose, whereas the face mask delivery system had the highest deposition on the nose-throat model of 74% of nominal dose. This is due to the size of the aerosol droplets entering the model for each of the systems, 1.4 μm and 5.0 μm for the mixer-heater and face mask systems, respectively. The low-volume mixer-heater was able to dry the aerosol droplets exiting the nebulizer sufficiently enough to navigate through the passageways of the nose-throat model to reach the filter for a high estimated % lung dose.

Incorporation of a realistic breathing profile significantly reduced the estimated % lung dose for both the low-volume mixer-heater and face mask standard of care systems, 12% and 5.2% of nominal dose, respectively. The significant difference observed in the estimated % lung dose is due to the rapid and shallow breathing pattern characteristic to infants; the profile consisted of a 0.5 s inhalation and 1 s exhalation with a tidal volume of 56 mL. The controller and delay timer settings were studied to maximize the estimated % lung dose for the low-volume mixer-heater system. With a driving amplitude of 4 Vpp, a nebulization trigger time of 0.4 s prior to the next inhalation and a nebulization duration of 0.2 s, the estimated % lung dose was increased to 35% of nominal dose, a significant improvement over the <4% of nominal dose using standard of care methods as reported in literature [103, 155]. However, sizing experiments showed that there was still room for improvement of the mixer-heater system.

Design changes to the low-volume mixer-heater were made to improve efficiency over the current design. The very low-volume mixer-heater was developed with an external heat source which allowed the mixer-heater volume to be reduced from 61.6 mL to 2.7 mL. Performance of the very low-volume mixer-heater system was determined with a surfactant-EEG formulation prepared with the Survanta[®] commercial formulation and mannitol. With the modulated controller

and nebulization duration of 0.3 s, the estimated % lung dose was determined to be 30% of nominal dose with a phospholipid delivery rate of 10 $\mu\text{g}/\text{min}$. Increased efficiency was observed with a lower nebulization duration of 0.1 s, estimated % lung dose of 52% of nominal, but a sacrifice in the phospholipid delivery rate to 6 $\mu\text{g}/\text{min}$. Use of the commercial controller was explored to increase the phospholipid delivery rate. At a nebulization duration of 0.1 s with the commercial controller, the estimated % lung dose was determined to be 31% of nominal dose with a phospholipid delivery rate of 19 $\mu\text{g}/\text{min}$, an improvement over that of the modulated controller.

A potential issue with this study is the low recovered doses seen with experiments performed both with and without exhalation incorporated. Due to the low solubility of DPPC in water, $<5 \mu\text{g}/\text{mL}$, the use of methanol was employed whenever possible. However, the nebulizer, mixer-heater, cannula, and nose-throat model are susceptible to breakdown when in contact with organic solvents, thus water was used to wash the components and then methanol was combined with the water wash to dissolve the drug. This procedure likely led to the low observed recoveries. Exploration of other washing techniques could possibly be explored in order to improve the percent of drug recovered.

CHAPTER 7

ASSESSMENT OF THE EFFECT OF SPRAY DRYING PROCESSES ON SURFACTANT PROTEIN CONCENTRATION

7.1 Introduction

The fundamental role that surfactant proteins play in proper pulmonary surfactant function necessitates the need to ensure their presence and activity in the final surfactant-EEG formulation. After processing for human use, commercially available natural surfactant formulations contain only the two hydrophobic proteins, SP-B and SP-C. The two proteins are subject to various stresses at multiple points throughout formulation processing such as: (i) thermal stress from sonication at elevated temperatures, (ii) shear stress due to cavitation during sonication, (iii) sheer stress, dehydration stress and stress due to adsorption of the proteins to the air-liquid interface during the atomization process of spray drying. The multiple stressors can lead to physicochemical degradation and possible loss of activity.

The most common physical deaggregation that proteins undergo is denaturation, or protein unfolding, which may occur during the atomization process in spray drying. During droplet formation, large air-liquid interfaces are produced causing the proteins to adsorb to the surface and unfold, which results in partial or total loss of the tertiary and possibly secondary structures of the proteins leading to loss of activity [110]. Covalent aggregation is a common chemical degradation mechanism of proteins. Since SP-B contains disulfide bonds, the hydrophobic protein may undergo degradation by covalent aggregation in which a free thiol of one protein carries out a

nucleophilic attack on the disulfide linkage of another protein molecule creating a new intermolecular disulfide bond [162]. Further propagation of this would lead to insoluble high molecular weight aggregates and loss of activity.

Another common chemical degradation mechanism that can significantly alter protein structure and function is deamidation – hydrolysis of the side chain amide on glutamine or asparagine residues to yield a carboxylic acid [110]. SP-B has four glutamine residues and SP-C has one asparagine residue, indicating that both proteins may undergo deamidation. Oxidation of proteins results in formation of sulfoxide derivatives, with methionine as the most susceptible amino acid; SP-B has two methionine residues and SP-C has one. As described, the hydrophobic surfactant proteins are expected to undergo protein conformation changes following processing, which further stresses the need to assess their presence and activity in the final surfactant-EEG formulation.

Analysis of the surfactant proteins pose a particularly difficult challenge as: (i) their hydrophobic nature makes them difficult to separate from the mixture of lipids, and (ii) there are low and variable quantities of protein present in the commercial formulations used to prepare the final EEG formulations. The concentration of the combined proteins (both SP-B and SP-C) in Survanta[®] is <1 mg/mL [30], which may differ from batch-to-batch since the surfactant is derived from bovine sources that naturally vary in components, approximately 0.10-0.13% w/w SP-B and 0.5% w/w SP-C compared to endogenous bovine surfactant [11, 163]. Survanta[®] is prepared by lavage of minced whole bovine lung that undergoes different levels of centrifugation followed by extraction with organic solvent and then supplementation with DPPC, palmitic acid, and tripalmitin. The last processing steps include organic solvent evaporation and resuspension in saline by sonication [164]. The surfactant formulation endures sonication for preparation of the

commercial product, which indicates that the hydrophobic proteins are able to withstand the energy input of sonication and should therefore be present following sonication employed during EEG formulation preparation.

Minocchieri et al. have studied the effect of nebulization on surfactant [165]. Using transmission electron microscopy and the Langmuir-Wilhelmy balance, the authors suggested that similarities in characteristics found between non-nebulized and nebulized surfactant would result in similar clinical effect and therefore concluded that vibrating mesh nebulizers are suitable for surfactant nebulization. Since spray drying employs similar methods of nebulization to atomize feed solutions and suspensions, the presence of surfactant proteins should be detected following the spray drying process.

The aim of this study was to establish a method for determining protein presence in the commercial Survanta[®] suspension and then apply the technique to samples from each step involved in preparation of surfactant-EEG formulations prepared with the commercial suspension.

7.2 Materials and methods

7.2.1 Protein purification by precipitation

Protein precipitation enables concentration and purification of the protein sample from interfering substances, such as salts and detergents (surfactants), for downstream applications. In the commercial Survanta[®] formulation, the proteins need to be separated from a complex mixture of salt and lipids. Lipids are insoluble in polar solvents like water, but highly soluble in non-polar or weakly polar organic solvents (e.g. chloroform, acetone, ether, benzene), while amino acids, the subunits of protein, are largely insoluble in the lipid solvents.

Pérez-Gil et al. [18] determined the solubilities of the hydrophobic surfactant proteins, SP-B and SP-C, isolated from minced porcine lungs. At the protein concentration of 7.5 $\mu\text{g}/\text{mL}$, the authors observed that only minimal amounts of SP-B were soluble in 100% acetonitrile, whereas pure trifluoroethanol or methanol dissolved SP-B almost completely (90-95%); in addition, neither methanol nor methanol/water mixtures dissolved an estimable amount of SP-C (Figure 7.1).

The use of different solvents was investigated for protein purification from Survanta[®], which included hexane/isopropanol, acetone, methanol/chloroform and trichloroacetic acid in acetone. Samples were then directly infused into the mass spectrometer (see section 7.2.2).

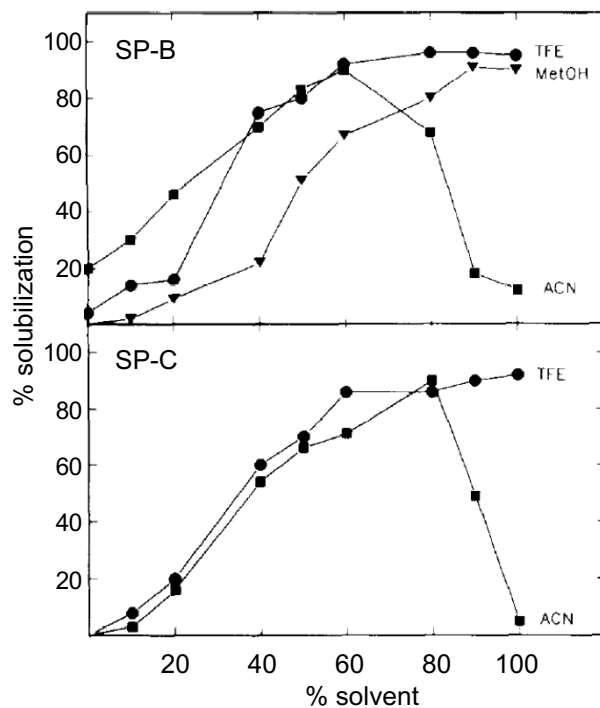


Figure 7.1 Solubility of SP-B (top) and SP-C (bottom) in different organic solvent/water mixtures at protein concentrations of 7.5 $\mu\text{g}/\text{mL}$; TFE = trifluoroethanol (circles), MeOH = methanol (triangles), ACN = acetonitrile (squares) [18].

7.2.1.1 Hexane/isopropanol

Methods described by Rodriguez-Vico et al. [113] for a protein precipitation procedure using a hexane-isopropanol mixture was applied to Survanta[®]. A 100 μ L aliquot of the commercial suspension was mixed with 5 mL of hexane/isopropanol (3:2, v/v). The mixture was then centrifuged for 15 min at 4000 $\times g$ (Sorvall[™] ST 16R, ThermoFisher Scientific Inc., Waltham, MA). The supernatant, containing lipids, was discarded and the pellet, containing protein, was dried off with a stream of nitrogen gas.

7.2.1.2 Methanol/chloroform

A methanol/chloroform procedure for protein purification was adapted from Wessel et al. [166]. In a microcentrifuge tube, methanol was combined with Survanta[®] in a ratio of 4:1 (0.40 mL methanol, 0.10 mL Survanta[®]) and vortexed. Chloroform was added in the same volume as the starting Survanta[®] sample volume, 0.10 mL, then vortexed. Deionized water was next added in a ratio of 3:1 of the starting Survanta[®] sample volume, 0.30 mL, then vortexed. The mixture was centrifuged for 5 min at 14000 $\times g$, which resulted in 3 layers: 1) large aqueous top layer, 2) protein interphase, and 3) smaller chloroform bottom layer. The top layer was carefully removed and discarded. An additional 0.40 mL of methanol was added to the interphase/chloroform mixture, then vortexed. The mixture was centrifuged for 5 min at 14000 $\times g$ to cause the precipitate to adhere to the tube walls. The supernatant was removed and the protein pellet was dried under a stream of air.

7.2.1.3 Acetone

The use of acetone for protein precipitation is a common method for precipitation and concentration of proteins. A straight forward method described by Pierce Biotechnology was

employed for acetone precipitation of proteins in Survanta[®] [167]. In an acetone-compatible polypropylene microcentrifuge tube (Fisherbrand[™], ThermoFisher Scientific Inc., Waltham, MA) cold acetone (-20 °C) was combined with Survanta[®] in a ratio of 4:1 (1.2 mL aliquot of acetone, 0.30 mL aliquot of Survanta[®]) and vortexed. The sample mixture was incubated for 60 min at -20 °C acetone, then centrifuged for 10 min at 14000×g. The supernatant was separated from the pellet and the acetone wash/incubation/centrifuge process was repeated two additional times with the collected pellet. After the third wash procedure, the acetone was dried, uncapped, at room temperature for 30 min.

7.2.1.4 Trichloroacetic acid in acetone

A method using trichloroacetic acid (TCA) in acetone was adapted from Nejadi et al [168]. A 15% w/v solution of TCA in acetone was prepared and cooled to -20 °C. The TCA solution was combined with Survanta[®] in a ratio of 4:1 (1.2 mL TCA in acetone, 0.30 mL Survanta[®]) and equilibrated at -20 °C for 60 min. After 60 min, the sample was centrifuged at 15000×g at 4 °C for 20 min. The supernatant was carefully removed and discarded and the pellet was dried at room temperature for 60 min.

7.2.2 Analysis by direct infusion into mass spectrometer

Pelleted samples prepared from protein precipitation methods were reconstituted in methanol and directly infused into a triple quadrupole mass spectrometer (Micromass[®] Quattro, Waters Corporation, Milford, MA) using positive electrospray ionization mode. A programmable syringe pump (Harvard Apparatus 55-1144 model 44, Harvard Apparatus, Holliston, MA) and a 500 µL glass syringe (GASTIGHT[®] 1750, Hamilton Co., Reno, NV) were used to infuse samples at a rate of 10 µL/min. The mass spectrometer (MS) was set to collect ≥ 60 scans from different

m/z ranges within 200-2000 (e.g. scans were collected every 2 s for m/z 1200-2000, therefore the MS was set to scan for a total time of 2 min). The initial mass spectrometer settings were set per manufacturer suggestions and from preliminary tuning studies with rabbit SP-B standards from an ELISA kit for detection of bovine SP-B (MyBioSource, San Diego, CA); parameter settings for the electrospray ionization are shown in Table 7.1.

Table 7.1 Starting electrospray mass spectrometer settings for analysis of surfactant samples

MS Parameter	Setting
Capillary voltage, kV	3.5
Cone voltage, V	35
Extractor voltage, V	3
RF lens voltage, V	0.3
Source temperature, °C	120
Desolvation temperature, °C	300
Desolvation flow, L/h	250
Cone flow, L/h	50
Multiplier	400

7.2.3 Protein purification by analytical chromatographic separation

Characteristics for the bovine surfactant proteins are listed in Table 7.2. Based on their amino acid sequence, the isoelectric point (pI) for SP-B and SP-C were predicted from an online computing tool, ExPASy Compute pI/Mw [169-171].

Amino acids are classified as hydrophilic or hydrophobic depending on their side chains and the side chain interaction with water is used to determine its hydrophathy index [172] – the larger the number, the more hydrophobic. The hydrophathy index values were estimated using an

online GRAVY calculator [173]. GRAVY is the grand average of hydropathy, the value of which is the sum of hydropathy values of all amino acids divided by the protein length.

Separation based on hydrophobicity was performed with a protein column (XBridge[®] protein Bridged Ethyl Hybrid (BEH) C₄ column, 300Å, 3.5 μm, 2.1 mm x 100 mm, 0.35 mL column volume, Waters Corporation, Milford, MA). The use of different mobile phase solvents were explored following published methods [174, 175]. The electrospray mass spectrometry conditions were the same as those used in the direct infusion experiments (Table 7.1).

Table 7.2 Comparison of bovine SP-B and SP-C characteristics [169-173].

Characteristic	SP-B	SP-C
Isoelectric point	9.03	8.96
Hydropathy index	1.09	2.58
Protein chain length	79	34
Monoisotopic mass (Da)	8699.78	3565.24
Cationic residues	8	2

7.2.4 Non-specific assay of proteins

Fluorescamine, sodium phosphate (Na₂HPO₄), and sodium phosphate monobasic (NaH₂PO₄•H₂O) were purchased from Fisher Scientific Co. (Hanover Park, IL). Survanta[®] (beractant) intratracheal suspension was purchased from Cardinal Health, Inc. (Greensboro, NC) and stored at 2-8 °C. Pearlitol[®] PF-mannitol was donated from Roquette Pharma (Lestrem, France).

For non-specific analysis of proteins, the reagent fluorescamine is commonly used for detection of primary amino acid groups [176]. The Survanta-EEG formulation was prepared and

spray dried as described in Chapter 4, but without leucine since it is an amino acid and its presence would be detected in the fluorescamine assay. Samples prepared for analysis and theoretical protein content based on the Survanta[®] label claim [30] are listed in Table 7.3. The theoretical protein concentration was first determined for the feed dispersion samples, then used to calculate the amount of Survanta[®] and Survanta-EEG powder needed to target the same concentration in the samples.

Table 7.3 Prepared protein samples and theoretical protein content for fluorescamine assay.

Protein sample	Sample aliquot	MeOH diluent, mL	Theoretical total protein concentration, mg/mL
Survanta [®]	0.35 mL	20	0.0175
Feed dispersion post-sonication	0.25 mL	n/a	0.0173
Bypass feed dispersion	0.25 mL	n/a	0.0173
Survanta-EEG powder (without leucine)	12.5 mg	10	0.0172

An aliquot (0.25 mL) of each prepared protein sample was combined with 1.25 mL of 0.05 M sodium phosphate buffer, pH 8, in a test tube. During vigorous shaking using a vortex mixer, 0.50 mL of fluorescamine in acetone (0.30 mg/mL) was rapidly added using a syringe. Aliquots of 100 μ L were transferred in triplicate to a 96-well plate and fluorescence measurements were made with excitation and emission wavelengths set to 390 nm and 475 nm, respectively, using a Synergy[™] H1 Hybrid Multi-Mode Reader (BioTek Instruments, Inc., Winooski, VT).

7.2.5 Enzymatic assay of proteins

Enzyme-linked immunosorbent assay (ELISA) kits (Bovine Pulmonary Surfactant-Associated Protein B (SP-B) ELISA kit MBS703513 and Bovine Pulmonary Surfactant-

Associated Protein C (SP-C) ELISA kit MBS700517, MyBiosource.com, San Diego, CA) were used to determine the presence of proteins at the different processing steps during formulation preparation. The assay used a sandwich enzyme technique specific for SP-B or SP-C.

Standards were prepared following manufacturer instructions. Samples were prepared by diluting Survanta[®], feed dispersions post-sonication, feed dispersions bypassed on the spray dryer, and leucine-Survanta-EEG powders in 60/40% v/v acetonitrile/water with theoretical protein concentrations of 100-500 $\mu\text{g/mL}$. Solvent selection was based on the work of Pérez-Gil et al. [18] (Figure 7.1). Standards were analyzed in duplicate, while samples were analyzed in triplicate. Repeat washing was performed with an automated microplate washer (Wellwash 4 Mk2, LabSystems, ThermoFisher Scientific Inc., Waltham, MA). Absorbance readings were measured at 450 nm using a microplate reader (Synergy[™] H1 Hybrid Multi-Mode Reader, BioTek Instruments, Inc., Winooski, VT).

7.3 Results and discussion

7.3.1 Protein precipitation

The precipitation of proteins from Survanta[®] was performed using hexane/isopropanol, methanol/chloroform, acetone, and TCA in acetone. The collected pellets were solubilized with methanol prior to direct infusion into the MS. A comparison of the scans collected from 200-2000 m/z is shown in Figure 7.2. The acetone (Figure 7.2c) and TCA in acetone (Figure 7.2d) precipitation samples were observed to provide spectrums with a lower number of individual molecular ions, compared to the other solvents, perhaps indicating greater extraction specificity. The highest intensity molecular ions for the four precipitation methods was observed at m/z of 734.7 and 757, indicating that DPPC was still present in the samples (DPPC+H⁺ of 734.6 m/z and

DPPC+Na⁺ of 756.6 *m/z*). The methanol/chloroform (Figure 7.2b) and TCA in acetone (Figure 7.2d) precipitation methods appeared to be better at removing salt from the commercial formulation as the DPPC sodium adducts were observed to be lower when compared to the hexane/isopropanol and acetone precipitation methods, with the methanol/chloroform precipitation method showing the lowest ratio of DPPC+Na⁺ to DPPC+H⁺. This is likely due to sodium chloride having the higher solubility in methanol compared to the other solvents (NaCl solubility at 25 °C per 100 g solvent: 1.4 g in methanol; 0.003 g in isopropanol, but insoluble in hexane; 0.000042 g in acetone). In addition, the methanol/chloroform procedure was the only method to use water as one of the wash solvents (NaCl solubility at 25 °C: 36 g /100 g water).

The presence of DPPC as the highest observed ion in the precipitation samples indicates that the procedures used were not effective in purifying the hydrophobic proteins from the commercial surfactant formulation. However, it was still of interest to determine if the multiply charged molecular ions of the intact hydrophobic proteins could be detected.

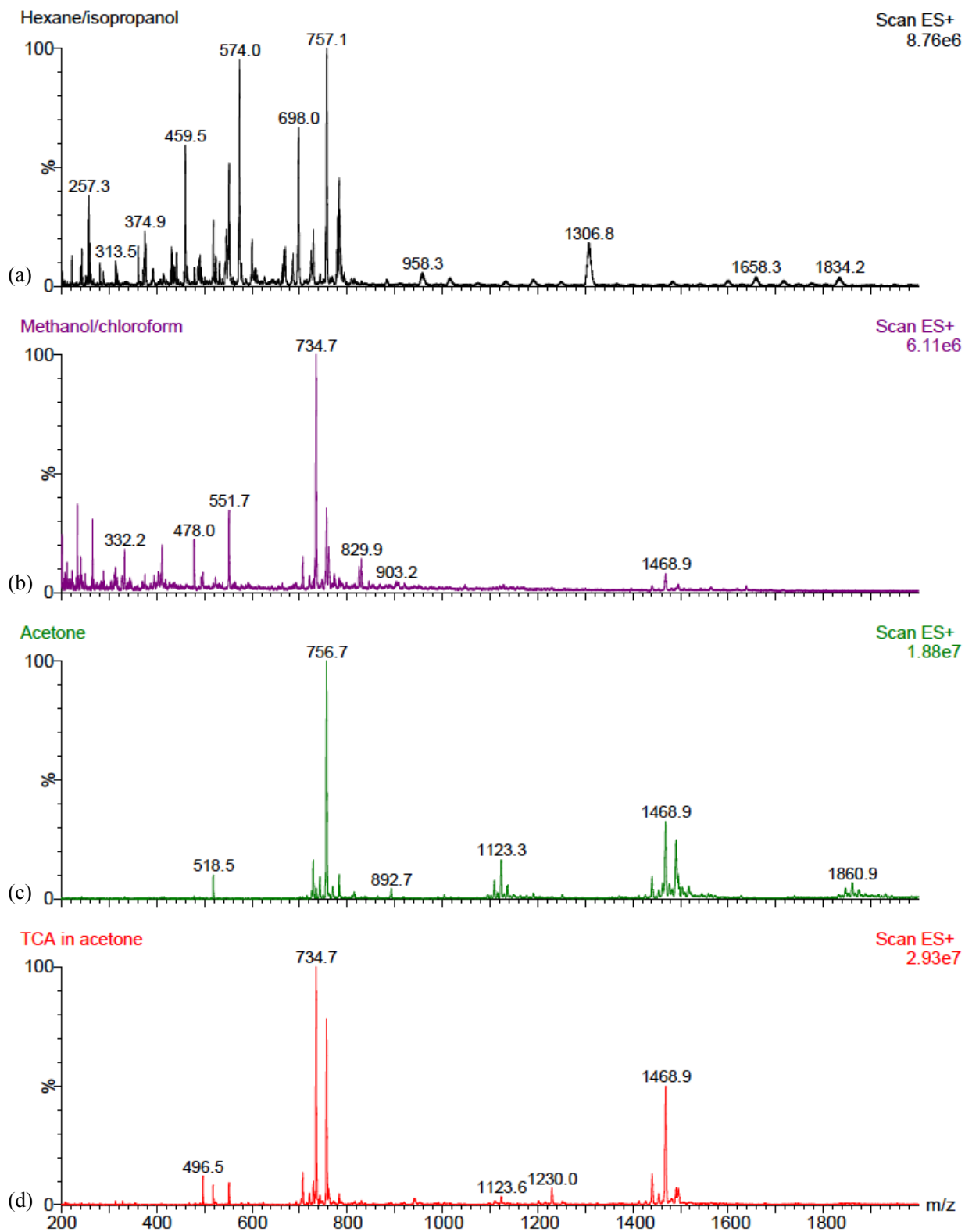


Figure 7.2 Mass spectrum comparison of protein precipitation methods on Survanta[®] with (a) hexane/isopropanol, (b) methanol/chloroform, (c) acetone, and (d) TCA in acetone.

Using Q-TOF nano-ESI, the primary structure of SP-B was determined by Liu et al. [26] as follows: FPIPI PYCWL CRTLI KRIQA VIPKG VLAMT VAQVC HVVPL LVGGI CQCLV ERYSV ILLDT LLGRM LPQLV CGLVL RCSS. There are 8 basic amino acid residues in the sequence of the SP-B monomer – lysine (K), arginine (R) and histidine (H) – indicating eight possible ionization sites. Each monomer has four amphipathic α -helices and the cysteines (C) are all oxidized to form disulfide bonds, three intra-molecular disulfide bonds and one inter-molecular disulfide bond that links two SP-B monomers to create a homodimer [26, 177]. The ExPASy Compute pI/Mw tool determined the theoretical monoisotopic mass of the SP-B monomer as 8699.78 Da. The mass of the dimer, with 7 disulfide bonds (2.016 Da decrease per disulfide bond [178]), was calculated to be 17395.53 Da.

The sequence of SP-C was determined by Q-TOF nano-ESI as LIPCC PVNIK RLLIV VVVVV LVVVV IVGAL LMGL [26]. Rich in valine (V) and leucine (L), SP-C is the most hydrophobic of the surfactant proteins [179]. A single α -helix monomer with 34 amino acid residues, SP-C has a theoretical monoisotopic mass of 3565.24 Da. The two cysteines of the protein are palmitoylated [26, 174], which enables SP-C to improve the lipid monolayer stability and re-spreading during expansion that occurs during inhalation [15]. Palmitoylation increases the monoisotopic mass of SP-C to 4041.70 Da (238.23 Da increase per palmitoylation [178]).

Two techniques were used to process the electrospray data, Transform and Maximum Entropy (MaxEnt). The Transform algorithm developed by Micromass[®] (Wilmslow, United Kingdom) was used to convert the m/z electrospray data from direct infusion of the precipitation samples onto a molecular mass spectrum. The protein molecular weights of 17395.5, 8699.8, and 4041.7 Da were assigned for the dimer of SP-B, the monomer of SP-B and the palmitoylated SP-C, respectively. The Transform spectrums for each sample is shown in Figure 7.3. Since the

Transform algorithm requires that component mass values are assigned and also that the entered mass values are accurate, the resulting spectrum does not definitively indicate the presence of proteins. The Transform spectra for each of the samples from the different precipitation methods show a peak at each of the mass values entered. For the hexane/isopropanol, methanol/chloroform and acetone samples (Figure 7.3a, Figure 7.3b and Figure 7.3c, respectively), the peak at the mass of the homodimer was shown to have the highest intensity, whereas the highest intensity peak was observed at the mass value of the SP-B monomer in the TCA in acetone sample (Figure 7.3d).

The MaxEnt tool, which uses the method of maximum entropy for deconvolution of electrospray data without the need to identify the proteins present, was also applied to the protein precipitation electrospray data to determine if the presence of proteins could be detected. The analysis was done over a broad mass range (3500 to 18500 Da) with a resolution of 1 Da/channel, to ensure that the entire mass range of the proteins was captured. Figure 7.4 shows the results from MaxEnt analysis for each precipitation method sample. As expected, many peaks were observed for all samples given their complex mixture. The precipitation sample prepared from acetone was observed to have a relatively distinct peak around 4400 Da. MaxEnt analysis was performed on this sample over a narrower output mass range (4000 to 5000 Da) using a finer resolution (0.5 Da/channel) to obtain a more accurate mass value; the resulting MaxEnt spectrum shown in Figure 7.5. The mass value was determined to be 4464.5 Da, which would be closest to that of palmitoylated SP-C (4041.7 Da), but a difference of 423 Da suggests that the hydrophobic protein could be associated with something else in the mixture or that this may be a fragment of the larger protein. Results were similar when the protein precipitation method with acetone was repeated (Figure 7.6).

Given the uncertainty with the precipitation methods explored when performed on the Survanta® formulation pre-processing, alternative methods were explored to separate the complex mixture of components in the commercial surfactant.

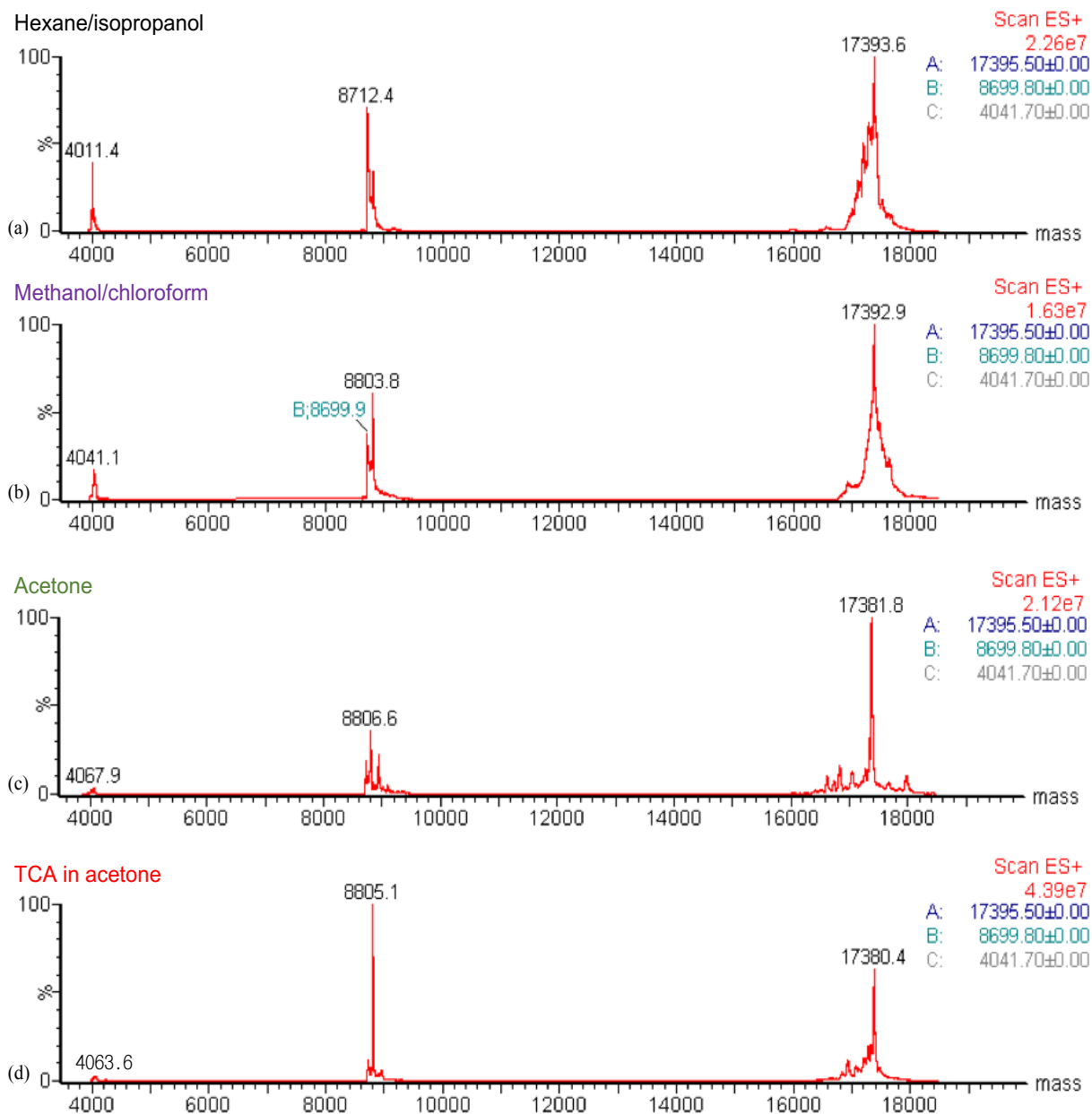


Figure 7.3 Transform spectrum comparison of protein precipitation methods on Survanta® with (a) hexane/isopropanol, (b) methanol/chloroform, (c) acetone, and (d) TCA in acetone with output mass range set from 3500 to 18500 Da.

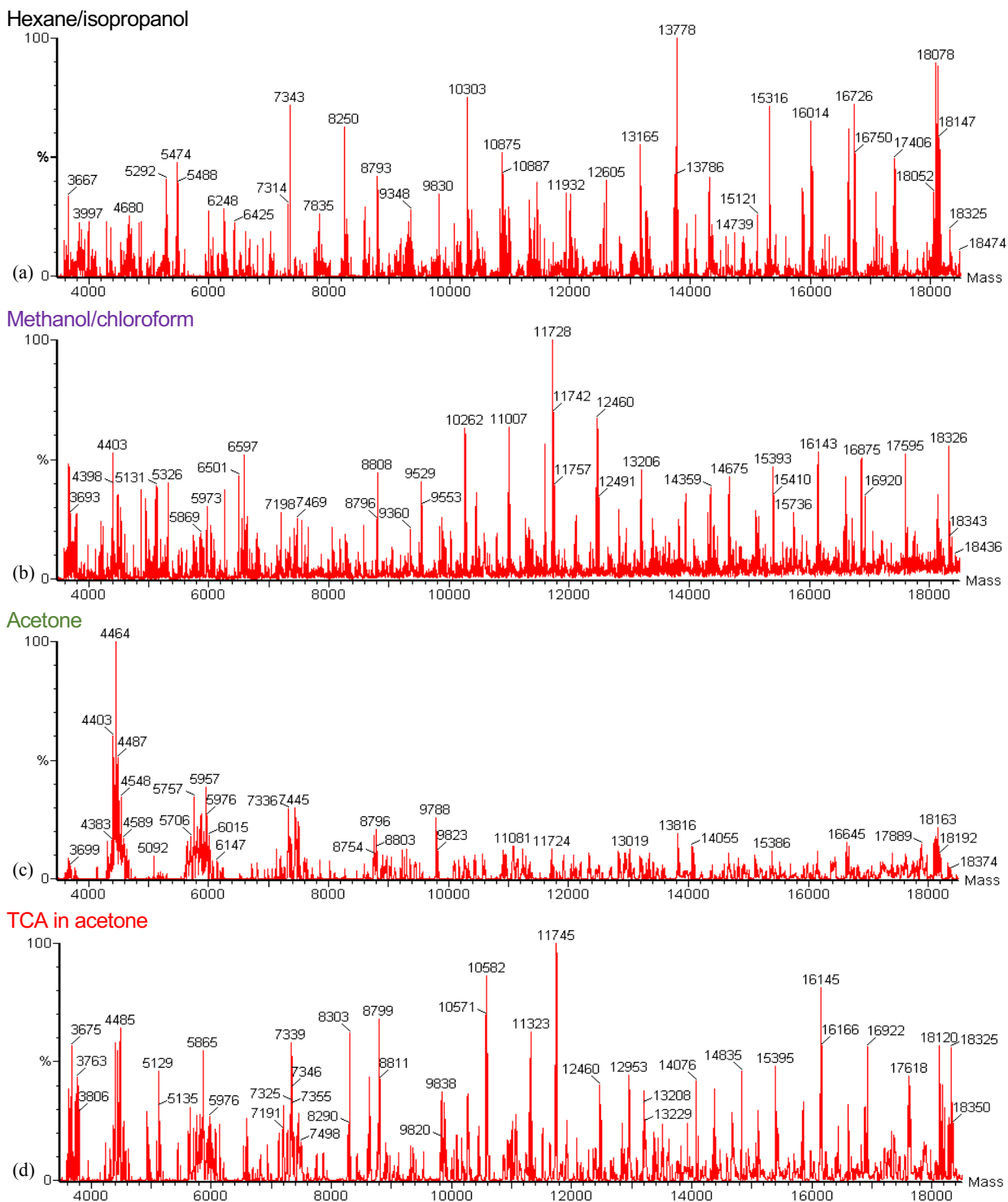


Figure 7.4 MaxEnt spectrum comparison of protein precipitation methods on Survanta[®] with (a) hexane/isopropanol, (b) methanol/chloroform, (c) acetone, and (d) TCA in acetone for output mass range set from 3500 to 18500 Da.

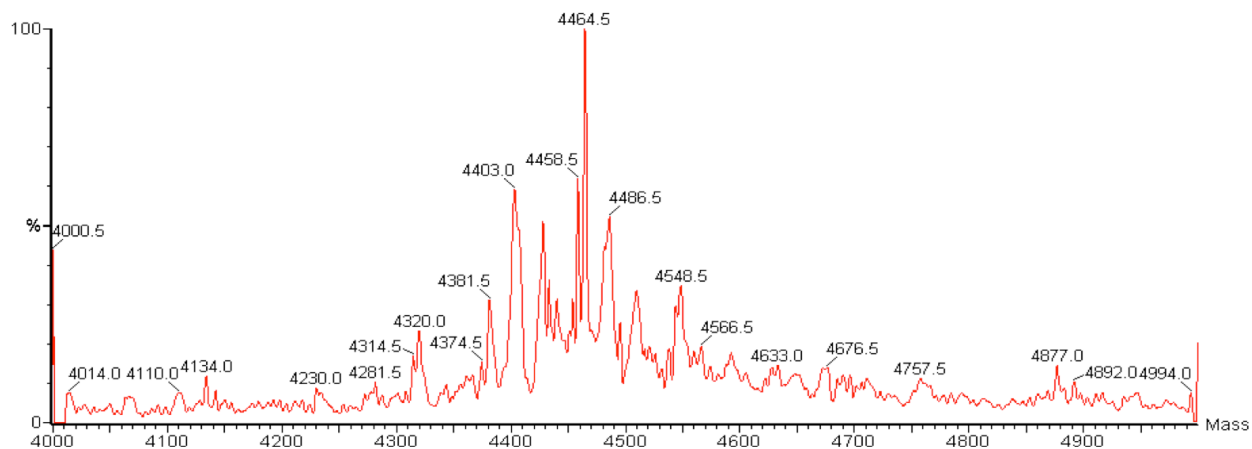


Figure 7.5 MaxEnt spectrum for acetone precipitate sample on Survanta[®] with output mass range of 4000 to 5000 Da with a resolution of 0.5 Da/channel.

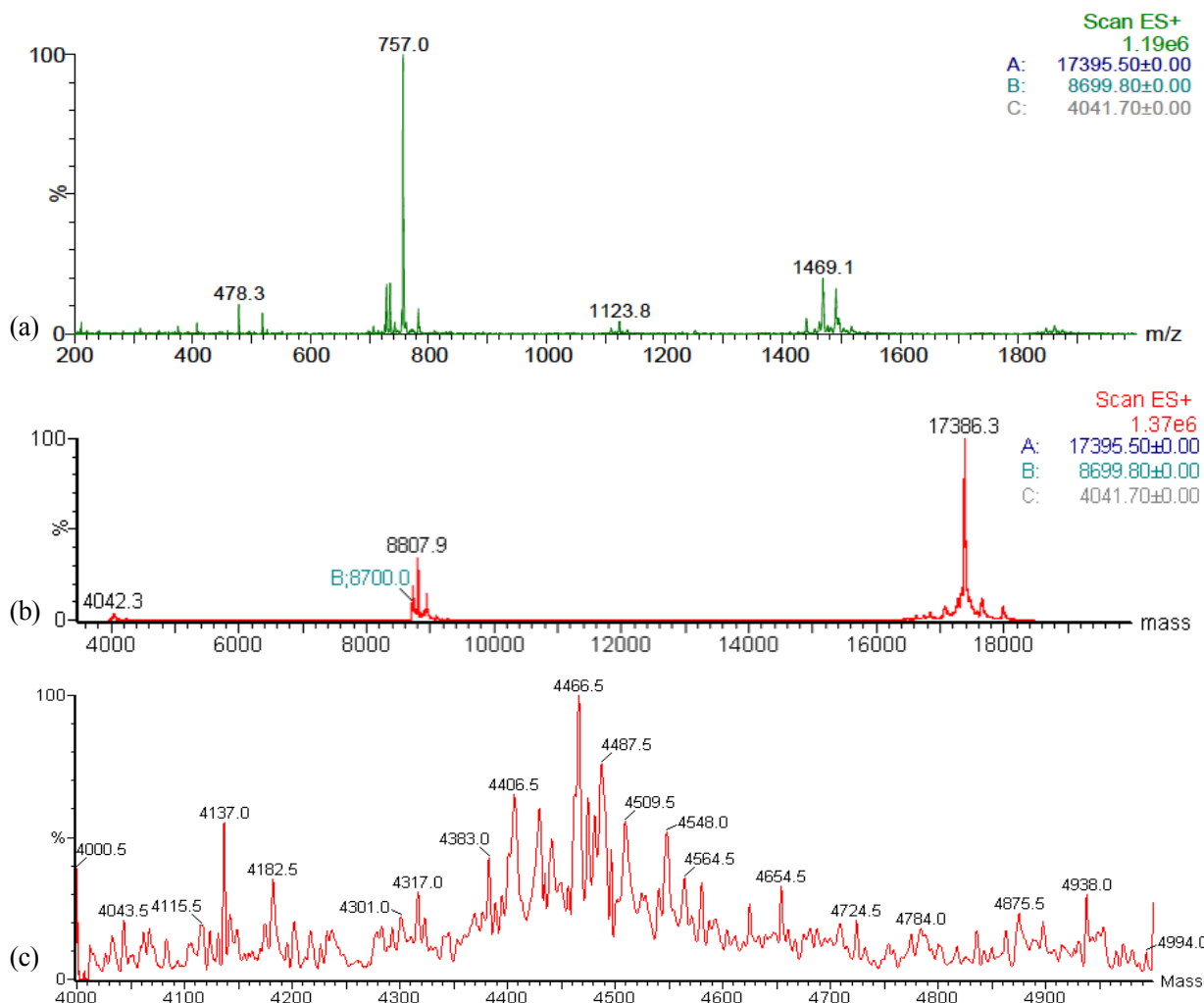


Figure 7.6 Repeat acetone protein precipitation sample (a) electrospray spectrum (b) Transform spectrum and (c) MaxEnt spectrum of Survanta[®].

7.3.2 Analytical separation of Survanta[®] components

Precipitation experiments to separate proteins from other hydrophobic components proved unsuccessful as a high concentration of lipids were still present in the samples, therefore, separation of the components using column chromatography was explored. A 300Å BEH C4 column was used for separation and coupled to an ESI-MS for detection. Samples were prepared by diluting Survanta[®] in methanol and dissolving the Survanta-EEG powder formulation in methanol prior to LC-MS analysis.

Following procedures adapted from Harayama et al. [174], initial experiments explored varying concentrations of methanol/water with 0.1% formic acid using both isocratic and gradient elution procedures. The MS parameters were as follows: capillary, 3.5 kV; cone, 35V; source temperature, 120 °C; desolvation temperature, 300 °C. Ion chromatograms showing the total ion count (TIC) were used as fingerprint patterns for evaluation of the separation of the constituent components of these complex formulations prior to analysis of their mass spectral profiles.

The mobile phase composition that resulted in the best separation of components was determined to be 80/20% v/v methanol/water with 0.1% formic acid at a flow rate of 0.2 mL/min with an injection volume of 5 µL and a run time of 22 min (Figure 7.7, top). The largest peak was observed at a retention time (T_r) of 9.07 min, which was identified as DPPC from the mass spectrum showing a m/z of 734.7 (Figure 7.8a). Figure 7.8b shows the mass spectrum for the peak at T_r of 6.97 min, which was observed to consist of a mixture of two phospholipids, palmitoyl-oleoyl phosphatidylcholine (PC 16:0/14:0, exact mass of 705.5 Da) and palmitoylpalmitol-eoyl phosphatidylcholine (PC 16:0/16:1, exact mass of 731.6 Da), which are the two major fluidizing components in pulmonary surfactant [180]. At the retention time of 2.13 min, the mass spectrum reveals a peak at 496 m/z , indicating the fragment after an acyl chain loss from DPPC, [DPPC+H]-

sn1 and [DPPC+H]⁺-sn2 [181] (PC 16:0/0:0, exact mass of 495.3 Da, Figure 7.8c). The peak at T_r of 1.21 min could possibly be that of the proteins since the mass spectrum shows multiple peaks spaced apart, a pattern typically observed with multiply charged species.

Although a good separation of the Survanta[®] components was observed with a mobile phase of 80/20% v/v methanol/water with 0.1% formic acid, a different separation profile was observed when a Survanta-EEG sample was run under the same conditions (Figure 7.7, bottom), which would make comparison of the two formulations problematic.

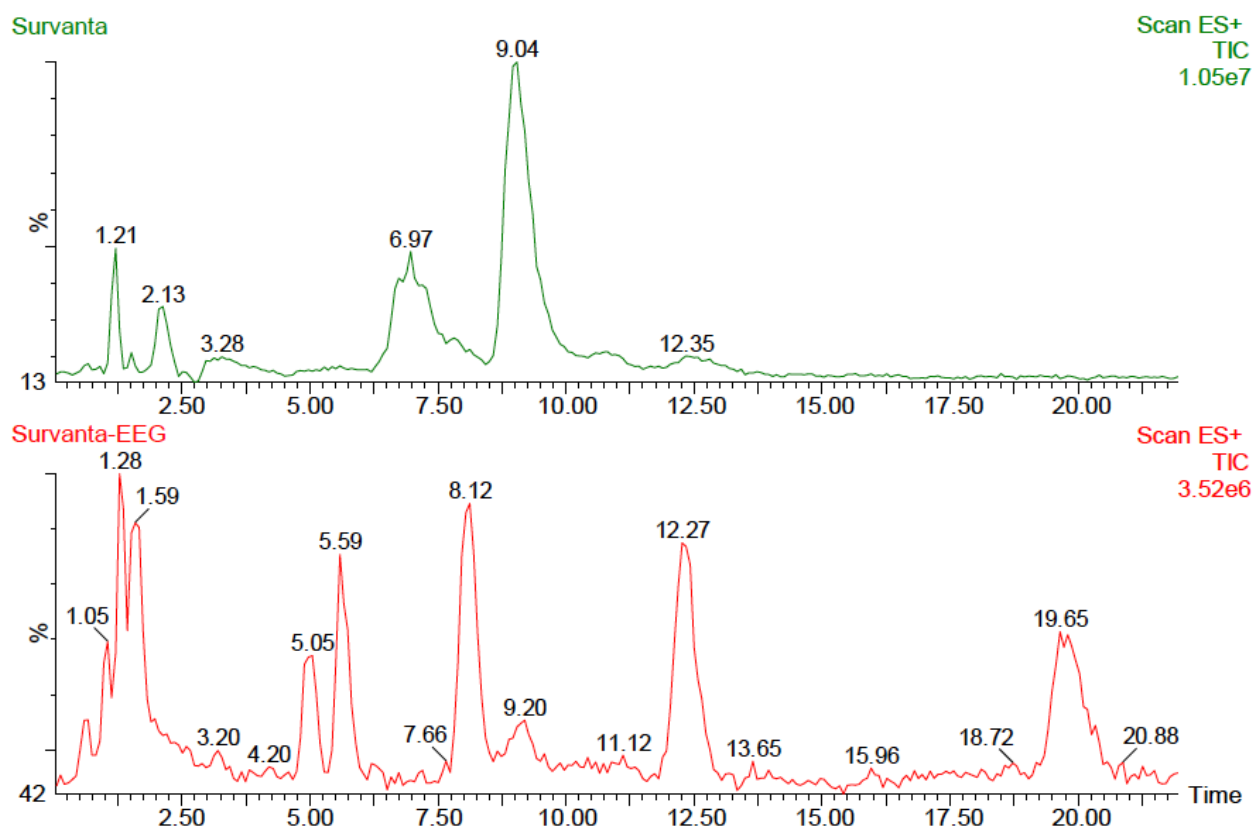


Figure 7.7 Comparison of total ion count chromatograms obtained for commercial Survanta[®] formulation (top) and Survanta-EEG spray dried powder (bottom) separation in mobile phase of 80/20% v/v methanol/water with 0.1% formic acid with injection volume of 5 μ L, 0.2 mL/min flow rate and 22 min run time.

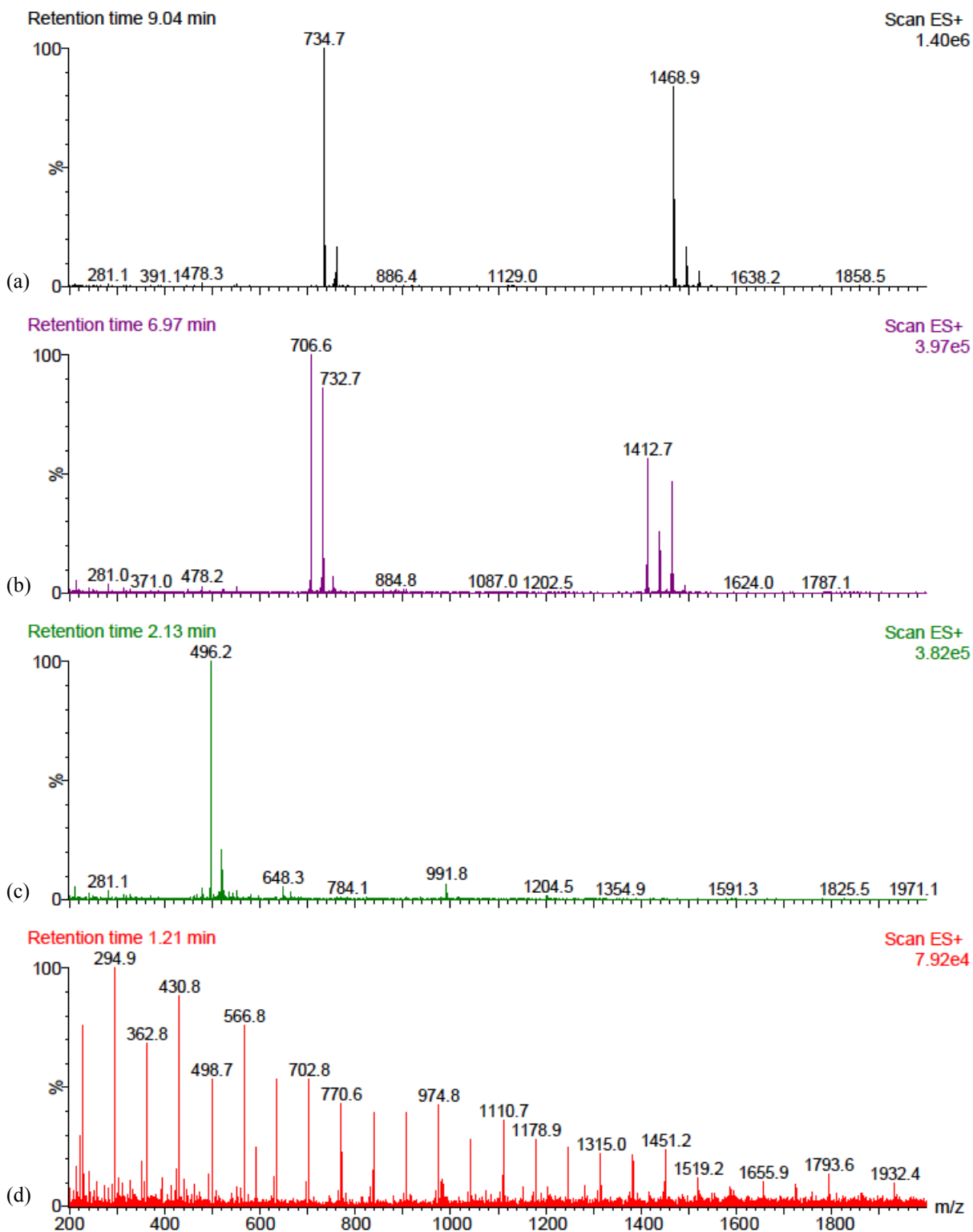


Figure 7.8 Mass spectra of Survanta® components separated using with 80/20% v/v methanol/water with 0.1% formic acid with injection volume of 5 μ L, 0.2 mL/min flow rate and 22 min run time. MS settings: capillary=3.5 kV, cone=35 V, source temperature=120 $^{\circ}$ C, desolvation temperature=300 $^{\circ}$ C.

The use of acetonitrile as the eluting solvent instead of methanol was explored. Using a mobile phase composition of 80/20% v/v acetonitrile/water, acetonitrile was shown to elute the components earlier in the chromatographic profile compared to methanol (Figure 7.9b compared to Figure 7.9a), which was expected as acetonitrile generally has a higher elution strength when compared to methanol. Different concentrations of acetonitrile in the mobile phase were explored while the flow rate was maintained at 0.2 mL/min. An improved separation was achieved by decreasing the concentration of acetonitrile to 60% (Figure 7.9c). A shorter run time of 15 min was used with the improved solvent mobile phase composition. Analysis of the spray dried powder formulation showed a similar finger print separation of the components compared to the Survanta[®] formulation using these chromatographic separation conditions. A blank injection of methanol was run and subtracted from both samples; a comparison of the Survanta[®] and Survanta-EEG total ion chromatograms are shown in Figure 7.10.

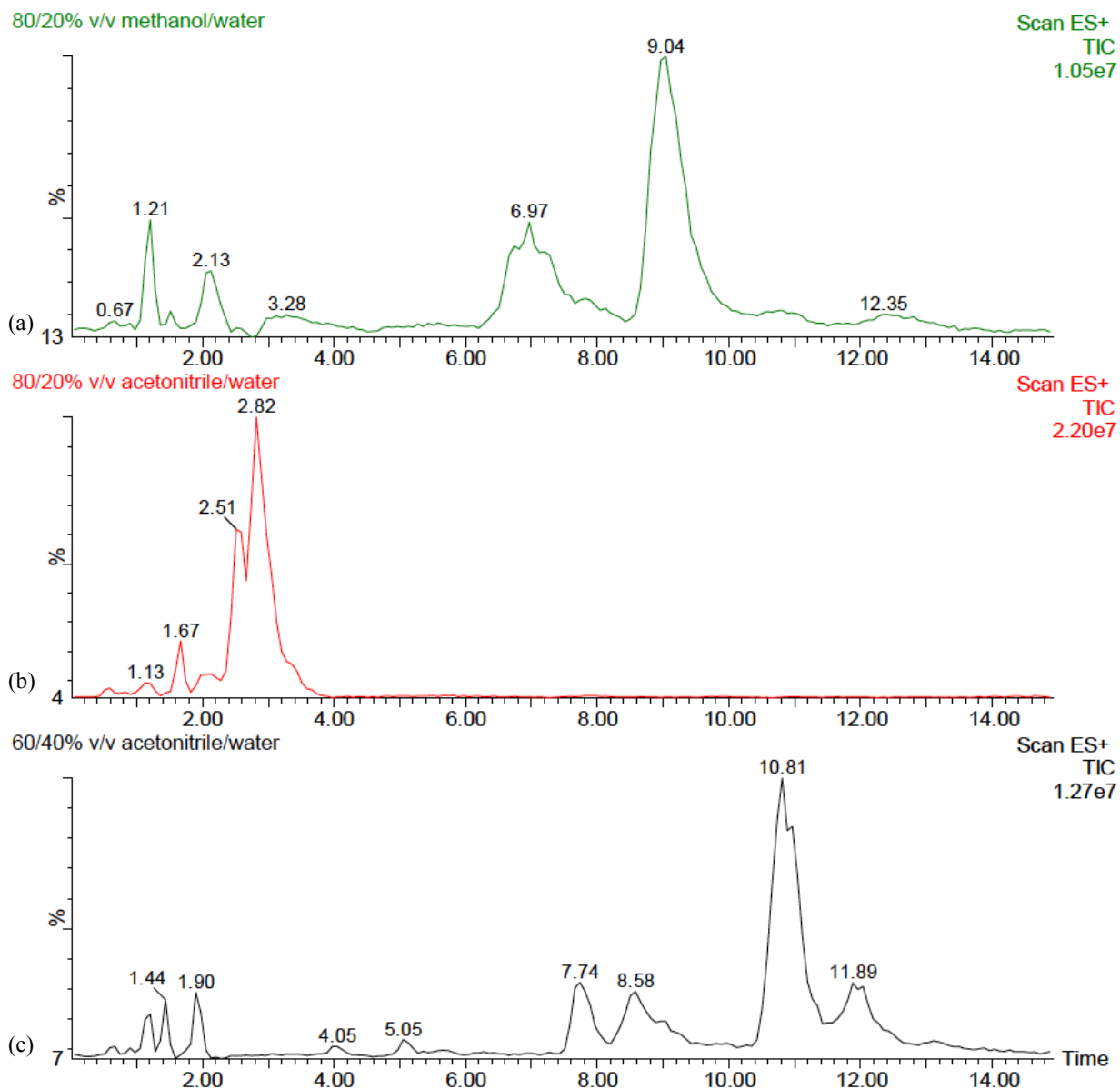


Figure 7.9 Comparison of mobile phase solvents (a) 80/20% v/v MeOH/H₂O with 0.1% formic acid, (b) 80/20% v/v ACN/H₂O with 0.1% formic acid, and (c) 60/40% v/v ACN/H₂O with 0.1% formic acid on separation of Survanta[®] components with 5 μ L injection volume and 0.2 mL/min flow rate. MeOH=methanol, H₂O=water, ACN=acetonitrile.

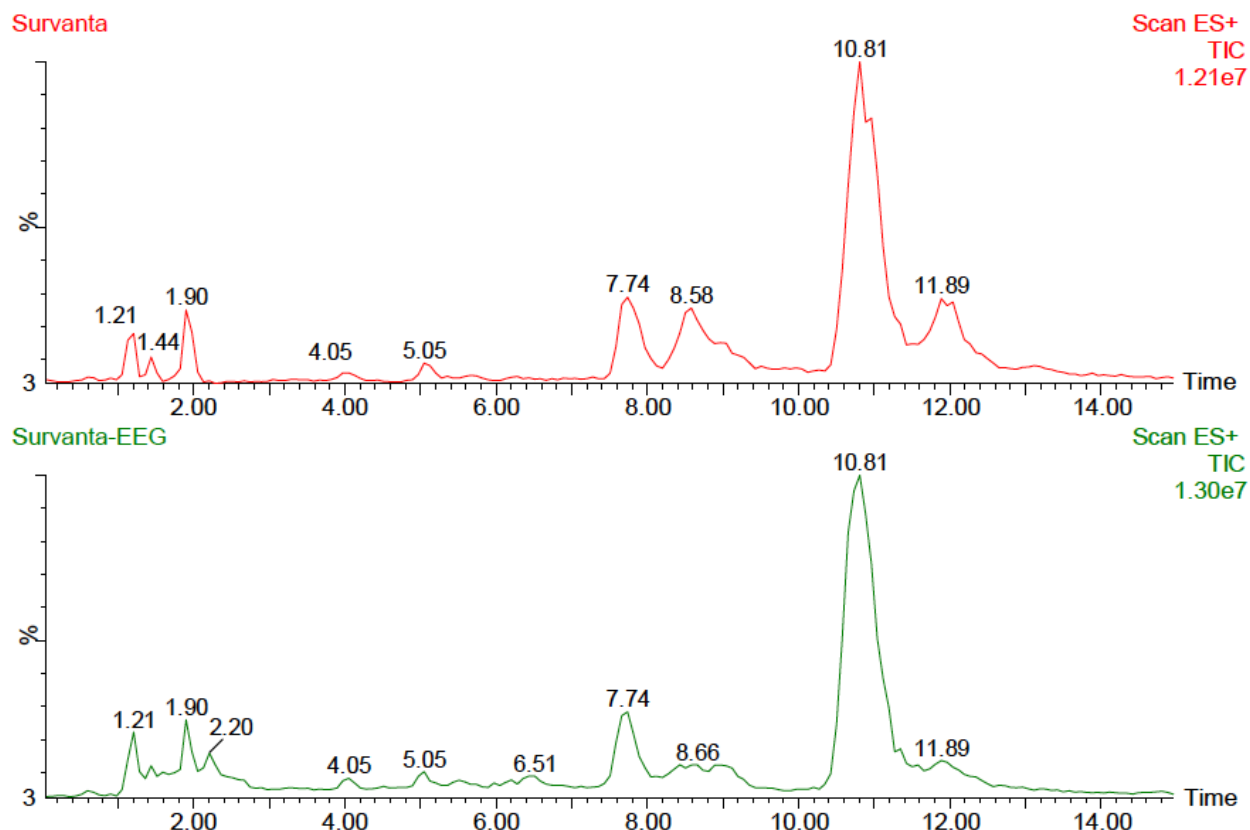


Figure 7.10 Comparison of commercial Survanta[®] formulation (top) with Survanta-EEG spray dried powder (bottom) separation in mobile phase of 60/40% v/v acetonitrile/water with 0.1% formic acid with 5 μ L injection volume, 0.2 mL/min flow rate and a 15 min run time.

Each of the separated chromatographic peaks in the Survanta[®] total ion mass chromatogram was assessed to determine its mass spectral profile, in an attempt to identify the surfactant proteins; mass spectrum results for each significant peak are shown in Figure 7.11. Given the highly hydrophobic nature of the proteins, it was expected that the proteins were to elute early in the run. The largest peak observed was at a T_r of 10.81 min, which was determined to be DPPC (m/z 734). Although the identification of some peaks was possible, the complexity of the commercial formulation made it difficult to assign a component to each peak without further fractional isolation and analysis, which was beyond the scope of this study; the peak components that were identified are shown in Table 7.4.

A similar mass spectral identification was performed for the Survanta-EEG formulation and is shown in Figure 7.12. In both total ion chromatograms, the peak at T_r of 1.21 min was identified as possibly that of the proteins since the mass spectrum showed multiple peaks spaced apart in a pattern, indicating the possibility of multiply charged species. The isotopic distributions in the spectrum could not be discerned since the triple quadrupole MS has low resolution that cannot fully distinguish a change in the m/z of less than 0.5 in a mass spectrum – a drawback to using a triple quadrupole mass spectrometer.

The Survanta[®] spectrum for the T_r peak at 1.21 min from 700-2000 m/z is shown in Figure 7.13 (top) with a comparison to the peak at the same retention time in the Survanta-EEG spray dried powder sample (Figure 7.13, bottom). The spectra show peaks with similar m/z values, with Survanta-EEG sample having a few additional peaks, suggesting that the samples have a similar composition.

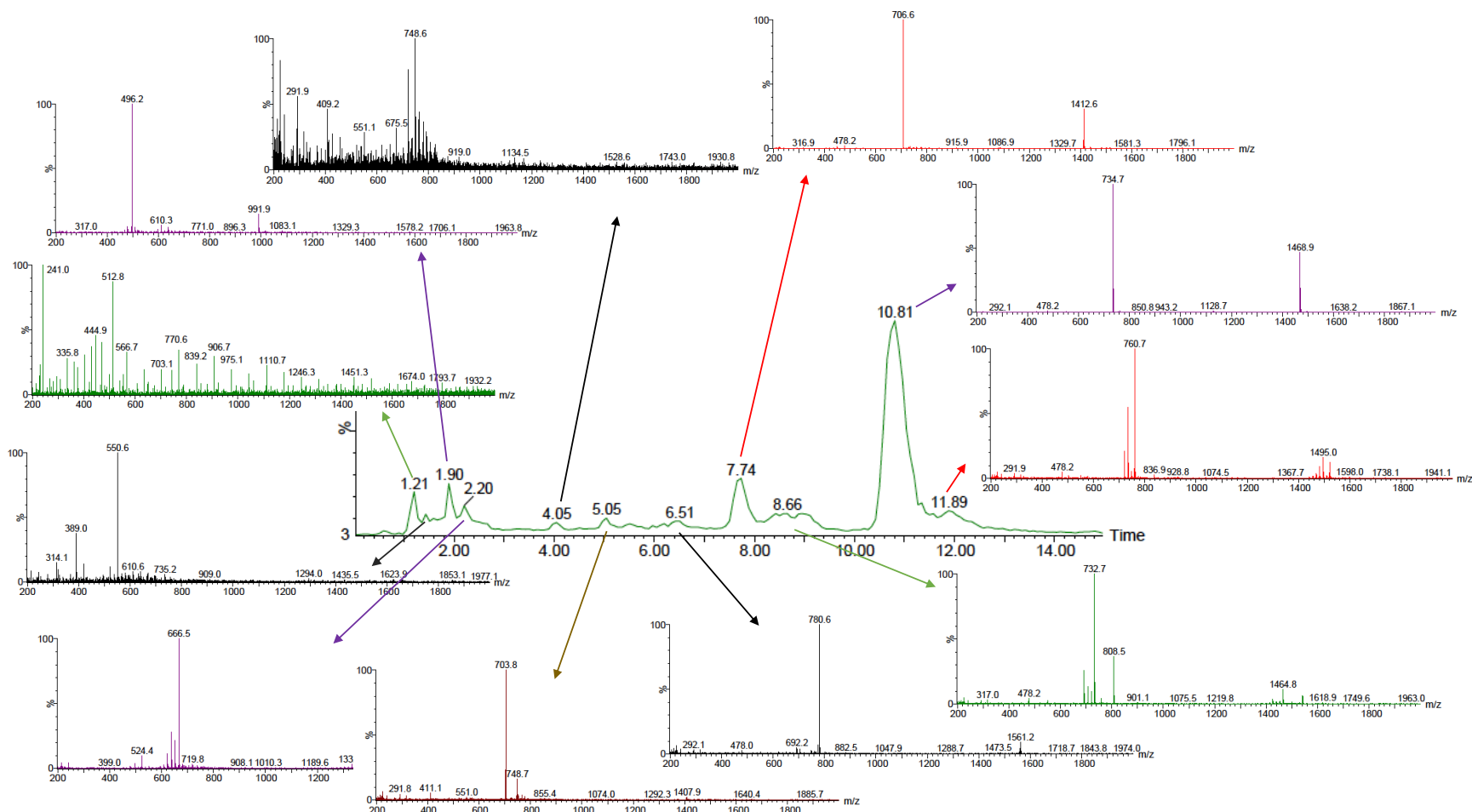


Figure 7.12 Mass spectra of Survanta-EEG components separated using with 60/40% v/v acetonitrile/water with 0.1% formic acid with injection volume of 5 μ L, 0.2 mL/min flow rate and 15 min run time. MS settings: capillary=3.5 kV, cone=35 V, source temperature=120 $^{\circ}$ C, desolvation temperature=300 $^{\circ}$ C.

Table 7.4 Identified peaks from mass spectra of Survanta[®] separated using with 60/40% v/v acetonitrile/water with 0.1% formic acid with injection volume of 5 μ L, 0.2 mL/min flow rate and 15 min run time. MS settings: capillary=3.5 kV, cone=35 V, source temperature=120 $^{\circ}$ C, desolvation temperature=300 $^{\circ}$ C. Exact mass values from [182].

Retention time, min	<i>m/z</i>	Component	Exact mass, Da
1.90	496.2	DPPC-sn1 and DPPC-sn2	495.3*
7.74	706.6	PC 16:0/14:0 (PMPC)	705.5
8.58	732.6	PC 16:0/16:1	731.6
10.81	734.7	PC 16:0/16:0 (DPPC)	733.5
11.89	760.7	PC 16:0/18:1 (POPC)	759.6

*Calculated using LipidMaps MS Tools [183].

PMPC=palmitoyl-myristoyl phosphatidylcholine, DPPC=dipalmitoylphosphatidylcholine, POPC=palmitoyl-oleoyl phosphatidylcholine

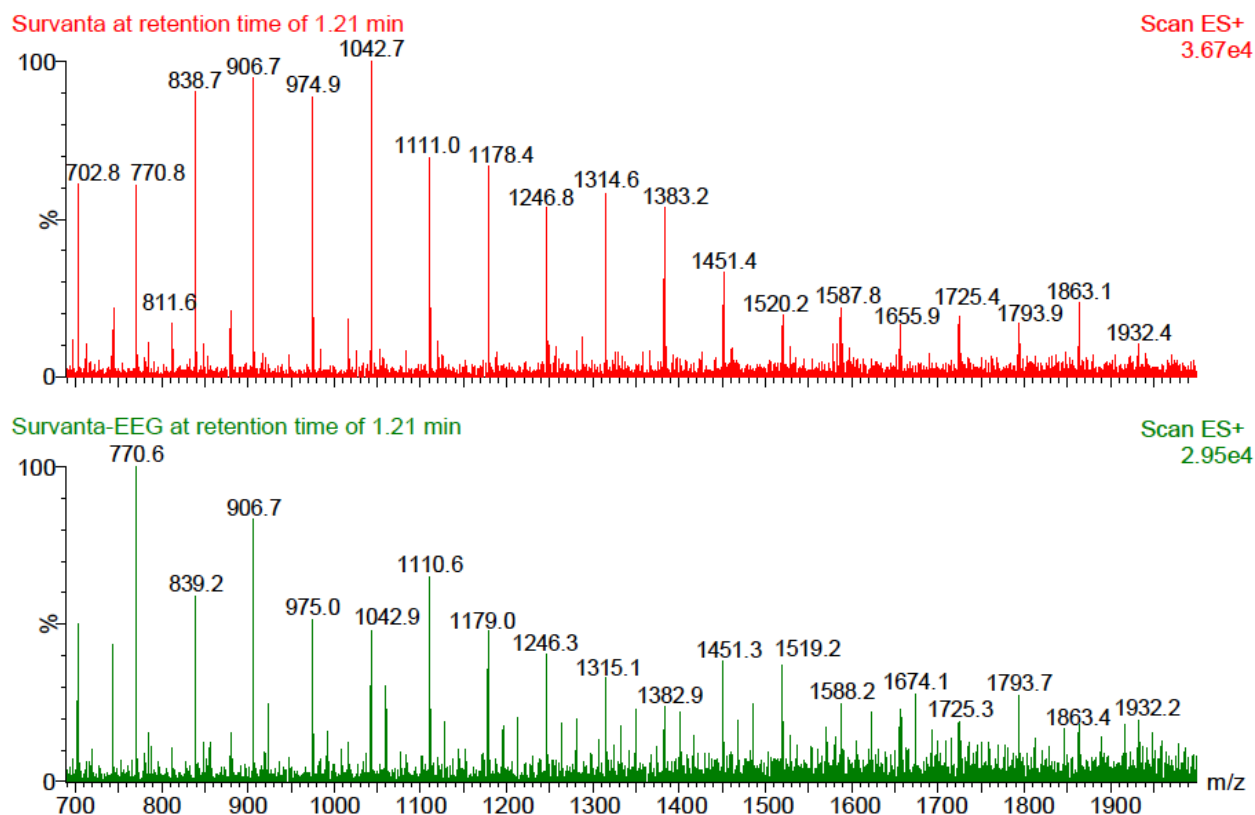


Figure 7.13 Mass spectra comparison of the peak at retention time of 1.21 min for the commercial Survanta[®] formulation (top) with Survanta-EEG spray dried powder (bottom). MS settings: capillary=3.5 kV, cone=35 V, source temperature=120 $^{\circ}$ C, desolvation temperature=300 $^{\circ}$ C.

The expected m/z values for the surfactant proteins were calculated from the exact mass values. The protonated (increase in 1.0073 Da) and sodium adduct (increase in 22.989 Da) m/z values for the ionized surfactant proteins are shown in Table 7.5. During sample preparation, methylation of proteins commonly occurs, especially when samples are prepared in methanol [26, 184]. Methylation is most commonly observed on arginine and lysine residues [184, 185]; SP-B has a total of seven arginine and lysine residues while SP-C has two. The expected m/z values for a single methylation are included in Table 7.5, although it is understood that as many as seven residues in SP-B or two residues in SP-C could be methylated. These modifications add to the difficulty of interpreting the peaks in the mass spectra. SP-C has been observed in its triple, quadruple and quintuple charge states [26, 174], and is therefore also included in Table 7.5.

A comparison of the peak table with the peaks observed in Figure 7.13 revealed random matching peaks (indicated with # symbol), however there were not enough matches to conclude that the peak at the retention time of 1.21 min was that of the proteins. The m/z range of 700 to 2000 was studied, in which a pattern with a consistent m/z increase of 68 was observed. This could represent cluster ions of sodium formate (formed from the sodium chloride present in the sample and the formic acid present in the mobile phase), which is often observed to have mass peaks 68 Da apart [186].

Both proteins may possibly have eluted at the same time from the column given that the mass spectra from the other peaks do not reveal patterns to be expected when analyzing proteins. Interpretation of the spectrum may be more difficult if both proteins eluted in the same peak, which contributes to the inconclusive results. Further studies could examine improving the chromatography to separate and identify the proteins.

Table 7.5 Predicted mass charges of SP-B dimer (17395.5 Da), SP-B monomer (8699.8 Da) and SP-C monomer (4041.7 Da), including sodium adducts and single methylation, within the range of the triple quadrupole MS (200-2000 *m/z*). H=hydrogen, Na=sodium, Me=methyl.

Protein	Charge	[M+H] ⁺ , <i>m/z</i>	[M+Na] ⁺ , <i>m/z</i>	[M+Me] ⁺ <i>m/z</i>
SP-B dimer	16	1088.2	1111.2 [#]	1088.1
	15	1160.7	1183.7	1160.6
	14	1243.6	1266.5	1243.5
	13	1339.1	1362.1	1339.2
	12	1450.6	1473.6	1450.8 [#]
	11	1582.4	1605.4	1582.7
	10	1740.6	1763.5	1741.0
	9	1933.8	1956.8	1934.4
SP-B monomer	8	1088.5	1111.5 [#]	1089.2
	7	1243.8	1266.8	1244.8
	6	1451.0 [#]	1474.0	1452.3
	5	1741.0	1764.0	1742.8
SP-C monomer	5	809.3	832.3	811.1 [#]
	4	1011.4	1034.4	1013.9
	3	1348.2	1371.2	1351.9

[#]Peaks identified within 0.5 *m/z* in Survanta[®] and Survanta-EEG formulations (Figure 7.13)

7.3.3 Non-specific assay of surfactant proteins

With inconclusive results from the previous experiments, a simple assay for the determination of primary amino groups (found in terminal amino acids of proteins) was performed. Fluorescamine was used for the non-specific determination of proteins in the commercial formulation, the feed dispersion samples, and the spray dried powders. Three batches of spray dried Survanta-EEG without leucine were prepared fresh and analyzed the following day with storage overnight in a desiccator in a fridge (2-8 °C). For comparison, the fluorescence results for

the processed samples were reported as a percentage of the fluorescence detected for the commercial formulation. The results are shown in Table 7.6.

For each of the three batches of feed dispersions that were prepared and spray dried, similar results were observed for the feed dispersion samples, both post-sonication and the bypass dispersion, with approximately 100% of the fluorescence detected compared to the unprocessed commercial Survanta[®] formulation.

A significant decrease in the fluorescence was observed for the Survanta-EEG spray dried powder sample compared to the commercial formulation; 42% of the fluorescence measured in the commercial Survanta[®] formulation was measured in the spray dried samples. Since the feed dispersion post-sonication and bypass feed dispersions were shown to maintain total primary amino acid values relative to Survanta[®], the observed decrease in relative absorbance is attributed to the spray drying process. In the spray dryer, the feed dispersions are nebulized to form micron-sized droplets, which is often associated with protein adsorption, partial unfolding and aggregation [187]. Protein adsorption to the air-liquid interface leads to increased occurrence of aggregation as interaction with hydrophobic residues is increased. Aggregation can lead to a change in the secondary structure of the proteins possibly resulting in decreased primary amino acids.

The fluorescamine assay provided a quick qualitative method for the determination of surfactant proteins following processes involved to produce spray dried powder. The use of bovine serum albumin (BSA) as a standard to generate a calibration curve with this assay would provide quantitative results for the total protein content. The use of BSA as a standard with fluorescamine has been described by Held [188]. It should also be noted that the spray dried Survanta-EEG powders did not contain leucine (as this would interfere with the fluorescence assay), and its

absence may have affected the spray drying process and offered less protection to the surfactant proteins present in the formulation.

Table 7.6 Fluorescence results for primary amino groups for three batches of spray dried Survanta-EEG formulations and feed dispersions, presented as percentages of the initial values obtained for the unprocessed Survanta[®] formulation. Values are mean (SD), n=3.

Batch	Survanta [®] absorbance	Fluorescence relative to Survanta [®] , %		
		Feed dispersion post-sonication	Bypass feed dispersion	Survanta-EEG (without leucine)
1	24385 (1574)	109.8 (6.8)	108.3 (5.8)	40.6 (2.2)
2	25194 (69)	100.2 (0.0)	102.2 (1.6)	43.9 (0.3)
3	24560 (247)	100.8 (1.1)	102.6 (6.4)	42.4 (1.4)
Overall mean	24713 (425)	103.6 (5.8)	104.4 (5.3)	42.3 (1.9)

7.3.4 Enzyme linked assay of surfactant proteins

For protein specific analysis of SP-B and SP-C, ELISA kits for bovine SP-B and SP-C were used for qualitative determination of the surfactant proteins in the spray drying feed dispersions and in the Survanta-EEG powder formulations. Samples were prepared in 60/40% v/v acetonitrile/water, then assayed per manufacturer protocol. The absorbance results were determined for all samples and the relative absorbance were calculated for the spray drying samples compared to the unprocessed commercial Survanta[®] formulation. The calculated relative absorbance values are shown in Table 7.7. Each of the samples (dispersion feed and powders) were found to quantitatively maintain the amount of surfactant proteins (SP-B and SP-C) throughout the spray drying process relative to the unprocessed commercial Survanta[®] formulation, with values in the range of 89-94% observed for SP-B and 82-91% for SP-C. The spray dried Survanta-EEG formulations had relative absorbance values for SP-B and SP-C of 92% and 91%,

respectively compared to the unprocessed commercial Survanta[®] formulation. This data together with the surface activity data presented in Chapter 3, supports the hypothesis that the Survanta-EEG formulations produced using a spray drying process retain their surfactant proteins during processing which helps maintain their surface activity and could offer a potential method of delivering lung surfactant replacement therapy as a powder formulation.

The quantitative results obtained for both SP-B and SP-C differ from the observations made with the non-specific assay for proteins, in which a decrease in total relative protein content was observed in the spray dried powder sample. The difference may possibly be due to sample preparation; spray dried powder samples for the fluorescamine assay were prepared in methanol, whereas spray dried powder samples for the ELISA assay were prepared in 60/40% v/v acetonitrile/water. Pérez-Gil et al. [18] determined that neither methanol nor methanol/water mixtures dissolved an estimable amount of SP-C (Figure 7.1). The poor solubility of SP-C in methanol would explain the less than 50% relative fluorescence observed as SP-C is present in the commercial Survanta[®] formulation at a higher concentration than SP-B [35, 163].

Table 7.7 Absorbance results of the spray dried Survanta-EEG formulation and feed dispersions relative to the commercial Survanta® formulation using ELISA kits for bovine SP-B and SP-C.

	Replicate	Absorbance relative to Survanta®, %		
		Feed dispersion post-sonication	Bypass feed dispersion	Survanta-EEG
SP-B	1	101.0	89.3	83.0
	2	91.2	92.1	96.7
	3	90.2	86.8	96.4
Overall mean (SD)		94.1 (6.0)	89.4 (2.7)	92.0 (7.8)
SP-C	1	86.1	90.0	95.6
	2	80.1	84.2	87.9
	3	80.6	84.2	89.1
Overall mean (SD)		82.2 (3.3)	86.1 (3.4)	90.9 (4.1)

7.4 Conclusion

This study explored different methods of protein separation and identification to determine the presence of the hydrophobic surfactant proteins in the commercial Survanta® formulation (Specific aim 2.4). The methods evaluated included protein precipitation using various solvents, column chromatography coupled to mass spectrometry, non-specific protein analysis using fluorescence and an enzyme-linked assay specific for the hydrophobic proteins. Protein precipitation methods followed by direct infusion into a mass spectrometer yielded inconclusive results. Column chromatography was successful in separating the components of the commercial Survanta® formulation, but identification of the protein proved difficult. However, the non-specific fluorescamine assay and the enzyme-linked assay were both able to determine the presence of the surfactant proteins in the commercial formulation. The determined methods were then applied to samples collected at different processing steps of Survanta-EEG preparation.

The fluorescamine assay and the enzyme-linked assay were both able to show the presence of the surfactant proteins following the processing methods involved in preparing Survanta-EEG formulations. Samples were prepared from the feed dispersions post-sonication, the bypass feed dispersion and the spray dried Survanta-EEG powder. The fluorescamine assay showed approximately 100% fluorescence for the dispersion samples relative to the commercial formulation, but lower fluorescence results for the spray dried powder sample relative to the commercial formulation, which is likely due to the solvent used during sample preparation. The enzyme-linked assay showed that the presence of both proteins was maintained above 80% for all Survanta-EEG formulation processing steps relative to the commercial formulation.

This study demonstrated that the presence of the hydrophobic surfactant proteins, SP-B and SP-C, are maintained following processing methods for Survanta-EEG formulation preparation suggesting that the EEG formulations remain active when administered to the lungs of infants.

CHAPTER 8

SUMMARY AND CONCLUSIONS

Immaturity-related respiratory distress results from pulmonary surfactant deficiency in underdeveloped lungs of preterm infants. Surfactant replacement therapy is approved for the prevention and treatment of neonatal respiratory distress syndrome (RDS) but employs invasive delivery techniques – instillation of a liquid bolus, resulting in non-uniform distribution of surfactant within the airways. The use of aerosolized surfactant coupled with non-invasive ventilation is a promising delivery technique for treating infants with RDS, but aerosolized surfactant has been met with challenges of poor delivery efficiency and long delivery times. The development of a dry powder surfactant formulation, using the excipient enhanced growth (EEG) application, administered via novel delivery devices and ventilation components, designed for minimal depositional losses, is hypothesized to provide improved lung delivery that will overcome the challenges of aerosolized surfactant therapy.

The first part of this project focused on developing methods to reproducibly produce micrometer sized spray dried powder surfactant formulations using the EEG technique which are highly dispersible and suitable for delivery using a dry powder inhaler with low device and capsule deposition losses. Given the high cost of commercially available naturally derived replacement surfactant formulations in the United States (\$400-800 per vial), the initial spray drying method development studies were performed with the dominant phospholipid present in pulmonary surfactant, dipalmitoylphosphatidylcholine (DPPC), as the model drug. A full factorial design of

experiments was performed to investigate the influence of spray drying process and formulation variables on the primary particle size, aerosol performance, and surface activity of a range of spray dried DPPC-EEG powders. The formulation factors included the percent solids concentration, the percentage of hygroscopic excipients, and the percent ethanol concentration in the feed dispersion. The spray drying process parameters studied were spray mesh size and inlet drying temperature. Preliminary experiments revealed that sodium chloride was a necessary component in the formulation as it enabled particle formation; and that stable feed dispersions for spray drying were required for homogenous powder production. The DOE revealed that DPPC-EEG powders were most influenced by the percent solids concentration in the feed dispersion, with the lower solids concentration (0.125 vs 0.250% w/v) resulting in smaller primary particle size, a higher primary particle fraction less than 1 μm , and improved aerosol performance with a smaller MMAD than powders produced at the higher solids concentration. The optimized formulation of the DPPC-EEG dry powders was characterized as having mean primary particle size of 1.03 μm with 48 % of particles less than 1 μm . Aerosol performance of this formulation was characterized by a mean MMAD of 1.6 μm which indicated good dispersion of the micrometer-sized primary particles for the DPPC-EEG formulation.

The optimal processing parameters determined with DPPC-EEG powders were applied to produce EEG formulations with commercial surfactants. The surfactants selected to study were naturally derived replacement surfactant formulations available in the United States: beractant (Survanta[®]), calfactant (Infasurf[®]), and poractant (Curosurf[®]). The formulations differ in the composition of proteins and lipids and consequently in their solids concentration, which was accounted for when preparing the EEG formulations. Overall, the commercial surfactant EEG formulations, which have a complex combination of lipids and proteins, were found to have a

larger primary particle size (1.2-1.8 μm), lower primary particle fraction less than 1 μm (24-39%), a larger span, and poorer aerosol performance (larger MMAD of 1.9-3.3 μm , lower particle fractions less than 1 μm of 0.5-7%) compared to that of the DPPC-EEG formulation. The commercial surfactant EEG formulations were, however, shown to maintain surfactant activity following feed dispersion preparation and spray drying, which indicated that the spray drying process did not appear to have a negative effect on the main therapeutic activity of the formulations. Optimization of a commercial surfactant-EEG formulation was then addressed in further studies.

The Survanta-EEG formulation was observed to be the most comparable to the DPPC-EEG formulation with respect to powder characteristics and aerosol performance and was therefore selected for further optimization. This study explored the effect of dispersion enhancers on the feed dispersion, powder characteristics and primary particle size distribution at different dispersion pressures. This study also investigated the influence of alcohol concentration in the feed dispersion on the aerosol performance of the spray dried powders using a novel dry powder inhaler in an attempt to improve the aerosol dispersion characteristics of the surfactant-EEG formulations.

Dispersions for spray drying were prepared by sonication of lipids in ethanol/water mixtures. This method is generally successful for small volumes of liposomes, but sonication conditions are difficult to reproduce resulting in size variations between batches produced at different times. Liposomes produced by sonication are also inherently unstable due to the high degree of curvature of the membranes that often spontaneously fuse to form larger vesicles when stored below their transition temperature. Therefore, it would be advantageous to explore the use of extrusion methods to produce liposomes with a more monodisperse size distribution in the final suspension prior to spray drying.

Of the two dry powder dispersion enhancers studied, leucine and trileucine, the powders prepared with leucine, at both 1.0 and 4.5 bar dispersion pressures, resulted in smaller primary particles, smaller spans, and higher fractions of submicrometer particles compared to powders prepared with trileucine at both ethanol concentrations studied (5 and 20% v/v ethanol in water). Aerosol performance of the EEG formulations prepared with leucine were evaluated at both ethanol concentrations with a novel low-volume dose containment unit dry powder inhaler. The powders prepared with 20% v/v ethanol in water were observed to produce more consistent emitted dose masses, size distributions, aerosol plume durations and obscuration parameters over three actuations that were less variable when compared to leucine powders prepared in 5% v/v ethanol in water. Effective powder delivery as an aerosol depends on a combination of both the drug formulation and the delivery device. The optimization of a novel dry powder inhaler (DPI) to deliver the surfactant-EEG formulations was investigated.

For applications of delivering drugs as aerosols to small rodent animal models and being suitable for delivery of aerosols to low birth weight infants, the inhaler design needs to disperse relatively high powder masses (3-10 mg) with very low volumes of dispersion air. Challenges to this design included 1) being restricted to a low dispersion air volume (~3 mL), and 2) a preference of delivering the dose in one actuation. The aim was to develop a device that was capable of delivering ≥ 2 mg/kg of lipids in one 3 mL actuation of air as this was the dose observed in small animal models that was required to elicit an effect [83]. For the surfactant-EEG formulation, this translates to approximately 2.2 mg of spray dried powder for a 300 g rodent.

The novel containment unit DPI developed in this study was based on design modifications to an active DPI prototype developed for use with 10 mL volumes of actuation air [141]. The design modification that was observed to have the largest impact on the emitted mass was reducing

the powder chamber volume from a size 0 capsule (0.68 mL) to a dose containment unit with a volume of 0.21 mL. With a 3 mg fill mass, the reduction in chamber volume resulted in a 100% increase in the emitted mass based on the nominal mass. Subsequent design modifications were then investigated to improve the aerosol dispersion, which included altering the entrainment air flow path through the device, increasing the number of air inlet holes (from one to three), and investigating the effects of the outlet delivery tube internal diameter on aerosol performance. Incremental increases in the % emitted mass were observed with changes to the entrainment air flow path and increasing the number of air inlet holes. Correlations were revealed when studying the effect of the delivery tube internal diameter – increasing internal diameter resulted in increasing % emitted mass and increasing Dv50 values.

The effect of delivery tube length and fill mass on the emitted mass and Dv50 values revealed an optimal device that was found to have powder dispersion characteristics independent of fill mass (3-10 mg) with good powder emptying in one actuation. At a 10 mg fill mass this lead design was able to deliver 5.3 mg of surfactant powder with an aerosol Dv50 of 2.7 μm in a single 3 mL actuation of dispersion air. The novel DPI developed in this study could be adapted for use in the treatment of infants on non-invasive ventilation. A low volume of air, as is used to disperse the powder formulations in the optimized containment unit DPI, is vital when dealing with preterm infants with tidal volumes as low as 4 mL/kg [81].

The dose containment unit dry powder inhaler developed in this research successfully dispersed spray dried surfactant-EEG formulations using a low volume of air. At the higher fill mass of 10 mg, however, a dense aerosol plume exited the DPI on the first actuation using 3 mL of dispersion air, which may cause unwanted deposition in small airways or narrow delivery tubing. The use of secondary flows, established by an inlet orifice smaller than the outlet orifice,

should be explored to decelerate the inlet airflow to improve deaggregation of the spray dried powders and possibly control the momentum cloud effect.

Surfactant therapy in infants has been observed to improve mucus hydration [189], suggesting its potential use in the treatment of lung diseases with airway mucus obstruction, such as viral bronchiolitis. With no cure, bronchiolitis treatment focuses on supportive care which includes delivery of supplemental oxygen via high flow nasal cannula therapy (HFNC). Ancillary delivery of nebulized surfactant during HFNC could potentially hasten resolution of symptoms.

A novel low-volume aerosol mixer-heater system designed to generate submicrometer EEG aerosols has the potential for use during HFNC administration [159]. Aerosol is generated by a commercial vibrating mesh nebulizer into the mixer-heater device, where it is mixed with room temperature ventilation gas and then heated to dry the aerosol to produce micrometer sized particles for inhalation with minimal deposition losses. The low-volume mixer-heater system was tested to determine the *in vitro* delivery efficiency with a realistic infant nose-throat model. Initial experiments were performed under steady state inhalation flow of 7 L/min to compare aerosol deposition and delivery efficiency with standard of care methods using an albuterol sulfate nebulizer formulation. The low-volume mixer-heater system was operated with a modified controller, which reduced the output of the nebulizer to approximately 25% of that observed with the commercial controller.

The estimated lung dose with the low-volume mixer-heater system was observed to be significantly higher than the face mask standard of care system (76 vs 14% of the nominal dose). The smaller droplets entering the *in vitro* model using the low-volume mixer-heater system compared to the face mask standard of care system, 1.4 μm vs the 5.0 μm , resulted in improved aerosol drug delivery efficiency through the realistic airway. When a realistic breathing profile

was incorporated, the estimated % lung dose for both systems decreased significantly (to 12% and 5.2% of the nominal dose for the mixer-heater and standard of care methods, respectively). In order to minimize drug losses and increase the estimated % lung dose, the use of aerosol synchronization with the low-volume mixer-heater system was explored to ensure that drug was only delivered to the airways during inhalation.

When optimized breath synchronization was used with the low-volume mixer heater, aerosol generated 0.4 s prior to inhalation with a nebulization duration of 0.2 s resulted in an estimated % lung dose of 35% of the nominal dose. Implementation of nebulization 0.4 s prior to inhalation is possible in the controlled laboratory environment with a breathing simulator, however it is not practical in a clinical environment as the breathing profile of infants with respiratory issues is erratic and nonuniform. These *in vitro* experiments however did clearly demonstrate that for this low-volume mixer heater, triggering the nebulizer 0.4 s prior to inhalation resulted in the highest estimated lung dose. These studies indicated that due to the residual volume of the low-volume mixer-heater, the timing of aerosol delivery relative to the inhalation cycle is of critical importance to ensure that the maximum dose of aerosol reaches the infant lung. Design modifications to the low volume mixer-heater were made to eliminate the need of breath synchronization.

The very low-volume mixer-heater was developed with an external heat source which allowed the mixer-heater volume to be reduced from 61.6 mL to 2.7 mL. The *in vitro* delivery of a nebulized surfactant-EEG formulation was studied with the modified device which now allowed aerosol delivery to be initiated at the start of each inhalation. Combinations of controller type (commercial, 50 V_{rms} ; modified, 14 V_{rms}) and nebulization duration (0.1 s, 0.3 s) were explored to determine the best settings to achieve an acceptable balance of phospholipid delivery rate and estimated % lung dose. The modified controller with 0.1 s nebulization duration was shown to

have the highest estimated % lung dose (52% of the nominal dose), but the slowest estimated delivery rate for phospholipids (6.3 $\mu\text{g}/\text{min}$). The commercial controller with 0.3 s nebulization duration was observed to have the highest delivery rate for phospholipids (28 $\mu\text{g}/\text{min}$), but the lowest estimated % lung dose (15% of the nominal dose). An acceptable compromise was the commercial controller with 0.1 s nebulization duration which had an estimated % lung dose of 31% of the nominal and an estimated phospholipid delivery rate of 19 $\mu\text{g}/\text{min}$, a significant improvement over the < 4% of the nominal dose using standard of care methods as reported in literature [103, 155]. Assuming 2 mg of phospholipids per kg of body weight elicits an effect, for an 8 kg infant, it would take 14 hours to deliver 16 mg of phospholipids which could be administered simultaneously with HFNC non-invasive ventilation. Considering that most children are hospitalized for 2 to 3 days when admitted for bronchiolitis, 14 hours to possibly hasten relief of symptoms may be an appropriate treatment option.

Finally, of importance for surfactant activity, the presence of the surfactant proteins (SP-B and SP-C) following formulation processing (which applies to feed dispersions for spray drying and nebulized formulations) and spray drying were determined using two methods: non-specific assay for primary amino acids and an enzyme-linked assay specific to SP-B and SP-C. Both assays were able to show the presence of proteins following processing methods involved with preparing Survanta-EEG formulations.

These studies using the Survanta-EEG powder formulations and nebulized formulations delivered using the newly developed aerosol generation devices indicate their viability as alternative non-invasive methods of surfactant delivery using the inhalation route to infants.

LIST OF REFERENCES

LIST OF REFERENCES

1. Cheng YS. Mechanisms of Pharmaceutical Aerosol Deposition in the Respiratory Tract. *AAPS PharmSciTech*. 2014; 15: 630–640.
2. Van Scott MR, Chandler J, Olmstead S, Brown JM, Mannie M. Airway Anatomy, Physiology, and Inflammation. In: *The Toxicant Induction of Irritant Asthma, Rhinitis, and Related Conditions*. Meggs WJ, editor. Boston, MA: Springer US; 2013. p. 19–61.
3. Brink DS, Lechner AJ. Development and Functional Anatomy of the Lungs and Airways. In: *Respiratory: An Integrated Approach to Disease*. Lechner AJ, Matuschak GM, Brink DS, editors. New York, NY: McGraw-Hill Education; 2015.
4. Hickey AJ, Thompson DC. Physiology of the Airways. *Pharmaceutical Inhalation Aerosol Technology* Taylor & Francis; 2003. p. 1–29.
5. Fahy JV, Dickey BF. Airway Mucus Function and Dysfunction. *New England Journal of Medicine*. 2010; 363: 2233–2247.
6. Rubin BK. Secretion properties, clearance, and therapy in airway disease. *Translational Respiratory Medicine*. 2014; 2: 6.
7. Banerjee R, Puniyani R. Exogenous Surfactant Therapy and Mucus Rheology in Chronic Obstructive Airway Diseases. *Journal of Biomaterials Applications*. 2000; 14: 243–272.
8. Dunsmore SE, Rannels DE. Extracellular matrix biology in the lung. *American Journal of Physiology-Lung Cellular and Molecular Physiology*. 1996; 270: L3–L27.
9. Smith LJ, McKay KO, van Asperen PP, Selvadurai H, Fitzgerald DA. Normal Development of the Lung and Premature Birth. *Paediatric Respiratory Reviews*. 2010; 11: 135–142.
10. El-Gendy N, Kaviratna A, Berkland C, Dhar P. Delivery and performance of surfactant replacement therapies to treat pulmonary disorders. *Therapeutic Delivery*. 2013; 4: 951–980.
11. Zuo YY, Veldhuizen RA, Neumann AW, Petersen NO, Possmayer F. Current perspectives in pulmonary surfactant — Inhibition, enhancement and evaluation. *Biochimica et Biophysica Acta (BBA) - Biomembranes*. 2008; 1778: 1947–1977.
12. Zhang H, Wang YE, Fan Q, Zuo YY. On the Low Surface Tension of Lung Surfactant. *Langmuir*. 2011; 27: 8351–8358.

13. Notter R. Lung Surfactants: Basic Science and Clinical Applications. Taylor & Francis; 2000.
14. Hislop A, Wigglesworth J, Desai R. Alveolar development in the human fetus and infant. *Early Human Development*. 1986; 13: 1–11.
15. Pérez-Gil J, Keough KM. Interfacial properties of surfactant proteins. *Biochimica et Biophysica Acta (BBA) - Molecular Basis of Disease*. 1998; 1408: 203–217.
16. Mozafari MR. Nanoliposomes: Preparation and Analysis. In: *Liposomes*. Weissig V, editor. Totowa, NJ: Humana Press; 2010. p. 29–50.
17. Gugliotti M, Politi M, Chaimovich H. A simple surface tension method for demonstrating the L β -L α transition in biological membranes. *Biochemical Education*. 1998; 26: 233–238.
18. Pérez-Gil J, Cruz A, Casals C. Solubility of hydrophobic surfactant proteins in organic solvent/water mixtures. Structural studies on SP-B and SP-C in aqueous organic solvents and lipids. *Biochimica et Biophysica Acta (BBA) - Lipids and Lipid Metabolism*. 1993; 1168: 261–270.
19. Chakraborty M, Kotecha S. Pulmonary surfactant in newborn infants and children. *Breathe*. 2013; 9: 476–488.
20. Schürch S, Qanbar R, Bachofen H, Possmayer F. The Surface-Associated Surfactant Reservoir in the Alveolar Lining. *Neonatology*. 1995; 67: 61–76.
21. Goerke J. Pulmonary surfactant: functions and molecular composition. *Biochimica et Biophysica Acta (BBA) - Molecular Basis of Disease*. 1998; 1408: 79–89.
22. Veldhuizen EJ, Haagsman HP. Role of pulmonary surfactant components in surface film formation and dynamics. *Biochimica et Biophysica Acta*. 2000; 1467: 255–270.
23. Hu G, Jiao B, Shi X, Valle RP, Fan Q, Zuo YY. Physicochemical Properties of Nanoparticles Regulate Translocation across Pulmonary Surfactant Monolayer and Formation of Lipoprotein Corona. *ACS Nano*. 2013; 7: 10525–10533.
24. Zimmermann L, Janssen D, Tibboel D, Hamvas A, Carnielli V. Surfactant Metabolism in the Neonate. *Neonatology*. 2005; 87: 296–307.
25. Robertson B, Halliday HL. Principles of surfactant replacement. *Biochimica et Biophysica Acta (BBA) - Molecular Basis of Disease*. 1998; 1408: 346–361.
26. Liu S, Zhao L, Manzanares D, Doherty-Kirby A, Zhang C, Possmayer F, Lajoie GA. Characterization of bovine surfactant proteins B and C by electrospray ionization mass spectrometry. *Rapid Communications in Mass Spectrometry*. 2008; 22: 197–203.
27. Seger N, Soll R. Animal derived surfactant extract for treatment of respiratory distress syndrome. Cochrane Neonatal Group, editor. *Cochrane Database of Systematic Reviews*. 2009.

28. Luchetti M, Casiraghi G, Valsecchi R, Galassini E, Marraro G. Porcine-derived surfactant treatment of severe bronchiolitis. *Acta Anaesthesiologica Scandinavica*. 1998; 42: 805–810.
29. Luchetti M, Ferrero F, Gallini C, Natale A, Pigna A, Tortorolo L, Marraro G. Multicenter, randomized, controlled study of porcine surfactant in severe respiratory syncytial virus-induced respiratory failure. *Pediatric Critical Care Medicine*. 2002; 3: 261–268.
30. Survanta® (beractant) [package insert]. AbbVie Inc., North Chicago, IL. 2012.
31. Infasurf® (calfactant) [package insert]. ONY, Inc., Amherst, NY. 2011.
32. Curosurf® (poractant alfa) [package insert]. Chiesi USA, Inc., Cary, NC. 2014.
33. Trembath A, Hornik CP, Clark R, Smith PB, Daniels J, Laughon M. Comparative Effectiveness of Surfactant Preparations in Premature Infants. *The Journal of Pediatrics*. 2013; 163: 955-960.e1.
34. Singh N, Halliday HL, Stevens TP, Suresh G, Soll R, Rojas-Reyes MX. Comparison of animal-derived surfactants for the prevention and treatment of respiratory distress syndrome in preterm infants. Cochrane Neonatal Group, editor. *Cochrane Database of Systematic Reviews*. 2015.
35. Logan JW, Moya FR. Animal-derived surfactants for the treatment and prevention of neonatal respiratory distress syndrome: summary of clinical trials. *Therapeutic Clinical Risk Management*. 2009; 5: 251–260.
36. March of Dimes, The Partnership for Maternal, Newborn & Child Health (PMNCH), Mary Kinney, World Health Organization (WHO). Born Too Soon: The Global Action Report on Preterm Birth. Howson C, Kinney M, Lawn J, editors. Geneva: World Health Organization; 2012.
37. Nkadi PO, Merritt TA, Pillers D-AM. An overview of pulmonary surfactant in the neonate: Genetics, metabolism, and the role of surfactant in health and disease. *Molecular Genetics and Metabolism*. 2009; 97: 95–101.
38. Ma CC-H, Ma S. The Role of Surfactant in Respiratory Distress Syndrome. *Open Respiratory Medicine Journal*. 2012; 6: 44–53.
39. Suresh GK, Soll RF. Overview of Surfactant Replacement Trials. *Journal of Perinatology*. 2005; 25: S40–S44.
40. Liechty EA, Donovan E, Purohit D, Gilhooly J, Feldman B, Noguchi A, Denson SE, Sehgal SS, Gross I, Stevens D, Ikegami M, Zachman RD, Carrier ST, Gunkel JH, Gold AJ. Reduction of Neonatal Mortality after Multiple Doses of Bovine Surfactant in Low Birth Weight Neonates with Respiratory Distress Syndrome. *Pediatrics*. 1991; 88: 19–28.
41. Walsh BK, Daigle B, DiBlasi RM, Restrepo RD. AARC Clinical Practice Guideline. Surfactant Replacement Therapy: 2013. *Respiratory Care*. 2013; 58: 367–375.

42. Committee On Fetus and Newborn. Respiratory Support in Preterm Infants at Birth. *Pediatrics*. 2014; 133: 171–174.
43. O'Donnell CP, Kamlin COF, Davis PG, Morley CJ. Endotracheal Intubation Attempts During Neonatal Resuscitation: Success Rates, Duration, and Adverse Effects. *Pediatrics*. 2006; 117: e16–e21.
44. Maheshwari R, Tracy M, Badawi N, Hinder M. Neonatal endotracheal intubation: How to make it more baby friendly: Neonatal endotracheal intubation. *Journal of Paediatrics and Child Health*. 2016; 52: 480–486.
45. Walsh BK, Vehse N. Pediatric Airway Disorders and Parenchymal Lung Diseases. *Perinatal and Pediatric Respiratory Care*. Third. St. Louis, Missouri: Saunders Elsevier; 2010. p. 554–581.
46. Meissner HC. Viral Bronchiolitis in Children. Ingelfinger JR, editor. *New England Journal of Medicine*. 2016; 374: 62–72.
47. Breary S, Smyth R. Pathogenesis of RSV in Children. In: *Respiratory Syncytial Virus*. Cane P, editor. Amsterdam, The Netherlands: Elsevier B.V.; 2007. p. 141–162.
48. Garzon LS, Wiles L. Management of Respiratory Syncytial Virus with Lower Respiratory Tract Infection in Infants and Children. *AACN Clinical Issues*. 2002; 13: 421–430.
49. Ralston SL, Lieberthal AS, Meissner HC, Alverson BK, Baley JE, Gadomski AM, Johnson DW, Light MJ, Maraqa NF, Mendonca EA, Phelan KJ, Zorc JJ, Stanko-Lopp D, Brown MA, Nathanson I, Rosenblum E, Sayles S, Hernandez-Cancio S. Clinical Practice Guideline: The Diagnosis, Management, and Prevention of Bronchiolitis. *Pediatrics*. 2014; 134: e1474–e1502.
50. Panitch HB. Respiratory syncytial virus bronchiolitis: supportive care and therapies designed to overcome airway obstruction: *The Pediatric Infectious Disease Journal*. 2003; 22: S83–S88.
51. Virazole® (Ribavirin for Inhalation Solution, USP) [package insert]. Valeant Pharmaceuticals North America, LLC, Bridgewater, NJ. 2016.
52. Doctor TN, Foster JP, Stewart A, Tan K, Todd DA, McGrory L. Heated and humidified inspired gas through heated humidifiers in comparison to non-heated and non-humidified gas in hospitalised neonates receiving respiratory support. Cochrane Neonatal Group, editor. *Cochrane Database of Systematic Reviews*. 2017.
53. Beggs S, Wong ZH, Kaul S, Ogden KJ, Walters JA. High-flow nasal cannula therapy for infants with bronchiolitis. Cochrane Acute Respiratory Infections Group, editor. *Cochrane Database of Systematic Reviews*. 2014.
54. Narasimhan R, Krishnamurthy S. A review of non-invasive ventilation support in neonates. *Paediatrics and Child Health*. 2014; 24: 7–11.

55. Mahmoud RA, Roehr CC, Schmalisch G. Current methods of non-invasive ventilatory support for neonates. *Paediatric Respiratory Reviews*. 2011; 12: 196–205.
56. Davis PG, Morley CJ, Owen LS. Non-invasive respiratory support of preterm neonates with respiratory distress: Continuous positive airway pressure and nasal intermittent positive pressure ventilation. *Seminars in Fetal and Neonatal Medicine*. 2009; 14: 14–20.
57. Manley BJ, Owen LS. High-flow nasal cannula: Mechanisms, evidence and recommendations. *Seminars in Fetal and Neonatal Medicine*. 2016; 21: 139–145.
58. Hess DR. Noninvasive Ventilation for Acute Respiratory Failure. *Respiratory Care*. 2013; 58: 950–972.
59. Frey B, Shann F. Oxygen administration in infants. *Archives of Disease in Childhood - Fetal and Neonatal Edition*. 2003; 88: F84–F88.
60. Manley BJ, Owen LS, Doyle LW, Davis PG. High-flow nasal cannulae and nasal continuous positive airway pressure use in non-tertiary special care nurseries in Australia and New Zealand. *Journal of Paediatrics and Child Health*. 2012; 48: 16–21.
61. Dysart K, Miller TL, Wolfson MR, Shaffer TH. Research in high flow therapy: Mechanisms of action. *Respiratory Medicine*. 2009; 103: 1400–1405.
62. Osman M, Elsharkawy A, Abdel-Hady H. Assessment of pain during application of nasal-continuous positive airway pressure and heated, humidified high-flow nasal cannulae in preterm infants. *Journal of Perinatology*. 2015; 35: 263–267.
63. Owen LS, Manley BJ. Nasal intermittent positive pressure ventilation in preterm infants: Equipment, evidence, and synchronization. *Seminars in Fetal and Neonatal Medicine*. 2016; 21: 146–153.
64. Bollen CW, Uiterwaal CSPM, van Vught AJ. Cumulative Metaanalysis of High-frequency Versus Conventional Ventilation in Premature Neonates. *American Journal of Respiratory and Critical Care Medicine*. 2003; 168: 1150–1155.
65. DiBlasi RM. Nasal Continuous Positive Airway Pressure (CPAP) for the Respiratory Care of the Newborn Infant. *Respiratory Care*. 2009; 54: 27.
66. Morley CJ, Davis PG, Doyle LW, Brion LP, Hascoet J-M, carlin JB. Nasal CPAP or Intubation at Birth for Very Preterm Infants. *New England Journal of Medicine*. 2008; 358: 700–708.
67. Narendran V, Donovan EF, Hoath SB, Akinbi HT, Steichen JJ, Jobe AH. Early Bubble CPAP and Outcomes in ELBW Preterm Infants. *Journal of Perinatology*. 2003; 23: 195–199.
68. Rojas MA, Lozano JM, Rojas-Reyes MX, Laughon M, Bose CL, Rondon MA, Charry L, Bastidas JA, Perez LA, Rojas C, Ovalle O, Celis LA, Garcia-Harker J, Jaramillo ML, for the Colombian Neonatal Research Network. Very Early Surfactant Without Mandatory

- Ventilation in Premature Infants Treated with Early Continuous Positive Airway Pressure: A Randomized, Controlled Trial. *Pediatrics*. 2009; 123: 137–142.
69. Wilkinson D, Andersen C, O'Donnell CP, De Paoli AG, Manley BJ. High flow nasal cannula for respiratory support in preterm infants. Cochrane Neonatal Group, editor. *Cochrane Database of Systematic Reviews*. 2016.
 70. Sreenan C, Lemke RP, Hudson-Mason A, Osioviich H. High-Flow Nasal Cannulae in the Management of Apnea of Prematurity: A Comparison with Conventional Nasal Continuous Positive Airway Pressure. *Pediatrics*. 2001; 107: 1081–1083.
 71. Finer NN. Nasal Cannula Use in the Preterm Infant: Oxygen or Pressure? *Pediatrics*. 2005; 116: 1216–1217.
 72. Newman S, Anderson P. Respiratory Drug Delivery: Essential Theory and Practice. Respiratory Drug Delivery Online; 2009.
 73. Cole CH. special Problems in Aerosol Delivery: Neonatal and Pediatric Considerations. *Respiratory Care*. 2000; 45: 6.
 74. Willson DF. Aerosolized Surfactants, Anti-Inflammatory Drugs, and Analgesics. *Respiratory Care*. 2015; 60: 774–793.
 75. Longest PW, Hindle M. Numerical Model to Characterize the Size Increase of Combination Drug and Hygroscopic Excipient Nanoparticle Aerosols. *Aerosol Science and Technology*. 2011; 45: 884–899.
 76. Son Y-J, Longest PW, Hindle M. Aerosolization characteristics of dry powder inhaler formulations for the excipient enhanced growth (EEG) application: Effect of spray drying process conditions on aerosol performance. *International Journal of Pharmaceutics*. 2013; 443: 137–145.
 77. Golshahi L, Tian G, Azimi M, Son Y-J, Walenga R, Longest PW, Hindle M. The Use of Condensational Growth Methods for Efficient Drug Delivery to the Lungs during Noninvasive Ventilation High Flow Therapy. *Pharmaceutical Research*. 2013; 30: 2917–2930.
 78. Ari A, Fink JB. Aerosol therapy in children: challenges and solutions. *Expert Review of Respiratory Medicine*. 2013; 7: 665–672.
 79. DiBlasi RM. Clinical Controversies in Aerosol Therapy for Infants and Children. *Respiratory Care*. 2015; 60: 894–916.
 80. Everard ML. Inhaler Devices in Infants and Children: Challenges and Solutions. *Journal of Aerosol Medicine*. 2004; 17: 186–195.

81. Walsh BK, DiBlasi RM. Mechanical Ventilation of the Neonate and Pediatric Patient. *Perinatal and Pediatric Respiratory Care* Third. St. Louis, Missouri: Saunders Elsevier; 2010. p. 325–347.
82. Rodenstein D, Perlmutter N, Stanescu D. Infants are not obligatory nasal breathers. *Pediatric Pulmonology*. 1985; 1: 230–230.
83. Lewis JF, Ikegami M, Jobe AH, Tabor B. Aerosolized surfactant treatment of preterm lambs. *Journal of Applied Physiology*. 1991; 70: 869–876.
84. Dijk P, Heikamp A, Oetomo SB. Surfactant nebulisation: lung function, surfactant distribution and pulmonary blood flow distribution in lung lavaged rabbits. *Intensive Care Medicine*. 1997; 23: 1070–1076.
85. Berggren E, Liljedahl M, Winbladh B, Andreasson B, Curstedt T, Robertson B, Schollin J. Pilot study of nebulized surfactant therapy for neonatal respiratory distress syndrome. *Acta Paediatrica*. 2000; 89: 460–464.
86. Jorch G, Hartl H, Roth B, Kribs A, Gortner L, Schaible T, Hennecke KH, Poets C. To the editor: Surfactant aerosol treatment of respiratory distress syndrome in spontaneously breathing premature infants. *Pediatric Pulmonology*. 1997; 24: 222–224.
87. Finer NN, Merritt TA, Bernstein G, Job L, Mazela J, Segal R. An Open Label, Pilot Study of Aerosurf® Combined with nCPAP to Prevent RDS in Preterm Neonates. *Journal of Aerosol Medicine and Pulmonary Drug Delivery*. 2010; 23: 303–309.
88. Ruppert C, Kuchenbuch T, Boensch M, Schmidt S, Mathes U, Hillebrand V, Henneke I, Markart P, Reiss I, Schermuly RT, Seeger W, Günther A. Dry powder aerosolization of a recombinant surfactant protein-C–based surfactant for inhalative treatment of the acutely inflamed lung. *Critical Care Medicine*. 2010; 38: 1584–1591.
89. Pohlmann G, Iwatschenko P, Koch W, Windt H, Rast M, de Abreu MG, Taut F, De Muynck C. A Novel Continuous Powder Aerosolizer (CPA) for Inhalative Administration of Highly Concentrated Recombinant Surfactant Protein-C (rSP-C) Surfactant to Preterm Neonates. *Journal of Aerosol Medicine and Pulmonary Drug Delivery*. 2013; 26: 370–379.
90. Ellyett K, Broadbent RS, Fawcett E, Campbell A. Surfactant Aerosol Treatment of Respiratory Distress Syndrome in the Spontaneously Breathing Premature Rabbit. *Pediatric Research*. 1996; 39: 953–957.
91. Lin Y-W, Wong J, Qu L, Chan H-K, Zhou Q. Powder Production and Particle Engineering for Dry Powder Inhaler Formulations. *Current Pharmaceutical Design*. 2015; 21: 3902–3916.
92. Telko MJ, Hickey AJ. Dry Powder Inhaler Formulation. *Respiratory Care*. 2005; 50: 19.
93. Chow AHL, Tong HHY, Chattopadhyay P, Shekunov BY. Particle Engineering for Pulmonary Drug Delivery. *Pharmaceutical Research*. 2007; 24: 411–437.

94. Arpagaus C, John P, Collenberg A, Rütli D. Nanocapsules formation by nano spray drying. In: *Nanoencapsulation Technologies for the Food and Nutraceutical Industries*. 1st ed. Jafari SM, editor. Academic Press; 2017. p. 346–401.
95. Vehring R. Pharmaceutical Particle Engineering via Spray Drying. *Pharmaceutical Research*. 2008; 25: 999–1022.
96. Nano Spray Dryer B-90 HP (Operation Manual). BUCHI Labortechnik AG, Flawil, Switzerland. 2017.
97. Lee SH, Heng D, Ng WK, Chan H-K, Tan RBH. Nano spray drying: A novel method for preparing protein nanoparticles for protein therapy. *International Journal of Pharmaceutics*. 2011; 403: 192–200.
98. Weers JG, Tarara TE, Dellamary LA, Riess JG, Schutt EG. Phospholipid-based powders for drug delivery. [Patent]. 2014.
99. Hancock BC, Zografi G. The Relationship between the Glass-Transition Temperature and the Water-Content of Amorphous Pharmaceutical Solids. *Pharmaceutical Research*. 1994; 11: 471–477.
100. Erickson B, DiMaggio SC, Mullen DG, Kelly CV, Leroueil PR, Berry SA, Baker JR, Orr BG, Banaszak Holl MM. Interactions of Poly(amidoamine) Dendrimers with Survanta Lung Surfactant: The Importance of Lipid Domains. *Langmuir*. 2008; 24: 11003–11008.
101. Taurozzi J, Hackley V, Wiesner M. Preparation of Nanoparticle Dispersions from Powdered Material Using Ultrasonic Disruption - Version 1.1. National Institute of Standards and Technology. 2012.
102. Lewis J, Tabor B, Ikegami M, Jobe AH, Joseph M, Absolom D. Lung function and surfactant distribution in saline-lavaged sheep given instilled vs. nebulized surfactant. *Journal of Applied Physiology*. 1993; 74: 1256–1264.
103. Fok TF, Monkman S, Dolovich M, Gray S, Coates G, Paes B, Rashid F, Newhouse M, Kirpalani H. Efficiency of aerosol medication delivery from a metered dose inhaler versus jet nebulizer in infants with bronchopulmonary dysplasia. *Pediatric Pulmonology*. 1996; 21: 301–309.
104. Fink JB. Aerosol Delivery to Ventilated Infant and Pediatric Patients. *Respiratory Care*. 2004; 49: 13.
105. Kramek-Romanowska K, Sosnowski TR. Application of maximum bubble pressure tensiometry in the studies of pulmonary surfactant activity. *Inzynieria I Aparatura Chemiczna*. 2014; 53: 263–264.
106. Rowe RC, Sheskey PJ, Cook WG, Fenton ME, editors. Mannitol. *Handbook of Pharmaceutical Excipients*. 7th ed. London: Pharmaceutical Press; 2012.

107. Daviskas E, Anderson S, Brannan J, Chan H-K, Eberl S, Bautovich G. Inhalation of dry-powder mannitol increases mucociliary clearance. *European Respiratory Journal*. 1997; 10: 2449–2454.
108. Eastoe J, Dalton JS. Dynamic surface tension and adsorption mechanisms of surfactants at the air–water interface. *Advances in Colloid and Interface Science*. 2000; 85: 103–144.
109. Dynarowicz-Łątka P, Dhanabalan A, Oliveira ON. Modern physicochemical research on Langmuir monolayers. *Advances in Colloid and Interface Science*. 2001; 91: 221–293.
110. Depreter F, Pilcer G, Amighi K. Inhaled proteins: Challenges and perspectives. *International Journal of Pharmaceutics*. 2013; 447: 251–280.
111. Wingfield PT. Protein Precipitation Using Ammonium Sulfate. *Current Protocols in Protein Science*. 2001; APPENDIX 3: Appendix-3F.
112. Duong-Ly KC, Gabelli SB. Salting out of Proteins Using Ammonium Sulfate Precipitation. *Methods in Enzymology*. Elsevier; 2014. p. 85–94.
113. Rodriguez-Vico F, Marlinez-Cayuela M, Zafra MF, Garc E, Ramirez H. A Procedure for the Simultaneous Determination of Lipid and Protein in Biomembranes and Other Biological Samples. *Lipids*. 1991; 26: 77–80.
114. Ferraz TP., Fiúza M., dos Santos ML., Pontes de Carvalho L, Soares N. Comparison of six methods for the extraction of lipids from serum in terms of effectiveness and protein preservation. *Journal of Biochemical and Biophysical Methods*. 2004; 58: 187–193.
115. Reis A, Rudnitskaya A, Blackburn GJ, Fauzi NM, Pitt AR, Spickett CM. A comparison of five lipid extraction solvent systems for lipidomic studies of human LDL. *Journal of Lipid Research*. 2013; 54: 1812–1824.
116. Mohsen-Nia M, Amiri H, Jazi B. Dielectric Constants of Water, Methanol, Ethanol, Butanol and Acetone: Measurement and Computational Study. *Journal of Solution Chemistry*. 2010; 39: 701–708.
117. Koontz L. TCA Precipitation. In: *Methods in Enzymology*. Elsevier; 2014. p. 3–10.
118. Zellner M, Winkler W, Hayden H, Diestinger M, Eliassen M, Gesslbauer B, Miller I, Chang M, Kungl A, Roth E, Oehler R. Quantitative validation of different protein precipitation methods in proteome analysis of blood platelets. *Electrophoresis*. 2005; 26: 2481–2489.
119. Curstedt T, Jornvall H, Robertson B, Bergman T, Berggren P. Two hydrophobic low-molecular-mass protein fractions of pulmonary surfactant. Characterization and biophysical activity. *European Journal of Biochemistry*. 1987; 168: 255–262.
120. Arnold T, Linke D. The Use of Detergents to Purify Membrane Proteins. *Current Protocols in Protein Science*. 2008; 53: 4.8.1-4.8.30.

121. Loo RRO, Dales N, Andrews PC. Surfactant effects on protein structure examined by electrospray ionization mass spectrometry. *Protein Science*. 1994; 3: 1975–1983.
122. Kramer HJ, Schmidt R, Gunther A, Becker G, Suzuki Y, Seeger W. ELISA Technique for Quantification of Surfactant Protein B (SP-B) in Bronchoalveolar Lavage Fluid. *American Journal of Respiratory and Critical Care Medicine*. 1995; 152: 1540–1544.
123. Zeta potential - An introduction in 30 minutes [technical note]. Malvern Instruments Ltd, Worcestershire, UK. 2017.
124. Sirsi S, Pae C, Taek Oh DK, Blomback H, Koubaa A, Papahadjopoulos-Sternberg B, Borden M. Lung surfactant microbubbles. *Soft Matter*. 2009; 5: 4835.
125. Morley CJ, Miller N, Bangham AD, Davis JA. Dry Artificial Lung Surfactant and its Effects on Very Preterm Babies. *The Lancet*. 1981; 317: 64–68.
126. Milner AD, Vyas H, Hopkin IE. Effects of artificial surfactant on lung function and blood gases in idiopathic respiratory distress syndrome. *Archives of Disease in Childhood*. 1983; 58: 458–460.
127. Sosnowski TR, Gradoń L. Modification of inhalable powders by pulmonary surfactant components adsorbed on droplets during spray-drying process. *Colloids and Surfaces A: Physicochemical and Engineering Aspects*. 2010; 365: 56–61.
128. Meenach SA, Vogt FG, Anderson KW, Hilt JZ, McGarry RC, Mansour HM. Design, physicochemical characterization, and optimization of organic solution advanced spray-dried inhalable dipalmitoylphosphatidylcholine (DPPC) and dipalmitoylphosphatidylethanolamine poly(ethylene glycol) (DPPE-PEG) microparticles and nanoparticles for targeted respiratory nanomedicine delivery as dry powder inhalation aerosols. *International Journal of Nanomedicine*. 2013; 8: 275–293.
129. Bosquillon C, Rouxhet PG, Ahimou F, Simon D, Culot C, Pr at V, Vanbever R. Aerosolization properties, surface composition and physical state of spray-dried protein powders. *Journal of Controlled Release*. 2004; 99: 357–367.
130. Bosquillon C, Pr at V, Vanbever R. Pulmonary delivery of growth hormone using dry powders and visualization of its local fate in rats. *Journal of Controlled Release*. 2004; 96: 233–244.
131. Vanbever R, Mintzes JD, Wang J, Nice J, Chen D, Batycky R, Langer R, Edwards DA. Formulation and Physical Characterization of Large Porous Particles for Inhalation. *Pharmaceutical Research*. 1999; 16: 1735–1742.
132. Li D, Zhao R. Development and validation of an LC-MS/MS method for quantification of dipalmitoylphosphatidylcholine as a promising biomarker for renal failure in urine. *Journal of Chinese Pharmaceutical Sciences*. 2015; 24.

133. Kramek-Romanowska K, Odziomek M, Sosnowski TR. Dynamic tensiometry studies on interactions of novel therapeutic inhalable powders with model pulmonary surfactant at the air–water interface. *Colloids and Surfaces A: Physicochemical and Engineering Aspects*. 2015; 480: 149–158.
134. Hancock BC, Shamblin SL. Water vapour sorption by pharmaceutical sugars. *Pharmaceutical Science & Technology Today*. 1998; 1: 345–351.
135. Kim SH, Franses EI. New protocols for preparing dipalmitoylphosphatidylcholine dispersions and controlling surface tension and competitive adsorption with albumin at the air/aqueous interface. *Colloids and Surfaces B: Biointerfaces*. 2005; 43: 256–266.
136. Wen X, Franses EI. Role of Subsurface Particulates on the Dynamic Adsorption of Dipalmitoylphosphatidylcholine at the Air/Water Interface. *Langmuir*. 2001; 17: 3194–3201.
137. Wan LSC, Poon PKC. Effect of salts on the surface/interfacial tension and critical micelle concentration of surfactants. *Journal of Pharmaceutical Sciences*. 1969; 58: 1562–1567.
138. Lechuga-Ballesteros D, Charan C, Stults CL, Stevenson CL, Miller DP, Vehring R, Tep V, Kuo M. Trileucine Improves Aerosol Performance and Stability of Spray-Dried Powders for Inhalation. *Journal of Pharmaceutical Sciences*. 2008; 97: 287–302.
139. Boraey MA, Hoe S, Sharif H, Miller DP, Lechuga-Ballesteros D, Vehring R. Improvement of the dispersibility of spray-dried budesonide powders using leucine in an ethanol–water cosolvent system. *Powder Technology*. 2013; 236: 171–178.
140. Li X, Anton N, Arpagaus C, Belleiteix F, Vandamme TF. Nanoparticles by spray drying using innovative new technology: The Büchi Nano Spray Dryer B-90. *Journal of Controlled Release*. 2010; 147: 304–310.
141. Farkas DR, Hindle M, Longest PW. Development of an Inline Dry Powder Inhaler that Requires Low Air Volume. Advance online publication. doi: 10.1089/jamp.2017.1424. *Journal of Aerosol Medicine and Pulmonary Drug Delivery*. 2018.
142. Ly HV, Longo ML. The Influence of Short-Chain Alcohols on Interfacial Tension, Mechanical Properties, Area/Molecule, and Permeability of Fluid Lipid Bilayers. *Biophysical Journal*. 2004; 87: 1013–1033.
143. Kuo M-C, Lechuga-Ballesteros D. Dry Powder Compositions Having Improved Dispersivity. [Patent]. 2003.
144. Laube BL, Sharpless G, Shermer C, Sullivan V, Powell K. Deposition of Dry Powder Generated by Solvent in Sophia Anatomical Infant Nose-Throat (SAINT) Model. *Aerosol Science and Technology*. 2012; 46: 514–520.
145. Longest PW, Golshahi L, Behara SRB, Tian G, Farkas DR, Hindle M. Efficient Nose-to-Lung (N2L) Aerosol Delivery with a Dry Powder Inhaler. *Journal of Aerosol Medicine and Pulmonary Drug Delivery*. 2015; 28: 189–201.

146. Grainger CI, Alcock R, Gard TG, Quirk AV, van Amerongen G, de Swart RL, Hardy JG. Administration of an insulin powder to the lungs of cynomolgus monkeys using a Penn Century insufflator. *International Journal of Pharmaceutics*. 2004; 269: 523–527.
147. Mitzner W, Brown R, Lee W. In vivo measurement of lung volumes in mice. *Physiological Genomics*. 2001; 4: 215–221.
148. Fairchild GA. Measurement of Respiratory Volume for Virus Retention Studies in Mice. *Applied Microbiology*. 1972; 24: 812–818.
149. Strohl KP, Thomas AJ, St. Jean P, Schlenker EH, Koletsky RJ, Schork NJ. Ventilation and metabolism among rat strains. *Journal of Applied Physiology*. 1997; 82: 317–323.
150. Hoppentocht M, Hoste C, Hagedoorn P, Frijlink HW, de Boer AH. In vitro evaluation of the DP-4M PennCentury™ insufflator. *European Journal of Pharmaceutics and Biopharmaceutics*. 2014; 88: 153–159.
151. Cryan S-A, Sivadas N, Garcia-Contreras L. In vivo animal models for drug delivery across the lung mucosal barrier. *Advanced Drug Delivery Reviews*. 2007; 59: 1133–1151.
152. Farkas D, Hindle M, Longest PW. Application of an inline dry powder inhaler to deliver high dose pharmaceutical aerosols during low flow nasal cannula therapy. *International Journal of Pharmaceutics*. 2018; 546: 1–9.
153. McKiernan C, Chua LC, Visintainer PF, Allen H. High Flow Nasal Cannulae Therapy in Infants with Bronchiolitis. *The Journal of Pediatrics*. 2010; 156: 634–638.
154. Gadomski AM, Scribani MB. Bronchodilators for bronchiolitis. Cochrane Neonatal Group, editor. *Cochrane Database of Systematic Reviews*. 2014.
155. Chua H, Collis G, Newbury A, Chan K, Bower G, Sly P, Le Souef P. The influence of age on aerosol deposition in children with cystic fibrosis. *European Respiratory Journal*. 1994; 7: 2185–2191.
156. El Taoum KK, Xi J, Kim J, Berlinski A. In Vitro Evaluation of Aerosols Delivered via the Nasal Route. *Respiratory Care*. 2015; 60: 1015–1025.
157. Longest PW, Walenga RL, Son Y-J, Hindle M. High-Efficiency Generation and Delivery of Aerosols Through Nasal Cannula During Noninvasive Ventilation. *Journal of Aerosol Medicine and Pulmonary Drug Delivery*. 2013; 26: 266–279.
158. Golshahi L, Longest PW, Azimi M, Syed A, Hindle M. Intermittent Aerosol Delivery to the Lungs During High-Flow Nasal Cannula Therapy. *Respiratory Care*. 2014; 59: 1476–1486.
159. Spence B, Longest PW, Wei X, Dhapare S, Hindle M. Development of a High Flow Nasal Cannula (HFNC) and Pharmaceutical Aerosol Combination Device. Manuscript submitted for publication. *Journal of Aerosol Medicine and Pulmonary Drug Delivery*. 2018.

160. Dhapare S, Boc S, Spence B, Bass K, Longest PW, Hindle M. Breath-synchronized Delivery of Aerosols to Infants. Manuscript in preparation. 2018.
161. Holbrook L, Hindle M, Longest PW. Generating charged pharmaceutical aerosols intended to improve targeted drug delivery in ventilated infants. *Journal of Aerosol Science*. 2015; 88: 35–47.
162. Chang L (Lucy), Pikal MJ. Mechanisms of protein stabilization in the solid state. *Journal of Pharmaceutical Sciences*. 2009; 98: 2886–2908.
163. Bernhard W, Mottaghian J, Gebert A, Rau GA, von der HARDT H, Poets CF. Commercial versus Native Surfactants: Surface Activity, Molecular Components, and the Effect of Calcium. *American Journal of Respiratory and Critical Care Medicine*. 2000; 162: 1524–1533.
164. Walti H, Couchard M, Relier J-P. Exogenous Surfactant in the Management of Hyaline Membrane Disease. In: *Pulmonary Surfactant: Biochemical, Functional, Regulatory, and Clinical Concepts*. Bourbon JR, editor. CRC Press, Inc.; 1991. p. 385–429.
165. Minocchieri S, Knoch S, Schoel WM, Ochs M, Nelle M. Nebulizing poractant alfa versus conventional instillation: Ultrastructural appearance and preservation of surface activity: Nebulized Surfactant Characterization. *Pediatric Pulmonology*. 2014; 49: 348–356.
166. Wessel D, Flügge UI. A method for the quantitative recovery of protein in dilute solution in the presence of detergents and lipids. *Analytical Biochemistry*. 1984; 138: 141–143.
167. Acetone precipitation of proteins (Tech Tip #49). Pierce Biotechnology Inc., Waltham, MA. 2009.
168. Nejadi N, Masti SM, Tavirani MR. Comparison of three routine protein precipitation methods: acetone, TCA/acetone wash and TCA/acetone. *Journal of Pharmaceutical Sciences*. 2014; 5: 58–60.
169. Bjellqvist B, Hughes GJ, Pasquali C, Paquet N, Ravier F, Sanchez J-C, Frutiger S, Hochstrasser D. The focusing positions of polypeptides in immobilized pH gradients can be predicted from their amino acid sequences. *Electrophoresis*. 1993; 14: 1023–1031.
170. Bjellqvist B, Basse B, Olsen E, Celis JE. Reference points for comparisons of two-dimensional maps of proteins from different human cell types defined in a pH scale where isoelectric points correlate with polypeptide compositions. *Electrophoresis*. 1994; 15: 529–539.
171. Gasteiger E, Hoogland C, Gattiker A, Duvaud S, Wilkins MR, Appel RD, Bairoch A. Protein Identification and Analysis Tools on the ExPASy Server. In: *The Proteomics Protocols Handbook*. Walker JM, editor. Totowa, NJ: Humana Press; 2005. p. 571–607.
172. Kyte J, Doolittle RF. A simple method for displaying the hydropathic character of a protein. *Journal of Molecular Biology*. 1982; 157: 105–132.

173. Fuchs S. Gravy Calculator [Internet]. 2011. Available from: <http://www.gravy-calculator.de/index.php>.
174. Harayama T, Shindou H, Kita Y, Otsubo E, Ikeda K, Chida S, Weaver TE, Shimizu T. Establishment of LC-MS methods for the analysis of palmitoylated surfactant proteins. *Journal of Lipid Research*. 2015; 56: 1370–1379.
175. Gustafsson M, Curstedt T, Jornvall H. Reverse-phase HPLC of the hydrophobic pulmonary surfactant proteins: detection of a surfactant protein C isoform containing Ne-palmitoyllysine. *Biochemical Journal*. 1997; 326: 799–806.
176. Böhlen P, Stein S, Dairman W, Udenfriend S. Fluorometric assay of proteins in the nanogram range. *Archives of Biochemistry and Biophysics*. 1973; 155: 213–220.
177. Johansson J, Curstedt T, Jornvall H. Surfactant Protein B: Disulfide Bridges, Structural Properties, and Kringle Similarities. *Biochemistry*. 1991; 30: 6971–6921.
178. Mass Changes [Internet]. Sigma-Aldrich [cited 2018 Jul 1]. Available from: <https://www.sigmaaldrich.com/life-science/proteomics/post-translational-analysis/phosphorylation/mass-changes.html>.
179. Beers MF, Bates SR, Fisher AB. Differential extraction for the rapid purification of bovine surfactant protein B. *American Journal of Physiology-Lung Cellular and Molecular Physiology*. 1992; 262: L773–L778.
180. Lang CJ, Postle AD, Orgeig S, Possmayer F, Bernhard W, Panda AK, Jürgens KD, Milsom WK, Nag K, Daniels CB. Dipalmitoylphosphatidylcholine is not the major surfactant phospholipid species in all mammals. *American Journal of Physiology-Regulatory, Integrative and Comparative Physiology*. 2005; 289: R1426–R1439.
181. Kind T, Liu K-H, Lee DY, DeFelice B, Meissen JK, Fiehn O. LipidBlast in silico tandem mass spectrometry database for lipid identification. *Nature Methods*. 2013; 10: 755–758.
182. Avanti Polar Lipids [Internet]. Available from: <https://avantilipids.com/>.
183. LIPID MAPS® Lipidomics Gateway [Internet]. Available from: <http://www.lipidmaps.org/tools/structuredrawing/masscalc.php>.
184. Chen G, Liu H, Wang X, Li Z. In vitro methylation by methanol: Proteomic screening and prevalence investigation. *Analytica Chimica Acta*. 2010; 661: 67–75.
185. Afjehi-Sadat L, Garcia BA. Comprehending Dynamic Protein Methylation with Mass Spectrometry. *Current Opinion in Chemical Biology*. 2013; 17: 12–19.
186. Tong H, Bell D, Tabei K, Siegel MM. Automated data massaging, interpretation, and e-mailing modules for high throughput open access mass spectrometry. *Journal of the American Society for Mass Spectrometry*. 1999; 10: 1174–1187.

187. Hertel SP, Winter G, Friess W. Protein stability in pulmonary drug delivery via nebulization. *Advanced Drug Delivery Reviews*. 2015; 93: 79–94.
188. Held PG. Fluorometric Quantitation of Protein using the Reactive Compound Fluorescamine (Application Note). BioTek Instruments, Inc., Winooski, VT. 2001.
189. Rubin BK, Ramirez O, King M. Mucus Rheology and Transport in Neonatal Respiratory Distress Syndrome and the Effect of Surfactant Therapy. *Chest*. 1992; 101: 1080–1085.

VITA

EDUCATION

- Doctor of Philosophy, Pharmaceutical Sciences 2014 – present
Virginia Commonwealth University (VCU), School of Pharmacy
Richmond, VA
- Bachelor of Science, Biochemistry 2002 – 2005
University of California, Los Angeles
Los Angeles, CA

PROFESSIONAL EXPERIENCE

- Novartis Pharmaceuticals Corporation 2009 – 2014
San Carlos, CA
- Nektar Therapeutics 2006 – 2008
San Carlos, CA

POSTER PRESENTATIONS and ABSTRACTS

1. Boc ST, Farkas D, Longest PW, Hindle M. Aerosolization of Spray Dried Pulmonary Surfactant Powder Using a Novel Low Air Volume Actuated Dry Powder Inhaler. In *Respiratory Drug Delivery 2018. Volume 2*, 2018: 639-642.
2. Boc ST, Farkas D, Longest PW, Hindle M. Spray Dried Pulmonary Surfactant Powder Formulations: Development and Characterization. In *Respiratory Drug Delivery 2018. Volume 2*, 2018: 635-638.
3. Dhapare S, Spence B, Boc ST, Wei X, Bass K, Longest PW, Hindle M. Breath-synchronized Delivery of Aerosols to Infants using a Very Low Volume Mixer-Heater. In *Respiratory Drug Delivery 2018. Volume 2*, 2018: 643-646.
4. Boc ST, Spence B, Bass KP, Longest PW, Hindle M. Improved Nose-to-Lung (N2L) Aerosol Delivery in an *In Vitro* Infant Nasal Cannula. *Journal of Aerosol Medicine and Pulmonary Drug Delivery*. June 2017, 30(3): A-32.
5. Bass KP, Boc ST, Hindle M, Longest PW. High Efficiency Nose-to-Lung (N2L) Aerosol Delivery in an Infant: Development of a Validated CFD Method. *Journal of Aerosol Medicine and Pulmonary Drug Delivery*. June 2017, 30(3): A-8.

6. Boc ST, Spence B, Bass K, Longest PW, Hindle M. High-Efficiency Delivery of Aerosols via an Infant Nasal Cannula. In *Respiratory Drug Delivery Europe 2017. Volume 2*, 2017: 385-388.
7. Kadrichu N, Dang T, Boc ST, Corkery K, Challoner P. Amikacin Inhale *In Vitro* Delivery with Tracheostomy Setup. In *Respiratory Drug Delivery Europe 2015. Volume 2*, 2015: 383-386.
8. Kadrichu NP, Boc ST, Day RF, Hayes MJ. Amikacin Inhale: Development of a Vibrating Mesh with Superior Performance. In *Respiratory Drug Delivery 2014. Volume 2*, 2014: 507-510.
9. Kadrichu NP, Boc ST, Corkery KJ, Challoner PB. *In vitro* Assessment of Aerosolized Amikacin Lung Dose Delivered by NKTR-061 PDDS Clinical During On-Ventilator and Off-Ventilator Use. *Journal of Aerosol Medicine and Pulmonary Drug Delivery*. 2013, 26(2): A-39.
10. Kadrichu NP, Boc ST, Corkery KJ, Challoner PB. In vitro efficiency of Amikacin Inhale, a novel drug-device delivery system. *Critical Care*. 2013, 17: P81. DOI: 10.1186/cc12019.

PODIUM PRESENTATIONS

Boc S. High-Efficiency Delivery of Aerosols via an Infant Nasal Cannula. *Respiratory Drug Delivery Europe 2017*, April 2017; Antibes, France.

SCHOLARSHIPS/HONORS/ACHIEVEMENTS

Charles T. Rector and Thomas W. Rorrer, Jr. Dean's Award Finalist for Excellence in Graduate Study, Virginia Commonwealth University	2018
John Wood Excellence in Pharmaceuticals, Virginia Commonwealth University	2018
Joseph P. Schwartz Award, Virginia Commonwealth University	2017
Phi Kappa Phi Honor Society	2016
Joseph P. Schwartz Award, Virginia Commonwealth University	2016
Jyotsan and Mavji Thakker Award, Virginia Commonwealth University	2015